A novel optogenetics-based therapy for obstructive sleep apnoea

Fiona L. Knapman

A thesis in fulfilment of the requirements for the degree of
Doctor of Philosophy

School of Clinical Medicine
Faculty of Medicine and Health

February 2023

Supervisor: Lynne E. Bilston
Co-supervisor: Peter G. R. Burke

UNSW SYDNEY

NeuRA
Discover. Conquer. Cure.

ORIGINALITY, COPYRIGHT AND AUTHENTICITY STATEMENTS

ORIGINALITY STATEMENT

☑ I hereby declare that this submission is my own work and to the best of my knowledge it contains no materials previously published or written by another person, or substantial proportions of material which have been accepted for the award of any other degree or diploma at UNSW or any other educational institution, except where due acknowledgement is made in the thesis. Any contribution made to the research by others, with whom I have worked at UNSW or elsewhere, is explicitly acknowledged in the thesis. I also declare that the intellectual content of this thesis is the product of my own work, except to the extent that assistance from others in the project's design and conception or in style, presentation and linguistic expression is acknowledged.

COPYRIGHT STATEMENT

☑ I hereby grant the University of New South Wales or its agents a non-exclusive licence to archive and to make available (including to members of the public) my thesis or dissertation in whole or part in the University libraries in all forms of media, now or here after known. I acknowledge that I retain all intellectual property rights which subsist in my thesis or dissertation, such as copyright and patent rights, subject to applicable law. I also retain the right to use all or part of my thesis or dissertation in future works (such as articles or books).

For any substantial portions of copyright material used in this thesis, written permission for use has been obtained, or the copyright material is removed from the final public version of the thesis.

AUTHENTICITY STATEMENT

☑ I certify that the Library deposit digital copy is a direct equivalent of the final officially approved version of my thesis.

INCLUSION OF PUBLICATIONS STATEMENT

UNSW is supportive of candidates publishing their research results during their candidature as detailed in the UNSW Thesis Examination Procedure.

Publications can be used in the candidate's thesis in lieu of a Chapter provided:

- The candidate contributed **greater than 50%** of the content in the publication and are the "primary author", i.e. they were responsible primarily for the planning, execution and preparation of the work for publication.
- The candidate has obtained approval to include the publication in their thesis in lieu of a Chapter from their Supervisor and Postgraduate Coordinator.
- The publication is not subject to any obligations or contractual agreements with a third party that would constrain its inclusion in the thesis.

☑ The candidate has declared that **their thesis has publications - either published or submitted for publication - incorporated into it in lieu of a Chapter/s. Details of these publications are provided below.**.

Publication Details #1

Full Title:	Direct optogenetic activation of upper airway muscles in an acute model of obstructive sleep apnoea
Authors:	Fiona L. Knapman, Myfanwy Cohen, Tom Kulaga, Nigel Lovell, Leszek Lisowski, Simon McMullan, Peter G.R. Burke, Lynne E. Bilston
Journal or Book Name:	American Journal of Respiratory and Critical Care Medicine
Volume/Page Numbers:	
Date Accepted/Published:	
Status:	submitted
The Candidate's Contribution to the Work:	Fiona performed all experiments and analysed all data, excluding the DNA and RNA quantification. With Professor Bilston, Fiona interpreted the data and wrote the initial draft.
Location of the work in the thesis and/or how the work is incorporated in the thesis:	Chapter 2 contains all work associated with this publication.

Candidate's Declaration

I confirm that where I have used a publication in lieu of a chapter, the listed publication(s) above meet(s) the requirements to be included in the thesis. I also declare that I have complied with the Thesis Examination Procedure.

TABLE OF CONTENTS

Originality, copyright and authenticity statements ..... **i**
Inclusion of publications statement ..... **ii**
Table of contents ..... **iii**
Acknowledgements ..... **vi**
Abbreviations and symbols ..... **vii**
List of figures ..... **viii**
List of tables ..... **xv**
Chapter 1 Introduction and literature review **1**
1.1 Breathing and the upper airway 2
1.1.1 Upper airway muscles 3
1.1.2 Neural control 9
1.1.3 Rodent upper airway 13
1.1.4 Characterising upper airway function 14
1.2 Obstructive sleep apnoea 17
1.2.1 Pathophysiology 18
1.2.2 OSA treatments 19
1.2.3 Rodent models of OSA 30
1.3 Optogenetics 31
1.3.1 Opsins 33
1.3.2 Gene transfer 36
1.3.3 Promoters 46
1.3.4 Restoration of skeletal muscle function 48
1.3.5 Optogenetics technology 55
Chapter 2 Optimising the viral construct: Promoters **60**
2.1 Introduction 60
2.2 Methods 61
2.2.1 Animals 61
2.2.2 AAV vectors 61
2.2.3 Intramuscular AAV injection 62
2.2.4 Electrophysiology measurements 63
2.2.5 Histology and immunofluorescence staining 64
2.2.6 DNA and RNA Quantification 65
2.2.7 Statistics 66
2.3 Results 66
2.3.1 Use of a muscle-specific promoter consistently induced strong ChR2 expression. 66

2.3.2 The muscle-specific promoter minimises off-target expression 67
2.3.3 Isoflurane titration in rodents mimics sleep associated pharyngeal hypotonia/atonia 70
2.3.4 Closed-loop photostimulation restores pharyngeal inspiratory dilator activity 70
2.3.5 Optimal functional responses depend on light stimulation parameters 71
2.4 Discussion 72
Chapter 3 Optimising the viral construct: rAAV serotypes 78
3.1 Introduction 78
3.2 Methods 80
3.2.1 AAV vectors 81
3.3 Results 81
3.3.1 AAVMYO produced equivalent distribution of opsin:reporter expression, but greater levels of viral DNA and RNA expression in the tongue 81
3.3.2 AAVMYO facilitated more robust light-evoked increases in muscle activity 84
3.4 Discussion 86
Chapter 4 Quantifying light-evoked airway dilation 90
4.1 Introduction 90
4.2 Methods 91
4.2.1 Animals 91
4.2.2 AAV vectors 91
4.2.3 Intramuscular AAV injection 92
4.2.4 High-resolution ultrasound imaging 92
4.2.5 Ultrasound image analysis 94
4.3 Results 95
4.3.1 Ultrasound-recorded light-evoked airway dilation was variable between animals . 95
4.3.2 Persistence of light-evoked muscle contractions 12 weeks after intramuscular injections 98
4.3.3 Light-evoked muscle contractions and airway dilation are dependent on the stimulation protocol and are visibly different to endogenous contractions 102
4.4 Discussion 102
Chapter 5 Quantifying the effects of chronic light stimulation 106
5.1 Introduction 106
5.2 Hardware development 107
5.2.1 Light delivery requirements 107
5.2.2 Recording hardware 111
5.3 Methods 111
5.3.1 Animals 111
5.3.2 AAV vectors 111
5.3.3 Intramuscular AAV injection 112

5.4 Pilot study #1 112
5.4.1 Surgical method 112
5.4.2 Results 117
5.5 Pilot study #2 121
5.5.1 Surgical method - Changes 121
5.5.2 Results 122
5.6 Pilot Study #3 124
5.6.1 Surgical method - Changes 124
5.6.2 Results 125
5.7 Pilot Study #4 128
5.7.1 Surgical method - Changes 128
5.7.2 Results 129
5.8 Pilot Study #5 130
5.8.1 Surgical method – Changes 130
5.8.2 Results 131
5.9 Discussion 134
Chapter 6 Summary, Discussion, and Conclusions 138
6.1 Summary of results 138
6.2 Developing an optogenetic stimulation therapy for OSA 139
6.2.1 Light stimulation 140
6.2.2 Targeted opsin expression and optimised safety profiles 142
6.2.3 Long term considerations 149
6.3 Contributions to Knowledge 150
6.3.1 Rodent research methods 151
6.3.2 Improved targeting of direct optogenetic control of skeletal muscle 152
6.3.3 Clinical applications outside of OSA 153
6.4 Conclusions 154
References 155
Appendices 179

ACKNOWLEDGEMENTS

Most importantly, I would like to express my deepest gratitude to Professor Lynne Bilston for her support, guidance and patience throughout my PhD. I consider myself extremely lucky to have had Lynne as my supervisor for the past four years and my employer for the preceding three years. I can honestly say that without her, I would not have made it through this thesis with my sanity intact.

I am also grateful to Peter Burke for his advice and endless enthusiasm. Every experiment I conducted would not have been possible without his practical support.

There are also several others whose support and contributions were invaluable. I want to thank Myfanwy Cohen for her help with experiments, particularly the DNA and RNA quantification, Tom Kulaga for developing various electronic components, and Peter Humburg for his expertise in statistical analysis. Also, thank you very much to Leszek Lisowski, Simon McMullan and Nigel Lovell for their respective expertise.

Finally, I'd like to thank my family for their unwavering support and belief in me. I could not have done this without them, and I love them very much.

ABBREVIATIONS AND SYMBOLS

AAV	Adeno-associated virus
CAG	A promoter derived from CMV, CBA, and rabbit beta globin genes
CBA	Chicken beta-actin
ChR	Channelrhodopsin
CMV	Cytomegalovirus
CNS	Central nervous system
CPAP	Continuous positive airway pressure
DMD	Duchenne muscular dystrophy
EMA	European Medicines Agency
FDA	Food and Drug Administration
FES	Functional electrical stimulation
ITR	Inverted terminal repeats
MAS	Mandibular advancement splint
MCK	Muscle creatine kinase
NAbs	Neutralising antibodies
OSA	Obstructive sleep apnoea
PNS	Peripheral nervous system
rAAV	Recombinant adeno-associated virus
SD	Sprague Dawley
SMA	Spinal muscular atrophy
tMCK	Enhanced muscle-specific promoter derived from the MCK promoter

LIST OF FIGURES

Figure 1-1 | Structures of the respiratory system. Primary respiratory muscle (diaphragm and external intercostal muscles) contractions induce inspiration (purple arrows), and the upper airway muscles maintain pharyngeal patency. 3

Figure 1-2 | Muscles of the human tongue and upper airway. (A) Muscles of the human tongue and upper airway have highly complex and interwoven fibres; superior longitudinal (SL), hyoglossus (HG), transverse (T), genioglossus (GG), vertical (V), geniohyoid (GH), styloglossus (SG), inferior longitudinal (IL), mylohyoid (MH), digastric (DG), combined longitudinal (CL – where IL, HG and SG merge) (R. Lloyd, unpublished). **(B)** Several upper airway muscles control the tongue position (orange highlight), the soft palate position (blue highlight), the hyoid position (green highlight) and the posterior pharyngeal walls (yellow highlight) [38]. During inspiration, they collectively maintain upper airway patency..... 6

Figure 1-3 | Neural innervation and drive to the tongue. (A) The hypoglossal motor neuron (XII) divides into lateral branches (l-XII) to innervate the styloglossus (SG), the superior longitudinal (SL), medial region of the inferior longitudinal (IL) muscles of the tongue. The following medial branches (m-XII) innervate the oblique and horizontal compartments of the genioglossus (GGo, GGh), the transverse and vertical (T/V), and the lateral IL muscles [30]. **(B)** The genioglossus receives six unique motor unit discharge patterns during quiet breathing, indicated by the raw electromyography, instantaneous discharge frequency plot and inspired volume plots [31]..... 10

Figure 1-4 | Therapeutic options for obstructive sleep apnoea. (A) Continuous positive airway pressure devices, **(B)** mandibular advancement splints, and **(C)** upper airway surgeries, including uvulopalatopharyngoplasty..... 19

Figure 1-5 | Hypoglossal nerve stimulators are increasing in prevalence for obstructive sleep apnoea. (A) The Inspire Medical device is clinically approved, and **(B)** the Genio System by Nyxoah, and **(C)** aura6000 by LivaNova have undergone clinical trials. 23

Figure 1-6 | Microbial opsins can induce depolarisation or hyperpolarisation with light stimulation. (A) Opsins in the channelrhodopsin family act as non-specific ion channels that open when illuminated to induce depolarisation. **(B)** Opsins in the halorhodopsin family act as chloride ion channels that open when illuminated to induce hyperpolarisation. **(C)** Different opsins can be activated by a range of visible light wavelengths but produce maximum photocurrents when exposed to a specific wavelength of light. 34

Figure 1-7 | Kinetic and spectral properties of opsin variants. While a range of wavelengths can activate an opsin, they demonstrate peak activation at specific wavelengths (y-axis). Opsin reactivation depends on their off-kinetics (τoff). Figure from [275]. 35
Figure 2-1 | Non-specific (CAG) and muscle specific (tMCK) promoter driven expression in the tongue. (A) Diagram of the ventral surface of a rat tongue, with the approximate location of the genioglossus identified. Viral vectors were injected intramuscularly at sites 1 to 4. Light was applied to the crosshatched region and tongue EMG activity measured via fine wire electrodes inserted near sites 1 to 4. For histology, the tongue was sectioned through the transverse planes in the tongue 'tip', 'middle' and 'base'. **(B)** The tMCK promoter (grey, n=6) produced greater protein expression in the tongue compared to the CAG promoter (blue, n=4) (p=0.013). **(C, D)** Weaker and less widespread membrane-bound ChR2(H134R):mCherry fusion protein (orange) expression is seen in representative images of the tongue tip, middle and base sections from a **(C)** CAG than a **(D)** tMCK animal. 67
Figure 2-2 | Biodistribution after intramuscular delivery of the tMCK and CAG constructs. (A) 3 weeks following intramuscular delivery of an rAAV construct, ChR2(H134R):mCherry fusion proteins are visible in 8.7±3.9% (mean±SD) of ChAT positive hypoglossal motor neurons in animals that received the CAG construct, **(B)** but are absent in animals that received the tMCK construct. **(C)** The tMCK cohort exhibited robust levels of viral DNA and **(D)** RNA expression in the tongue, and minimal or no expression in organs (spleen, liver and heart), and other skeletal muscles (gastrocnemius and diaphragm), thus confirming the specificity of the tMCK construct (^=diaphragm, gastrocnemius and brainstem viral DNA levels were below the limits of detection). *** P<0.001 and **** P<0.0001 by one-way ANOVA and Tukey Test. 68
Figure 2-3 | Optogenetic stimulation of the tongue muscles in an isoflurane-based model of pharyngeal muscle atonia. (A) Increased isoflurane concentration results in reductions of genioglossus electromyography (EMG) activity (blue) while diaphragm EMG activity (red) is preserved, mimicking pharyngeal muscle hypotonia in human sleep. **(B)** During the electrophysiology studies, isoflurane is delivered via a nose cone, and fine wire electrodes monitor genioglossus and diaphragm EMG. **(C)** Sample data illustrates that pulsed blue light (470 nm), triggered by the onset of inspiratory diaphragm EMG activity (dotted line), restores genioglossus EMG when 3.5% isoflurane reduces endogenous activity and when 5% isoflurane removes endogenous activity. Light application does not affect diaphragm EMG. **(D)** Adjacent unstimulated and stimulated EMG activity is normalised to maximal unstimulated EMG activity (n=4, mean±SD). The tMCK construct induced sufficient expression for light stimulation to

significantly (p<0.001) increase EMG activity. Note that visible tongue protrusions were only observed in animals injected with the tMCK construct. *** P<0.001 by linear mixed model. ..69
Figure 2-4 | Light-evoked EMG in the genioglossus varies with light simulation protocol characteristics. (A) Relationship between light pulse durations and the area under the induced genioglossus EMG curve, i.e. EMG restoration with a single pulse (n=4, mean±SEM). **(B)** Representative examples of genioglossus and diaphragm EMG prior to isoflurane induced EMG reduction ('Endogenous Maximum'), after isoflurane induced EMG elimination ('Endogenous Absent') and when EMG is increased by 10 ms long pulses with increasing frequencies ('Light Applied'). **(C)** When pulsed stimulation is maintained for 300 ms, the greatest increase in EMG was achieved with pulse widths of 5 ms and frequencies between 40 Hz and 60 Hz (n=4, mean±SEM). **(D)** The stimulated EMG declines with sequential pulses within a stimulation protocol (n=4, mean±SEM). Duration for all stimulation trains is ~ 300 ms. 72
Figure 3-1 | Opsin expression and biodistribution following intramuscular injections of AAVMYO and AAV9. (A) Both serotypes achieved similar distributions of opsin:reporter expression in the tongue, and **(B)** did not induce opsin:reporter expression in the hypoglossal motor nucleus of the brainstem (only ChAT positive hypoglossal motor neurons and dorsal motor neurons of the vagus are highlighted in the AAVMYO brainstem sections). **(C)** A three-way mixed model ANOVA (tissue type x time point x serotype) reported that at three weeks, viral DNA copy numbers in the tongue were significantly greater for the AAVMYO serotype than AAV9 (Tukey, P < 0.0001). DNA copy numbers in the tongue fell significantly between 3 and 12 weeks for both serotypes (Tukey, AAVMYO: P < 0.0001; AAV9: P = 0.011), and there were no differences in DNA copy numbers in the tongue between serotypes at 12 weeks (Tukey, P > 0.999). **(D)** Using the same statistical analysis, RNA expression in the tongue at three weeks was significantly greater for the AAVMYO serotype than AAV9 (Tukey, P < 0.0001) and, regardless of serotype. RNA expression fell significantly between 3 and 12 weeks after for both serotypes (Tukey, AAVMYO: P < 0.0001; AAV9: P = 0.035), and there were no differences between RNA expression in the tongue at 12 weeks (P > 0.999). **** P < 0.0001, * P < 0.05 . 83
Figure 3-2 | Light-evoked EMG responses in animals receiving AAV9 and AAVMYO packaged optogenetic constructs. Increases in EMG responses with light stimulation were greater in the animals that received the AAVMYO serotype than the AAV9 serotype (linear mixed model, Bonferroni post hoc, P < 0.0001); however, both serotypes facilitated significant EMG increases with light stimulation (Univariant tests, AAVMYO: F(1, 221) = 163.4, P < 0.0001; AAV9: F(1, 221) = 16.0, P < 0.0001). **** P < 0.0001. 85
Figure 4-1 | Ultrasound imaging for airway dilation. (A) During ultrasound imaging, animals were placed supine on a physiological monitoring platform, and images were acquired using a

fixed transducer. **(B)** The airway was imaged during three conditions; i) no stimulation, ii) stimulation only (i.e. stimulation applied 'out-of-phase' with the respiratory cycle), and iii) light stimulation applied 'in-phase' with the respiratory cycle. **(C)** B-mode images (400 frames, acquired at 45 frames per second) were captured in a sagittal plane, **(D)** a mid-axial plane, and **(E)** a posterior-axial plane. Airway dilation was quantified as the vertical displacement of the dorsal surface of the tongue along three vertical lines, labelled 'left', 'centre' and 'right'. **(F)** The coordinates of the dorsal surface and vertical line intersections were recorded during expiration, **(G)** and inspiration (no stimulation), and when **(H)** stimulation was applied 'out-of-phase' with inspiration (stimulation only), and 'in-phase' with inspiration (not pictured). These coordinates were then used to calculate the ventral displacement of the tongue's dorsal surface. 93

Figure 4-2 | Sample data from three weeks after intramuscular injections in an animal where light-evoked upper airway muscle contraction and airway dilation was observed. **(A)** Dorsal surfaces of the tongue during expiration (yellow dashed lines), inspiration (i.e. no stimulation, orange dashed lines), stimulation only (red dashed lines), and 'in-phase' stimulation (i.e. stimulation and inspiration, purple dashed lines) are indicated. **(B)** Light stimulation produces laterally dominant airway dilation (red), which persists when light stimulation is applied in phase with inspiration. **(C)** Airway dilation is strongest in the caudal/posterior region of the tongue rather than the rostral/anterior region where the mid-axial plane is located. 97

Figure 4-3 | Light-evoked airway dilation following intramuscular injections of an optogenetics construct . (A) At three weeks, two animals (green) displayed light-evoked muscle contractions and airway dilation and two (orange) displayed light-evoked muscle contractions but did not achieve light-evoked airway dilation. The four remaining animals (grey) did not display any light-evoked muscle contractions **(B)** The animals that displayed light-evoked airway dilation at three weeks maintained these responses until ~ 8 to 10 weeks after injections. At this time, light-evoked muscle contractions weakened and airway dilation was not visible in an axial plane. 98

Figure 4-4 | Sample data from 6 to 12 weeks after intramuscular injections indicates that when functional responses to light are present three weeks after injections, they persist, albeit at reduced strengths for 9 weeks. (A) At 6 weeks and **(B)** 8 weeks after injection, airway dilation remains strong. Dilation is greater on one side of the tongue, and in the posterior-axial frame. **(C)** 10 weeks after injection, contraction strength declined and airway dilation is minimal. In this animal, it has not been captured in either axial plane, but can be seen in the mid-sagittal plane 'behind' the tongue following light-evoked geniohyoid contraction. **(D)** 12 weeks after injection, contraction strength has declined further, and airway dilation is no

longer visible. In all panels, dashed lines indicate the dorsal surface of the tongue during expiration (yellow), inspiration (no stimulation, orange), stimulation only (red), and in-phase stimulation (stimulation and inspiration, purple)..... 102
Figure 5-1 | Construction of light-delivery hardware (A) Iterations of the implantable flexible printed circuit boards (PCBs, WellPCB, ShijiaTzhuang Hebei, China) with locations for soldering two light emitting diodes (LEDs). The progression of the development goes from left to right. (**B)** The final flexible PCB design, employs a six-channel electrode system, with two locations for surface-mounted chip LEDs and one for an additional recording component. Four suture points for securing the PCB within the tongue are included. (**C)** Implantable optical fibre for the delivery of visible light from an external source to the tongue. Two suture points are included. 110
Figure 5-2 | Ventral surface of a rat tongue. Four intramuscular injection locations are labelled 1 to 4. 112
Figure 5-3 | Preparation for hardware implantation. Skull, submandibular and diaphragm (left to right) regions must be shaved and sterilised (grey ovals) and incisions made (black dotted lines). Approximate subcutaneous tunnelling routes and the insertion locations for EMG electrodes are indicated. Created with BioRender.com..... 113
Figure 5-4 | Head stage set up for Pilot 1 and Pilot 2 A) Approximate locations for screws, pedestals, and the transcutaneous pocket for electrode slack storage. **B)** Two diaphragm EMG (diaEMG) electrodes, two genioglossus EMG (ggEMG) electrodes, two EEG electrodes, and two LED connections were connected to specific sites on two six-channel electrode pedestals. The 'spare' connection points were reserved for the third EEG electrode and any additional recording components. The figure indicates pedestal orientation from the insertion side (the larger holes). **C)** The pedestals were secured to the skull via dental composite. Patch cables deliver data from the pedestal to amplifiers and power to the flexible PCB via the pedestals. Epoxy resin was used to isolate the PCB pins. **D)** Female sockets were crimped to the EMG and EEG electrodes and inserted into the 6-channel pedestals, split end first. 115
Figure 5-5 | The recording chamber was fabricated by combining a pressure sensor and a glass vacuum desiccator. Light stimulation and air (1 L/min) enter the chamber, and recorded data (chamber pressure, EEG and EMG) and air (passive) exit. 116
Figure 5-6 | Endogenous EMG recording was difficult to obtain, and light stimulation produced increases in muscle activity and artefacts (A) Brief and low amplitude periods of endogenous respiratory-linked genioglossus EMG (ggEMG) were present. However, no endogenous respiration-linked diaphragm EMG (diaEMG) was recorded. ECG artefacts were present in the **(A)** ggEMG and **(B)** diaEMG channels. Light stimulation induced **(C)** increases in

ggEMG activity and **(D)** artefacts in both the EMG and EEG channels. **D) A**rtefacts generated by 10 ms pulses repeated at 20 Hs, 40 Hz and 60 Hz. Artefacts in the EEG channel are evident at the stimulating frequency and the associated harmonics. 118

Figure 5-7 | Pilot study #1 recorded periods of EEG, genioglossus EMG (ggEMG) and respiratory data (pressure). (A) ~ 2 hours of data show distinct periods of theta activity (~ 7 Hz). When high-frequency respiratory rates are also recorded (RespRate), the animal is likely awake (e.g. ~ 5400 s). When the RespRate is stable with only occasional bursts of activity the animal is likely in REM sleep. The grey box identifies a transition period between REM and NREM. This is enlarged in **(B),** where the periods of NREM and REM are identified. Light-induced ggEMG activity was recorded during **(C)** NREM and **(D)** REM sleep 120

Figure 5-8 | Adapted version of Figure 5-3 indicates the new locations for electrode 'slack', i.e. the loops included in the genioglossus EMG (ggEMG) and diaphragm EMG (diaEMG) electrode routes. Created with BioRender.com 121

Figure 5-9 | Pilot #2 produced periods of clear EEG and genioglossus EMG (ggEMG) data. (A) Under isoflurane anaesthesia, clean EEG data was recorded. **(B)** In the recording chamber (not anaesthetised), brief periods of endogenous ggEMG activity were recorded. **(C)** Wakefulness could be identified by a weak theta band (~ 7 Hz) in the EEG channel and behaviour-related activity in the ggEMG channel, i.e. **(D)** teeth grinding and grooming. 123

Figure 5-10 | Data acquired during Pilot #4. (**A)** The chamber pressure signal afforded closed-loop light stimulation. **B)** EEG data was recorded while the animal was under isoflurane, and **C)** during NREM and REM sleep. Augmented breaths indicated transitions between sleep stages or REM sleep when accompanied by slowed breathing..... 126

Figure 5-11 | Altered version of Figure 5-4, describing head stage set up for Pilots 4 and 5. (**A)** Approximate locations for screws, pedestal, and optical fibre ferrule. (**B)** Two genioglossus EMG (ggEMG) electrodes and three EEG electrodes connect to specific sites on a six-channel electrode pedestal. The figure indicates the orientation from the insertion side of the pedestals (the larger holes). (**C)** The pedestal and ferrule are secured to the skull by a dental composite and, during recording, connect to patch cables for data and light transfer, respectively. (**D)** The female pins are crimped to the wires at the solid end and inserted into the pedestal split end first. 128

Figure 5-12 | Chronic implantation of an optical fibre for Pilot 5. A) Skull, sub-mandibular and shoulder (left to right) regions must be shaved and sterilised (grey ovals) prior to incisions (black dotted lines). Approximate routes for subcutaneous tunnelling for the genioglossus EMG (ggEMG) electrodes (blue) and optical fibre (orange) are indicated. The optical fibre was secured at three points (green), and the EMG electrodes were inserted at two points (purple).

The inset image displays the region where the tissue was separated (red) immediately posterior to the mandibular symphysis for effective light source placement. Created with BioRender.com **B)** One set of sutures was secured to the optical fibre via shrink wrap, and two additional single sutures were unattached and loosely applied. 130
Figure 5-13 | Pilot #5 generated excellent EEG recordings (A) while the animal was anaesthetised, with sparser activity when greater isoflurane concentrations were applied. **(B)** EEG was also consistently recorded when the animal was in the recording chamber, and wakefulness (e.g. 100 to 400 seconds) and sleep stage identification were possible. A NREM and a REM stage are identified. 131
Figure 5-14 | Daisy-chained EEG patch cables produce two different EEG channels. (A) Each channel displays different intensities of activity bands characteristic of wakefulness, REM and NREM. **(B)** During REM sleep, the 'EEG #2' channel displayed theta wave activity (~ 7 Hz). This was absent in the 'EEG #1' channel. **(C)** Both channels display increases in delta wave activity (0 to 4 Hz) during NREM sleep 134

LIST OF TABLES

Table 3-1 | Study Design. 80

Table 3-2 | Summary of main and interaction effects of viral DNA copy numbers and RNA expression following a three-way mixed model ANOVA in GraphPad. Variables are tissue (i.e. tongue, diaphragm, gastrocnemius, liver, spleen, heart, brainstem and bladder), time point (i.e. 3- and 12- weeks after viral vector administration), and serotype (i.e. AAV9 or AAVMYO). 84

Table 3-3 | Summary of main and interaction effects of EMG activity following a linear mixed model in SPSS. Variables are intercept (i.e. animal ID), serotype (i.e. AAV9 or AAVMYO), endogenous group (i.e. method of grouping equivalent levels of endogenous/unstimulated EMG activity – 1 to 10), and stimulation (i.e. unstimulated/endogenous EMG and stimulated EMG). 86

Table 4-1 | Qualitative ultrasound observations from three to twelve weeks after vector administration. 'Any' indicates where light-evoked contractions were visible regardless of whether they were associated with airway dilation, and 'Dilate' indicates when the light-evoked muscle contractions achieved airway dilation. No further ultrasounds were performed (indicated by '-') on animals in which no light-evoked movement was detected (✖) 96

Table 5-1 | Summary of devices able to deliver light stimulation to the tongue. Flexible PCBs, optical fibres and fully implanted devices have different characteristics that make them suitable for the presented application..... 109

Chapter 1 INTRODUCTION AND LITERATURE REVIEW

Obstructive sleep apnoea (OSA) is a chronic, sleep-related breathing disorder characterised by repeated airway narrowing and/or collapse during sleep. Currently, nearly 1 billion adults worldwide (~ 1/7 of the population) have OSA. Diagnosis is nearly twice as high in men as in women (25% versus 13%), and those over 50 years old are more than three times more likely to be diagnosed than those under 50 years (39% versus 12%) [1]. Despite the increasing prevalence of OSA in our aging and overweight population [2, 3] and the significant clinical, social and economic consequences [4], therapeutic options remain suboptimal. The 'gold-standard' therapy, Continuous Positive Airway Pressure (CPAP) devices, are efficacious but poorly tolerated, with between 46 and 83% of patients reported as non-adherent [5]. Second-line treatments such as mandibular advancement splints, upper airway surgeries, and hypoglossal nerve stimulators have superior adherence but variable and unpredictable efficacy [3, 6-8].

To address this gap, this thesis describes proof-of-concept studies for a proposed novel, minimally invasive optogenetics-based muscle stimulation therapy that aims to combat inadequate upper airway muscle activity, which, combined with anatomical risk factors, is a significant contributor to OSA [9-11]. Patients will receive local intramuscular injections into specific upper airway muscles of a viral vector construct to induce light sensitivity. An oral appliance worn during sleep will detect inspiration onset and, in response, will apply light stimulation to the targeted muscle(s) to induce contractions and airway dilation. The proposed therapy will be significantly less invasive than existing options (e.g. upper airway surgeries and hypoglossal nerve stimulators) and will achieve greater patient adherence than CPAP. Due to optogenetics' high spatial and temporal specificity, the proposed therapy could target the patient-specific site of airway collapse and allows temporally precise feedback-driven, 'closed-loop' control of muscle stimulation titrated to individual requirements and/or adapted throughout the night, potentially overcoming limitations of existing and proposed muscle stimulation therapies for OSA, including hypoglossal nerve stimulators [6, 12-14] and chemogenic [15, 16] approaches.

This thesis encompasses early pre-clinical studies for the proposed therapy, focusing on optimising opsin expression for effective light-evoked upper airway muscle contractions and airway dilation. This literature review will cover several topics. First, the role upper airway muscles play in respiration and the primary differences between rodent and human upper airway anatomy and physiology. Second, OSA pathophysiology, current therapeutic options for OSA patients, rodent models of OSA and methods of quantifying upper airway function will be

described. Third, the review will describe the primary elements of the proposed therapy, specifically opsins and optogenetics, adeno-associated viral vectors, and how they can be optimised to generate functional light-evoked responses. Potential challenges to clinical translation will also be described, including immune responses and technological changes for light delivery to skeletal muscle. Finally, the current status of optogenetics for direct and indirect optogenetic stimulation of skeletal muscle will be discussed.

1.1 BREATHING AND THE UPPER AIRWAY

Inspiration during quiet breathing is an unconscious process initiated by the primary respiratory muscles. The main contributor, the diaphragm, contracts and flattens (the centre moves caudally, and the edges move rostrally), expanding the thoracic cavity. This expansion is aided by the contraction of the external intercostal muscles that move the ribs caudally and laterally (Figure 1-1). The resultant pressure gradient between the thoracic cavity and the atmosphere generates a vacuum, drawing air into the lungs. In contrast, expiration during quiet breathing is passive. The elasticity of the lung tissue causes recoil, and primary respiratory muscle relaxation returns the thoracic cavity to its original volume, increasing intrapulmonary pressure and driving movement of air out of the system [17].

The upper airway extends from the anterior nares (nostrils) and the oral cavity to the glottis and can be divided into four anatomical regions; the nasal cavity, the oral cavity, the pharynx, and the larynx. The pharynx or pharyngeal airway can be further divided into three regions; the nasopharynx, oropharynx and laryngopharynx (also referred to as the hypopharynx, Figure 1-1). The nasopharynx is the most rostral portion of the pharynx and lies between the cranium base and the soft palate, posterior to the nasal cavity [18, 19]. The nasopharynx can be divided into the nasopharynx and the velopharynx (also known as the retropalatal oropharynx). The latter is the inferior portion of the initially described nasopharynx, lies between the hard and soft palates [20, 21], and is commonly isolated when referring to obstructive sleep apnoea (OSA) as it is a common site of airway collapse [22-24]. The oropharynx is posterior to the oral cavity, between the soft palate and the pharyngoepiglottic fold (bilateral mucus membranes that extend from the tongue base to the epiglottis). The laryngopharynx sits caudal to the epiglottis, extending to the upper oesophageal sphincter [18, 19].

Following much of the literature in respiratory and sleep medicine, this thesis will use ‘upper airway’ interchangeably with ‘pharynx’ and ‘pharyngeal region’. This is primarily due to the region's importance in sleep apnoea diagnosis, resulting from its increased susceptibility to collapse during inspiration.

1.1.1 Upper airway muscles

The pharynx contains 24 muscles that receive complex and synchronised activity patterns from motor neurons [21, 25, 26], although the details of their control and actions are incompletely understood. This complexity translates to significant roles in tasks including speech, swallowing and mastication, and loss of drive to these muscles and/or deviations from the precisely synchronised activation patterns can lead to disorders such as dysarthria [27], dysphasia[28], and OSA [11]. For respiration, the primary role of these muscles is to maintain pharyngeal airway patency. Due to a lack of rigid supports, the pharynx is significantly more compliant and collapsible than the nasal cavity and the larynx. The primary respiratory muscles generate negative intrapulmonary pressure in the thoracic cavity during inspiration, drawing air into the upper airway. Without pharyngeal muscle activation, the upper airway is at risk of collapse in the face of large inspiratory (i.e. negative) pressure swings [11, 29]. The upper airway muscles can be divided into four groups based on the 'macro' structures they primarily control i.e. the tongue, soft palate, hyoid bone, and pharyngeal walls [21]. However, some muscles contribute to the position of more than one macrostructure.

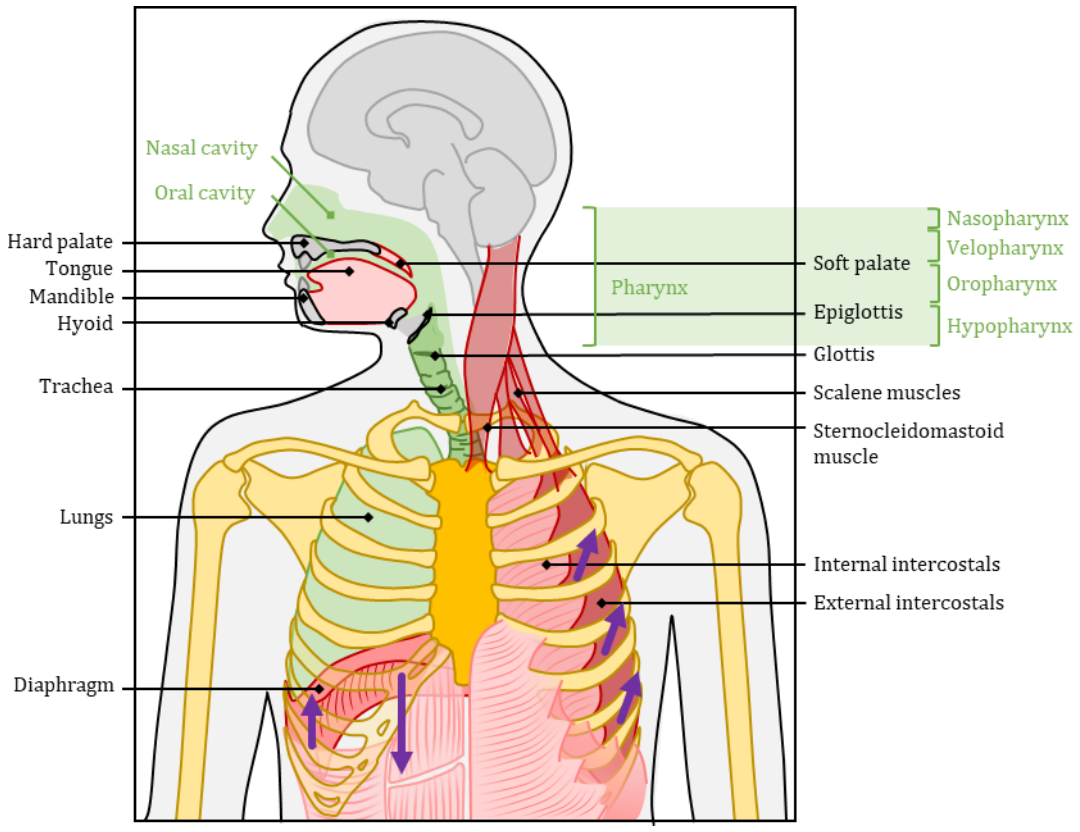

Figure 1-1 | Structures of the respiratory system. Primary respiratory muscle (diaphragm and external intercostal muscles) contractions induce inspiration (purple arrows), and the upper airway muscles maintain pharyngeal patency.

1.1.1.1 Tongue muscles

The tongue is an entirely muscular organ, critical for speech, swallowing and respiration. It is separated medially by the lingual septum and is composed of at least eight complex muscles [26]. Each muscle receives highly synchronised activation patterns from motor neurons [30-32], is composed of uniquely orientated myofibres and, in some regions of the tongue, profoundly interdigitated. The tongue can be elevated or depressed, shortened or elongated, retracted or protruded and/or articulated, i.e. dorsoflexion (tongue tip curled superiorly), ventroflexion (tongue tip curled inferiorly) or retroflexion (simultaneous tongue base elevation and tongue body depression) [26, 33]. As a muscular hydrostat, i.e. the tongue's biomechanics are more akin to a hydraulic system rather than a mechanical lever as per most of the skeletal system, a constant muscle volume is maintained [34]. When isolated longitudinal muscle fibres contract, the tongue will shorten and widen, with some increase in thickness. When isolated fibres in the cross-sectional plane contract, the tongue will flatten and elongate. When both groups co-contract, the tongue will adopt a certain rigidity [34]. Currently, the contributions of individual muscles to gross tongue movement remain poorly understood, and hypotheses are largely assumptions based on anatomical arrangement and extrapolations from animal experiments [26]. What is agreed on is that gross movements are produced by the coordinated activation of several individual muscles acting as agonists, antagonists and stabilisers. [26, 30, 33, 35].

The muscles of the tongue can be classified based on origin (extrinsic and intrinsic) and functionality (retractors and protruders). Extrinsic muscles have a bony origin, i.e. the mandible, hyoid bone or styloid process, and insert into the tongue body. These muscles include the genioglossus, hyoglossus, styloglossus and palatoglossus and typically alter tongue position. Intrinsic muscles originate and terminate within the tongue and primarily contribute to the tongue shape and assist in protrusion and retraction. Intrinsic muscles include the inferior and superior longitudinal muscles and the vertical and transverse muscles [26, 33]. The functionality-based divisions are 'retractors', i.e. those that draw the tongue posteriorly towards the posterior pharyngeal wall and therefore reduce upper airway lumen, and 'protruders', i.e. those that draw the tongue forward and out of the mouth and therefore increase upper airway lumen. Retractors include the hyoglossus, styloglossus and intrinsic inferior and superior longitudinal muscles. Protruders include the genioglossus, vertical and transverse muscles. These functional classifications represent oversimplifications of each muscles contribution to tongue movement and airway dilation [26, 36, 37].

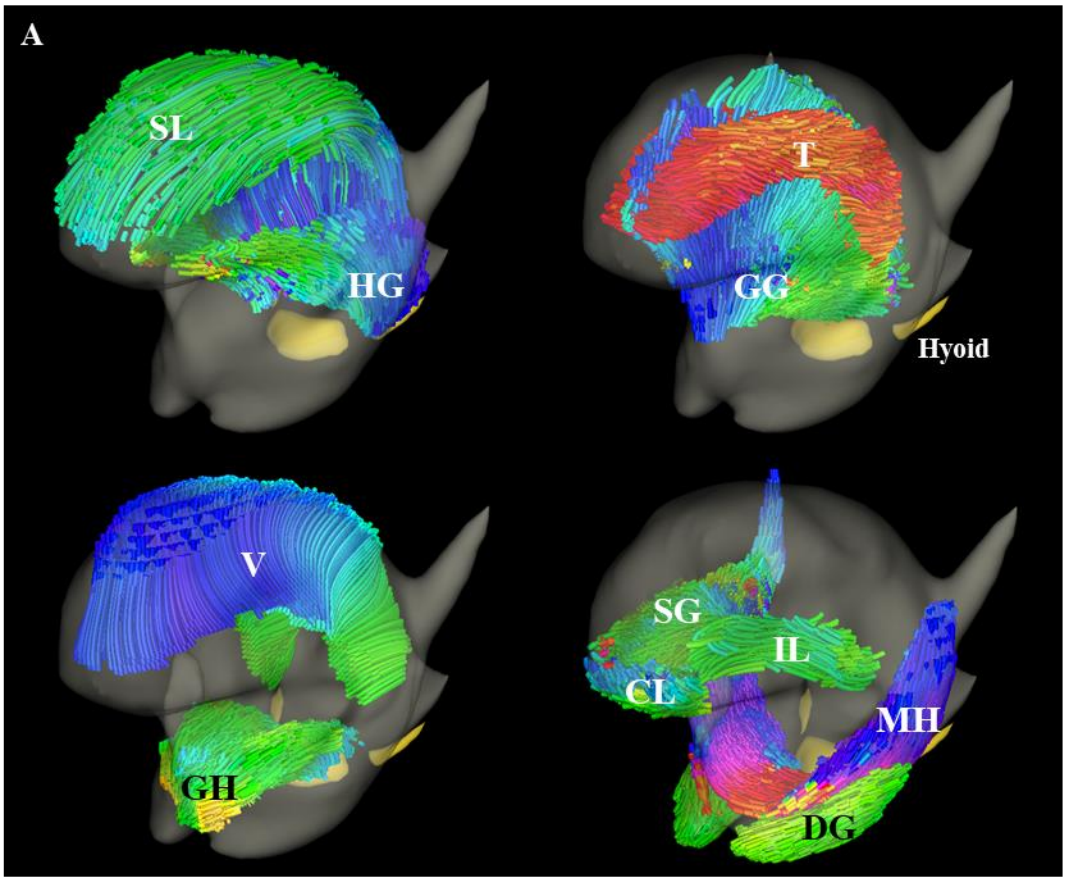
A
SL
HG
T
GG
Hyoid
V
GH
SG
IL
CL
MH
DG

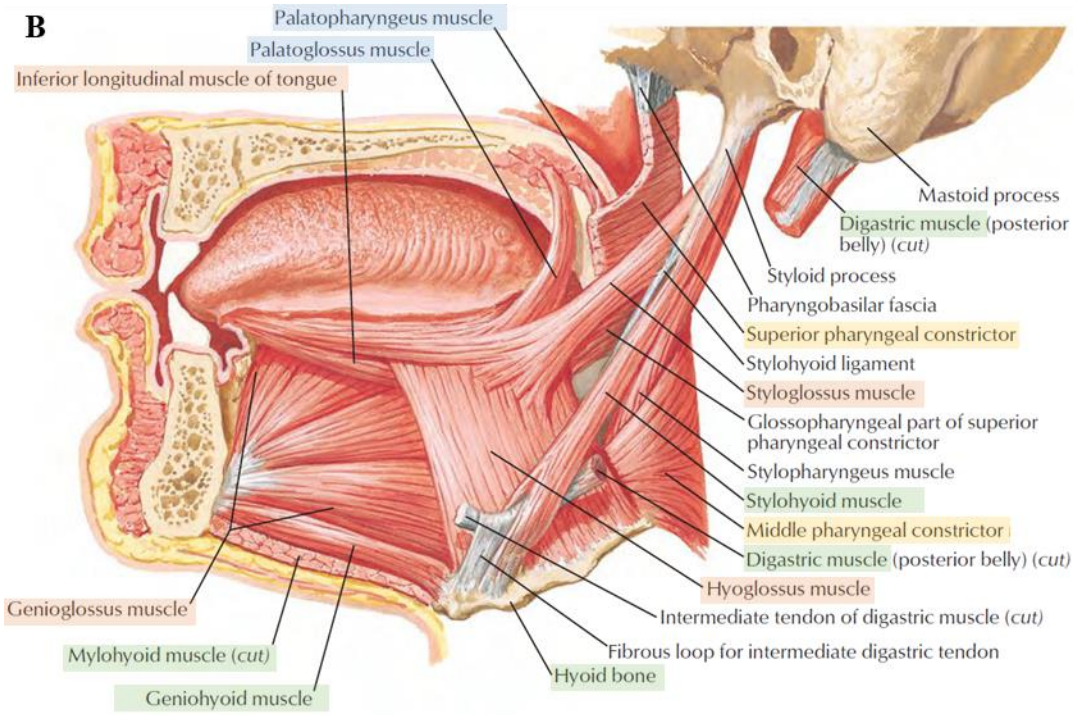
B
Palatopharyngeus muscle
Palatoglossus muscle
Inferior longitudinal muscle of tongue
Mastoid process
Digastric muscle (posterior belly) (cut)
Styloid process
Pharyngobasilar fascia
Superior pharyngeal constrictor
Stylohyoid ligament
Styloglossus muscle
Glossopharyngeal part of superior pharyngeal constrictor
Stylopharyngeus muscle
Stylohyoid muscle
Middle pharyngeal constrictor
Digastric muscle (posterior belly) (cut)
Hyoglossus muscle
Intermediate tendon of digastric muscle (cut)
Fibrous loop for intermediate digastric tendon
Hyoid bone
Genioglossus muscle
Mylohyoid muscle (cut)
Geniohyoid muscle

Figure 1-2 | Muscles of the human tongue and upper airway. (A) Muscles of the human tongue and upper airway have highly complex and interwoven fibres; superior longitudinal (SL), hyoglossus (HG), transverse (T), genioglossus (GG), vertical (V), geniohyoid (GH), styloglossus (SG), inferior longitudinal (IL), mylohyoid (MH), digastric (DG), combined longitudinal (CL – where IL, HG and SG merge) (R. Lloyd, unpublished). **(B)** Several upper airway muscles control the tongue position (orange highlight), the soft palate position (blue highlight), the hyoid position (green highlight) and the posterior pharyngeal walls (yellow highlight) [38]. During inspiration, they collectively maintain upper airway patency.

The genioglossus is the largest and most studied muscle in the human tongue and the upper airway (Figure 1-2)[31, 39-41]. Genioglossus fascicles originate at the midline of the inner mandible and fan out in a 90° arc. The muscle is divided into two neuromuscular compartments separated by a thin layer of connective tissue. The horizontal genioglossus is located inferiorly and its fascicles course posteriorly from the mandible to insert into the hyoid bone or the connective tissue above [26, 30]. The oblique compartment has muscle fascicles fanning out from the mandible, extending through the bulk of the tongue and inserting into the dorsum, with fascicles at the centre of the tongue passing between transverse and superior longitudinal muscle fascicles [26, 30]. The fascicles that insert into the posterior dorsum, like those of the horizontal compartment, contribute to tongue protrusion by drawing the posterior tongue anteriorly during inspiration [42-44]. The more vertically oriented fibres may induce tongue depression, the more anterior fibres may contribute to ventroflexion and tongue tip retrusion, and the fascicles that insert into the midline of the dorsum midline may contribute to creating a concave superior tongue surface, a feature essential for speech and swallowing [26, 35].

The styloglossus (Figure 1-2) is the most lateral tongue muscle, and originates at the styloid process of the temporal bone, descends anteriorly, and inserts into the tongue's side. Separate bundles of fascicles pass through or merge with other longitudinally oriented muscles, including the hyoglossus and inferior longitudinal [26, 45]. The hyoglossus (Figure 1-2) originates at the hyoid bone, inserts into the posterior tongue, and is bordered by the genioglossus and inferior longitudinal muscles medially and the stylogossus laterally. In different tongue regions, the hyoglossus appears continuous with and virtually indistinguishable from the styloglossus, the transverse and genioglossus muscles [26, 45]. The styloglossus and hyoglossus contribute to tongue retrusion and elevation or depression, respectively [26]. At least three smaller extrinsic muscles also insert into the tongue; the palatoglossus (which also contributes to soft palate position, described below), glossopharyngeus and chondroglossus. These are not thought to contribute significantly to tongue movement and are often not included in tongue models [26].

Intrinsic tongue muscles are widely thought to contribute to tongue shape rather than position. This contrasts with the muscular hydrostat theory, which supports the constant interaction of intrinsic and extrinsic muscles in all tongue movements [34]. Moreover, there is increasing

evidence for their respiratory-modulated activation under certain stimuli [32, 46]. The superior longitudinal muscle, the only unpaired muscle, sits below the superior dorsum, spans the length of the tongue, and is well-defined by a thin layer of connective tissue (Figure 1-2). It appears as a 'muscular sheet' of longitudinally and obliquely oriented fascicles, through which vertically oriented fascicles of other muscles pass to terminate at the dorsum [26, 47]. The paired inferior longitudinal similarly spans the length of the tongue (Figure 1-2). It originates near the tongue base, travels anteriorly with other longitudinally oriented muscles (e.g. genioglossus, hyoglossus and styloglossus), and ascends to the tongue apex [26, 47]. Like the genioglossus, the inferior longitudinal muscle is divided into two compartments arranged in parallel (lateral and medial)[30]. Contractions of both longitudinal muscles contribute to tongue shortening. The superior longitudinal additionally contribute to tongue tip curling (dorsiflexion), and the inferior contributes to retroflexion of the tongue base [26].

The transverse muscle originates at the median septum and courses laterally, inserting into the connective tissue overlying the longitudinally oriented muscles (Figure 1-2). The vertical muscle fascicles originate at this connective tissue and extend almost vertically, intersecting the transverse fascicles and terminating at the dorsum (Figure 1-2). Vertical muscle fascicles can appear as a continuation of the genioglossus in the medial third of the tongue. The transverse and vertical muscles contribute to tongue narrowing and flattening, elongating the tongue [26, 47].

1.1.1.2 Palatal muscles

The soft palate is a flap of muscular tissue attached to the posterior region of the hard palate. The palatal muscles control the channel between the oral cavity and the nasopharynx and determine the route of respiration (oral versus nasal) [48]. Despite the importance of the soft palate, the exact movements and the roles of the muscles in performing these movements remains poorly understood [21].

The position of the soft palate is determined by five paired muscles, the levator veli palatini, tensor veli palatini, palatoglossus, palatopharyngeus, and musculus uvula. All palatal muscles attach to the palatine aponeurosis, a thin, firm and fibrous lamella that supports the muscles and provides strength to the soft palate. The levator veli palatini (a thick rounded muscle) and the tensor veli palatini (a broad, thin muscle) originate at the temporal and sphenoid bones, respectively. During oral breathing, levator veli palatini contractions produce soft palate elevation and nasopharynx constriction [49]. In contrast, tensor veli palatini contractions stiffen the soft palate and facilitate nasal ventilation [49, 50].

The paired palatoglossus muscles (Figure 1-2B, also an extrinsic tongue muscle) appear continuous and form the palatoglossal arch. From the palatine aponeurosis, the muscles descend anteriorly, insert into the side of the tongue, and the myofibres spread over the dorsum or intertwine with transverse muscle fibres. Similarly, the palatopharyngeus forms the palatopharyngeal arch, descends posterolaterally down the pharyngeal wall, and terminates at the thyroid cartilage. During nasal breathing, contractions of both muscles pull the soft palate inferiorly, occluding the oropharynx and opening the nasopharynx [21, 49, 51]. The palatoglossus also contributes to tongue elevation and pulls it posteriorly, and the palatopharyngeus potentially contributes to pharyngeal wall elevation [21]. Finally, the musculus uvulae form the bulk of the uvula, and contractions result in uvular broadening and shortening [21].

1.1.1.3 Hyoid muscles

The hyoid bone is horse-shoe shaped, is located at the midline of the anterior neck and, unlike other bones, is solely anchored by muscles (Figure 1-2). The hyoid bone is vital to several physiological functions, including breathing, swallowing and sleep, and provides attachment sites for the muscles that form the floor of the mouth, the tongue, the larynx, the epiglottis and the pharynx. Seven paired muscles, i.e. the geniohyoid, mylohyoid, stylohyoid, digastric, thyrohyoid, sternohyoid, and omohyoid, attach to and control the position of the hyoid bone. During inspiration, these muscles aim to pull the hyoid anteriorly and caudally to dilate the airway [21].

The mylohyoid and geniohyoid run between the hyoid bone and the mandible. The mylohyoid is a thin, flat muscle that forms the oral cavity floor, and the geniohyoid is more medial and sits between the genioglossus and mylohyoid (Figure 1-2). The digastric muscle has two independent muscular bellies that connect to the hyoid bone via an intermediate tendon and its fibrous sling (Figure 1-2). The anterior belly connects to the mandible, and the posterior connects to the mastoid process of the temporal bone. The contraction of these three muscles elevates the hyoid. The digastric and geniohyoid also contribute to the mandible depression, and the mylohyoid elevates the floor of the mouth [21].

The stylohyoid is a thin muscle that sits superior and anterior to the posterior digastric and runs between the hyoid and the styloid process of the temporal bones (Figure 1-2B). Stylohyoid contraction pulls the hyoid posteriorly and superiorly for the initiation of swallowing [21].

Finally, the thyrohyoid, sternohyoid and omohyoid are inferior to the hyoid and run between the hyoid and the thyroid cartilage, sternum and scapula, respectively. The omohyoid, like the

digastric, has two bellies, a superior and an inferior, separated by an intermediate tendon. The superior belly, along with the sternohyoid and the thyrohyoid, predominantly depresses the hyoid bone and, like the stylohyoid, plays an active role in swallowing [21].

1.1.1.4 Pharyngeal muscles

Three circularly oriented muscles, the superior, middle and inferior pharyngeal constrictors, form a 'muscular sleeve', known as the outer posterior pharyngeal wall. The pharyngeal raphe, a fibrous band that runs down the posterior wall, provides attachments and separates pairs of constrictor muscles. However, significant individual variation is seen [52]. The superior constrictor (Figure 1-2C) originates at the pterygoid hamulus, the pterygomandibular raphe and the posterior end of the mandible mylohyoid line and inserts into the pharyngeal tubercle as well as the pharyngeal raphe. The middle constrictor (Figure 1-2C) originates at the stylohyoid ligament, and the greater and lesser horns of the hyoid bone and the inferior pharyngeal constrictor is composed of two parts that originate at the thyroid cartilage and the cricoid cartilage [53].

Fibres of the three pharyngeal constrictors blend and sometimes link to adjacent muscles [54]. Sequential contractions of the pharyngeal constrictors (superior to inferior) convey food bolus downwards from the oral cavity to the oesophagus during and after swallowing. In addition to bolus shifting, the pharyngeal constrictors may contribute to the prevention of pharyngeal collapse by increasing the rigidity of the pharyngeal tube [55]. As the middle pharyngeal constrictor attaches to the hyoid, it contributes to hyoid elevation [53].

1.1.2 Neural control

All tongue muscles, excluding the palatoglossus, are innervated by the hypoglossal nerve. This is a largely motor nerve that originates at the hypoglossal nucleus in the ventral portion of the medulla. Retrograde labelling studies have reported somatotopic organisation of motor neurons within the hypoglossal motor nucleus, reflecting the anatomical and functional organisation of tongue muscles in rodents [56-58] and non-human primates [59]. Hypoglossal axons then travel caudally and dorsally towards the tongue. Upon initial entry at the ventrolateral aspect of the posterior tongue, the hypoglossal nerve projects its first branch to the geniohyoid. It then projects multiple lateral branches directly (Figure 1-3A) or via a short main trunk, which go on to innervate longitudinally oriented muscle fibres that form the 'cover layer' of the tongue, i.e. the styloglossus, hyoglossus, superior longitudinal and the lateral belly of the inferior longitudinal [30, 56, 60]. After the lateral branches, the remaining medial hypoglossal nerve continues anteriorly before splitting into branches that innervate the tongue's 'core', i.e. the genioglossus, the transverse and vertical muscles, and the medial belly of the inferior

longitudinal [30, 56, 60]. The only tongue muscle not innervated by the hypoglossal nerve is the palatoglossus, which receives neural inputs from the superior branches of the glossopharyngeal and vagus nerves [25]. The inferior and superior longitudinal muscles receive additional innervation from the lingual nerve [30].

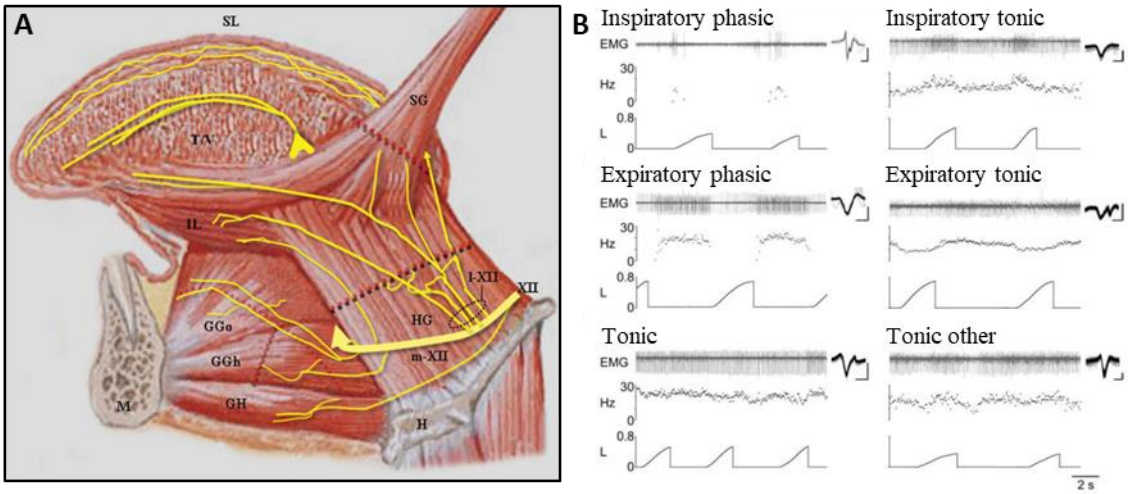

Figure 1-3 | Neural innervation and drive to the tongue. (A) The hypoglossal motor neuron (XII) divides into lateral branches (l-XII) to innervate the styloglossus (SG), the superior longitudinal (SL), medial region of the inferior longitudinal (IL) muscles of the tongue. The following medial branches (m-XII) innervate the oblique and horizontal compartments of the genioglossus (GGo, GGh), the transverse and vertical (T/V), and the lateral IL muscles [30]. **(B)** The genioglossus receives six unique motor unit discharge patterns during quiet breathing, indicated by the raw electromyography, instantaneous discharge frequency plot and inspired volume plots [31].

As noted, most research investigating respiratory modulation of the upper airway muscles focuses on the genioglossus. EMG recordings typically indicate that genioglossus muscle fibres are recruited phasically immediately before and during inspiration to counteract intraluminal negative pressures and are tonically recruited during expiration to maintain tongue position [61-63]. Single motor unit studies suggest greater complexity, reporting up to six distinct motor unit discharge patterns (Figure 1-3B). In a study of 110 genioglossus units, only 39.1% displayed phasic inspiratory activity. 11.8% of the motor units exhibited inspiratory tonic activity (continuous firing with increases during inspiration), 4.5% displayed expiratory phasic activity, 10.9% displayed expiratory tonic activity and 29.1% displayed tonic activity with no respiratory modulation evident. The remaining 4.5% were classified as ‘tonic other’, indicating that variation in firing rate was observed but was unrelated to respiration [31]. These proportions vary somewhat between studies (e.g. [39, 64, 65]), but the existence of 6 patterns and the dominance of inspiratory-related activity (phasic and tonic) is consistent. With sleep onset, approximately 50% of genioglossus inspiratory units (phasic and tonic) cease activity, and those that continue firing exhibit significant reductions. In contrast, tonic and expiratory units remain

relatively unchanged [39]. Motor units have also been reported to shift between firing pattern 'types'. Motor units that displayed tonic inspiratory firing patterns during wakefulness shifted to phasic inspiratory firing patterns with sleep onset, whereas tonic units exhibited an increase in drive [40]. The opposite shifts occur with arousal from sleep; phasic inspiratory units return to tonic inspiratory patterns, and drive to tonic units declines [40]. Neural drive to the genioglossus also varies with changes in sleep stage, with the lowest activity recorded during REM sleep [66], and the onset of hypercapnia and hypoxia [61, 67]. There is also evidence of differing drive to the two genioglossus compartments (oblique and horizontal) during specific tasks [41].

The profound interweaving of tongue muscles makes it technically challenging to identify and isolate intrinsic and non-genioglossus extrinsic tongue muscles. As a result, few studies investigate neural drive via EMG recording and muscle function is often extrapolated from anatomical arrangement and/or animal research. Other extrinsic muscles, such as the hyoglossus and styloglossus, have shown similar elevations in activity during inspiration [32, 60, 68] whereas intrinsic muscles are often inactive during quiet breathing [32]. During hypercapnia, drive increases to the muscles, and both extrinsic and intrinsic muscles are phasically active [32, 69]. Extrinsic and intrinsic muscles can have different activity patterns during tasks. With increasing force generated during an impeded tongue protrusion, drive to the intrinsic muscles proportionally increased whereas drive to the genioglossus remained constant, suggesting that the intrinsic muscles play a greater role in generating protrusional forces [70]. Interestingly, in rodents, retractor muscles (hyoglossus and styloglossus) generate up to ten times more force than the genioglossus [69]. Electrical stimulation studies have reported that co-activation can produce either a net retraction force [69, 71] or greater airway dilation, pharyngeal stiffening, and/or airflow than achieved following the stimulation of a single muscle group (intrinsic/extrinsic or protrudors/retractors) [37, 60, 72].

Excluding the tensor palatini, which is innervated by the trigeminal nerve, all palatal muscles are innervated by the pharyngeal branch of the vagus nerve. Only a few studies have targeted these muscles. The tensor palatini has shown a similar range of single motor unit types as reported in the genioglossus but has a greater proportion of expiratory units (18% inspiratory phasic, 25% inspiratory tonic, 21% expiratory phasic, 7% expiratory tonic, and 29% tonic units). With sleep onset, significant expiratory and inspiratory motor unit de-recruitment occurs, with expiratory phasic motor units virtually silenced. Conversely, tonic units (with no respiratory modulation) receive constant drive [73]. Unlike the genioglossus, sleep stage dependence is not evident [66]. The palatoglossus and levator veli palatini muscles alter their activity with 'route of respiration'. Palatoglossus activity is strong during nasal breathing

(inspiratory phasic dominant), drawing the soft palate inferiorly to occlude the oropharynx and open the nasopharynx. This activity is silenced when breathing shifts to oral [49], with 78% fewer inspiratory phasic and 58% fewer inspiratory tonic motor units active. In contrast, the levator palatini displays greater activity during oral breathing to elevate the soft palate, and constrict the nasopharynx [49]. However, this activity is typically inconsistently present [74], and patterns vary between individuals (inspiratory phasic versus expiratory phasic) [49].

The geniohyoid is innervated by the first hypoglossal motor nerve branches, and reports of respiratory modulation during quiet breathing vary. Typically it is reported to have strong inspiratory phasic activity during wakefulness, and the phasically active motor units remain relatively constant with sleep onset, whereas tonically active units decline in activity [75, 76]. In contrast, other studies have found that the geniohyoid displays predominantly tonic activity and minimal respiratory-modulated, leading to the conclusion that the geniohyoid may not play an active role in maintaining airway stability during quiet breathing [77].

Pharyngeal constrictors receive combined contributions from the glossopharyngeal and vagal nerves via the pharyngeal plexus [53, 54]. They have been reported to have two distinct and specialised layers of fibres, a slow twitch inner layer and a fast twitch outer layer, that receive independent innervation from the glossopharyngeal and vagal nerves, respectively [53]. Sustained contraction of pharyngeal constrictors, particularly the slow inner layer, which appears to be unique to ‘normal’ adult humans, is thought to produce pharyngeal wall stiffening during respiration and shape the walls for speech. Conversely, the fast inner layer may play a role during swallowing [53]. In general, the three constrictors display similar patterns of activation. They display respiratory modulation during wakefulness [74, 78] and are activated to generate specific sounds and to swallow [78, 79]. The superior pharyngeal constrictor displays inconsistent expiratory phasic activation, and high inter- and intra-subject variability are reported [74]. Activity is typically absent during NREM sleep and sporadic with no respiratory modulation during REM sleep [78, 80].

Besides the genioglossus and perhaps the tensor palatini, limited conclusive data is available on the activation of upper airway muscles during quiet breathing. Generally, while these muscles display different activation patterns, they seem to have similar single motor unit types (expiratory and inspiratory tonic and phasic, or tonic without respiratory modulation), and the primary differences are in the proportion of these different motor units present in each muscle. The upper airway muscles also seem to respond to stimuli in similar ways, i.e. the onset of sleep seems to produce a universal reduction of overall muscle activity; however, how each muscle achieves those global changes may differ.

1.1.3 Rodent upper airway

Rodents make up approximately 95% of all laboratory animals. Their appeal stems from their size, which facilitates accessible housing and maintenance, their short reproductive cycle and lifespan, the ease of genetic manipulation and their genetic similarities to humans [81]. Their popularity extends to investigations into the upper airway, despite the significant size and postural differences. While humans have a curved tongue and a flexed pharynx (the nasopharynx turns ~ 90°), the rodent tongue is comparatively flat, and the nasopharynx comparatively straight, flexing only ~ 15° [20, 30]. Due to the olfactory dominance in rodents, they have significantly more complex nasal passages [20, 82], and like all non-human mammals, they have a high larynx with the epiglottis overlapping the soft palate. Consequently, rodents are almost exclusively nasal breathers, and the connection between the soft palate and epiglottis is only broken for vocalization and swallowing large boluses of food [83]. In humans, where breathing is the dominant function of the nasal passages, the region is comparatively simple, and more space between the epiglottis and soft palate allows both nasal and oral breathing [20, 82].

Despite these gross differences, tongue musculature, neural innervation, and mechanical actions are remarkably well conserved, and general structures are consistent across species. Eight muscles divide into two structural groups; extrinsic muscles originating on bony structures (genioglossus, hyoglossus, styloglossus and palatoglossus) and intrinsic muscles contained within the tongue (superior and inferior longitudinal, transverse and vertical). In both species, muscle fibres attributed to different muscles extensively intertwine within the tongue, and the muscles are loosely classified as protrudors or retractors [26, 84, 85], with co-activation stiffening and dilating the pharynx [36, 86]. Innervation is relatively conserved across species with the medial and lateral branches of the hypoglossal motor nerve supplying all muscles [30, 85], and drive increases with hypercapnia, hypoxia [36, 67] and arousal from sleep [39, 40, 87]. Finally, both species display evidence of neuromuscular compartments, particularly within the genioglossus [26, 56].

Despite these similarities, human tongue musculature and innervation are more complex. Human neural innervation is more dense, the muscles have more variable motor end plate morphologies, and there is a greater prevalence of neuromuscular compartmentalisation (in humans, compartmentalisation is present in the genioglossus, superior and inferior longitudinal, and transverse and vertical muscles) [30]. In rodents, the hypoglossal motor nerve divides into a single medial and lateral branch before dividing further to innervate the muscles [85]. Conversely, in humans, the hypoglossal nerve has approximately 50 to 60 primary nerve

branches along the length of the tongue [30]. While in both species, the medial hypoglossal nerve supplies the genioglossus, transverse and vertical muscles, and the lateral supplies the styloglossus and hyoglossus muscles, differences arise with the innervation of the superior and inferior intrinsic muscles [30, 85]. In rodents, both are supplied by the lateral branch [85]. In contrast, human inferior longitudinal muscles receive inputs from both the medial and lateral branches (to the medial and lateral compartments of the inferior longitudinal muscle, respectively), and the superior longitudinal muscles receive input from lateral branches [30]. Both receive additional input from the lingual nerve [30]. Finally, the human transverse and vertical muscles are much larger, and innervation is more dense and complex than in other mammalian tongues [26, 30, 84, 85]. Notably, many differences between human and rodent tongues are associated with the general complexity and the intrinsic muscles that are thought to be primarily responsible for tongue shape and speech [88].

1.1.4 Characterising upper airway function

In order to demonstrate the efficacy of the novel therapy for OSA proposed in this thesis, an appropriate method of quantifying upper airway function must be used. Feasible methods include pharyngeal critical closing pressure (Pcrit), electromyography (EMG), magnetic resonance imaging (MRI) and ultrasound imaging. Each modality has its own pros and cons and has utility in different applications.

1.1.4.1 Pharyngeal critical closing pressure

The ‘gold standard’ for quantifying upper airway collapsibility is the pharyngeal critical closing pressure (Pcrit) approach. In humans, Pcrit is determined during sleep and requires a continuous positive airway pressure (CPAP) device, more commonly used as a treatment for OSA. The device applies multiple brief pressure reductions to the airway for at least five breaths to induce airflow limitations and/or airway collapse. A pressure-flow relationship is calculated via linear regression, and the pressure at which zero airflow occurs is referred to as the Pcrit value [66, 89, 90]. A negative Pcrit indicates the airway remains open even when negative pressures are applied, and a positive Pcrit indicates the airway opens only when positive airway pressures are applied. In other words, during sleep, individuals with a high Pcrit (values > 0–2 cmH_2O) have collapsible airways, and their muscles struggle to counter inspiratory-related negative pressures [10, 11]. While this is an effective method of quantifying upper airway collapsibility, the technique is invasive, labour-intensive and time-consuming. Consequently, alternatives have been proposed, including a comparatively simple ‘upper airway collapsibility index’ test conducted during wakefulness [91].

Pcrit is also quantified in animals, and animals with high Pcrit values have been used as models for obstructive sleep apnoea [92]. As in human studies, Pcrit measurements require invasive instrumentation, including the implantation of cannulas via trachea incision and head-out plethysmographs, and often end with animal euthanasia [92, 93].

1.1.4.2 Electromyography

EMG signals measure the electrical activity in a muscle during a mechanical action. It is a complex signal generated by the innervating neuron(s) and depends on the muscle's anatomical and physiological characteristics. EMG recordings obtained via surface electrodes are composites of the action potentials generated in all motor units lying beneath. In contrast, EMG signals obtained via wire or needle electrodes inserted directly in the muscle are more localised and can be readily decomposed into single motor unit action potentials [31, 73, 77]. Single motor unit action potentials' shapes and firing rates can improve understanding of muscle control and neuromuscular disorders. EMG signals have elucidated the highly coordinated neural control of upper airway muscles throughout the respiratory cycle [31, 73, 77] and during speech, swallowing, and mastication [79]. They have also been used to describe how the drive to these muscles varies with task [41], and how the loss of drive or deviations from the synchronised activation patterns can lead to disorders such as dysphagia [94], dysarthria [27], dysphasia [28], and OSA [11]. Finally, EMG signals have been used to provide evidence for muscle stimulation therapies for disorders associated with upper airway dysfunction [16, 86].

The use of EMG as an indicator of muscle contraction can be challenged as EMG reflects neural inputs rather than mechanical output and local activity at the EMG electrode location rather than global activity. In the upper airway, this is compounded by the anatomical complexity of the muscles [26, 84], as electrical activity recorded may not always correspond predictably to muscle movement.

1.1.4.3 Magnetic resonance imaging

MRI is a non-invasive imaging technology that can produce static and dynamic, two-dimensional and three-dimensional images. Briefly, powerful magnetic fields within the bore of the scanner force randomly oriented paramagnetic atoms (typically hydrogen atoms or ‘protons’) into alignment. A rapidly repeating series of radiofrequency pulses then cause ‘excitation’ and ‘resonance’ of the protons. When a pulse dissipates, the protons relax and return to realign with the magnetic field. During realignment, a radiofrequency signal is detected and transformed into an image dependent on the tissue type-specific resonance characteristics.

Two MRI protocols are typically used to quantify upper airway muscle function and airway dilation in humans and rodents; mDixon and Tagged MRI sequences. mDixon protocols produce high-contrast, static anatomical images for fat quantification and fat suppression by exploiting the different resonance frequencies of fat and water in a homogeneous magnetic field. In a gradient echo sequence, transverse magnetisation of fat and water particles begins immediately after MR-induced proton excitation. At this time, soft tissue fat and water components are 'in phase'. Due to their different resonance frequencies, dephasing occurs at different rates and depending on the type of scanner (i.e. magnet strength measured in Tesla), they will be 'out of phase' (in opposition at 180°) at a precise time following initial excitation. In Dixon protocols, images are acquired during the 'in-phase' and 'out-of-phase' conditions, so 'water only' images can be obtained via image summation, and 'fat only' images can be obtained via image subtraction. Water-only images can be used for 'fat suppression', i.e. reducing fat signals that can be intense in other MR sequences causing exaggerated motion artefacts and reducing lesion visibility [95, 96]. In the upper airway, Dixon protocols have been used to quantify intramuscular tongue fat in obese and non-obese rats [97] and explore the link between tongue fat, airway dilation and obstructive sleep apnoea in humans [98, 99].

Dynamic images of the upper airway can be obtained via tagged MRI (also known as Spatial Modulation of Magnetization, SPAMM), which uses a series of radio frequency and magnetic field gradient pulses to generate an evenly spaced grid of dark lines or 'tags' on the targeted tissue. These tags distort with tissue movement, and the resulting image series can be analysed using the deforming grid lines as fiducial markers [100-102]. Tagged MR imaging has been used extensively in the upper airway, aiding our understanding of upper airway biomechanics in rats [97, 100, 103, 104] and humans [99, 105, 106], predicting treatment outcomes of mandibular advancement splints in OSA patients [107-109] and quantifying tongue movement during phonation [110, 111].

1.1.4.4 Ultrasound imaging

Like MR imaging, ultrasound is a non-invasive imaging technology that can produce static and dynamic two-dimensional and three-dimensional images. Briefly, a transducer emits pulses of ultrasound that propagate into the body. These pulses are scattered and reflected when they encounter inhomogeneous tissue or impedance jumps at the transition between two tissue types or structures. These events create returning waves or 'echoes' with different amplitudes and transit times, which are converted into 'points of brightness' on an image. The high speed at which echoes return and the complete image frames are created means that real-time motion is captured. Ultrasound presents several advantages over other medical imaging modalities. In

addition to providing ‘real-time’ images, ultrasound is comparatively low-cost, does not use harmful ionising radiation, and requires minimal technical knowledge.

Ultrasound imaging has been used in human upper airways to quantify airway dilation and tongue movement in OSA patients and healthy controls [43, 112]. It is at least as effective as MRI for quantifying inspiratory tongue movement [43]. Ultrasound has not been used in rodent upper airways but has been extensively used to quantify muscle contractions in other skeletal [113] and cardiac muscle applications [114].

1.2 OBSTRUCTIVE SLEEP APNOEA

Obstructive sleep apnoea (OSA) is a chronic sleep-related breathing disorder characterised by repeated airway narrowing and/or collapse during sleep. A 2019 literature-based analysis estimated that nearly 1 billion people worldwide between 30 to 69 years have OSA, equating to approximately 14% of the population [1]. In the same demographic range in Australia, it was estimated that 24.5% had OSA. However, in other countries, OSA prevalence exceeded 50%. OSA is almost twice as prevalent in males (25% vs 13% in females), and over three times more prevalent in individuals over 50 years old (39% vs 12% in those under 50 years) [1]. As increased weight also dramatically increases the risk of OSA (a 10% increase in weight gain predicts a 32% worsening of OSA severity [4]), the prevalence of the disease continues to rise in our increasingly overweight and aging population. Between 2019 and 2020, the overall costs of OSA in Australia were approximately $US13.1 billion, including health system costs, productivity losses, and non-financial costs associated with loss of well-being [115].

OSA severity is defined by the average number of times the upper airway partially (hypopnea) or completely (apnoea) collapses per hour of sleep, as classified in accordance with SaO2 and levels of desaturation. This measure is referred to as the apnoea-hypopnoea index (AHI) and is most accurately obtained during in-lab polysomnography (PSG) however, support for multi-night in-home PSGs is increasing [116]. An AHI between 5 to 15 events per hour is classified as mild OSA, 15 to 30 events as moderate OSA, and more than 30 events as severe OSA [117]. The acute effects of apnoea and hypopnoea events include reductions or cessations of airflow during sleep, intermittent hypoxia, fragmented sleep and exaggerated fluctuations in cardiovascular measures, including heart rhythm and blood pressure. During wakefulness, OSA patients often experience fatigue, poor concentration and irritability [2] and are at greater risk of workplace and motor vehicle accidents [118]. OSA is associated with significant long-term concerns such as hypertension and cardiovascular morbidities (e.g. stroke and heart failure) [3, 119-121], reductions in mood and quality of life [122, 123], increased prevalence of

neurodegenerative disorders (dementia, vascular dementia and Alzheimer's disease) [124, 125] and premature mortality [126, 127].

1.2.1 Pathophysiology

Understanding the multifactorial pathogenesis of upper airway collapse and OSA, as well as the heterogeneous OSA patient population, is essential for treating OSA [10]. Many sleep clinicians and researchers endorse a 'personalised medicine' approach, considering each 'phenotypic trait' of OSA pathogenesis a potential therapeutic target [10, 128]. Respiratory and sleep phenotyping studies have divided pathophysiological contributors to OSA into anatomical and non-anatomical traits.

Some degree of upper airway anatomical or structural impairment is a prerequisite for pharyngeal collapse and OSA pathogenesis [10]. Compared to control subjects, OSA patients typically have a longer and narrower pharynx [129, 130], greater volumes of and/or fat accumulation in upper airway soft tissues, and subsequently, a narrow or crowded airway [35, 98, 130-132] with a greater propensity for collapse. Caudally located hyoid bones [133], greater neck circumferences to height ratio [134], and some craniofacial morphologies [133, 135], such as increased anterior facial heights [133] and reduced mandible length and depth in males [136], are also associated with greater OSA risk and severity.

Approximately 70% of OSA patients present with one or more non-anatomical contributors to OSA pathogenesis. 36% of patients are reported to have impaired pharyngeal dilator muscle function, where negative airway pressures stimulate inadequate levels of neural drive to the upper airway muscles during sleep [10]. Individuals with anatomically compromised airways that would otherwise predispose them to OSA can be 'protected' by robust muscle responsiveness [137, 138]. Similarly, neuromuscular compensation is present in OSA patients during wakefulness [63]. 30 to 50% of patients have low arousal thresholds [10, 21, 139, 140], where only mild airway narrowing and small changes in intrathoracic pressures stimulate arousal from sleep. Low arousal thresholds can produce recurrent shifts between wakefulness and sleep and prevent adequate muscle recruitment and stable sleep [66, 139, 141, 142]. Low arousal thresholds are particularly prevalent in non-obese OSA patients (> 86%) [143]. Finally, 36% of patients display oversensitive ventilatory control systems or 'high loop gain' [10]. During sleep, afferent feedback from chemoreceptors tightly regulates ventilation, and the ratio of ventilatory response to ventilatory disturbance is known as 'loop gain'. High loop gain indicates respiratory control instability, where the system induces excessive responses to small changes in CO_2, resulting in hypocapnia, reductions in respiratory drive, and a diminished

ability to prevent obstruction and/or reopen the airway post-obstruction, thus perpetuating recurring upper airway collapse [10, 90, 142, 144].

1.2.2 OSA treatments

Numerous OSA treatments are currently clinically available. Traditionally, they have targeted anatomical contributors to OSA; however, increased research into non-anatomical contributors has spurred the development of other therapies targeting impaired pharyngeal muscle function, low arousal thresholds, and high loop gain have increased in prominence. As ~70% of patients have anatomical and non-anatomical contributors, combined therapies are also increasing. Therapies vary considerably concerning efficacy in reducing AHI, invasiveness and adherence to treatment. Due to the vast heterogeneity of the OSA population, no single treatment is effective for everyone.

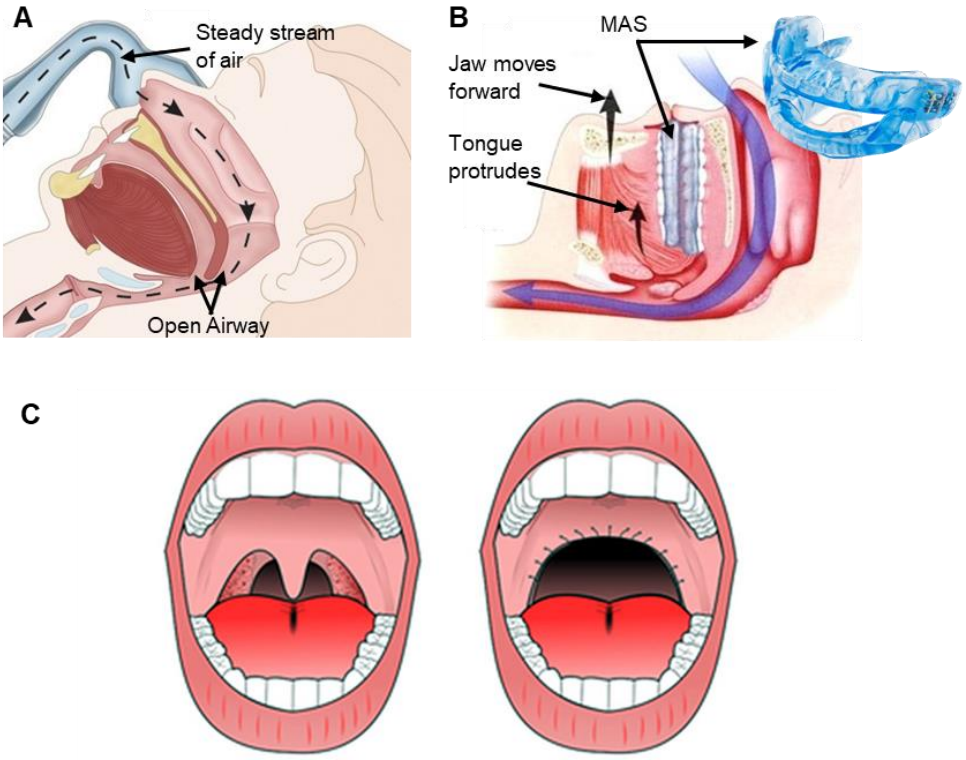

Figure 1-4 | Therapeutic options for obstructive sleep apnoea. (A) Continuous positive airway pressure devices, **(B)** mandibular advancement splints, and **(C)** upper airway surgeries, including uvulopalatopharyngoplasty

1.2.2.1 Continuous positive airway pressure

Continuous positive airway devices (CPAP) are considered the 'gold-standard' therapy for OSA. By delivering constant pressurised air via a facial or nasal mask (Figure 1-4A), CPAPs mechanically maintain airway patency. When appropriately used, CPAP can be highly efficacious in reducing sleep-disordered breathing. Moreover, CPAP improves blood pressure

[145] and quality of life measures [146-148] and reduces daytime OSA symptoms such as sleepiness and cognitive deficits [7] and the risk of motor vehicle accidents [149].

While CPAP devices should be used daily for the duration of a patient's sleep, practically, this occurs in the minority of patients, and most studies use ≥ 4 hours per night on 70% of nights as 'acceptable' compliance [2, 8]. Despite this low goal, over half of all patients are partially adherent or completely intolerant due to perceived invasiveness, claustrophobia and inconvenience [5, 8, 10]. As several studies have found dose-dependent relationships between clinical improvements and CPAP use [146-148], this is a major barrier to achieving clinically effective therapy. For instance, improvements in quality of life questionnaires, including the 'Epworth Sleepiness Scale', the 'Multiple Sleep Latency Test' and the 'Functional Outcomes associated with Sleepiness Questionnaire', were achieved when CPAP was used daily for 4, 6 and 7.5 hours, respectively [146]. Furthermore, 6 hours per night was required for memory function improvement [150], and 5.6 hours was required for blood pressure improvements [147]. Despite efforts to improve CPAP compliance, it remains a suboptimal therapy for a substantial proportion of people with OSA.

1.2.2.2 Mandibular advancement splints

Mandibular advancement splints (MAS) or oral appliances (Figure 1-4B) are a common second-line treatment for people with OSA who either refuse or cannot tolerate CPAP. They are designed to protrude the mandible and subsequently shift the tongue and soft palate anteriorly to increase the dimensions of the airway lumen. MASs are rapidly growing in use, particularly in patients with mild to moderate OSA [7, 145, 151]. Complete response rates to MAS (AHI < 5, MAS in situ) vary between 29% to 71% of participants in different studies, averaging 48% of all participants [152]. While MAS efficacy (as measured by PSG studies) is inferior and more variable than CPAP, particularly in those with severe OSA [7, 152-154], MAS achieved significantly greater compliance [7, 153, 154] and is comparable to CPAP for improvements in daytime sleepiness, quality of life [151], and blood pressure [145].

Despite ongoing research, predicting who will respond to a MAS remains difficult. Various combinations of phenotypic traits have had some success, with patients with mild anatomical compromise and low loop gain [155], and patients with mild non-anatomical traits (low loop gain, high arousal threshold, low response to arousal), moderate pharyngeal collapsibility, and weaker muscle compensation [89] associated with improved outcomes. Similarly, models using baseline PSG measures and patient characteristics have had some promising results. 74% prediction success was achieved using age, BMI, event depth, and 'pinching' in expiratory flow rate (palate prolapse and sudden nasopharyngeal blockage) [156]. These associations are

relatively weak and unreplicated, and decisions based solely on these factors are not recommended [152].

Finally, MAS use typically requires multiple dentist appointments for device fitting, has high costs and has been associated with mostly mild side effects including dental changes, pain and excess salivation [128].

1.2.2.3 Upper airway surgeries

Numerous upper airway surgeries are available to OSA patients, and the fundamental aim is to reduce anatomical obstructions in the nasal cavity and pharynx. Surgeries targeting nasal obstructions include septoplasty, tubinoplasty, and radiofrequency of turbinates. Surgeries for soft palate reduction include uvulopalatopharyngoplasty (UPPP, Figure 1-4C), tonsillectomy or adenoidectomy, and surgeries aiming to reduce the tongue base and/or achieve greater oropharyngeal lumen, include radiofrequency ablation of the posterior tongue, hyoid suspension, and maxillomandibular advancement (MMA).

While upper airway surgeries are curative for some, response to surgery is unpredictable, and many patients have residual OSA [157, 158]. Moreover, upper airway surgeries are contentious due to insufficient or inadequate research. Research predominantly consists of retrospective or single-centre case studies with small cohorts and limited demographics, excluding several at risk groups including the elderly, obese and those with comorbidities [157, 159, 160]. Low 'responder' classifications are common, i.e. a $\geq$ 50% AHI reduction, compared to a post-treatment AHI of $\leq$ 10 for studies exploring more conventional treatment options, including MAS and CPAP devices. Studies often lack standardisation of anatomical reference points, and have variations in pre-operative evaluations and post-operative follow-up [157, 159, 160]. Retrospective studies commonly group all standalone, staged and simultaneous multi-level surgeries together regardless of the ablated soft tissue [158]. A 'quality assessment' of studies investigating upper airway surgeries found that, based on study design and limitations, all were considered 'low' or 'very low' quality [157]. In a study considered one of the more rigorous trials, the SAMS (Sleep Apnea Multilevel Surgery) randomised clinical trial [159], surgeons explicitly trained to conduct the multi-level surgery (modified uvulopalatopharyngoplasty and minimally invasive tongue volume reduction) produced significantly greater AHI and ESS reductions than that achieved using 'medical management', i.e. advice on sleep positioning and weight loss. However, this study had a highly selective population, and only 26% of patients experienced a 'complete' or 'near complete' OSA resolution (i.e. AHI < 10) [159].

Despite this variation, there has been some success. Nasal surgery in patients with significant obstructions reduced therapeutic CPAP pressures and improved adherence [161]. MMA, i.e. the enlargement of the airway luminal area by surgically advancing the bones of the upper and lower jaw, has been indicated as a promising surgery for improving oximetric (including AHI) and quality of life measures [157, 160] and in a meta-analysis, MMA was found to reduce AHIs by 80 and 92%, resulting in a mean post-operative AHI of 7.7. In comparison, UPPP reduced AHIs by 23 to 42%, and post-op AHI remained elevated at 29.8 events/hour. Moreover, MMA studies reported fewer adverse events versus other surgeries, including UPPP, radiofrequency ablation, and other multi-level and multi-phased procedures [157]. Upper airway surgeries have improved cardiovascular measures (systolic and diastolic blood pressure) and reduced the need for antihypertensive medication [162], and have improved quality of life measures despite the absence of concurrent AHI improvements [163]

The success of surgery is commonly attributed to the reduction of anatomical obstruction, but is difficult to predict. Non-anatomical OSA traits have been proposed as contributors to and predictors of surgical success. While low loop gain has been associated with AHI reductions [164], muscle responsiveness has deteriorated post-surgery [165]. Conversely, other studies have found no changes in non-anatomical traits post-surgery and no predictive abilities [166]. Obesity has also been postulated as a predictor or contributor to post-operative outcomes; however, it too has been found ineffective [167]. Due to this inability to predict surgical outcomes, and surgery's invasive and irreversible nature, it is commonly considered a ‘salvage’ treatment for a restricted group of patients who have failed (due to poor efficacy or adherence) conventional OSA therapies, including CPAP and MAS devices [168].

1.2.2.4 Hypoglossal nerve stimulators

The hypoglossal nerve innervates all tongue muscles, excluding the palatoglossus. The medial branches innervate ‘protrudor’ muscles that comprise the ‘core’ of the tongue, i.e. the genioglossus, posterior transverse and vertical muscles, and medial inferior longitudinal muscles. The lateral branches innervate ‘retractors’ that form the ‘cover layer’ of the tongue, i.e. the superior longitudinal, styloglossus, hyoglossus and lateral inferior longitudinal muscles [30, 33, 85]. Impaired muscle function is considered a primary contributor to OSA pathogenesis [10, 11], and conversely, robust muscle responsiveness can ‘protect’ individuals with anatomically compromised airways that would otherwise predispose them to OSA [137, 138]. Finally, activation of protrudor muscles, or co-activation of protrudor and retractor muscles, have improved upper airway flow mechanics in rodent research [36, 37], and electrical stimulation of

the medial branch (e.g. Inspire Medical, Figure 1-5A) or main trunk of the hypoglossal nerve (e.g. aura6000, LivaNova, Figure 1-5C) have been developed as OSA therapies.

The U.S. Food and Drug Administration (FDA) approved the first hypoglossal nerve stimulator in 2014 (Figure 1-5A). This device, by Inspire Medical, remains the only clinically available one; however, two others are undergoing clinical trials. The Inspire device consists of three surgically implanted components and a remote control. The device detects respiratory effort via a pressure-sensitive membrane implanted between the intercostal muscle layers in the extrapleural space. The signals are sent via a 'respiratory sensing lead' to an implantable pulse generator (IPG) that sits subcutaneously in the patient's chest. The IPG delivers stimulation, synchronised with the respiratory cycle, via the stimulating lead that terminates at the medial hypoglossal nerve within the neck as a 'self-sizing stimulation cuff'. The patient uses the remote to turn the therapy on before sleep and turn it off when they wake. The remote also can adjust stimulation parameters within physician-defined limits [169]. As of April 2020, the FDA specifies that patients eligible for hypoglossal nerve stimulation must be over 18 years old, non-obese (BMI $\leq$ 32 kg/m^2), and with moderate to severe OSA (AHI $\geq$ 15 and $\leq$ 65). Apnoea/hypopnoea events must be predominantly obstructive (> 75%), and the patient must have failed or be intolerant of CPAP, and lack concentric upper airway collapse at the level of the soft palate [169].

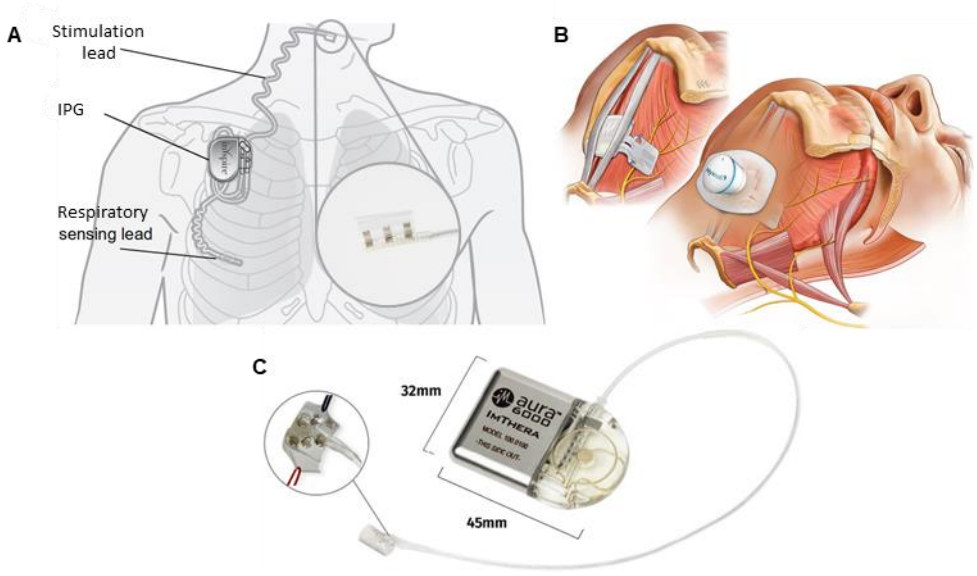

Figure 1-5 | Hypoglossal nerve stimulators are increasing in prevalence for obstructive sleep apnoea. (A) The Inspire Medical device is clinically approved, and **(B)** the Genio System by Nyxoah, and **(C)** aura6000 by LivaNova have undergone clinical trials.

Three other devices have been tested in clinical trials but have not received FDA approval. A similar device by Apnex Medical targets the medial branch of the hypoglossal nerve but uses

two respiratory sensing leads to monitor respiration via thoracic bioimpedance. While initial results were promising [14], Phase III trials failed to meet efficacy targets. Another device, aura6000 by LivaNova (formerly ImThera, Figure 1-5C), is similar to the Inspire Device but lacks the respiratory sensing lead, and the nerve cuff wraps around the trunk of the hypoglossal nerve rather than the medial branch. Both protruders and retractors receive continuous stimulation to maintain muscle tone during sleep via six independent electrodes in two rows inside the cuff. These are alternately activated to minimise fatigue during continuous activation. This device remains in Phase III trials ("THN3", NCT02263859). Another device is the Genio System by Nyxoah. In mid-2022, Nyxoah received an investigational device exemption approval from the FDA for clinical trials of its Genio system for bilateral hypoglossal nerve stimulation (Figure 1-5B, NCT03763682). This device claims to be the first 'battery-free, leadless, and single incision neurostimulator' and, unlike the Inspire device, also aims to treat patients with complete concentric collapse at the soft palate. The Genio system consists of a neurostimulator implanted in the submental region over the genioglossus and an external activation unit. This stimulator uses bilateral paddle electrodes in contact with more distal hypoglossal nerve branches and aims to stimulate the genioglossus exclusively. Cyclical pauses in stimulation allow rest periods to prevent fatigue; however, stimulation is not synchronized with inspiration. Instead, stimulation is determined by the external activation unit connected to the paddles by a disposable adhesive patch placed under the chin by the patient before sleep. The activation unit is removed in the morning, the patch is discarded, and the activation chip is recharged for subsequent use [13].

The Inspire Medical device's clinical approval and the current implantation eligibility criteria are largely based on the 'Stimulation Therapy for Apnoea Reduction' trial (STAR trial, NCT01161420). In the restricted cohort described above, the median AHI 12 months after device implantation decreased by 68% (an AHI of 29.3 at pre-implantation reduced to 9.0). Median ODI scores decreased by 70%, and quality of life improved. 66% of patients were considered responders to treatment (AHI reduction $>$ 50% to $<$ 20 events per hour), and self-reported daily adherence was 86%. Unfortunately, 15% of participants exhibited a significant increase in AHI at 12 months, with 6% exhibiting an increase greater than 15 events per hour. Two of 124 participants exhibited serious device-related adverse events that required secondary surgery for implantation correction. 33 additional serious adverse events were reported but were unrelated to the surgery or the device. Most (88%) non-serious adverse events were related to the procedure and included sore throat from intubation, pain at the incision site, and muscle soreness. Tongue weakness was not uncommon post-surgery (18%) but resolved in all patients. 40% of participants reported discomfort during stimulation, and 21% reported tongue soreness,

including abrasions on the lower side of the tongue; however, most of these non-serious events resolved with acclimatisation to the therapy [170]. In follow-up reporting three and five years after implantation, response rate, AHI reductions, self-reported adherence and quality of life improvements were maintained. After five years, 8 participants reported 9 serious device-related events that required repositioning or replacement. Between one and five years after implantation, discomfort due to stimulation reports fell from 81 to 5 reports per year, and tongue abrasions reports fell from 26 to 2 reports per year, supporting the need for acclimatisation [171, 172]. Unfortunately, no predictors for treatment success were identified [170].

A 2019 meta-analysis compared the Inspire, ImThera and Apnex devices. AHI reductions significantly differed between devices six months after implantation (55.1%, 27%, and 54.4%, respectively) but were comparable at 12 months (56.2%, 53.5%, and 44.3%). In terms of 'responders' to HNS (AHI reduction $>$ 50% to $<$ 20 events per hour), the Inspire, ImThera, and Apnex devices were successful in 70%, 35%, and 59.8% of patients at 6 months and 72.4%, 76.9% and 55% at 12 months. Adverse event rates, when reported, were comparable to those in the STAR trial, and analysis concluded that hypoglossal nerve stimulation presented an effective and safe surgical procedure for adult patients with moderate to severe OSA [12]. In a similar cohort, the Genio system decreased AHI by $\sim$ 47.3% 6 months after implantation, and the responder rate was 50% following the STAR trial definition. Other PSG measures (oxygen saturation, sleep efficiency etc.) improved; however, sleepiness and quality of life changes did not. No device-related significant adverse events were reported, but 3 of 27 participants experienced significant adverse events related to the surgery, including painful swallowing (30% participants), dysarthria (26% participants), hematoma (19% participants), and swelling/bruising around the incision (19% participants), resolved spontaneously. 30% of participants experienced local skin irritation due to the adhesive patch; however, this resolved in all but one case where irritation persisted at 6 months. Non-serious device-related adverse events were largely resolved via stimulation parameter adjustments. Adherence was high (91% using the system at least 5 days a week, and 77% reported using it for more than 5 hours per night) and exceeded CPAP adherence [13]. Genio system efficacy is similar to that of the unilateral devices [13, 173]; however, it has also shown efficacy in a single patient complete concentric collapse (an exclusion criterion for unilateral devices), reducing AHI from 33.6 to 1.6 events per hour [174]. This is the focus of an ongoing clinical trial (NCT03763682).

Despite promising results and superior compliance versus CPAP, hypoglossal nerve stimulators remain clinically approved for a highly selective population, and research outside this population remains incomplete. Research indicates that 30 to 50% of the restricted cohorts

remain non-responders. While not an irreversible intervention per upper airway surgeries, the implantation of these devices is highly invasive and comes with associated risks. Precise placement of the electrode on select branches of the hypoglossal nerve is essential for the HNS success [175], and synchronisation with respiration or alternating between electrode contacts is required to avoid muscle fatigue [176, 177].

As with other second-line therapies, no criteria currently predicts hypoglossal nerve stimulation success, apart from the absence of concentric pharyngeal collapse visible during Drug Induce Sleep Endoscopy, and investigations into endotype-based predictions are increasing. Using baseline PSG data obtained from the STAR trial and a 'responder' definition of an AHI reduction > 50% to < 10 events per hour, it was determined that patients with high arousal thresholds or patients with strong muscle compensation, lower loop gain and milder airway collapsibility were more likely to respond. The resulting 'predicted responders' had a four-fold lower on-treatment AHI than the predicted non-responders, however this has yet to be replicated. It was concluded that patient-specific causes of OSA could explain heterogeneity in hypoglossal nerve stimulation outcomes and that these traits could hold promise for precise therapy administration [178].

1.2.2.5 Pharmacotherapies

OSA pharmacotherapies target non-anatomical traits, namely impaired upper airway muscle function, low arousal thresholds and high loop gain.

Pharmacologic methods for improving upper airway muscle activity and responsiveness during sleep target several pathways associated with muscle control. Desipramine, a tricyclic antidepressant with noradrenergic, mild antimuscarinic and mild serotonergic effects, virtually abolished the natural decrease in tonic genioglossus muscle activity between wakefulness and non-REM sleep, reduced airway collapsibility [179, 180], and subsequently AHI [180]. Noradrenergic agents have increasingly been combined with antimuscarinic agents to increase muscle responsiveness during sleep. Reboxetine (noradrenaline reuptake inhibitor) and hyoscine butylbromide (antimuscarinic) reduced AHI by 17 ± 17 events/h by increasing tonic genioglossus muscle activity, reducing loop gain, and improving measures of airway collapsibility, without altering arousal thresholds [181]. Reboxetine and oxybutynin (antimuscarinic) have similarly produced AHI reductions (mean reduction of 59%) and improved next-day vigilance [182]. To a lesser extent, reboxetine alone reduces OSA severity; however, in that study, the addition of oxybutynin did not produce further improvements [183]. Atomoxetine, another noradrenergic agent, has been combined with several antimuscarinics with varied success. With oxybutynin, AHIs were reduced by over 60%, and it was theorised

that the effect was due to an increase in central stimulation of hypoglossal motor neurons and, subsequently, the upper airway dilators [184]. Later investigations found improved upper airway collapsibility and breathing stability (loop gain) and slightly reduced arousal thresholds. The success of this combined drug therapy was predicted by 'passive' anatomy, the proportion of events that were hypopneas rather than apnoeas, and baseline AHI [185]. Following this success, an exploration of more selective antimuscarinics was conducted. Atomoxetine and solifenacin succinate reduced event severity, increased the proportion of hypopneas during NREM, and improved oxygenation. Atomoxetine and biperiden hydrochloride improved quality of life measures (e.g. next-day sleepiness, perceived sleepiness). Unfortunately, despite both combinations reducing loop gain, neither altered AHI, heart rate during sleep increased, and REM sleep reduced [186].

Another method being explored to increase muscle tone and activate upper airway musculature is 'Designer Receptors Exclusively Activated by Designer Drugs' or DREADDs. DREADDs are bioengineered G-protein coupled receptors exclusively activated by designer synthetic ligands, traditionally clozapine-N-oxide (CNO) [15, 187, 188]. In rodents, viral vector-mediated expression of excitatory DREADD receptors, e.g. hM3Dq [188] or hM3Gq [15], in the hypoglossal motor nucleus, facilitated increases in tonic motor neuron firing, and subsequently, improved upper airway muscle contractions and pharyngeal dilation following acute systemic CNO administration [15, 187-189]. However, pharmacokinetic studies demonstrated that there was reverse metabolization of CNO into clozapine, an endogenously bioactive compound that exerts atypical antipsychotic behavioural effects in mice and rats [190], rendering it unsuitable for widespread clinical use. More recent DREADDs research has improved clinical potential. Rather than direct stereotactic administration of viral vectors to the brainstem, these studies use intralingual injections of viral vectors with established efficacy for retrograde transport and transgene expression. A novel and highly-specific DREADD ligand, J60, was used rather than CNO, and similarly increased tonic genioglossus muscle activation and pharyngeal dilation [16]. This chemogenetic approach to treating OSA requires repeat ligand administration before sleep onset and does not provide temporally precise muscle activation but rather a general elevation of tonic firing. This approach seems more efficient during NREM sleep than REM sleep, and the long-term safety and efficacy of chemogenetic ligands and nervous system-targeted gene therapies have yet to be established.

Hypnotics, particularly benzodiazepines (e.g. temazepam) and z-drugs (e.g. zopiclone, eszopiclone), are of interest to the sleep apnoea field due to their potential ability to reduce OSA severity and promote stable sleep by increasing arousal thresholds without concurrent

reductions in upper airway muscle activity. Both hypnotics work by potentiating GABA activity; however, Z-drugs have largely replaced older benzodiazepines, as they do not reduce deep sleep, are associated with fewer adverse side effects, particularly residual daytime effects, and have a shorter action duration and half-life [191]. As initial investigations into benzodiazepines [192] and high dose z-drugs [193] found that the resultant CNS depression prolonged apnoeic events, worsened hypoxia and reduced REM sleep [192, 193], the focus has shifted to newer non-myorelaxant sedatives including zopiclone [194]. Unfortunately, these investigations have produced varied results. While some have increased arousal thresholds without concurrent changes in genioglossus activity [140, 194, 195], others have indicated that they have no effect [196, 197] even when high doses are used [197]. Moreover, where arousal threshold reductions occurred, they did not always equate to reductions in OSA severity [194, 195]. Low arousal thresholds were initially identified as a predictor for response to z-drugs [140]; however, in studies that recruited explicitly from this population, no significant changes in AHI were found [197]. Finally, eszopiclone combined with oxygen therapy successfully reduced AHI by increasing arousal thresholds and reducing loop gain. This was particularly effective in patients with mild to moderate OSA, less collapsible airways, and more responsive upper airway muscles [198], however, replication is still required.

Pharmacotherapies have also targeted high loop gain (ventilatory response/ventilatory disturbance). Respiratory stimulants, e.g. acetazolamide (carbonic anhyrase inhibitor), have successfully reduced loop gain by 40% and NREM AHI by 50% without concurrent reductions in other OSA traits (airway collapsibility, arousal threshold or muscle responsiveness) [199]. Acetazolamide has also reduced blood pressure and AHI in hypertensive patients at high altitudes, and when combined with CPAP, AHI is reduced further [200]. Unfortunately, in both acetazolamide studies, other clinical scores remained unchanged (e.g. sleepiness and quality of life), and side effects, including paresthesia, taste disturbances and dyspepsia, were common, limiting long-term viability [199, 200]. Other respiratory stimulants show varied results. Zonisamide, another carbonic anhydrase inhibitor, also decreased AHI in overweight to obese people with moderate to severe OSA [201]. Aminophylline, a bronchodilator, showed no effects on obstructive events, significant disruptions in sleep efficiency and increased sleep fragmentation [202]. Finally, a combination therapy using oxybutynin and betahistine (histaminergic agent) increased loop gain and ventilatory instability but did not significantly change AHI [203].

While pharmacotherapy investigations benefit from double-blind, randomised, placebo-controlled trials, they frequently leave patients with residual OSA, present insufficient clinical

data (e.g. quality of life measures including daytime sleepiness), and are underpowered with small effect sizes. Positive results, even when statistically significant, should be interpreted with caution. Ongoing adequately powered and long-term studies will be required to establish concrete pathomechanisms and clinical outcomes of long-term use.

1.2.2.6 Other

Several other OSA interventions have been explored, including positional sleep therapy, oxygen therapy, weight loss, and various combination therapies.

As supine sleep significantly contributes to OSA in up to 75% of OSA patients [204], positional sleep therapy devices that promote lateral sleep have been proposed to reduce OSA severity. Various devices have been used, from 'home-made' options where the patient tapes a tennis ball to their back to devices that vibrate or emit sound when the patient is supine. In participants with mild to moderate positional OSA (i.e. ≥ twice as many disordered breathing events per hour when in supine [204]), positional therapies effectively reduce the percentage of supine sleep and improve OSA severity and subjective measures of sleepiness and quality of life [205, 206]. In restricted cohorts, AHI reductions are equivalent to those achieved with CPAP [207]. There is little standardisation amongst positional therapy studies, and many devices are available, including the Zzoma Positional Sleeper, a 'backpack-like' semi-rigid foam structure strapped to the patient [207] and the SONA Pillow with a 45° incline that promotes lateral sleep with the jaw positioned downward [206] – and generalising results concerning compliance levels and efficacy can be difficult.

As obesity is a primary risk factor for OSA, weight loss has also been proposed as an OSA therapy for overweight and obese patients. Most research shows that weight loss from lifestyle changes (diet and exercise) can reduce OSA severity and improve quality of life measures; however, the amount of weight loss required is unknown, and the resultant AHI reductions are highly variable. Moreover, long-term data is limited, and significant methodological limitations are present [208, 209]. Bariatric surgery for weight loss and OSA management has also been proposed. Interestingly, in an RCT, the greater weight reduction following surgery rather than lifestyle changes (~ 28 kg versus ~ 5 kg, respectively) did not produce a statistically greater AHI reduction. It was concluded that while mild to moderate weight loss is beneficial, further losses are associated with only limited additional benefits [210]. Unfortunately, substantial weight loss can be difficult to achieve and hard to maintain [209], and only a minority of individuals, usually those with mild OSA, experience a complete resolution of OSA symptoms with weight loss alone [211], and adjunct therapies are often required [209].

Oxygen therapy has also been shown to reduce loop gain and AHI by approximately 50% in a cohort with high loop gain [212]. In unselected patients, oxygen therapy has variable efficacy [213] and is less effective than CPAP in reducing AHI. Currently, no standardised protocols for oxygen delivery (flow rate and duration) have been established [214].

Finally, as most OSA patients have multiple contributors to their pathophysiology [215], combined therapies are increasing in popularity. Positional therapy combined with a mandibular advancement splint was found superior to either therapy alone [216]. This was also seen when atomoxetine was combined with oxybutynin [185]. Nasal surgery and mandibular advancement splints have significantly reduced CPAP pressure requirements and improved tolerance [161, 217]. Moreover, oxygen to reduce loop gain and a hypnotic to increase arousal threshold have also successfully resolved OSA in selected patients whose anatomy is not severely compromised [198]. While research into these combined methodologies is growing and is particularly encouraging for patients intolerant of CPAP, large-scale investigations are still required.

1.2.3 Rodent models of OSA

OSA is almost exclusively a human disorder, and the few animals that exhibit spontaneous obstructive apnoeas, e.g. British bulldogs [218], are not feasible for large-scale, non-recoverable pre-clinical studies due to size, availability and economic constraints. While central apnoeic events have been recorded in more rodents [219], obstructive events require additional interventions. Obese Zucker rats [97] and obese and leptin-resistant New Zealand mice [92, 220] have exhibited spontaneous airway narrowing during volumetric MRI or PSG assessment. Leptin-deficient ob/ob mice have upper airway neuromechanical control deficits, which can be reversed with leptin administration, suggesting that leptin deficiency may increase vulnerability to airway collapse and obstructive apnoeas [92]. Unfortunately, comorbidities, including arterial hypertension, hyperinsulinemia and hypercholesterolemia, make it difficult to attribute these findings to airway obstruction [213]. Moreover, in obese Zucker rats, despite narrower and more collapsible airways compared to lean controls, no concurrent loss of pharyngeal muscle activity (a non-anatomical contributor to human OSA) was present [221], indicating that while these models may mimic airway closure, they may not replicate other important aspects of human OSA pathophysiology.

Intermittent hypoxia can be induced via hypoxic chambers with timed nitrogen administration to replace oxygen, simulating the brief repetitive hypoxic periods and re-oxygenation associated with recurrent obstructive events [222]. Arousals and reductions in REM sleep accompany the induced hypoxias, therefore simulating human OSA [223]. Various protocols induce

intermittent hypoxia in rodents, and each likely impacts the associated physiologic and pathologic processes differently. Rodent models of OSA have also used various methods to occlude the upper airway and simulate obstructive events mechanically. These include external, computer-controlled, collapsible chambers attached to a tracheotomised rodent [224], external chambers that deliver high inspiratory resistance to force airway collapse [225, 226], and small balloons expanded externally to obstruct nasal flow [227] or expanded internally to obstruct the airway itself [228]. As per the obese models, neither the intermittent hypoxia nor the mechanical occlusion models are likely to reflect the non-anatomical contributors to human OSA, and the complex hardware may restrict how novel therapies can be tested.

Pharmacologic methods have also induced airway collapse. Serotonin injections that augment vagal tone can produce a single, immediate, transient apnoea [229]. In rats, this model has been used to demonstrate the therapeutic potential of systemic administration of cannabinoids that increase genioglossus muscle activity and suppress serotonin-induced apnoeas [230, 231]. Unfortunately, this model does not generate repeat apnoeas or hypopneas, and the injections may interact with additional interventions, thus limiting their utility in some applications. Inhibitory DREADDs can reversibly silence hypoglossal motor neurons and genioglossus activity in lean mice and induce flow-limited breaths in REM and NREM sleep without an anatomically compromised airway [232]. While this model may lend itself to studies examining the impact of pathogenic factors of OSA on other outcomes (e.g. cardiometabolic) and potentially aid in identifying novel targets for OSA therapies [232], they require costly or time-consuming viral vectors or transgenic animal lines to generate the expression of inhibitory designer receptors.

Despite OSA being almost exclusive to humans, several rodent models reflect elements of human OSA. Careful consideration of which animal model is best for a specific application is required, particularly concerning the non-anatomical contributors to OSA, which are less likely to be accurately replicated.

1.3 OPTOGENETICS

In 1999, while describing techniques of molecular biology and their utility in neuroscience, Francis Crick stated that to understand how our brains work, researchers require a tool that can ‘turn the firing of one or more types of neuron on and off in the alert animal in a rapid manner’. He stated that ‘the ideal signal would be light’ and that while ‘rather farfetched… it is conceivable that molecular biologists could engineer a particular cell type to be sensitive to

light' [233]. Ten years later, optogenetics, the combination of light stimulation and genetic engineering, was coined Nature Methods 'Method of the Year [234].

In contrast with traditional neuromodulation methods (e.g. irreversible lesions, pharmacotherapies and electrical stimulation), optogenetics provides a minimally invasive, cell-type specific method of inducing cellular change with high temporal and spatial resolution. In brief, cells are engineered to express membrane-bound proteins or 'opsins', which act as ion pumps or channels when illuminated with a specific wavelength of visible light and alter downstream cellular activity [235-239]. The central nervous system (CNS) is the most common target for optogenetics. In the CNS, optogenetics has been used to improve understanding of neural circuitry and proposed as a potential therapy for various neurological diseases, including Alzheimer's [240, 241], Parkinson's [242, 243], schizophrenia [244], pain [245] and epilepsy [246]. More recently, peripheral optogenetics has expanded. Optogenetics has been proposed as an alternative to electrical stimulation for arrhythmia management and cardiac pacemakers [247-251], urinary and bowel incontinence [252, 253], and the restoration of skeletal muscle function following disease (e.g. muscular dystrophies or motor neuron diseases) or injury (e.g. spinal cord injury) [235, 254, 255]. Clinically, optogenetics remains in its infancy, restricted to clinical trials for retinitis pigmentosa [256-259]. An initial human case study used viral vectors to induce opsin expression in the retinal ganglion cells and achieved partial recovery of visual function using goggles that detect changes in local light intensity and project corresponding light pulses to the retina. Following these results, no evidence of ocular or systemic adverse events [260], and the unmet need for a novel therapy, the FDA granted a Fast Track designation in late 2021.

The success of optogenetics depends on several factors. First, numerous naturally occurring or engineered opsins are available, each with unique characteristics that can help or hinder their use in specific applications. Second, the targeted cells must generate sufficient opsin expression for functionally effective light-evoked responses. This can be achieved via three primary mechanisms; transgenic animal lines, electrotransfer or viral vectors. Third, the optimal location for opsins to be expressed must be considered. For peripheral targets, e.g. skeletal muscle, optogenetic activation can be achieved 'directly', i.e. where opsin expression and light stimulation are applied to the muscle, or 'indirectly', i.e. where opsin expression and light stimulation are applied to the innervating peripheral nerve or associated motor nuclei. Finally, the technology required for delivering light to the targeted cells must be established.

1.3.1 Opsins

Ooptogenetics uses membrane-bound proteins or ‘opsins’ that, when illuminated by a specific wavelength of light, can modify the activity of the cell in which they are expressed. Two types of opsins exist in nature. Type I opsins, or ‘microbial’ opsins, are used by prokaryotes and some microbial eukaryotes (e.g. fungi and algae) for tasks including navigation towards energy sources or away from hazards. They act as single-component systems, conferring both light sensitivity and ion conductance. Photon absorption triggers isomerisation of the opsin-bound retinal molecule from all-trans to 13-cis configuration. Opsin configuration then changes, activating ion channel opening or pump activation. The transmembrane ion movement ultimately leads to depolarization or hyperpolarisation, and neural activation or inhibition, respectively [261, 262]. Type 2 opsins are more complex and used in higher eukaryote vision and circadian rhythm modulation. As G-protein coupled receptors, photon absorption and the isomerisation of 11-cis retinal into the all-trans configuration initiates intracellular signalling cascades rather than immediate cellular change [262]. As Type 1 opsins are smaller, induce rapid neural change, and are easier to engineer, they are more frequently used in optogenetics-based research than Type 2 opsins. As the studies presented in this thesis aim to induce temporally and spatially precise muscle contractions, this literature review will focus on depolarizing Type 1 or ‘microbial’ opsins.

Following the initial ex vivo use of opsins in 2003 [263], numerous microbial opsins have been discovered or engineered. The first and most commonly used microbial opsins are from the channelrhodopsin (ChR) family, particularly channelrhodopsin-2 (ChR2, Figure 1-6A). ChR2 is derived from unicellular green algae, and illumination results in an influx of positively charged ions initiating depolarisation and neuronal spiking [264, 265]. Conversely, illumination of bacteriorhodopsins or halorhodopsins (Figure 1-6B), outward proton pump and inward chloride pumps, respectively, produces hyperpolarisation and neuronal silencing [261, 266]. Each opsin has unique characteristics, including shifted absorption/action spectra [267-270], increased photosensitivity and photocurrents [271], and varied kinetics [268, 269, 271, 272], that either help or hinder its suitability for specific applications.

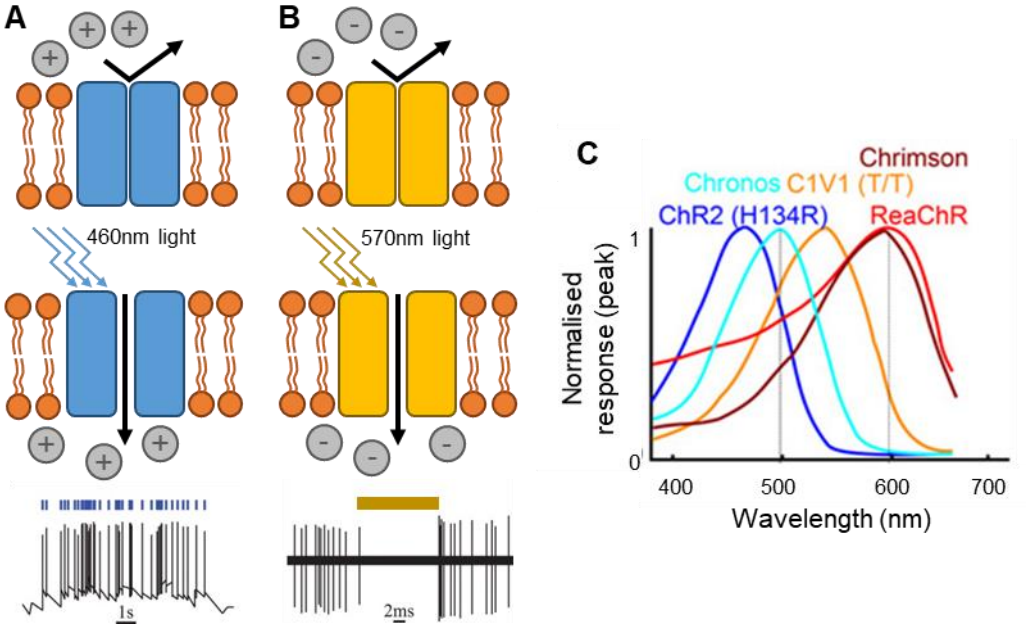

Figure 1-6 | Microbial opsins can induce depolarisation or hyperpolarisation with light stimulation. **(A)** Opsins in the channelrhodopsin family act as non-specific ion channels that open when illuminated to induce depolarisation. **(B)** Opsins in the halorhodopsin family act as chloride ion channels that open when illuminated to induce hyperpolarisation. **(C)** Different opsins can be activated by a range of visible light wavelengths but produce maximum photocurrents when exposed to a specific wavelength of light.

While a limited spectrum of visible light can activate microbial opsins, optimal photocurrents are generated when exposed to a specific wavelength (Figure 1-6C, Figure 1-7). ChR2(H134R), a ChR2 variant with a single point gain of function mutation at position H134R, can be activated by a range of visible light but produces maximum photocurrents with blue light, i.e. ~ 470 nm (Figure 1-6C) [263-265]. Conversely, Chrimson is considered a 'red-shifted' or 'red light sensitive' opsin and produces maximum photocurrents with 600 nm wavelengths (Figure 1-6C) [268]. Spectrally distinct opsins, i.e. those activated by different wavelengths, can be simultaneously expressed in single or neighbouring cells/tissues and independently activated. ChR2 and Arch3 (an inhibitory archaerhodopsin variant) expressed in the same V3 interneurons induced and suppressed muscle spasms when illuminated by blue and green light, respectively [273]. Spectrally distinct opsins also allow alternate activation of agonist and antagonist muscles innervated by a single mixed peripheral nerve. After rodent tibialis anterior and gastrocnemius muscles received viral vector injections to generate CsChrimson (a red light sensitive depolarising opsin derived from Chrimson [268]) and ChR2(H134R) in their respective portions of the sciatic nerve, alternating blue and red light stimulation to the surgically exposed sciatic nerve induced plantar flexion and dorsiflexion in vivo [274].

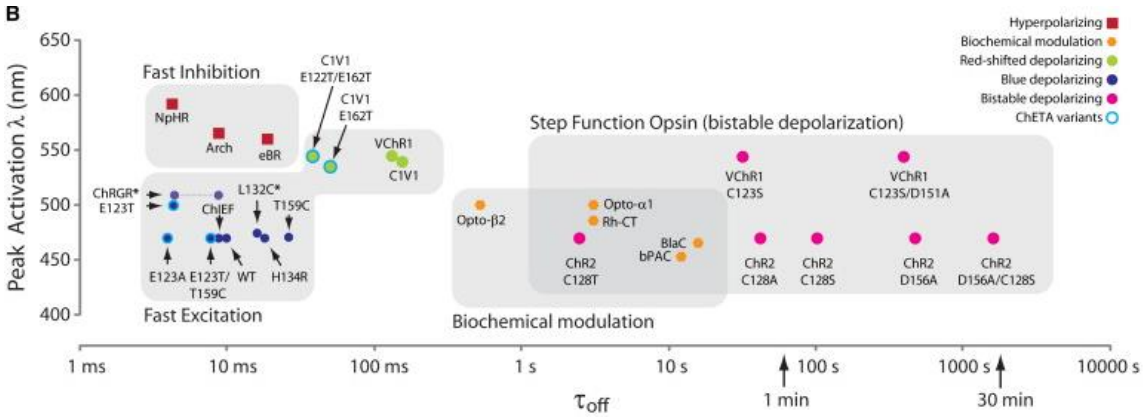

Figure 1-7 | Kinetic and spectral properties of opsin variants. While a range of wavelengths can activate an opsin, they demonstrate peak activation at specific wavelengths (y-axis). Opsin reactivation depends on their off-kinetics (τoff). Figure from [275].

As visible light is absorbed as it passes through tissue in a wavelength-dependent manner, spectral sensitivity also determines the depth at which opsins can be effectively activated. As intensity reductions are greater with shorter wavelengths (e.g. blue light, ~ 430 – 500 nm) [276], red-shifted opsins activated by 630 – 710 nm, e.g. ChrimsonR [277], ReaChR [278] and ChRmine [267], can be activated at greater depths and with reduced light intensities [279, 280]. Similarly, opsins with greater photosensitivity, e.g. CatCh [281], can be activated despite light attenuation [238, 282]. These opsins reduce power requirements, tissue heating risks, and the necessity for invasive implants [282]. Further, due to CatCh's enhanced Ca^{2+} permeability [283], it is particularly suitable for Ca^{2+} influx induced muscle contraction. In contrast, ChRmine [267], while red-light sensitive, exhibits little to no Ca^{2+} conductance so may prove ineffective for skeletal muscle activation [283]. In silico investigations of cardiac optogenetics have indicated that red-shifted and highly photosensitive opsins likely will be vital for clinical applications where light must penetrate human tissues several orders of magnitude larger than rodents [250].

Opsin kinetics dictate optimal stimulation protocol. For most applications, an ideal opsin rapidly activates and shows minimal desensitisation during illumination. Rapid deactivation following the end of stimulation (off-kinetics, τ_{off}) permits immediate and effective repolarization (and retinal re-isomerisation) and repeat activation [238]. Indeed, poor off-kinetics associated with standard ChR2 variants, e.g. ChR2(H134R), may fail to achieve high fidelity action potentials exceeding 30Hz, and the evoked responses to successive light pulses can decline due to ineffective repolarisation (τ_{off} for ChR2(H134R) ~ 20.9 ms [265]) [235, 264, 284]. 'Ultrafast' opsins, such as ChETA [272] and Chronos [268], have more rapid off-kinetics (τ_{off} ~ 5.2 ms and 3.6 ms, respectively) and reduced desensitization to allow faster reactivation. In mouse

brain tissue expressing ChETA, spike trains up to 200Hz produced high fidelity responses [272].

Optimal kinetics can come at the cost of light sensitivity and photocurrent strength, with highly light sensitive opsins often displaying poor τ_{off} [238], e.g. the mutagenesis of ChR2 to ChR2(H134R) resulted in enhanced light sensitivity and photocurrents but reduced τ_{off} values (~ 11.9 ms to 20.9 ms [238, 265]). Red-shifted opsins also tend to display poor kinetics, with τ_{off} values of approximately 60 ms for C1V1 variants (C1V1(E162T), C1V1(E122T/E162T)) [238]. However, mutagenesis of Chrimson to ChrimsonR reduced τ_{off} from approximately 21.4 ms to 15.4 ms [268], and ChRmine (τ_{off} ~ 70 ms) [285], yeilded variants with reduced τ_{off} values (~ 30 ms) and equivalent peak photocurrent amplitudes [270].

Opsins with slow kinetics, known as step function opsins (SFOs), may also reduce light intensity and energy requirements. SFO channels remain open for over 30 minutes after light stimulation stops or until deactivation with orange light [271]. SFO activation can induce stable and subthreshold depolarisation that sensitises cells to further excitation. Thus, co-expression of SFOs and spectrally distinct 'standard' activating opsins, e.g. ChrimsonR, may elevate resting thresholds and reduce light intensity and power requirements for effective activation of the 'standard' opsin. New SFOs with additional ultra-high light sensitivity [286] hold promise for clinical applications.

1.3.2 Gene transfer

Therapeutic applications of optogenetic stimulation require sufficient, specific, and persistent opsin expression. This is achieved by optimising the method of opsin gene delivery to the targeted cells/tissues. Gene transfer typically occurs via three primary approaches; transgenesis, electrotransfer and viral transduction.

1.3.2.1 Transgenic animals

The first example of transgenic animals for optogenetics was a ChR2-YFP expressing mouse line for in vivo activation and neural circuitry mapping [287]. Since then, the toolbox of transgenic mice and rats expressing opsins has grown rapidly and been successfully employed in various applications [266, 288]. Transgenic animals permit widespread, stable and heritable transgene expression [288]. In contrast to viral vectors, there are no packaging restrictions, so larger and stronger promoters (further discussed in Section 1.3.3) can induce specific and saturated expression of larger transgenes [289]. However, the development and validation of transgenic animal lines is expensive and time-consuming, potentially taking several generations [288]. New animal lines are required for different opsins, and extensive use of sometimes

poorly characterised animal lines can hinder the ability to anticipate potential risks [43]. Transgenic animals can also lack the desired spatial specificity as the transgene is expressed in all promoter-defined cells rather than being restricted to a distinct region/s [290]. Most importantly, while transgenic animals provide proof of principle [235], they are not suitable for clinical applications.

1.3.2.2 Electrotransfer

Electrotransfer (or electroporation) is a non-viral method for delivering molecules, including DNA, RNA and proteins, into cells following electric pulses [239, 291]. It has been used in in-utero research [290], DNA vaccinations [292], transdermal gene delivery [293, 294] and the treatment of non-healing and chronic cutaneous wounds [295]. Despite emerging in the late 1980s to increase the efficiency of chemotherapeutic drugs, the mechanisms of electrotransfer are still contested. Traditional theories postulate that molecule transfer is achieved via the generation of pores [293, 296], whereas more recent studies indicate that endocytosis plays a role [291, 297-299]. Regardless of mechanisms, electrotransfer is now employed in over 150 centres in the European Union [295, 300, 301] to treat refractory cutaneous and subcutaneous tumour nodules [302, 303]. Electrochemotherapy remains the primary application of electrotransfer in a clinical setting [302, 303], with some 90 clinical trials (predominantly cancer treatments) have been completed to date [291].

Electrotransfer has demonstrated efficacy and reproducibility in skeletal muscles as a therapy for muscular dystrophies [304, 305] and the systematic secretion of therapeutic proteins [305]. Notably, it can increase transgene expression up to 100 times compared to direct injection [305, 306]. Electrotransfer is well suited to use in skeletal muscle due to the ease of access and transfection [295]. Moreover, transgene expression is considered stable due to the post-mitotic nature of muscle fibres that, when damaged, do not fully degenerate [304, 305, 307]. Several electrotransfer studies investigating therapies for Duchenne muscular dystrophy (DMD) have reported the delivery of the entire dystrophin cDNA construct (12.5kb) driven by ubiquitous promoters (see Section 1.3.3) delivered into tibialis anterior muscle fibres in mdx mice (an animal model of DMD) [308, 309]. In some studies, the levels of gene electrotransfer to skeletal muscle fibres have been equivalent to viral vector-mediated transfer [304], however the uptake of plasmid varies across myofibers [310].

Electrotransfer is considered a safe, simple and inexpensive gene transfer method [291, 306, 311, 312] without requirement for chemicals and viruses [303]. As with transgenic animals, this method can quickly and efficiently transfer large payloads [306, 308] and deliver multiple unique plasmids into cells [295, 308]. Moreover, electrotransfer of naked pDNA can facilitate

repeated transgene expression without protocol alterations due to the lack of immune response [291, 308]. This contrasts with viral vector-mediated gene delivery systems that can require viral capsid manipulation or immune suppression for re-administration [313].

Electrotransfer for transgene delivery has two significant limitations that restrict its use in human subjects. First, while electrotransfer significantly increases transgene expression compared to direct DNA injections, expression typically remains low and unstable compared to viral delivery methods. Second, there is a risk of adverse effects on the transduced tissues when high voltages are used [304, 312], and intense stimulation and electrode implantation can elicit pain [314, 315]. Finally, it is virtually impossible to use electrotransfer on large volumes of tissue due to the high voltages required, and surgery is necessary when targeting internal organs [305].

Thus, an optimal gene electrotransfer will maximise transgene expression but minimise tissue damage and associated pain [305, 316]. While the manipulation of stimulation protocols may reduce the risk of tissue damage, standardised protocols have yet to be established. Moreover, establishing a standardised protocol is challenging as protocols necessarily will differ in accordance with tissue type [304] and volume [317], and electrode type [318], shape and position [318].

1.3.2.3 Viral vectors: Adeno-associated viral vectors

Viruses are near-perfect nano-machines for gene delivery. The rapid development of viral vector technology and the inclusion of novel promoters and enhancers have produced numerous highly efficient transgene delivery systems. Not all viral vectors are suitable for human applications that require replication-deficient viruses that induce fast, robust, and spatially localised transgene expression via natural infectious pathways [236, 239, 319, 320].

Adeno-associated viruses (AAV) are one of the most actively investigated and promising vehicles for in vivo gene delivery to dividing and non-dividing cells. First discovered in the mid-1960s as a contaminant of adenovirus preparation [321, 322], AAVs were first FDA-approved for lipoprotein lipase deficiency in 2012 (Glybera); however, this product was withdrawn due to low demand and high cost. Currently, four FDA or European Medicine Agency (EMA) approved rAAVs vectors are approved for use in Leber congenital amaurosis (Luxturna), spinal muscular atrophy (Zolgensma), aromatic L-amino acid decarboxylase deficiency (Upstaza) and Haemophilia A (Roctavian). Approximately 150 clinical trials for various ophthalmological, neurologic, metabolic, hematologic and musculoskeletal diseases and disorders have employed AAV gene therapies, indicating that AAV gene therapy is a safe, well

tolerated and efficacious modality [323]. Importantly, AAVs can transform a patient's genome with a single injection, and unique molecular specificity and minimal off-target effects can be achieved with optimised serotype and promoter selection.

AAVs are icosahedral, non-enveloped protein capsids that surround and protect small (≈ 4.7kb) single-stranded DNA genomes that contain three genes; *Rep* (Replication) encodes four proteins required for viral replication and packaging*; Cap* (Capsin) encode the viral capsid proteins that form the outer capid shell, protect the genomic DNA and are involved in cell binding and internalisation*;* and *app* (assembly activating protein) that provides a scaffold for capsid assembly. Two t-shaped inverted terminal repeats (ITRs) that flank the genes are required for genome replication and packaging. As a 'dependovirus', AAVs are replication defective and rely on coinfection by a helper virus, commonly adenovirus, to replicate and produce a productive infection in the body. Without a helper virus, AAVs cannot enter the lytic cycle and establish latency by site-specific integration into a unique locus on human chromosome 19 [319, 324-328]. Recombinant AAVs (rAAVs) have the same capsid sequence and structure as their wild-type counterparts; however, the viral DNA components (Rep, Cap and App genes) are replaced with an 'expression cassette' composed of a transgene, promoter and other regulatory elements. The lack of viral DNA contributes towards rAAVs suitability for gene therapies, as after receptor-mediated endocytosis, the genome does not effectively integrate with the host genome [239, 324-326], minimising the risk of insertional mutagenesis and long-term and irreversible side effects [329]. In the nucleus, the vector genome forms double-stranded episomes that pose a low risk of genotoxicity. Moreover, as loss of transgene expression is a function of the transduced cell turnover rate, rAAVs can provide long-term transgene expression in non-dividing cells, both critical features for safe and effective gene delivery [319, 325, 327, 330, 331]. rAAV-mediated gene expression has been recorded for up to 10 years in human muscle [332], and 7.5 years after clinical administration of Luxturna, i.e. the FDA-approved rAAV-mediated therapy for inherited retinal dystrophy [333].

1.3.2.3.1 Serotypes

A major advantage of rAAVs over alternative gene transfer methods is the specificity afforded by the countless 'wild-type' and engineered AAV serotypes. As each serotype differs in efficacy and tropism, transgene expression can be restricted to targeted tissues, and minimised in non-target tissues, reducing risks associated with over-expression, including immune responses and toxicities [330, 334-337].

rAAVs are commonly derived from naturally occurring serotypes [338] that present specific tissue tropisms, i.e. each preferentially infects specific cell types. AAV2 was the first serotype

used for transgene delivery, remains the most commonly used (~30% of clinical trials) [338], and is FDA-approved for RPE65-mediated inherited retinal dystrophy (Luxturna) [339]. Other wild-type rAAVs, AAV1 and AAV9, are used for the FDA-approved therapies for lipoprotein lipase deficiency and spinal muscular atrophy, respectively. A 2021 meta-analysis found that of the 125 studies that disclosed the rAAV used, 87% were derived from natural serotypes or were pseudo-typed (the transgene was flanked by AAV2 ITRs and packaged within another natural serotype). Each disease group in their analysis had a capsid prevalence, e.g. AAV8 dominated blood disorders, AAV1 and AAV9 dominated neuromuscular disorders, and AAV9 dominated liposomal storage disorders [338].

rAAVs infect target cells by binding primary receptors and co-receptors on the cell surface, which triggers their endocytosis into endosomes. The primary receptors dictate serotype tropisms and kinetics, and considerable cross-over between serotypes is evident [340, 341]. Definitive tropisms are challenging to define due to considerable variations in study design, including vector titres, doses, administration routes, animal models, promoters and transgenes [342]. However, new DNA/RNA barcoding methods combined with next-generation sequencing [343] now allow side-by-side comparisons of hundreds of capsids in a single animal at consistent doses [344, 345]. In mice, a comparison of systemically administered wild-type AAVs found that serotypes 1 to 3, 5 to 8, rh10 and 12 were sequestered mainly in the liver. Conversely, AAV4 had weak liver expression and strong expression in the lung. AAV9 exhibited the broadest distribution and the highest efficiency in most organs, but most viral copies (~ 50%) still ended up in the liver [344].

Despite the established efficacy for gene transfer by wild-type rAAVs, there are several disadvantages. First, the equivalent wild-type AAVs are pervasive in human populations, and subsequently, so are pre-existing adaptive immunities, including neutralising antibodies [346]. Low titres of neutralising antibodies (NAb titre of 1:5 and 1:10, i.e. a titre of 1:10 indicates that diluting one part of sample with 10 parts saline, produces a sample with undetectable antibody level) have eliminated large viral loads in gene therapy studies for haemophilia B and DMD [347] [313, 348], and can potentially lead to reductions in transduced cells and transgene expression. As a result, functional efficacy can be reduced and vector re-administration may not be safe or effective. Second, these wild-type rAAVs typically have broad tropisms and are biased towards the liver, which requires high viral loads for therapeutically effective expression levels in other tissues [342, 349]. High viral loads can, in turn, produce therapy-limiting toxicities [349], as documented in a recent clinical trial [350].

Novel-engineered rAAVs offer the opportunity to overcome these limitations. In the absence of previous exposure, engineered serotypes are subject to reduced immune surveillance and responses and can be designed with increased tissue specificity, strong liver detargeting, and/or an improved ability to evade antibody neutralization [344, 345, 351]. In turn, their use may improve long-term transgene expression, reduce viral loads and immunogenicity, and improve safety profiles. Various methods have been used to develop novel rAAVs. So-called rational design employs a bottom up approach that exploits knowledge of capsid biology and host cell targets to apply site-specific modifications to existing capsids to improve tissue specificity and/or modify antigenic sites [352]. Directed evolution, a 'top-down' approach, generates diverse capsid libraries via gene shuffling and random mutagenesis. High throughput testing methods using barcoding are applied to identify the most effective capsids [344, 345, 351]. Finally, in silico design uses computational approaches to predict novel capsid designs not seen in nature, e.g. by reconstructing ancestral AAVs from contemporary capsids [353].

Recently. several highly muscle-specific rAAVs have been developed and identified. In 2020, AAVMYO, generated via directed evolution, displayed excellent efficiency and specificity in musculature following systemic administration in mice. Compared to AAV9, previously considered the most efficient serotype for muscle transduction, AAVMYO produced eYFP mRNA expression ~ 61-, 17-, and 11-fold greater in the diaphragm, quadriceps femoris, and heart, respectively, with concurrent liver detargeting (nine-fold less than AAV9). These findings were supported at the protein level, in other mouse strains, and with different transgenes and reporters [344]. The same group later generated AAVMYO2 and AAVMYO3 via rational additions, which maintained high efficacy in striated muscle and high vector yields but further reduced off-target expression [354]. A second highly myotropic serotype, MyoAAV was identified the following year (2021 [345]). Like AAVMYO, systemic delivery of MyoAAV generated greater RNA and transgene expression in skeletal muscle and greater liver detargeting than AAV9 [345]. Moreover, compared to AAV9, MyoAAV produced 14 times greater RNA expression following intramuscular injections in mice and transduced 35 to 52 times more human myocytes [345].

1.3.2.3.2 Limitations

rAAV-mediated gene therapies have been approved for use in several disorders and are the subject of 100s of clinical trials. Despite this, barriers to their widespread use still exist, soecifically (1) rAAVs have limited capacities for the 'expression cassette' [328, 330]; (2) high viral loads are often required for therapeutic efficacy [350], and (3) rAAVs are commonly

subject to pre-existing, acute and delayed immune responses that can reduce transgene expression and functional efficacy [354].

1.3.2.3.2.1 Packaging restrictions

rAAVs are one of the smallest known viral vectors with expression cassettes limited to 4.5 to 5 kb (compared to 9-10 kb for lentiviruses) [328, 330, 355]. Larger cassettes can reduce viral production yield, and induce transgene truncation or rearrangement, and unexpected changes in the viral vector properties (e.g. virulence, tissue tropism and the susceptibility of the vector to the immune system) [319, 356, 357]. Due to this limitation, large gene and promoter sequences are not yet feasible in rAAV-mediated gene therapies [236, 319], and efforts to minimise the cassette size are essential for effective transgene expression [355].

Truncated transgenes and promoters have been developed to circumvent these limitations. For example, the entire cDNA sequence for the large dystrophin gene (11.5 to 13.9 kb), dysfunctional in DMD [356, 358] has been the subject of several rAAV-mediated gene therapy clinical trials (NCT03362502, NCT03368742, and NCT0376911) following the successful development of novel micro-dystrophins (~ 3.7kb) [328] with enhanced functionality. Truncated promoters have also been developed as several of the most effective, tissue-specific promoters exceed the rAAV size restrictions. Muscle creatine kinase promoters (MCK), initially 6.5kb, have been abbreviated to dMCK (509bp) and tMCK (720bp) promoters. The tMCK promoter proved particularly strong in muscles, superseding the strength of the highly active ubiquitous CMV promoter, but essentially inactive in non-muscle cells lines (over 200 fold-weaker than the CMV promoter) [330]. Truncation is not unique to tissue-specific promoters, for instance the CMV promoter (approximately 600bp) can be shortened to 173bp and maintain expression in most cell types [356].

Where transgenes and/or promoters cannot be truncated, dual or triple rAAV gene strategies, where the cassette is split over multiple vectors, can be used [319, 356]. By splitting coding sequences for Factor VIII proteins into heavy and light chains and delivering them separately in a dual rAAV strategy, transgene functionality and long-term phenotypic corrections for Haemophilia A were achieved [359, 360]. Dual strategies have also been used to treat oculopharyngeal muscular dystrophy where two different transgenes were required; one to inhibit the expression of the endogenous mutated gene and a second to induce the expression of the same sequence-optimised transgene. Individually these methods were ineffective however, the dual strategy increased muscle strength and decreased degeneration [361]. The authors noted that this dual AAV method could be applied to other neurological gain-of-function aggregate pathologies such as Parkinson’s Disease, Alzheimer’s Disease and Huntington’s Disease [361].

1.3.2.3.2.2 High viral loads

rAAV dosing is a compromise between efficacy and toxicity. In animals, typical doses range from 10^{11} to 10^{13} vector copies, but in non-human primates and humans, vector copies have exceeded 10^{16}, and are particularly common in applications that use systemic delivery [338]. Zolgensma, FDA-approved for spinal muscular atrophy, systemically delivers 1.1×10^{14} vg/kg of an AAV9 capsid driven by a non-specific promoter for survival motor neuron protein expression (NCT03306277)[362]. Simiarly, clinical trials for DMD-targeted therapies systemically deliver 2.0×10^{14} vg/kg of rAAVrh74 (an NHP-derived serotype similar to AAV8) driven by a muscle-specific promoter (MHCK7, [363]) for micro-dystrophin expression [364]. While functionally effective results are achieved, and administration is typically well tolerated [362, 364], high viral loads have been reported to increase immunogenicity, liver injuries, and other side effects. Recently the manufacturer of Zolgensma reported two fatalities due to acute liver failure [365], and transient (non-lethal) liver failure has also been reported [337]. A clinical trial using AAV8 to treat X-linked myotubular myopathy similarly reported three patients experiencing severe hepatotoxicity, two of whom died. These patients had received a 'high dose' (3×10^{14} vg/mL) of the AAV8 construct, and those treated with a low dose (1×10^{14} vg/kg) exhibited no liver-related adverse events [350]. These outcomes are supported by studies in non-human primates (2×10^{14} vg/kg), where severe toxicity and liver failure resulted in 1 of 3 animals being euthanased [349], and in ex vivo studies (primary human hepatocyte mixed cultures) where the 'high dose' (1×10^{15} vg/cell) produced innate immune responses, and the 'low dose' (1×10^{13}) did not [334]. This highlights the importance of minimising viral doses and targeted AAV administration (systemic delivery requires higher viral loads [338]).

High viral loads are often associated with wild-type rAAVs due to their liver sequestering [344], and systemic delivery and the associated dilution of the viral product [338]. As previously stated, engineered serotypes that actively detarget the liver and enhance targeted transgene expression (e.g. [344, 345, 354]) may reduce the required loads for therapeutic efficacy and, subsequently, the risk of toxicities. Tissue-specific promoters can minimise the potentially harmful effects of off-target expression [319, 330], and compared to systemic delivery, intramuscular injections typically have low vector dissemination to non-targeted tissue [366], are less susceptible to pre-existing anti-AAV humoral immunity [367, 368], and are associated with fewer serious adverse events [323]. Targeted delivery allows reduced viral loads, with clinical trials administering a maximum of 7.5×10^{15} vector copies versus 1.5×10^{17} for systemic administration [338].

Viral dosage is application-specific and depends on many factors, including the route and location of vector administration, the AAV variant, and the transgene. Controlled dose-dependent studies, focussing on transduction efficiency and immunogenicity, are required to establish optimal application-specific dosages.

1.3.2.3.2.3 Immune responses to rAAVs

rAAVs were initially described as non-immunogenic; however, as research expanded from mice to larger animal models and humans, it became evident that administration can trigger immune responses to the capsid and the/or transgene [335, 369]. It remains accepted that rAAVs are not strongly immunogenic, likely due to the ITRs being the only viral elements. Viral peptide presentation on MHCs is minimal, as is the intensity of cellular immune responses. Despite this, humoral and cellular immune responses are one of, if not the most frequently cited, barriers to efficient rAAV-mediated gene therapies in clinical practice.

Anti-AAV antibodies develop within hours of AAV exposure and can limit transduction when rAAV-mediated gene therapy is delivered intravenously or intramuscularly [313, 348]. Wild-type AAVs are endemic in the human population, and due to high serotype cross-reactivity, the human population also have high rates of anti-AAV antibodies [340, 346, 367, 370]. The prevalence of anti-AAV antibodies for specific serotypes varies from 30 to 70% of the population [346]. Clinical trials frequently exclude subjects based on pre-existing antibody titres, regardless of whether they are neutralising. For instance, DMD-related clinical trials have required either anti-AAVrh75 antibody titers < 1:400 [364] or the complete absence of anti-AAV9 neutralising antibodies (NAbs) [371]. Moreover, after the initial administration of an rAAV therapy, a previously seronegative patient may be excluded from future therapy re-administration [370]. While anti-AAV antibodies have long been considered the leading cause of therapeutic failure [367, 372-374], mixed evidence exists. Binding anti-AAVs (non-neutralising antibodies that recognise the capsid but do not neutralise it) have increased transgene expression in the liver [374], and anti-AAV NAbs have altered rAAV tropisms and directed vector particles to the spleen [375]. While high rAAV doses may combat pre-existing antibody-induced reductions in transduction, this increases the risk of peripheral toxicities and innate immune responses [335].

Where circulating antibodies develop rapidly in response to rAAV or AAV administration, T cell responses to novel antigens are much slower and are associated with losses in established transgene expression [367, 370, 376]. In an early study investigating clotting factor IX over-expression in the liver of hemophilia B patients, T-cell mediated immune response produced elevated blood levels of liver enzymes and reversed the successful factor IX over-expression

[367]. Like anti-AAV antibodies, AAV-specific memory T cells can recognise multiple rAAV serotypes [376].

With the increasing use of rAAVs in clinical trials, many studies have proposed strategies to minimise the effects of pre-existing immunities or reduce immune responses in AAV naïve subjects. As previously noted, tissue-specific promoters can minimise off-target effects and immune responses [319, 330, 335, 336], and engineered rAAVs are less susceptible to immune surveillance and responses due to patient naivety and can be engineered to evade neutralising antibodies [371][346]. Alternatively, empty viral capsids injected alongside the transgene-containing capsid act as decoys and prevent NAbs from inhibiting internalisation and transgene expression [377]. Crosslinking synthetic polymers onto AAV vectors can reduce NAb recognition, innate immune responses and adaptive immune responses to enhance gene transfer and allow repeat administration [378, 379]. AAV vectors associated with extracellular vesicles can also evade pre-existing NAbs and, compared to standard non-enveloped AAV vectors, have produced 4000-fold greater transduction in mice [380, 381]. Finally, plasmapheresis can also effectively reduce NAb levels [382].

Adjunct pharmacotherapies are commonly prescribed in clinical trials to minimise immunological risks. Transient immunosuppressive and corticosteroid treatments are commonly used [338], and effectively suppress T cell-mediated responses [373, 383, 384] and the development of anti-AAV antibodies [348, 385]. Moreover, rAAV vector re-administration is possible when the initial rAAV dose is administered with synthetic vaccine particles encapsulating immunosuppressants [386]. rAAV administration may also prove feasible in patients with pre-existing anti-AAV antibodies following endopeptidase infusions that degrade circulating antibodies. This approach has been successful in formerly anti-AAV seropositive mice, non-human primates and human plasma samples *in vitro* [387]. While various pharmacotherapy interventions have succeeded in evading pre-existing immunities and the onset of immune responses, there is significant variation between studies with different anatomical targets, rAAV serotypes and animals. For instance, dexamethasone (glucocorticoid) improves AAV9 transduction of the liver but reduces transduction of the heart following retro-orbital injections in mice [388]. Similarly, prednisone (corticosteroid) reduces cytotoxic T-cell infiltration of muscle after intravenous rAAV injection in non-human primates [389] but does not affect transgene expression after intramuscular rAAV injections in mice [390].

Tissue type and route of administration influence immune responses to rAAVs [391, 392]. With direct tissue permeation, AAV vector and NAb contacts are minimised [393]. Intramuscular injections, in particular, allow only modest vector dissemination outside the target tissue [392],

are associated with low adverse events versus other administration routes [323], and pre-existing NAbs have also shown less impact on transgene expression. In rhesus monkeys with pre-existing AAV8 NAb titers of 61:160, there was no effect on expression levels, and re-administration was possible [368].

The transgene product can also trigger immune responses. In the case of optogenetics, as opsins are typically phylogenetically distinct from human cells, human immune systems will consider them 'foreign'. As the only optogenetics-based clinical trials are for retinitis pigmentosa, where the viral vector is administered via intravitreal injection, and transgene expression occurs in retinal ganglion cells [394-396], data is limited. In preclinical rodent studies, intravitreal injection of AAV2-ChR2 produced low and clinically insignificant levels of ChR2-specific antibodies, and while there was recognition by T cells, inflammation-like immune reactions persisted for only one month after injections [396]. Similar results have been reported with the expression of other ChR variants [395]. As the eye is considered immune privileged [397], these results cannot be directly translated to opsin expression in other tissues.

Immunogenicity following opsin expression in the peripheral nervous system has also been studied. In rats, anterior compartment injections of AA6 and opsin expression in the peroneal nerve, resulted in the detection of ChR2-specific antibodies, and ChR2-mediated immunogenicity was confirmed as the primary cause of opsin expression loss, motor neuron death and ipsilateral muscle atrophy. As this occurred with low and high viral loads, it suggests that all dosages of rAAV-mediated optogenetic expression within the PNS may be unsafe. However, the administration of slow-release immunosuppressants subdued ChR2-mediated immunogenicity and resulted in persistent opsin expression and functional responses to light stimulation for up to 12 weeks [335].

Finally, it is crucial to recognise the differences in immune systems between species [376, 398]. Mice, in particular, may have very different T-cell responses compared to other animals [398], with 'aberrant' T-cell responses to rAAVs, where they fail to proliferate when re-exposed [399]. NHPs may also have unique T-cell responses to AAVs, which allows them to respond better to rAAV-based gene therapy than humans [400].

1.3.3 Promoters

The promoter is a short DNA sequence that indicates where RNA polymerase commences gene transcription. Regarding rAAV-mediated gene therapy, promoters drive transgene expression and dictate the overall strength and cell-specificity of expression [319]. Promoters are

considered specific or non-specific (or ubiquitous). Non-specific promoters are active in any virally transduced cells or tissues whereas specific promoters are restricted to select tissues.

1.3.3.1 Ubiquitous promoters

Ubiquitous promoters such as CMV (cytomegalovirus promoter), CBA (chicken beta-actin) and CAG (a synthetic promoter consisting of CMV enhancer, CBA promoter and a rabbit beta-globin splice acceptor) produce robust gene expression across a broad range of cell types, and are particularly suited to cases where a gene product is secreted from multiple tissues [401]. In a 2022 meta-analysis of clinical trials using rAAVs, 50% of all studies used one of these three promoters [338]. Moreover, FDA-approved therapies for lipoprotein lipase deficiency and spinal muscular atrophy (SMA) use CMV and CBA, respectively [401-403].

Generally, CBA and CAG produced the most robust expression of the non-specific promoters. However, superior performance often equates to greater size, and at ~ 1.7kb, the use of CBA and CAG in rAAV gene therapies can be restrictive. Smaller alternates such as CMV, human elongation factor 1α subunit (EF1α) or β glucuronidase (GUSB) promoters (approximately 0.8kb, 1.2kb and 378b respectively) produce weaker expression but may be more suitable for rAAV-mediated expression of larger transgenes [404-407]. CMV and CBA also have miniaturised hybrid forms, e.g. CBh (~ 800bp [408]), that provide equivalent strong and persistent expression while allowing greater packaging capacity for other sequences.

While powerful, non-specific promoters can cause over-expression [409-411] or off-target expression [412-414], including that in antigen-presenting cells [415] and liver cells [337] that can trigger immune responses and toxicities. Finally, non-specific promoters, particularly CMV, are prone to inactivation or ‘silencing’, which can result in varied expression levels in different cell types or loss of expression over time [406, 416-418].

1.3.3.2 Tissue-specific promoters

In comparison, tissue-specific promotors limit the potential for of over- or off-target expression [319, 330, 335]. Various tissue-specific promoters exist; human synapsin (hSyn) and Calcium/calmodulin-dependent protein kinase II (CaMKII) restrict expression to neurons [274, 279], glial fibrillary acidic protein (GFAP) promoters restrict expression to astrocytes [419] and muscle creatine kinase (MCK), desmin and their derivatives restrict expression to muscle [330, 389]. Unlike non-specific promoters, tissue-specific alternatives are inert in antigen-presenting cells [416] and the potential for leakage of rAAV particles and resultant unwanted expression correspondingly, is reduced [319]. Moreover, due to attenuated immune responses and lack of

promoter silencing [416, 417], tissue-specific promoters typically improve transgene expression longevity [330, 416, 420].

The use of tissue-specific promoters can come at the expense of expression levels and size [416, 417, 421]. For example, the 6.5kb MCK is incompatible with rAAVs, and the standard truncated version is still relatively large (3.8 to 4.2kb) and typically produces weaker transgene expression than non-specific promoters [330, 331]. However, when modified, achieved by ligating a modified MCK enhancer sequence (2RS5) to a highly truncated MCK basal promoter, produced novel alternatives containing double or triple enhancers (dMCK and tMCK, respectively) with significantly higher expression levels [330]. In this de novo form, tMCK drove improved expression specificity and persistence compared to CMV [422], and clinical trials for DMD have generated strong expression in patients for up to three months [423].

Enhancer elements and modifications can be employed if tissue-specific promoter-induced expression remains insufficient. Post-transcriptional regulatory elements such as WPRE can boost expression and prevent long–term silencing [404], and CMV enhancers with tissue-specific promoters have induced tissue-specific expression levels greater than non-specific promoters alone [424]. In mice, MCK enhancer sequences combined with a robust, ubiquitous promoter (SV40) have successfully induced long-term expression (over six months) with enhanced tissue specificity, transcriptional activity and expression longevity by reducing immune responses, significantly improving CMV or CAG promoter results, where expression was maintained for only a few weeks [416].

1.3.4 Restoration of skeletal muscle function

Skeletal muscle is innervated by motor neurons whose cell bodies cluster in elongated motor nuclei within the brainstem or spinal cord. Upon reaching the muscle, motor neuron axons extensively branch to innervate a few to several thousand muscle fibres. As each branch approaches a single fibre, it splits and forms clusters of terminal branches whose tips expand and form small synaptic bulbs, which form neuromuscular junctions along the muscle fibre. When synaptic inputs exceed motor neuron depolarisation thresholds at the brainstem or spinal cord, an action potential propagates along the axon to the muscle fibre. At the neuromuscular junction, the action potential triggers the release of acetylcholine, which stimulates ion channel receptors on the muscle cell surface. Channel opening allows calcium influx, and the ensuing opening of voltage-gated sodium channels initiates the spread of depolarisation along the muscle cell and eventual muscle contraction [425-428].

Motor units, i.e. a motor neuron and associated myofibres, vary in size and composition. Small motor units typically consist of a small number of Type I myofibres that contract slowly, generate low forces, and resist fatigue. With fewer parallel ion channels across a smaller surface area, reduced myelination, and higher input resistances, small motor neurons respond to synaptic currents with larger membrane potential changes and more efficient action potential generation. Consequently, small motor units are quickly recruited for tasks requiring precise and sustained control. In contrast, large motor units are typically composed of Type IIa and Type IIx myofibres. These fibres contract faster, generate large forces and fatigue quickly. They are recruited after small motor units for tasks requiring short-term, maximal forces [425-427, 429, 430].

Where there is damage at any stage of the described pathway, skeletal muscle function can be disrupted or lost. Currently, the only clinically available method of restoring muscle function is via electrical stimulation of the peripheral nerves. Unfortunately, this is not feasible in all patients.

1.3.4.1 Electrical stimulation

Restoration of skeletal muscle function typically has been attempted via electrical stimulation applied directly to the muscle or indirectly via the descending motor tract. Clinically, direct stimulation is difficult due to large power requirements and indiscriminate co-activation of surrounding tissues, potentially resulting in poor contraction specificity and unwanted pain, sensation or movement [431]. Moreover, the mechanical and coordinative complexity and the variety and episodic nature of skeletal muscle generated movements, create significant barriers for clinical translation due to the associated hardware requirements. For instance, Hasse and colleagues (2022) [432] demonstrated progress in in achieving a repertoire of upper limb movements in monkeys by combining machine learning with kinematic and EMG data. The produced artificial neural network aimed to predict activation patterns associated with new movements. While the predicted patterns and associated stimulation trains generated upper limb movements good fidelity in some cases, substantial error was observed in others [432]. Notably, this protocol required 29 pairs of electrodes (with 58 electrode leads) to be chronically embedded within the muscles of the upper limb [432], thus limiting its clinical applicability.

In contrast, indirect electrical stimulation, or ‘functional electrical stimulation’ (FES), typically target spinal circuits below the lesion [433], or motor axons that innervate the targeted muscle [432]. These techniques are more clinically feasible, and have been used to successfully restore upper airway function in OSA patients [12, 13] or limb function following spinal cord injury or stroke [433-435]. However, like direct electrical stimulation, significant challenges remain

when aiming for ‘complex’ movements, and early applications tended to produce indiscriminate activation of local, non-targeted motor nerves and/or afferent sensory nerves [436]. That being said, more recent studies have achieved greater success. In three individuals with complete sensorimotor paralysis, a novel paddle electrode was precisely implanted, utilizing a novel computational framework, to target an ensemble of dorsal roots associated with leg and trunk movements. Within one day, activity-specific stimulation protocols elicited standing, walking, cycling, swimming, and trunk control movements, although these movements did not resemble typical endogenous movements [433].

While these advances are promising, electrical stimulation for skeletal muscle control faces several challenges. First, all applications require invasive surgery and precise electrode positioning [432, 433, 437]. Slight deviations in positions can result in varied activation patterns and/or activation of sensory afferents or non-targeted muscles. Second, motor unit recruitment via FES has typically been thought to occur in a ‘reverse’ or ‘random’ order, with larger and fatigable motor units preferentially recruited due to low input resistances [438-441]. As such, the metabolic cost of FES-induced muscle contractions is high, and rapid muscle fatigue occurs [439, 442]. Moreover, prolonged contractions require continued activation of the same fibres, and reactivation of electrically fatigued fibres is not possible [439]. Conversely, studies using epidural stimulation of the spinal cord have demonstrated both orderly and reverse motor unit recruitment in patients with chronic motor complete spinal cord injury [443]. Fatigue can be reduced via low frequency stimulation which recruits a greater proportion of slow-twitch, fatigue resistant fibres [444, 445], or via the application of multiple electrodes that recruit multiple motor axons [446]. However, regardless of the method employed, the total duration of FES should be limited, particularly when ‘optimal’ stimulation frequencies are used [445].

Currently, applications of FES are best suited to cases where motor neurons and neuromuscular junctions are intact, and coarse control with high but fatigable output is acceptable, e.g. where one motor neuron or peripheral nerve innervates a singular muscle group, performing a binary ‘on’/’off’ task. Achieving efficacy in cases where a peripheral nerve innervates multiple muscle groups and is responsible for executing complex or multiple actions will pose greater challenges.

1.3.4.2 Optogenetic stimulation

Compared to FES, indirect and direct optogenetic stimulation generate comparable contractile forces, and enhanced contractile control and resistance to fatigue [254, 439, 447]. Importantly, optogenetic stimulation preserves normal physiologically orderly recruitment of motor units [439, 440, 448], offering potential for finely controlled chronic and dynamic activation.

The high stimulating currents and subsequent risks of tissue heating and damage associated with electrical stimulation are lesser concerns with optogenetic stimulation, provided stimulation parameters are maintained within recognised safe bounds [279, 280, 449-451]. These risks can be further reduced with highly photosensitive opsins and/or red-shifted opsins that minimise light intensity requirements [267, 452]. Heating of implanted optical stimulation devices is a valid concern, particularly for preclinical to clinical translation. Fortunately, numerous strategies and technologies are being developed to overcome these challenges, including novel powering strategies, fibre optics, heat sinks and transdermal illumination which negates the need for implanted devices [253, 271, 453, 454].

Optogenetic stimulation of motor neurons and myofibres can be achieved invasively via surgical exposure and illumination of the targeted tissue [279, 455], implantation of optical devices e.g. optical nerve cuffs [440, 456] and optic fibres [455], or non-invasively by transdermal or transcranial illumination [279, 439]. While transdermal illumination was initially considered impractical due to high levels of blue light attenuation in biological tissue [457], this is likely to be more achievable with the recent development of highly photosensitive opsins [281] and red-shifted opsins [267, 452]. Activation of ReaChR opsins (red-light sensitive) in the rat vibrissa motor cortex through the skull elicited stronger whisker motions compared to blue-light sensitive ChR2 opsins in the same location. Reliable motion was achieved with the light source up to 1 cm above the skin surface [452]. Similarly, transdermal illumination has induced rodent hind limb muscle contractions and movements. Alternating contractions of the gastrocnemius and tibialis anterior were generated using two-colour transdermal illumination of spectrally different opsins expressed in the same mixed nerve [274]. In another study, transdermal illumination of the triceps surae muscles induced contractions with the light source located 1 cm above the intact musculature and skin [254]. Positioning of light sources requires significantly less precision than electrodes in FES, and they can remain a distance from their targets without unwanted activations of other muscles, nociceptors or otherwise. Therefore the risk of motor neuron and myofibre damage and inflammation [439].

1.3.4.2.1 Indirect optogenetic stimulation

Research investigating indirect optogenetic activation of skeletal muscle typically employs ChR-transgenic animals [439, 440, 455] or achieves opsin expression in motor neurons by intramuscular rAAV injection(s). Intramuscular injections frequently use AAV6, and neuronal promoters such as hSyn to target motoneurons. The optogenetic construct migrates retrogradely, and opsin expression occurs along, and is limited to, the innervating motor neurons specific to the injected muscle [274, 279, 439, 458]. This minimises any effects of incidental illumination

of adjacent motor neurons, afferent sensory neurons or the injected muscle itself [274, 279, 456]. For instance, the sciatic nerve bifurcates into the tibial and peroneal nerves which innervate the gastrocnemius and tibialis anterior respectively. Following rAAV injection into the gastrocnemius, and retrograde transport and opsin expression, illumination of the entire sciatic nerve induced muscle contractions in the gastrocnemius alone [274, 279, 456]. This allows muscles innervated by nerves too short, too deep or too highly branched for effective optic stimulation at the innervation site (e.g. the piriformis, vastus intermedius or laryngeal muscles), to be stimulated 'upstream' in a mixed nerve. Importantly, and unlike FES, selectivity for the specific muscle is retained with this strategy, and off-target activation of sensory afferents does not occur [274, 456].

Optogenetics is particularly promising for applications requiring closed-loop and activity-guided stimulation, where muscles are recruited in a cyclical and orderly manner, and/or in response to physiological conditions. Indirect optogenetics has been successfully applied to control respiratory muscles that drive airflow, e.g. illumination of the phrenic nerve to drive diaphragm contractions [459], and muscles that maintain airway patency, e.g. illumination of the hypoglossal motor nucleus to drive upper airway muscle contractions [455]. Limb muscles have also been targeted via the peroneal and tibial nerves in rodents [274, 279, 439, 440, 456] and non-human primates [460]. Illumination has resulted in the restoration of muscle activity in the hind limb and tongue in-sync with stimulation protocols [274, 279, 439, 440, 455, 456], as well as the restoration of diaphragmatic activity that persisted long after (~24 hours) illumination ceased (albeit at a reduced amplitude) linked to endogenous respiratory activity rather than the illumination protocol [459].

Optogenetic stimulation also allows greater titratability of muscle activity and contractile forces than FES.Responses can be modulated with stimulation protocol – muscle recruitment increases with greater optical power, but responses to variations in pulse width and frequency depend on the opsin expressed [272, 439]. Illumination of ChR2(H134R) results in brief and distinct muscle activations with each pulse applied. When longer pulses are used, e.g. 20ms pulses, decreases in activity with sequential pulses are observed at all frequencies [455, 460]. Shorter pulse durations, e.g. 5ms, result in similar declines at higher frequencies (>25Hz) however, at low frequencies, each light pulse produces a distinct and consistent muscle activation [456, 460]. Declines with sequential pulses are typically attributed to opsin desensitization and slow channel kinetics rather than muscle fatigue or progressive reductions in neurotransmitter release at the motor end plate [456, 460]. While ChR2(H134R) has faster kinetics than ChR2 due to its H134R gain of function mutation, optimal performance is typically restricted to frequencies

under 25Hz [456, 460]. However, improved performance and tunability of muscle activation can be achieved with ultra-fast opsins whose faster kinetics allow high-frequency protocols up to 200Hz [272], and can produce finely controlled tetanic contractions with high temporal resolution [268, 272, 461].

Optical stimulation can maintain muscle activation by recruiting additional fibers or reactivating optically fatigued fibers [439]. Indirect optical stimulation (1 Hz) can induce sustained tetanic tension for over 20 minutes, whereas FES-induced tension rapidly declined after onset, maintaining an equivalent tension for ~ 20 seconds and dropping to zero after 4 minutes [440]. Periodic activation via FES still induced fatigue at approximately 20 seconds, and further increases in stimulation could not maintain contractions. Opsin reactivation then permits a gradual return to and maintenance of chronic cyclic plantarflexion [439]. Optogenetic stimulation also allows alternating motor neuron recruitment with sub-maximal stimulation levels, thus enabling reactivation and persistent periodic activation. This suggests that opsin-expressing tissues undergo cyclic sensitivity and are amenable to long-term, fatigue-resistant stimulation [439].

Unlike FES, opsin expression in the PNS and CNS are subject to immune responses, and ChR-mediated immunogenicity has produced motor neuron death and muscle atrophy [335]. While the immune responses were inhibited using slow-release tacrolimus pellets, caution is required when targeting these systems [335].

Finally, the efficacy of indirect optogenetic stimulation of skeletal muscle depends on the integrity of the motor neurons and neuromuscular junctions. Accordingly, it is unsuitable for use in conditions where there is axonal damage/degeneration such as in amyotrophic lateral sclerosis (ALS). While restoring innervation and function via transplanting ChR2 expressing embryonic motor neurons or motor neurons derived from pluripotent cells is feasible [462, 463], this approach has significant technical and biological restrictions that hinder clinical applications. Direct optogenetic stimulation of skeletal muscle overcomes many of these issues.

1.3.4.2.2 Direct optogenetic stimulation

As the name suggests, ‘direct’ optogenetic stimulation of skeletal muscle cells entails opsin expression and light stimulation applied directly to the muscle. Direct optogenetic stimulation has been achieved as proof-of-concept [235, 254, 255] and could overcome the risks of neurally-targeted therapy [335]. To date, four studies report direct optogenetic stimulation of skeletal muscle. Two used ChR2(H134R)-transgenic animals with complete or near complete opsin expression and demonstrated strong light-evoked muscle contractions in explanted soleus

muscle, laryngeal muscles [235], and triceps surae muscles [254]. Contractions were also achieved in denervated, but intact triceps surae muscles following transdermal illumination [254]. Continuous illumination of muscle produced transient force generation, with an initial peak in activity followed by an eventual decline to baseline levels [235, 254]. In the laryngeal muscles, this equated to initial vocal cord opening and subsequent reclosure [235]. In contrast, pulsed illumination produced strong and sustained forces that could be modulated with light intensity, pulse duration and pulse frequency. Increased light intensity produced greater force by efficiently traversing tissue and activating more myofibres expressing ChRs [235, 254]. Increased pulse widths initially increased force generation [235, 254]. Bruegmann et al found that these increases plateaued at ~50 ms pulse widths (maximum duration tested was 150 ms) [235]. In contrast, Magown et al found that the generated forces plateaued between 10 and 100 ms, but further increased when illumination exceeded 100 ms (to 1,000 ms) [254]. Both studies found higher frequencies of pulsed illumination produced greater forces [235, 254]. Low repetition rates ($\leq$ 10 - 20 Hz) produced incomplete tetanic contractions with brief relaxations between light pulses, but frequencies exceeding ~ 30 Hz produced tetanic contractions [235, 254]. Efficacy then reduced when frequencies exceeded 40 Hz [235], likely due to ChR2(H134R)'s slow off-kinetics which precluded repolarization (time constant of deactivation ~ 20 ms [265]). 10 ms and 40 Hz stimulation of the laryngeal muscles produced maximal vocal cord opening, however with the optimization of duty cycles to minimize the risk of photodamage, 2 ms pulses at 40 Hz was considered the optimal protocol [235]. Importantly, optimised pulsed illumination protocols were able to generate forces equivalent to those achieved via electrical stimulation [235, 254], and the greatest forces generated using optogenetics were approximately 84% of the greatest forces generated by the most effective electrical stimulation protocol [235]. Fatigue was comparable to that seen with FES protocols when 350 ms long stimulation patterns were repeated 10 minutes [235], but optical stimulation was found to be inferior when similar protocols were applied over 2 minutes [254].

While these results in transgenic animals are promising, implementation of optogenetics in humans requires gene transfer. To date, three studies have used rAAVs for opsin expression in laryngeal muscles, the diaphragm and more recently (2023) the tongue [235, 255, 464]. All used a standard rAAV serotype, rAAV9 and a non-specific promoter to drive the expression of a standard channelrhodopsin variant (ChR2(H134R) [235] or ChR2 [255, 464]) fused to a fluorescent reporter protein for expression visualization [235, 255, 464]. In Bruegmann et al. (2015) [235], systemic injection into the left jugular vein of 2×10^{11} genome copies produced ChR2(H134R):mCherry expression in only 10.2±3.6% of the posterior cricoarytenoid muscle fibres four weeks after administration, and pulsed illumination produced a poor functional

response in explanted larynges with transient vocal cord opening, which declined to baseline during stimulation [235]. In Benevides et al. (2022), which exclusively looked at rAAV-mediated opsin expression, 6.12×10^{11} genome copies delivered to the diaphragm via microinjection to the intrapleural space produced ChR2:mVenus expression in 18±2% of diaphragm myofibres. Expression levels remained up to 18 weeks after vector administration, and in a paralysed diaphragm (in vivo), pulsed illumination applied via a laparotomy evoked diaphragm EMG potentials and contractions sufficient to generate respiratory airflow [255]. Similar results were recorded in the tongue following intralingual injections of the same construct (8.29×10^{11} genome copies). Light-evoked EMG responses recorded while the animal was anaesthetized, and light stimulation was applied intraorally to the tongue [464]. As in the transgenic animal experiments, responses to light stimulation could be graded by altering stimulation protocol, with EMG amplitudes increasing with intensity or duration of the light pulse [255, 464].

The aformentioned studies provide initial proof of concept for direct optogenetics for skeletal muscle, however significant work is required prior to clinical translation. Greater muscle-specificity and intramuscular injections have been recommended for improved rAAV-mediated opsin expression [235] and may aid in reducing off-target expression and systemic distribution of the rAAV and subsequently reduce the risk of immune responses and improve safety [323]. Advances in vial transduction and opsin technology may aid this. Novel AAV serotypes [344] and muscle-specific promoters [330] have generate stronger expression in muscle fibres [330, 344] and liver detargeting [344]. Ultrafast opsins may increase efficacy at greater frequencies [268, 272, 461], and due to the superior penetration of red-light, red-shifted opsins may facilitate stronger light-evoked muscle contractions at greater tissue depth [267, 452]. Additional considerations for clinical translation, including immune responses to rAAV administration, biodistribution of viral particles and off-target gene expression, also need systematic research.

1.3.5 Optogenetics technology

Successful optogenetic activation of skeletal muscle requires an efficient light delivery method to the target tissue. Optogenetics in animals began in neural applications with ‘tethered’ hardware, i.e. external light sources connected to surgically implanted optical fibres protruding into brain tissue and secured to the skull. Naturalistic behaviour was impossible [465] and tissue damage was common due to the stiffness mismatch between hardware and surrounding soft tissues [466, 467]. On the other hand, tethered systems benefit from comparatively unrestricted optic power, ease of device manufacture, surgical implantation, and data acquisition.

Lightweight and flexible patch cables and rotary joints can relieve torsional stress during movement and aid natural behaviour. Early ‘wireless’ hardware requires bulky externally mounted stages affixed to static bony structures (typically the skull), have limited battery lives and therefore limited experimental durations/protocols. Movement remains somewhat restricted, and the bulky devices present a potential danger to the animal and its cage mates [468]. Both systems (tethered and wireless head-mounted) increase the risk of infection at the interface site.

However, optogenetic technology in animals is rapidly evolving, and advances in material science, wireless power and data transfer, and hardware miniaturisation allow light stimulation to be delivered by wireless and completely or partially implanted devices that allow free animal behaviour, with minimal tissue trauma and environmental risks [469-473]. Robust but soft, thin, bendable and stretchable materials minimise potential damage to the device and the surrounding tissues during implantation and natural post-surgery movements [466, 467]. Technologies such as ‘serpentine-shaped’ electrodes on hyperelastic substrates [474] or soft, polymer-based kirigami [472, 475] or mesh structures [476] with integrated LED chips and recording electrodes aim to conform to tissues (e.g. heart), minimise damage and allow natural tissue movements (e.g. heart beating) by minimising mechanical mismatch [472, 474-476]. Additionally, the versatility of these stretchable and bendable materials increases the accessibility of complex and dynamic tissues. Indirect optogenetic stimulation of skeletal muscle can be achieved via novel optic cuffs with LEDs implanted along the internal diameter. Spiral optic cuffs around the sciatic nerve were well tolerated by awake and moving mice, and successfully stimulated contractions specific to the muscle that received rAAV injections [456]. Nerve cuffs have also been developed to simultaneously record neural activity and deliver light stimulation to peripheral nerves. One such cuff successfully monitored and altered limb position in freely moving animals [477].

Additional options are available when the muscle or neural targets cannot be effectively reached with visible light due to complex anatomy that restricts local device implantation and/or significant tissue depth that restricts transdermal illumination. ‘Luminopsins’ are fusion proteins of luciferase (light-generating protons) and opsins (light-activated proteins) which can be activated by extrinsic and intrinsic light sources. Luciferase bioluminescence is triggered by injections of the equivalent luciferin, which can then trigger opsin activation. While this method cannot achieve temporally precise activation, it can sensitise cells to fire action potentials in response to subthreshold synaptic currents, be they endogenous or technologically derived. Luminopsins also allow greater volumes of opsin-expressing tissue to be activated, as the light source is not limited by light attenuation but is fused to every opsin [478-480].

Another approach that has been explored is the use of embedded nanomaterials that convert wavelengths such as focused ultrasound or near-infrared light (NIR) to visible wavelengths, allowing distant muscle to be reached by subcutaneous or transcutaneous devices. Lanthanide-doped upconversion nanoparticles (UCNPs) locally convert NIR light into the visible wavelength required for opsin activation. A small UCNP device (~2 mm long, ~500 um diameter) implanted in the spinal cord evoked hind limb EMG activity in ChR2 expressing rodents with transdermal pulsed NIR stimulation [481]. Alternatively, zinc sulfide nanoparticles co-doped with trace amounts of silver and cobalt can be injected into the bloodstream, charged with 400nm light when passing through superficial vessels, and subsequently triggered with ultrasound to emit blue light in deep tissues to stimulate ChR [482]. Finally, radioluminescent nanoparticles, which absorb external x-rays and emit photons with wavelengths of ~ 610 nm, have been used for transcranial stimulation of deep cortical structures where neurons express red-shifted ReaChR [483].

1.3.5.1 Translation into human applications

Despite the rapid technological advancements in preclinical settings, the equivalent technology required for human translation remains in its infancy. While some advances from preclinical research will translate well, i.e. materials advances such as flexible substrates and/or mesh-like materials with embedded electronic components, several hurdles remain. A key issue is the poor penetration of visible light through the much larger human muscles (preclinical research is often conducted in rodents), and the associated scaling of technology.

Optogenetics in humans is currently limited to clinical trials for retinitis pigmentosa, where visual function can be partially restored. Unlike all but the most superficial skeletal muscle cells, retinal ganglion cells are optically accessible, and stimulation of the ChrimsonR (a red-shifted opsin) expressing cells is possible via red-light projected by goggles that detect changes in local light intensity [484]. For light delivery to most skeletal muscles, optogenetic control will need either implanted light sources or external light sources delivering light at wavelengths that can penetrate into the target tissues. Moreover, while indirect optogenetic stimulation of muscle may be able to adapt existing technology used in electrical stimulation of peripheral nerves, by substituting electrical for light stimuli [12] and nerve cuffs used in preclinical optogenetic applications [477], direct muscle optogenetics will likely require significantly greater technological innovation due to the complexity of delivering light to contracting muscles.

Hardware for light delivery to skeletal muscle will depend on the location and size of the target muscle. While superficial muscles may potentially be transcutaneously stimulated by wearable

devices (e.g. the small and relatively accessible upper airway muscles, such as those within the tongue, are involved in breathing, swallowing and/or speech, and accessible via the oral cavity), deep muscles, e.g. the diaphragm, may require surgically implanted light sources and/or the use of nanoparticles that locally convert highly penetrating wavelengths (NIR or ultrasound) to visible light wavelengths [481, 482] as described above When implanted devices are used, LEDs can be implanted near or within the target muscle or alternatively where space is limited, remote light sources can connect to optical fibres whose tips are near or within the target muscle. Due to the size of many human muscles, single LEDs or optical fibres will likely be insufficient for all but the smallest of muscles targeted. LED arrays, or optical fibres with splitters, multiple mirrored exposed points, or tapered ends are potential solutions to maximise the field of illumination [472, 475, 476, 485]. However, these methods come at the cost of optical power, as each light emitting site will reflect only a portion of the power generated by a single primary light source. The use of multiple light sources, on the other hand, increases power requirements and subsequent risk of tissue damage. It is worth noting that heating induced damage can typically be mitigated by considered selection of stimulation parameters (i.e. pulse width, frequency, duty cycle etc.) [235, 248, 453] and, while the degree of heating is application-specific, most pre-clinical devices report operational temperature increases of less than 1°C [252, 470], well below the ~2°C safety threshold for implanted biomedical devices (ISO-14708-1), and irreversible tissue damage [486, 487].

Optogenetic stimulation devices must be integrated with any required sensing and control hardware, plus a power source, and novel technology used in preclinical may be feasibly translated to clinical applications. Existing clinically approved electrical devices already use ‘closed loop’ stimulation, e.g. some hypoglossal nerve stimulators use pressure sensors implanted in the extrapleural space to detect inspiration onset, and novel technology e.g. implanted stretchable strain gauges encircling the target muscle to identify pathological behaviours have also been proposed to as inputs to control delivery of optogenetic stimuli [252, 488]. In contrast, transdermal devices may use more basic technology such as external inertial measurement units to monitor joint velocity and angle and control limb position and movement, e.g. in patients with foot drop as a result of a neurological, anatomical, or muscular problem [489].

In summary, while there remain many challenges in developing technology for clinical applications of direct optogenetic muscle control, the outlook is positive and developments are progressing rapidly. Successful, clinically acceptable technology must address the needs to each therapeutic application, and this requires careful consideration of the anatomy (target muscle

size, location, and type), stimulation requirements (light penetration, intensity, temporal profile and duty cycle) and control elements (sensors, control systems). In turn, the combination of these parameters will define the power requirements and possible methods of powering the system (battery, inductive power etc). Such systems must also be safe and comfortable for patients to use and meet all the required regulatory standards for medical devices.

Chapter 2 OPTIMISING THE VIRAL CONSTRUCT: PROMOTERS

2.1 INTRODUCTION

Inadequate activity of upper airway muscles during sleep, when combined with anatomical risk factors (e.g. a longer and narrower pharynx [129, 130], fat accumulation in upper airway soft tissues, and a narrow/crowded airway [35, 98, 130-132]) is a major contributor to obstructive sleep apnoea (OSA) [9-11]. Despite increasing OSA prevalence, due in part to aging and overweight populations [2, 3], and the significant clinical, social and economic consequences [4], therapeutic options remain suboptimal. 'Gold-standard', Continuous Positive Airway Pressure (CPAP), is efficacious but variably tolerated, with 46-83% of patients reported to be non-adherent [5]. Second line treatments including mandibular advancement splints, upper airway surgery, and hypoglossal nerve stimulators have superior adherence, but variable and unpredictable efficacy [6, 7, 490]. Of these, only hypoglossal nerve stimulation directly targets upper airway muscle activation.

Recently, gene therapy approaches for neural and muscle cell stimulation have emerged, including optogenetics, chemogenetics, and magnetogenetics using light, chemical and magnetic stimuli respectively to activate genetically modified cells [16, 232, 235, 254, 491]. In the context of OSA, a chemogenetic approach using designer receptors exclusively activated by designer drugs (DREADDs) targeting hypoglossal motor neurons has increased dilator muscle tone and widened the pharynx in transgenic animals and after intralingual viral vector injections [16, 232]. However, the safety of chemogenetic ligands and the long-term safety and efficacy of gene therapy targeting the nervous system remain to be established.

Optogenetics involves light stimulated activation of excitable cells modified to express light-sensitive ion channels, e.g. channelrhodopsins (ChR), an algae derived non-selective cation channel [262]. A key advantage of optogenetics is that spatially and temporally precise control of activity is achievable by adjusting the frequency and duration of light pulses. This enables pain-free tetanic muscle contractions similar to electrical stimulation [235, 254, 439].

Optogenetic induced muscle contraction is commonly achieved via 'indirect' stimulation of upstream motor neurons [439, 440, 456]. Unfortunately, peripheral and central nervous system targets have been associated with motor neuron death and muscle atrophy in rats, thought to be elicited by ChR-mediated immunogenicity [335]. 'Direct' optogenetic stimulation of skeletal muscle cells, while less studied, has been achieved as proof-of-concept [235, 254, 255, 464], and could overcome the risks of neurally-targeted therapy. Implementation in humans requires gene transfer, such as via recombinant adeno-associated viruses (rAAVs), similar to the

approach used for in vivo chemogenetic activation of hypoglossal motor neurons in mice [16]. Importantly, rAAV vectors are approved for use in humans for the treatment of RPE65-mediated inherited retinal dystrophy [339] and pediatric spinal muscular atrophy [492], demonstrating potential for clinical translation of other rAAV-based gene therapies.

The success of any gene therapy is influenced by the choice of promoter that controls gene transcription. While non-specific promoters are more frequently used, tissue-specific promoters that restrict gene expression to target tissues/cells minimise off-target effects and immune responses, improving the safety profile [319, 330, 335, 336]. For muscle stimulation therapy, an optogenetic construct that incorporates a muscle-specific promoter, packaged in an rAAV vector that efficiently delivers it to muscle cells, has potential to overcome poor expression and suboptimal efficacy seen with systemic delivery of non-specific promoter-driven constructs [235]. In the context of an OSA therapy, local intramuscular delivery enables targeting of specific upper airway muscles necessary for maintaining patency [16, 235].

The objective of the current study is to assess the potential for optogenetic stimulation of specific upper airway muscles to effect airway dilation in a rodent model of OSA simulating reduced dilator muscle activity akin to that experienced by OSA patients during sleep. The specific aims of the study were to (1) identify a suitable rAAV serotype and promoter combination for efficient, localised muscle-selective optogenetic transduction of lingual dilator muscles; (2) characterise biodistribution of the optogenetic construct following intramuscular tongue delivery; and (3) determine optimal optical illumination parameters to generate robust muscle activity in phase with the respiratory cycle.

2.2 METHODS

2.2.1 Animals

All procedures were approved by the Animal Ethics Committee, Macquarie University, Australia and accord with The Australian Code of Practice for the Care and Use of Animals. Sprague-Dawley (SD) rats were purchased from the Animal Resources Centre (Perth, Australia). All animals were group-housed in a dedicated housing room under a 12-hour light/12-hour dark cycle, and food and water were available ad libitum.

2.2.2 AAV vectors

Two AAV9 vectors were used in this study, one incorporating a non-specific promoter (CAG) and one a muscle-specific promoter (tMCK). Both vectors included a channelrhodopsin-2 variant with a gain of function substitution (ChR2(H134R)).

The AAV9-CAG-ChR2(H134R)-mCherry vector (titre: 3.3×10^{13} vg/mL) was purchased from the AddGene Plasmid Repository. The plasmid was donated to the repository by Karl Deisseroth's lab (Addgene viral prep # 100054-AAV9; http://n2t.net/62ncorpo:100054; RRID: Addgene_100054). This vector employs a strong synthetic and non-specific promoter, CAG, to drive high levels of gene expression. This promoter combines the cytomegalovirus early enhancer element I, the promoter, first exon and first intron of the chicken beta-actin gene (A) and the splice acceptor of the rabbit beta-globulin gene (G) [493]. The ChR2 expression levels can be visualised by fluorescent microscopy due to the incorporation of mCherry, a red fluorescent protein.

A muscle-specific promoter was employed to determine whether ChR expression could be restricted to the skeletal muscle of the tongue. Due to its size, standard muscle creatine kinase (MCK) promoters are incompatible with viral vector applications. MCK can be condensed by ligating a triple tandem of MCK enhancer (206-bp) to its 87-bp basal promoter resulting in a compact (720-bp), muscle-specific tMCK promoter [330]. The muscle-specific expression cassette sequence, pAAV-tMCK-ChR2(H134R)-mCherry, was developed by GenScript (New Jersey, USA), and packaged into an AAV9 vector by the Vector and Genome Engineering Facility (Children's Medical Research Institute, Westmead, Australia). The ChR2 expression levels can be visualised by fluorescent microscopy due to the incorporated mCherry, a red fluorescent protein. The final product, AAV9-tMCK-ChR2(H134R)-mCherry had a titre of 9.04×10^{12} vg/mL.

2.2.3 Intramuscular AAV injection

4 male SD rats received intramuscular injections of the CAG construct (mean ± SD, age = 8.00 ± 0.00 weeks, weight = 278.8 ± 8.93 g), and 6 male SD rats received intramuscular injections of the tMCK construct (mean±SD, age = 8.07 ± 0.07 weeks, weight = 256.5 ± 9.67 g) under general anaesthesia, induced with 5% Isoflurane in oxygen in an induction chamber and maintained using 2-3% Isoflurane in oxygen delivered at a rate of 1 L/min through a nose cone. Adequacy of the anaesthesia was assessed using the negative pedal withdrawal response and was regularly monitored until the end of the procedures. Animals received an injection of carprofen (an NSAID, 5 mg/kg) for pain relief, and cefazolin (an antibiotic, 25 mg/kg).

A 25 µL syringe (model 702 LT SYR, Hamilton Company) connected to a sterile 26-gauge needle was used to inject 20 µL of the viral vector construct into four locations (5µL per site) in the animal's tongue (Figure 2-1A). The solutions were injected slowly, and the syringe held in place for an additional 30 seconds after the injection before being slowly retracted from the

muscle to avoid virus loss. Animals were then allowed to recover from the anaesthesia before being returned to their cage.

These injections aimed to saturate the tongue muscles with opsin expression. This objective was informed by prior studies utilizing electrical stimulation that observed greater airway dilation, pharyngeal stiffening and increased airflow when multiple tongue muscles (i.e. intrinsic and extrinsic, protruders and retractors) rather than a single muscle group was stimulated [36, 37, 46, 72].

2.2.4 Electrophysiology measurements

All tMCK animals underwent electrophysiology studies 3 weeks following vector administration to allow for sufficient ChR expression in the tongue (mean ± SD, age = 11.0 ± 0.07 weeks, weight = 405.0 ± 30.3g). Anaesthesia was induced using 5% isoflurane in oxygen in an induction chamber and was maintained via using 2-3% isoflurane in oxygen delivered at a rate of 1L/min through a nose cone. Adequacy of the anaesthesia was assessed based on the negative pedal withdrawal response and was regularly monitored until the end of the procedure. The animal's body temperature was monitored via a rectal thermometer and maintained via a temperature controlled warming blanket. The animal's breathing rate was monitored to prevent respiratory depression.

Genioglossus and diaphragm activity was monitored via 0.005" diameter isonel-insulated stainless steel wire (MWS Wire Industries, CA, USA) with the hook stripped bare. EMG signals were amplified, band-pass filtered (30 – 1000Hz; Bioamplifier from CWE Inc., PA, USA) and sampled at 5kHz with an analogue-digital converter (CED1401 plus, Cambridge Electronic Designs, UK). Optical stimulation (LED, 470nm) was delivered intraorally to the ventral and posterior surface of the tongue (crosshatching, Fig.1A). Single pulses (1 to 300ms) and pulse trains (1 to 20 ms, 10 to 60 Hz) tested. Following initial data acquisition, endogenous genioglossus activity was reduced by gradually increasing isoflurane concentrations to 5%.

After data was acquired and with isoflurane concentration at 5%, rats were deeply anaesthetised using sodium pentobarbitone (>200 mg/kg) and intracardially perfused with phosphate buffered saline (PBS) followed by 4% paraformaldehyde.

EMG data was processed in MATLAB. The effect of the 470 nm light on the genioglossus was quantified by calculating the area under the rectified EMG trace from light onset until its return to basal levels. Adjacent stimulated and unstimulated EMG activity was collected and 'normalised' against the same calculations of the genioglossus activity associated with one inspiratory phase that produced visible tongue movement prior to isoflurane induced reductions

in activity. This produced a percentage to which the application of light restored EMG activity to maximal levels.

2.2.5 Histology and immunofluorescence staining

Following perfusion of both the CAG (mean ± SD, age = 11.0 ± 0.00 weeks, weight = 406.5 ± 21.8 g) and tMCK cohorts (mean ± SD, age = 11.0 ± 0.07 weeks, weight = 405.0 ± 30.3 g) three weeks following the intramuscular injections, the brainstem and tongue were extracted and post-fixed with 4% paraformaldehyde overnight at 4°C. They were then washed three times in PBS and stored in PBS.

Brainstems were sectioned with a vibratome (Vibratome VT1200S, Leica) into 80 µm thick, transverse slices. 1 in 4 sections were washed three times in PBS with 0.1% Tween-20 (PBT). Immunohistochemical staining was performed in a primary antibody solution (tris phosphate buffered saline (TPBS) with rabbit anti-RFP (Abcam AB62341, 1:1000), goat anti-Chat (Merch Millipore AB143, 1:1000) and normal donkey serum (NDS, 1:10)) for 24 hours at room temperature on a shaker. Following another three washes in PBT, the sections were incubated in a secondary antibody solution (TPBS with donkey anti-rabbit 555 (Invitrogen A32794, 1:500), donkey anti-goat 647 (Invitrogen A32816, 1:500) and NDS (1:20)) for 4 hours at room temperature on a shaker before a final washing with PBS. The brainstem sections were then mounted with a fluorescent mounting media (ProLong™ Golf Antifade Mountant, ThermoFisher) and imaged using a confocal microscope (LSM800 with Airyscan, Zeiss). Opsin:reporter protein expression in the brainstem was quantified as the percentage of ChAT positive cells that co-express the ChR2(H134R):mCherry fusion protein. In ImageJ, ChAT-positive and ChR2(H134R):mCherry-positive cells were identified via fluorescence intensity thresholding and segmentation. This was performed in 7 brainstem sections that included the hypoglossal motor nucleus per animal. All other brainstem sections were visualised to ensure no other fusion protein expression was present.

The tongue tissue was cryopreserved in a 30% sucrose solution until the specimens sank (24 to 48 hours). The tissue was then sectioned with a cryotome (Cryostat CM1950, Leica) into 80 µm thick, transverse slices. 3 main regions of the tongue were sectioned. The ‘tip’, ‘middle’ and ‘base’ regions were located approximately 5 mm, 10 mm and 15 mm from the rostral end of the tongue respectively. The tongue sections were then mounted with a fluorescent mounting media and imaged using a confocal microscope. Expression of the ChR2(H134R):mCherry fusion protein was quantified in ImageJ by determining the percent of tissue pixels over a ‘no expression’ brightness threshold.

2.2.6 DNA and RNA Quantification

An additional cohort of animals (n = 4) received intramuscular injections of the tMCK construct as described above. Three weeks later fresh tissue was harvested from the heavily anaesthetised animals undergoing saline perfusion immediately prior to paraformaldehyde fix. The tissue was snap-frozen in liquid nitrogen. Liver, spleen, gastrocnemius and diaphragm muscles were collected. Tongue, heart, and brainstem were removed from one animal, to serve as a comparison for the gene expression data from other organs[1].

Fresh frozen tissue samples were minced and divided for separate DNA and RNA extraction. DNA extraction was performed by homogenising the tissue samples in equal volumes of phenol-chloroform-isoamyl alcohol and TE buffer, to a total volume of 1 mL. Samples were centrifuged at 20,817 xg for 20 minutes. The aqueous layer was removed to 0.5 mL phenol-chloroform-isoamyl alcohol, mixed thoroughly, and centrifuged again. The second aqueous layer was removed and added to a 2.5× volume of 100% ethanol with a 0.1× volume of 3M sodium acetate (Sigma Aldrich), then incubated at -80ºC for 1 hour. DNA was pelleted by centrifugation, washed twice with 70% ethanol, and resuspended in TE buffer.

RNA was extracted by homogenising the samples in 1 mL of Trizol, followed by the addition of 200µL 1-bromo-3-chloropropane. Samples were centrifuged at 20,817 xg for 20 minutes, then the aqueous layer was removed to 70% isopropanol and incubated at -20ºC overnight. RNA was pelleted by centrifugation at 20,817 xg for 20 minutes, then pellets were washed twice with 70% ethanol, dried, and resuspended in nuclease-free water.

DNA and RNA samples were quantified using a Nanodrop spectrophotometer (Thermo Fisher) and diluted to 100 ng/µL (DNA) or 200 ng/µL (RNA). After 2 hours of ezDNase treatment at 37C (Invitrogen), RNA was used to generate cDNA using SuperScript IV VILO Master Mix (Invitrogen) in a 20 µL reaction. cDNA and genomic DNA were quantified with PowerUp SYBR Green Master Mix (Invitrogen) using 1 µL template in each 10 µL qPCR reaction, using a Viia 7 PCR machine (Thermo Fisher). Primers for ChR2, and for the housekeeping genes YWHAZ and RPL13, were purchased from Integrated DNA Technologies and used at a final concentration of 500 nM each. Primer sequences and thermal cycling protocols are listed in supplementary data.

Relative expression quantification was used for RNA by comparing ChR2 expression with YWHAZ expression. Genomic DNA was assessed with absolute quantification, by calculating vector copy number per ng of the housekeeping gene RPL13, compared to standard curves.

[1] DNA and RNA tissue harvesting and analysis was conducted by Dr Myfanwy E. Cohen, NeuRA

Standard curves used for ChR2 calculations were constructed from linearised plasmid DNA (plasmid 100054, AddGene). For absolute quantification of DNA, one sample was assessed with a Qubit to determine the exact DNA concentration, then serial dilutions of this sample were used to construct the standard curve.

All reagents were purchased from Sigma Aldrich (NSW, Aus) unless otherwise specified.

2.2.7 Statistics

Gene quantification statistical analysis was performed with GraphPad Prism (v9.3, GraphPad software LLC). A repeated-measures 2-way ANOVA with Bonferroni post hoc analysis was conducted to compare the tMCK and CAG construct induced ChR2(H134R)-mCherry fusion protein expression in the tongue.

Gene quantification in the tongue, diaphragm, gastrocnemius, liver, spleen, heart and brainstem following tMCK construct injections was analysed via a one-way ANOVA with multiple comparisons, using Tukey post-hoc corrections.

The effect of light stimulation on EMG activity within the tMCK cohort was analysed in SPSS via a linear mixed model with fixed and random effects to account for multiple data sets from each animal, with an unstructured covariance structure, and Bonferroni post hoc tests. Adjacent 'unstimulated' and 'stimulated' EMG data sets were binned based on the 'unstimulated' EMG data. Bins were created in 10% intervals from 0% to 100% of the maximum unstimulated EMG activity. Equivalent bins for each animal were then compared.

2.3 RESULTS

2.3.1 Use of a muscle-specific promoter consistently induced strong ChR2 expression

Intramuscular injections of the optogenetic constructs resulted in opsin expression in the muscles of the tongue. The muscle-specific tMCK promoter produced stronger and more widespread expression than the non-specific CAG promoter (Figure 4-1B-D) despite a lower titre (1.81×10^{11} vector copies for tMCK vs 6.60×10^{11} vector copies for CAG). Across the tongue, tMCK produced 4.7-fold greater expression than CAG (RM-ANOVA, $F(1,8)=10.0$, $p=0.013$, Figure 4-1B), with the greatest differences in the middle region (4.4-fold higher expression with tMCK, Bonferroni post hoc, $p=0.032$). There were no significant differences in expression in the base and tip regions of the tongue between the promoters (Bonferroni post hoc, $p=0.053$ and $p=0.94$ respectively). Additional opsin expression distribution details are illustrated in Figure S2.

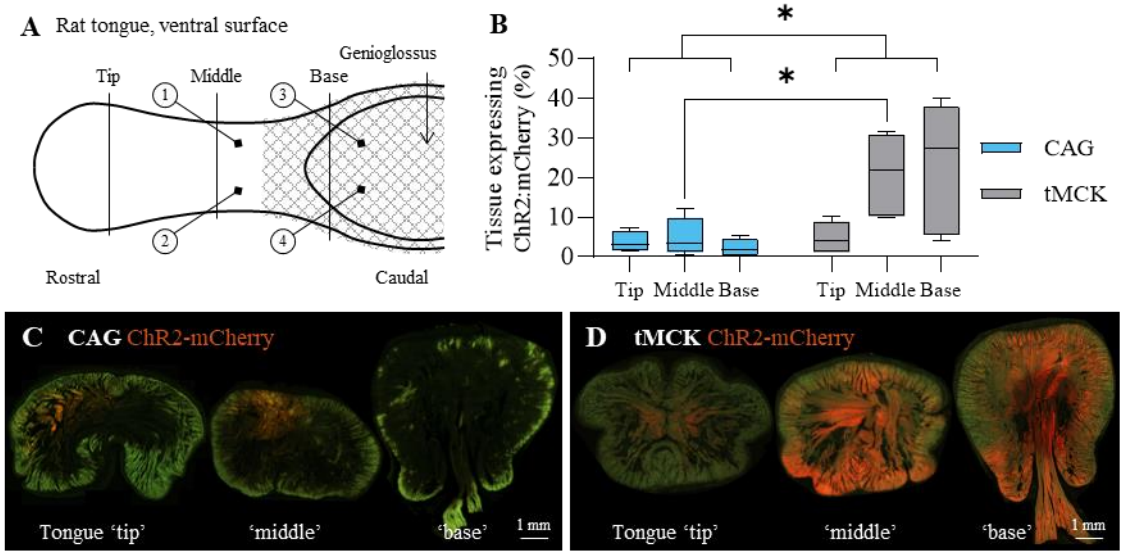

Figure 2-1 | Non-specific (CAG) and muscle specific (tMCK) promoter driven expression in the tongue. (A) Diagram of the ventral surface of a rat tongue, with the approximate location of the genioglossus identified. Viral vectors were injected intramuscularly at sites 1 to 4. Light was applied to the crosshatched region and tongue EMG activity measured via fine wire electrodes inserted near sites 1 to 4. For histology, the tongue was sectioned through the transverse planes in the tongue 'tip', 'middle' and 'base'. **(B)** The tMCK promoter (grey, n=6) produced greater protein expression in the tongue compared to the CAG promoter (blue, n=4) (p=0.013). **(C, D)** Weaker and less widespread membrane-bound ChR2(H134R):mCherry fusion protein (orange) expression is seen in representative images of the tongue tip, middle and base sections from a **(C)** CAG than a **(D)** tMCK animal.

2.3.2 The muscle-specific promoter minimises off-target expression

Protein expression in the brainstem was seen with the CAG promoter but not the tMCK promoter. ChR2(H134R):mCherry fusion protein expression in the brainstem hypoglossal motor nucleus due to retrograde transport along the hypoglossal motor neuron was quantified by the co-expression of the fusion protein and choline acetyltransferase (ChAT). Co-expression was found in 8.7±3.9% (mean±SD) of motor neurons in the CAG animals (Figure 2-2A), with no evidence of preferential expression in hypoglossal nucleus subdivisions amongst the cohort [56-59]. Co-expression was absent in all tMCK animals (Figure 2-2B). Neither construct induced expression in any other brainstem region, motor nuclei, sensory tract or terminal fields, including but not limited to facial, trigeminal and vagal motor nuclei, sensory trigeminal nuclei and the nucleus of the solitary tract.

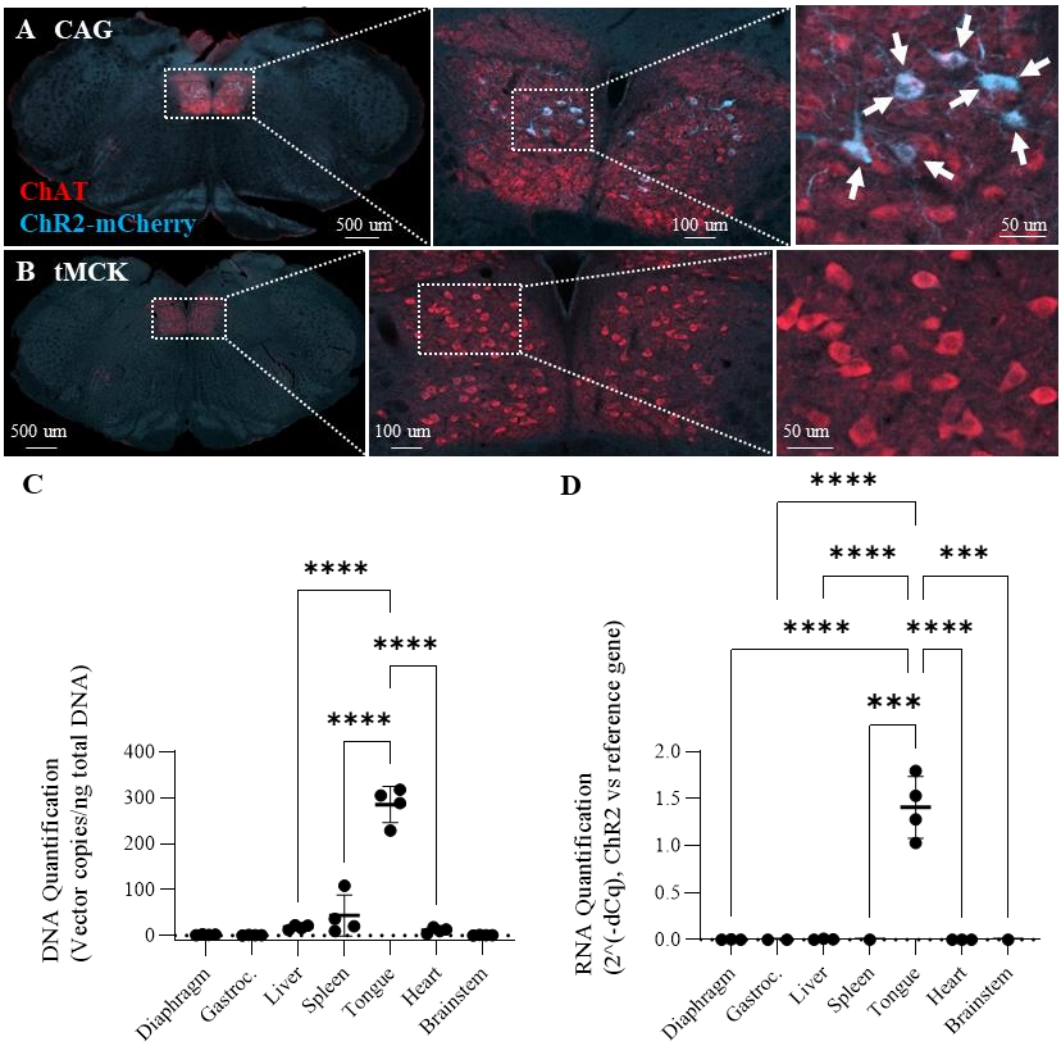

Figure 2-2 | Biodistribution after intramuscular delivery of the tMCK and CAG constructs. (A) 3 weeks following intramuscular delivery of an rAAV construct, ChR2(H134R):mCherry fusion proteins are visible in 8.7±3.9% (mean±SD) of ChAT positive hypoglossal motor neurons in animals that received the CAG construct, **(B)** but are absent in animals that received the tMCK construct. **(C)** The tMCK cohort exhibited robust levels of viral DNA and **(D)** RNA expression in the tongue, and minimal or no expression in organs (spleen, liver and heart), and other skeletal muscles (gastrocnemius and diaphragm), thus confirming the specificity of the tMCK construct (^=diaphragm, gastrocnemius and brainstem viral DNA levels were below the limits of detection). *** P<0.001 and **** P<0.0001 by one-way ANOVA and Tukey Test.

Viral DNA from animals administered the tMCK construct was found abundantly in the tongue, but was not detectable in other skeletal muscles (diaphragm, gastrocnemius) (Figure 2-2C). Viral DNA was also found in the liver, heart and spleen in very low copy numbers, but was not detectable in brainstem tissue samples. RNA expression was only found in the tongue, where it was abundantly expressed relative to the housekeeping gene (Figure 2-2D).

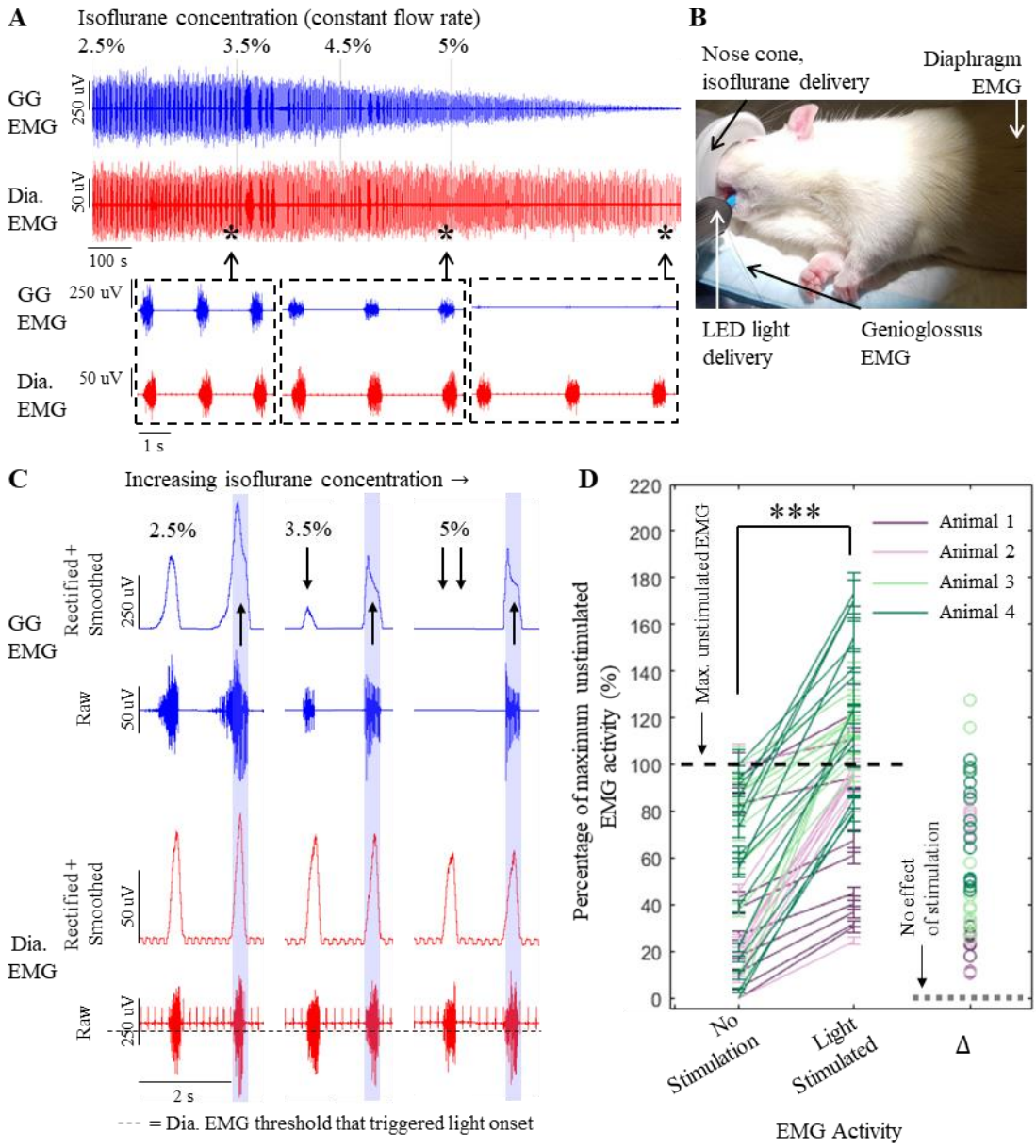

Figure 2-3 | Optogenetic stimulation of the tongue muscles in an isoflurane-based model of pharyngeal muscle atonia. (A) Increased isoflurane concentration results in reductions of genioglossus electromyography (EMG) activity (blue) while diaphragm EMG activity (red) is preserved, mimicking pharyngeal muscle hypotonia in human sleep. **(B)** During the electrophysiology studies, isoflurane is delivered via a nose cone, and fine wire electrodes monitor genioglossus and diaphragm EMG. **(C)** Sample data illustrates that pulsed blue light (470 nm), triggered by the onset of inspiratory diaphragm EMG activity (dotted line), restores genioglossus EMG when 3.5% isoflurane reduces endogenous activity and when 5% isoflurane removes endogenous activity. Light application does not affect diaphragm EMG. **(D)** Adjacent unstimulated and stimulated EMG activity is normalised to maximal unstimulated EMG activity (n=4, mean±SD). The tMCK construct induced sufficient expression for light stimulation to significantly ($p<0.001$) increase EMG activity. Note that visible tongue protrusions were only observed in animals injected with the tMCK construct. *** $P<0.001$ by linear mixed model.

2.3.3 Isoflurane titration in rodents mimics sleep associated pharyngeal hypotonia/atonia

The next step was to test whether light stimulation of this construct could produce tongue dilator muscle activity. To achieve this, an animal model of sleep-associated pharyngeal muscle hypotonia/atonia was required. Several existing rodent models mimic OSA using external apparatus and/or mechanical obstructions [224-227, 494] to collapse or block the airway. The few animal models that do exhibit spontaneous apnoea are either not feasible for large scale non-recoverable pre-clinical studies, e.g. British bulldogs [218], or do not adequately mimic sleep-associated dilator muscle hypotonia that contributes to human OSA e.g. obese Zucker rats [97] and Ob/Ob mice [92]. As such, they are unsuitable for testing pharyngeal muscle activity restoration.

This novel model was inspired by the common clinical problem where isoflurane general anesthesia causes pharyngeal muscle hypotonia and increases upper airway collapsibility [495]. Reversible reductions in phasic inspiratory dilator activity of the genioglossus were induced by increasing isoflurane concentration delivered via a nose cone to SD rats (Figure 2-3A, B). Isoflurane had minimal effects on concurrent diaphragm inspiratory activity (Figure 2-3A). This simple model recapitulates the hypotonia of human upper airway muscles during sleep that contributes to OSA [10], providing a suitable model for testing therapies targeting this trait.

2.3.4 Closed-loop photostimulation restores pharyngeal inspiratory dilator activity

To confirm that this optogenetic construct resulted in a meaningful functional response to light, three weeks after intramuscular injections diaphragm and genioglossus EMG were recorded in this rodent model of upper airway hypotonia. The ventral and posterior tongue surface (crosshatching, Figure 2-1A) was intermittently illuminated with a blue LED (470 nm, ~0.58 mW, NTE Electronics, NJ, USA) during inspiration, triggered by the onset of inspiratory diaphragm EMG activity exceeding the amplitude of the negative component of the QRS complex of the ECG artefact visible in the diaphragm signal (dotted line under the raw DiaEMG trace, Figure 2-3C). EMG data were normalised to the maximum unstimulated EMG activity recorded prior to the onset of isoflurane-induced EMG reduction when respiration-linked tongue contractions were still visible. Light-induced EMG during inspiration was compared to that during an adjacent unstimulated breath.

All tMCK animals (n=6) exhibited robust increases in EMG during light stimulation, accompanied by strong visible tongue protrusions in all animals (see Appendix Video A2-1). Data from two animals was excluded from quantitative analysis as initial isoflurane anesthesia abolished respiration-linked tongue movements/contractions prior to the insertion of EMG

electrodes, preventing normalisation of stimulated EMG activity, although blue-light evoked robust EMG in both cases. In the remaining four animals, light stimulation increased EMG by 55.6±24.7% (mean±SD) compared to an adjacent unstimulated breath (Figure 2-3D, linear mixed model, $F=140.0$, $p<0.001$). The magnitude of light-evoked increases in EMG were consistent across all levels of unstimulated EMG (linear mixed model, $F=1.9$, $p=0.072$).

Significant EMG variability (unstimulated and stimulated) between tMCK animals was observed (linear mixed model, $F=160.0$, $p=0.001$) and is most likely due to a combination of variability in opsin expression and strong dependence of light-evoked EMG on the relative positions of the EMG electrodes and light stimulus.

2.3.5 Optimal functional responses depend on light stimulation parameters

Amplitude and duration of light-induced muscle activity can be optimised by tailoring the illumination protocol. In the absence of endogenous genioglossus activity (i.e. high isoflurane concentration), single pulses of light (1 ms to 300 ms duration) produced EMG peaks approximately 10 ms after light onset, followed by a return to baseline at approximately 20 ms, regardless of pulse duration (Figure S3). Increasing pulse duration from 1 ms to 10 ms increased peak EMG 8-fold, but further increases in duration did not further increase EMG (Figure 2-4A).

However, since EMG evoked by single pulses returned to baseline after approximately 20 ms irrespective of pulse duration (Figure S3) these are insufficient to maintain airway patency. Therefore the next step was to investigate pulsed illumination protocols with pulse widths of 1-20 ms repeated at frequencies of 10-60 Hz over 300 ms, chosen to match the duration of endogenous inspiratory activity (Figure 2-4B). Maximum EMG over this 300ms period was generated with 5 ms pulse widths and frequencies over 50 Hz. For pulse widths less than 5 ms, higher frequencies induced only small, albeit consistent, increases in EMG. Conversely, when pulse widths exceeded 5 ms, initial rapid gains in EMG eventually plateaued and/or declined when frequencies exceeded 20 Hz (Figure 2-4C,D).

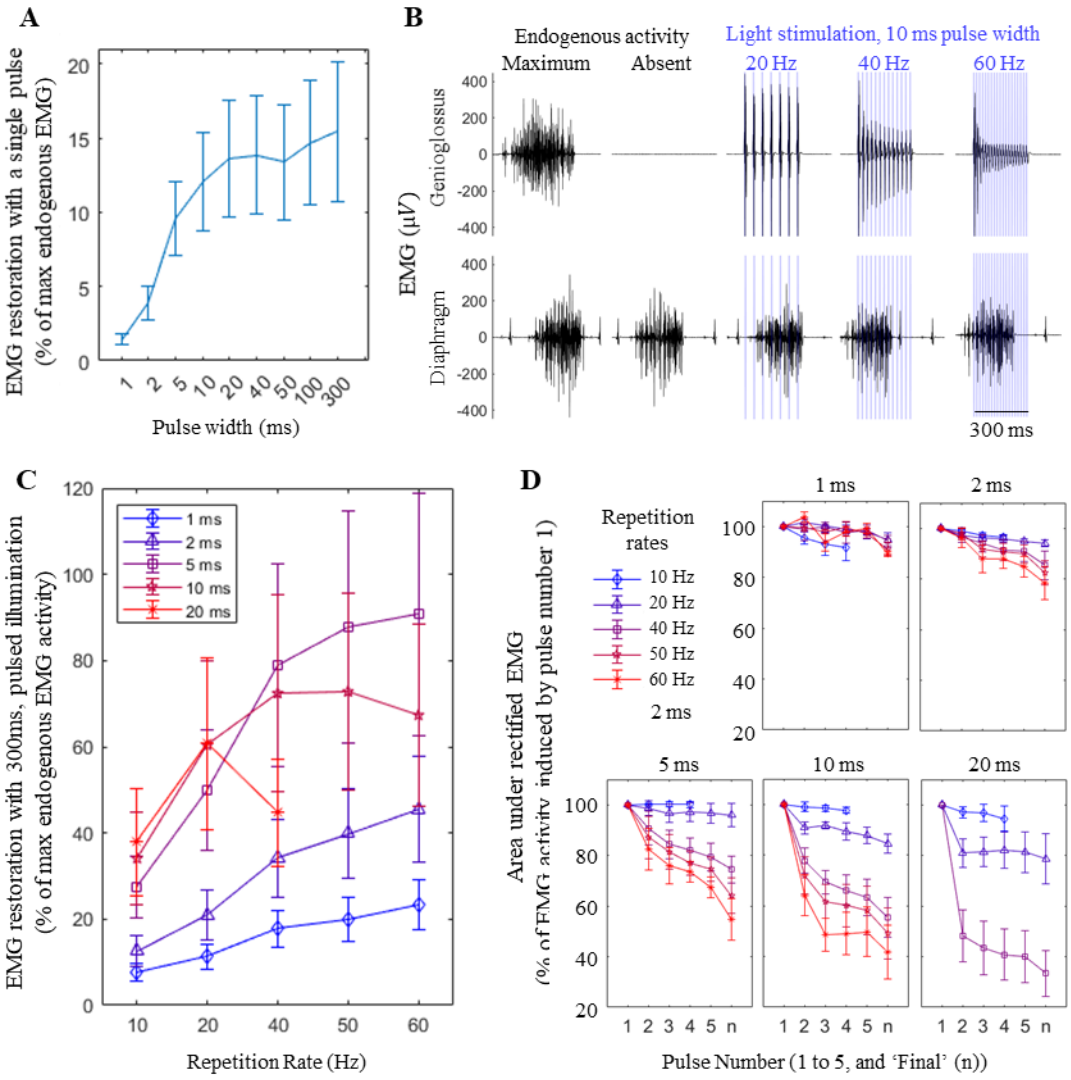

Figure 2-4 | Light-evoked EMG in the genioglossus varies with light simulation protocol characteristics. (A) Relationship between light pulse durations and the area under the induced genioglossus EMG curve, i.e. EMG restoration with a single pulse (n=4, mean±SEM). **(B)** Representative examples of genioglossus and diaphragm EMG prior to isoflurane induced EMG reduction ('Endogenous Maximum'), after isoflurane induced EMG elimination ('Endogenous Absent') and when EMG is increased by 10 ms long pulses with increasing frequencies ('Light Applied'). **(C)** When pulsed stimulation is maintained for 300 ms, the greatest increase in EMG was achieved with pulse widths of 5 ms and frequencies between 40 Hz and 60 Hz (n=4, mean±SEM). **(D)** The stimulated EMG declines with sequential pulses within a stimulation protocol (n=4, mean±SEM). Duration for all stimulation trains is ~ 300 ms.

2.4 DISCUSSION

The key finding of this study is that light stimulation, following direct administration of a novel muscle-specific optogenetic construct to the tongue, can consistently restore or enhance phasic activity and contraction of dilator muscles in a rodent model of OSA that recapitulates sleep-associated hypotonia of the upper airway dilator muscles seen in human OSA patients. The

light-evoked EMG can be similar in magnitude to endogenous respiratory-related tongue muscle activity, and the response evoked is independent of the level of endogenous activity present, confirming that this approach can boost inadequate dilator muscle function. Considerable inter-animal variation was observed, potentially resulting from differences in opsin expression and the relative positions of the light source and EMG electrodes. The timing of light-evoked EMG activity differed from the endogenous respiratory-related tongue muscle activity, as there was an absence of pre-inspiratory activation. To address this discrepancy, future studies aim to employ a simple predictive algorithm based on diaphragm EMG. This algorithm would enhance the coordination of the light-evoked tongue muscle activity with the respiratory cycle, preparing the airway to defend against large negative inspiration related pressure swings. Finally, this study has demonstrated that this can be achieved using intralingual injection with minimal systemic expression of the optogenetic construct, and no CNS expression, providing a promising safety profile. Together, these findings provide proof-of-concept for optogenetic stimulation of upper airway muscles that could form the basis for a novel therapy for OSA.

Prior to this study, very little successful direct optogenetic muscle activation had been reported, and most researchers used transgenic animals, achieving muscle contractions in the presence of near-complete muscle expression of the opsin [235, 254]. That approach is not feasible for human therapeutic applications. Bruegmann et al. [235] showed that systemic delivery of an AAV-opsin construct driven by a non-specific promoter produced limited skeletal muscle opsin expression, and was unable to achieve sustained contractions. More recently, two studies have demonstrated functionally effective and optogenetics-based activation of the diaphragm [255] and tongue [496] following intrapleural and intramuscular rAAV injections, respectively. These studies used a non-specific promoter driven vector delivered intramuscularly (AAV9-CAG-ChR2) – i.e. comparable to our initial vector. They demonstrated opsin expression in the targeted muscles and light-evoked EMG responses. In contrast, the current study used a novel construct that incorporated a muscle-specific promoter and local intramuscular injections, improves the efficacy of opsin expression in the target tissue with demonstrated functional muscle contraction while minimising off-target expression. Moreover, this was achieved using viral loads 3.4- and 4.6-fold lower than those applied in the diaphragm [255] and tongue [496] applications mentioned previously. Despite this achievement, further improvements in the efficiency of transgene expression are desirable. Potential avenues for exploration include novel synthetic AAV capsids with greater skeletal muscle affinity than the AAV9 used here, such as AAVMYO [345], which may enable further reductions in viral dosages, thereby reducing immune responses and improving long-term expression [497].

Interestingly, the five studies that have investigated direct optogenetic stimulation of skeletal muscle (including this thesis) compared vastly different stimulation protocols despite using very similar opsins (ChR2 and ChR2(H134R)). This thesis and the two early studies (Bruegmann et al., [235] and Magown et al., [254]) used ChR2(H134R) and applied 'pulsed stimulation', i.e. pulse widths ranging from 1ms to 150 ms [235], 300 ms (this study) or 1000 ms [254], applied at frequencies between 10 and 60 Hz. In contrast, the more recently published literature (Benevides et al., 2022 [255] and Singer et al., 2023 [496]) used ChR2 and aimed to 'mimic the effects of continuous light' via pulse widths between 0.1 and 1 ms, and interpulse intervals between 0.1 and 5 ms. This equated to extremely fast frequencies between ~ 167 Hz and 5000 Hz [255, 496]. Moreover, rather than a constant light intensity [235, 254] these studies gradually increased light intensity from 10 to 60 mW/mm^2 before gradually returned it to 10 mW/mm^2 within each stimulation train [255, 496]. The purpose of this was not outlined, however the resultant light-evoked EMG activity may better reflect the profile of endogenous EMG activity. Whether this represents a clinical benefit is unclear, however, preclinical studies of hypoglossal nerve stimulation suggest that this is unlikely, as efficacy is typically based on airway dilation (static cross sectional area measures from imaging protocols) [46, 72, 498] or flow mechanics (rate of airflow and pharyngeal critical closing pressure and resistances) [37]. The 'profile' of the contraction is not considered. These vastly different protocols also make direct comparisons difficult. In the more recent studies, increasing pulse widths from 0.1 to 1 ms produced increases in light-evoked responses [255, 496]. This may be continuous with the earlier findings (and those presented in this thesis) where greater pulse widths produced increases in light-evoked responses until a plateau was reached between 10 and 20 ms [235, 254]. Trends associated with stimulation frequencies are more challenging to combine, particularly due to the different off-kinetics of ChR2 (τ_{off} ~ 11.9 ms [238]) and ChR2(H134R) (τ_{off} ~ 20 ms [265]), the strong dependence on the very different pulse widths, and the different light intensity protocols [235, 254, 255, 496]. The recent studies reported that 1 ms pulses and 5 ms interpulse intervals, i.e. the lowest frequency protocol (~167 Hz), produced the greatest light-evoked responses [255, 496]. This may correlate with the findings presented here and in the earlier studies [235, 254] where higher frequencies eventually resulted in a plateau and decline in light-evoked responses – i.e. Fullers extremely fast protocols (up to 5000 Hz) were subject to greater declines per successive pulse. Finally, as previously stated, all stimulation protocols are specific to the opsin expressed. As alternate opsins are likely to be required for clinical translation (e.g. red-shifted and/or ultrafast opsins), these protocol optimisation studies will be repeated, and will therefore these differences to be directly compared.

This data supports using muscle-specific promoters, specifically tMCK, and local intramuscular injections to produce strong, targeted opsin expression to generate reliable and robust EMG activity and visible muscle contractions. Moreover, no CNS gene expression due to retrograde motoneuronal transport was observed with the muscle-specific promoter despite AAV9's demonstrated capacity to do so [499, 500]. Minimal systemic distribution and uptake by internal organs (liver, spleen, heart) and other skeletal muscles (diaphragm, gastrocnemius) was found. This indicates that, in addition to inducing strong and localised opsin expression, muscle-specific promoters and intramuscular injections may allow reduced total viral loads and minimise the risk of toxicity, immune responses and other adverse events resulting from off-target delivery including, but not limited to, motor neuron death and muscle atrophy [335].

The transition from preclinical to clinical studies is a significant hurdle for optogenetics-based therapies, particularly the challenges of managing the effect of immune responses on long-term opsin expression and function [335, 501]. These results, with strong tissue specificity and minimal systemic distribution, indicate that immune responses to this novel construct should be manageable [323, 417, 502]. Increasing evidence suggests this is possible via transient or slow-release subcutaneous immunosuppressants [335, 385]. Moreover, rAAV vector re-administration has been achieved when the initial rAAV dose is administered concurrently with synthetic vaccine particles encapsulating immunosuppressants [386], or is preceded by endopeptidase infusions that aim to degrade circulating antibodies [387]. There is already a considerable evidence base demonstrating safety of AAV-based gene therapies. AAV-based gene delivery is the basis of three FDA-approved treatments for an inherited retinal disorder, spinal muscular atrophy, and lipoprotein lipase deficiencies, and hundreds of AAV-based gene therapy trials have been completed or are underway with hematologic, ophthalmologic, neurologic, metabolic, and musculoskeletal targets [323]. In these trials, intramuscular AAV injections produced low rates of adverse events related to the transgene, capsid and/or the patient's immune response to the transgene or capsid [323], supporting this approach. More specific to this construct, several clinical trials investigating the safety, tolerability, and efficacy of AAVs optogenetic therapy for retinitis pigmentosa are ongoing [256-259], and an initial human case study, where the patient received a low dose ($5x10^{10}$ vg) of an AAV2-ChrimsonR gene therapy, resulted in partial functional recovery and no evidence of ocular or systemic adverse events [260].

Despite achieving sustained muscle contractions, further improvements in contraction duration, which may be needed in humans due to a longer respiratory cycle, are currently limited by opsin channel kinetics, as suggested by the stimulation protocol results (Figure 2-4). 'Ultrafast'

opsins, e.g. ChETA (time constant of deactivation ≈ 4 ms vs 18 ms for ChR2(H134R) [503]), may allow faster reactivation and reduced EMG 'decay' with sequential pulses, therefore allowing higher frequency stimulation protocols and greater EMG responses. Red-shifted ChR variants (e.g. ChRmine [267], ChrimsonR) may also aid the translation to larger human muscles since red light has greater penetration through soft tissues than blue light. Red-shifted opsins may also enable light stimulation to be applied transcutaneously or with an oral appliance, providing practical, safety, and ease-of-use benefits over even the least invasive existing electrical stimulation system, which uses implanted electrodes that are powered transcutaneously [13].

The demonstrated efficacy of the targeted optogenetic stimulation of the upper airway muscles, taken together with promising human results of rAAV-delivered optogenetic therapy for other conditions [260], indicate that this method has a potentially easier translation pathway than the also promising chemogenetic (DREADDs) approach [16, 232]. While both use localised delivery to target specific muscles in the pharynx, the direct muscle optogenetic approach does not require regular administration of a synthetic ligand at sleep onset, nor does it involve genetic modification of the peripheral or central nervous system. It can also deliver temporally precise stimulation and enable feedback-driven control that could be titrated on an individual basis and/or adapted as required throughout the night. Conversely, the DREADDs approach increases tonic muscle activity and may be more efficacious in NREM than REM sleep [16].

This study provides initial proof-of-concept of a novel stimulation-based OSA therapy. As a proof-of-concept study, there are several limitations and considerable further work is required before translation to humans. Firstly, the isoflurane anaesthesia model used to test optogenetic stimulation recapitulates sleep-related muscle hypotonia, but is not fully representative of natural sleep. Notwithstanding this, the model clearly demonstrates that it is possible to restore endogenous levels of respiratory-related muscle activity, similar to the approach used in a recent study of optogenetic diaphragm stimulation [255]. Finally, a demonstration of the effects of optogenetic stimulation on airway patency rather than EMG activity is required. Existing experimental techniques such as tagged magnetic resonance imaging [29, 100, 103, 106, 138, 504] and ultrasound [43, 44, 112] protocols have proven utility in quantifying airway dilation and tongue movement in humans and rodents.

This study has demonstrated the feasibility of a direct optogenetics approach to restoring or boosting upper airway dilator muscle activity, which has potential to maintain airway patency in OSA patients with inadequate dilator muscle activity during sleep. Muscle-specific promoters and local intramuscular injections maximise the efficiency and targeting of the construct, and

light stimulation protocols provide highly customisable, and temporally precise stimulation. Future studies exploring novel opsins and AAV capsids to improve the optogenetic response, and longer-term studies will develop this potential therapy further towards clinical application. Additionally, this approach has potential applications in other clinical conditions involving skeletal or respiratory muscle dysfunction, particularly where the integrity of the innervating motor neurons is poor, rendering neural stimulation approaches unsuitable, such as in motor neuron disease.

Chapter 3 OPTIMISING THE VIRAL CONSTRUCT: RAAV SEROTYPES

3.1 INTRODUCTION

Recombinant adeno-associated viruses (rAAVs) are akin to biological nanoparticles able to efficiently transverse cell membranes to deliver an 'expression cassette', i.e. a promoter, transgene and regulatory components, into a cell's nucleus for transcription and transgene expression. Once there, rAAV genomes predominantly persist as non-integrating episomes; therefore, non-dividing cells, such as myocytes, are most stably transduced. rAAVs are currently the only viral vector approved for gene therapies in humans. FDA approval has been granted for RPE65-mediated inherited retinal dystrophy, lipoprotein lipase deficiencies and pediatric spinal muscular atrophy. According to a 2022 meta-analysis, 136 clinical trials have investigated the efficacy, safety, and tolerability of 134 AAV drug products targeting 55 diseases [338], providing evidence that rAAVs are promising vehicles for gene delivery.

rAAVs are most commonly derived from naturally occurring serotypes [338] that present specific tissue tropisms, i.e. each preferentially infects specific cell types. For instance, rAAV serotype 9 (AAV9) is efficient at transducing skeletal muscle, used in clinical trials targeting neuromuscular disorders [338], and in FDA-approved gene therapy for spinal muscular atrophy. While naturally occurring rAAV serotypes have been successful, they are associated with several disadvantages. First, the equivalent wild-type viruses are endemic in human populations, and subsequently, so are pre-existing adaptive immunities, including neutralising antibodies [346]. Low levels of neutralising antibodies (titres between 1:5 and 1:10) have eliminated large vector doses [313, 348], and an absence of neutralising anti-AAV antibodies [371] or minimal titres of anti-AAV antibodies (e.g. $\geq$ 1:50) are commonly used as exclusion criteria regardless of neutralising abilities [505]. The presence of these antibodies can potentially lead to reductions in transgene expression and/or transduced cells and may undermine clinical efficacy and prevent re-administration. As a result, they are likely to require concurrent interventions that aim to suppress immune responses and/or allow transgene expression in the presence of pre-existing antibodies [354]. Second, these serotypes are often sequestered in the liver following administration [344], potentially limiting transduction efficacy in other organs and increasing the risk of liver toxicities [349, 350] and increasing the viral loads required to achieve therapeutic levels of transgene expression [342, 349] which can, in turn, increase the risk of generating immune responses [334, 350].

Engineered rAAVs can overcome some of these limitations. With the absence of previous exposure, engineered serotypes are subject to reduced immune surveillance and immune

responses and can be manufactured with increased tissue specificity, liver detargeting, and/or an improved ability to evade antibody neutralisation [344, 345, 351]. In turn, they may improve long-term expression, reduce viral loads and immunogenicity, and improve safety profiles. Novel serotypes are commonly engineered via rational design, where site-specific modifications to existing capsids improve tissue specificity and/or modify antigenic sites [352]. Alternatively, directed evolution methods generate huge libraries of diverse capsids via gene shuffling and random mutagenesis [344, 345, 351]. While the use of engineered capsids significantly lags behind naturally occurring capsids, used in only 13% of clinical trials [338], there is increasing support for their use in preclinical studies where they improve transduction [344, 345] and reduce immunogenicity [506].

AAV9 has long been considered the most efficient rAAV serotype for muscle transduction. It is approved for use in the treatment of spinal muscular atrophy, and is the sole serotype used in preclinical optogenetics-based muscle stimulation [235, 255, 496]. In 2020, a novel rAAV serotype, AAVMYO, with excellent efficiency and specificity in musculature was identified following systemic administration. Compared to AAV9, AAVMYO produced eYFP mRNA expression ~ 61-, 17-, and 11-fold greater in the diaphragm, quadriceps femoris, and heart, respectively, and concurrent liver detargeting (nine-fold less than AAV9). These findings were supported at the protein level, in other mouse strains, and with different transgenes and reporters [344]. Since then, AAVMYO has been further enhanced via rational additions [354]. Moreover, in 2021 a second similarly myotropic serotype, MyoAAV, was also developed via directed evolution and identified via barcoding [345]. These engineered rAAV serotypes represent a significant improvement in rAAV-mediated muscle transgene expression.

When work for this thesis commenced in 2019, AAV9 was considered the optimal serotype for muscle transduction, and its efficacy was confirmed in pilot studies comparing AAV9, AAV2, and AAV1 for opsin expression in the tongue. The next step for optimising serotype selection was to use barcoding methods to screen for potentially superior rAAVs (wild-type or engineered) for muscle transduction. Due to the COVID pandemic, these experiments were suspended in 2020. Fortunately, the development of AAVMYO in late 2020 and its direct comparison with 183 rAAV variants [344] obviated the need for an rAAV library screen. Consequently, after the research presented in Chapter 2 described strong and specific opsin expression and functional light-evoked responses following intramuscular injections of AAV9 driven by a muscle-specific promoter, the research described in the current Chapter aimed to determine whether AAVMYO could improve upon these results. Specifically, this study aimed to determine whether the engineered serotype would increase opsin expression in the tongue and

therefore facilitate greater light-evoked responses, while maintaining the specificity afforded by the muscle-specific promoter. The persistence of AAV9 and AAVMYO facilitated expression and biodistribution were also examined.

3.2 METHODS

The data acquired in Chapter 2 from the animals that received the muscle-specific promoter-driven construct (AAV9-tMCK-ChR2(H134R):mCherry) were compared to new data from animals that received an AAVMYO serotype packaging an identical expression cassette (Table 3-1). The viral loads and volumes for both constructs are provided in Section 3.2.1.

Table 3-1 | Study Design.

Capsid	Histology^		EMG		Viral DNA copies*		RNA expression*	
	Weeks post intramuscular injections							
	3	12	3	12	3	12	3	12
AAV9	N = 6†	-	N = 6†	-	N = 4†	N = 4	N = 4†	N = 4
AAVMYO	N = 6	-	N = 9	-	N = 3	N = 4	N = 3	N = 4

† Data from the AAV9 cohort at 3 weeks was previously reported in Chapter 2.

^ Tongue and brainstem opsin:reporter protein expression in the tongue and brainstem

* Quantified in the tongue, diaphragm, gastrocnemius, liver, spleen, heart, bladder, brainstem

In Chapter 2, three weeks after male SD rats (n = 6) received intramuscular injections of the AAV9 packaged construct to the tongue, light-evoked responses were quantified via EMG recording in a rodent model of human sleep-associated upper airway muscle impairment (high concentration isoflurane). After completion, tongue and brainstem tissue were harvested for histology analysis. In an additional cohort (male SD rats, n = 4), tissues were harvested at the same time point (3 weeks after injections) to quantify viral DNA copy numbers and RNA expression in the tongue, diaphragm, gastrocnemius, liver, spleen, heart, bladder, and brainstem (Table 3-1, indicated by †).

In the current study, new data were collected three weeks after male SD rats (n = 9) received intramuscular injections of the AAVMYO packaged construct to the tongue. After acquiring EMG data from all animals, tissues were harvested from six animals for histology analysis (tongue and brainstem) and from three animals to quantify viral DNA copy numbers and RNA expression (tongue, diaphragm, gastrocnemius, liver, spleen, heart, bladder, and brainstem).

An additional two cohorts of animals received intramuscular injections of either the AAV9 (n = 4) or AAVMYO (n = 4) packaged constructs, and tissues (tongue, diaphragm, gastrocnemius,

liver, spleen, heart, bladder, and brainstem) were harvested 12 weeks later for 'long-term' DNA and RNA quantification.

All tissue harvesting, analysis methods and statistics were performed as described in Chapter 2. The exception was the statistics used to compare the 3- and 12-week DNA and RNA data from the AAV9 and AAVMYO cohorts. This data was analysed using a Mixed Model ANOVA (with serotype, tissue, and time-point as variables), with Tukey post hoc tests.

3.2.1 AAV vectors

An AAV9-packaged construct and an AAVMYO [344]-packaged construct were compared in this study. Both vectors contained identical expression cassettes; a muscle-specific promoter (tMCK, [330]), a channelrhodopsin-2 variant with a gain of function substitution (ChR2(H134R)) fused to mCherry, a red fluorescent reporter, and the required regulatory components, i.e. pAAV-tMCK-ChR2(H134R):mCherry.

The muscle-specific expression cassette sequence, pAAV-tMCK-ChR2(H134R):mCherry, was developed by GenScript (New Jersey, USA) and packaged into AAV9 and AAVMYO capsids by the Vector and Genome Engineering Facility (Children's Medical Research Institute, Westmead, Australia). The AAVMYO plasmid was provided by Dirk Grimm (University of Heidelberg, Germany) [344].

The AAV9 construct, AAV9-tMCK-ChR2(H134R)-mCherry, had a titre of 9.04×10^{12} vg/mL, and the AAVMYO construct, AAVMYO-tMCK-ChR2(H134R)-mCherry, had a titre of 4.75×10^{13} vg/mL. 20µL of the AAV9 construct (4×5µL) contains 1.81×10^{11} vector copies per animal. 3.8 µL of the AAVMYO construct, diluted in 16.2 µL of injectable saline, was injected in the second cohort (4×5µL), equating to $1.\ 81 \times 10^{11}$ vg per animal.

3.3 RESULTS

3.3.1 AAVMYO produced equivalent distribution of opsin:reporter expression, but greater levels of viral DNA and RNA expression in the tongue

Histology. Confocal imaging of tongue tissue harvested at the 3-week time point indicates that the AAV9 and AAVMYO serotypes produced similar ChR2:mCherry expression three weeks after injections (Figure 3-1A, two-way RM-ANOVA, $F(1,10) = 0.00$, $p = 0.98$). Moreover, neither construct produced ChR2:mCherry expression in the hypoglossal motor nucleus of the brainstem following retrograde transport along the hypoglossal motor neuron (Figure 3-1B). Opsin expression was also absent in all other brainstem regions, motor nuclei, sensory tracts or

terminal fields, including but not limited to the facial, trigeminal and vagal motor nuclei, the sensory trigeminal nuclei and the nucleus of the solitary tract.

Viral DNA copy numbers. A three-way mixed model ANOVA, with tissue type, time point (3 and 12 weeks) and serotype (AAV9 or AAVMYO), showed significant main effects for tissue ($F(7,8) = 19.72$, $P < 0.0001$) and time point ($F(1,88) = 18.32$, $P < 0.0001$), indicating that DNA expression varied between tissues and time points. There were significant two-way interactions between tissue and time point ($F(7, 88) = 13.86$, $P < 0.0001$) and tissue and serotype ($F(7, 88) = 2.126$, $P = 0.0489$) and a significant three-way interaction between tissue, time point and serotype ($F(7, 88) = 2.855$, $P = 0.0099$). At three weeks, viral DNA copy numbers in the tongue were significantly greater for the AAVMYO serotype than AAV9 (Tukey, $P < 0.0001$) and, regardless of serotype, DNA copy numbers in the tongue were significantly greater than in all other tissues (Tukey, AAVMYO: tongue vs all other tissues, $P < 0.0001$; AAV9: tongue vs spleen, $P < 0.005$; tongue vs all other tissues, $P < 0.001$). DNA copy numbers in the tongue fell significantly between 3 and 12 weeks for both serotypes (Tukey, AAVMYO: $P < 0.0001$; AAV9: $P = 0.011$), and there were no differences in DNA copy numbers in the tongue between serotypes at 12 weeks (Tukey, $P > 0.999$). No other significant differences between serotypes were found.

RNA expression. The same statistical method was used to analyse RNA expression between tissues, time points, and serotypes. Significant main effects were found for tissue ($F (7, 88) = 33.09$, $P < 0.0001$) and time point ($F (1, 88) = 18.32$, $P < 0.0001$), indicating that RNA expression varied between tissues and time points. There were significant two-way interactions between tissue and time point ($F (7, 88) = 18.11$, $P < 0.0001$), tissue and serotype ($F (7, 88) = 2.555$, $P = 0.0192$) and time point and serotype ($F (1, 88) = 5.396$, $P = 0.0225$) and a significant three-way interaction between tissue, time point and serotype ($F (7, 88) = 5.393$, $P < 0.0001$). At three weeks, RNA expression in the tongue was significantly greater for the AAVMYO serotype than AAV9 (Tukey, $P < 0.0001$) and, regardless of serotype, RNA expression in the tongue was significantly greater than that in all other tissues (Tukey, AAVMYO: tongue vs all other tissues, $P < 0.0001$; AAV9: tongue vs all other tissues, $P < 0.0001$). RNA expression in the tongue fell significantly between 3 and 12 weeks after for both serotypes (Tukey, AAVMYO: $P < 0.0001$; AAV9: $P = 0.035$), and there were no differences between RNA expression in the tongue at 12 weeks (Tukey, $P > 0.999$). No other significant differences between serotypes were found.

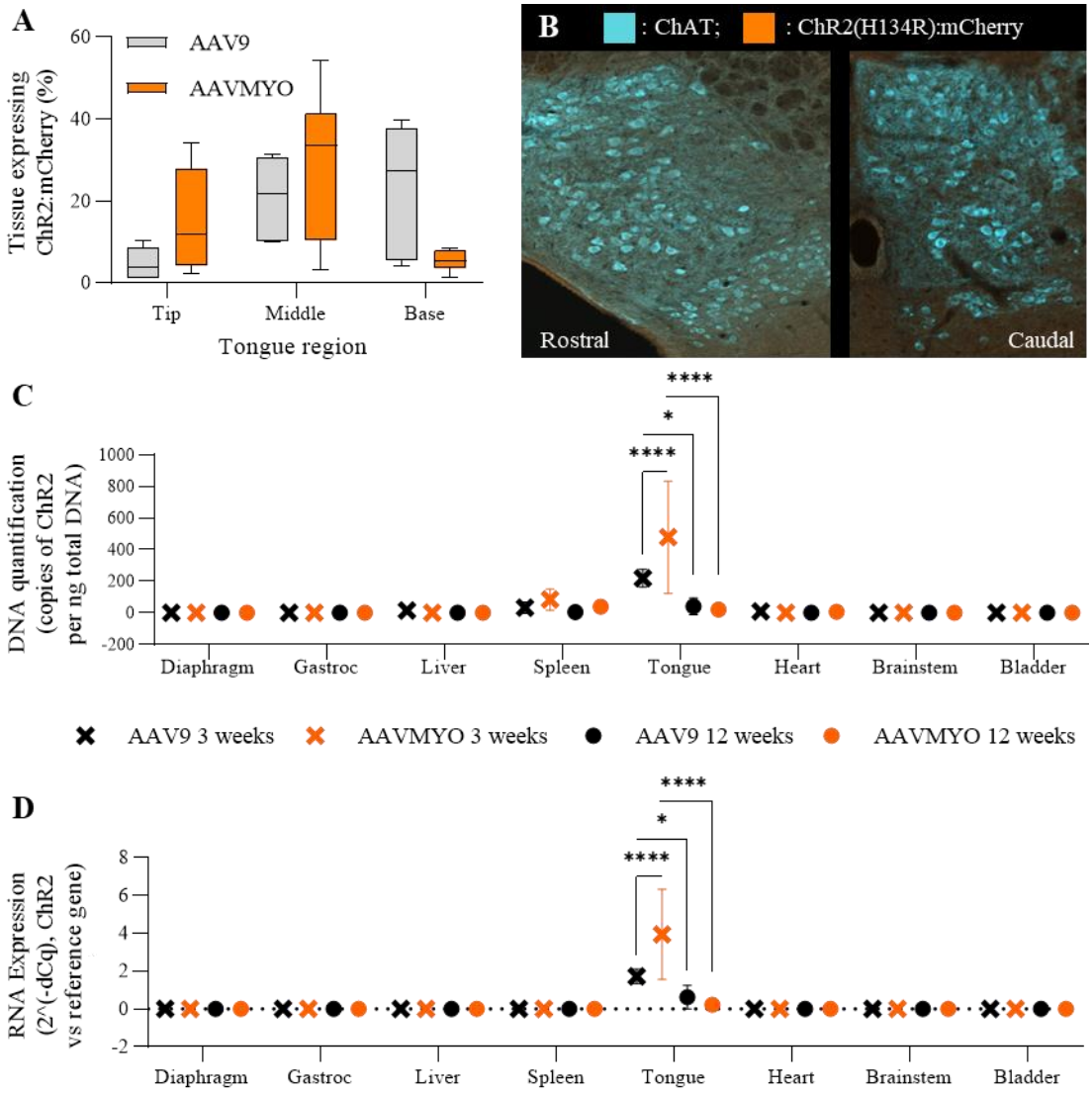

Figure 3-1 | Opsin expression and biodistribution following intramuscular injections of AAVMYO and AAV9. (A) Both serotypes achieved similar distributions of opsin:reporter expression in the tongue, and **(B)** did not induce opsin:reporter expression in the hypoglossal motor nucleus of the brainstem (only ChAT positive hypoglossal motor neurons and dorsal motor neurons of the vagus are highlighted in the AAVMYO brainstem sections). **(C)** A three-way mixed model ANOVA (tissue type x time point x serotype) reported that at three weeks, viral DNA copy numbers in the tongue were significantly greater for the AAVMYO serotype than AAV9 (Tukey, $P < 0.0001$). DNA copy numbers in the tongue fell significantly between 3 and 12 weeks for both serotypes (Tukey, AAVMYO: $P < 0.0001$; AAV9: $P = 0.011$), and there were no differences in DNA copy numbers in the tongue between serotypes at 12 weeks (Tukey, $P > 0.999$). **(D)** Using the same statistical analysis, RNA expression in the tongue at three weeks was significantly greater for the AAVMYO serotype than AAV9 (Tukey, $P < 0.0001$) and, regardless of serotype. RNA expression fell significantly between 3 and 12 weeks after for both serotypes (Tukey, AAVMYO: $P < 0.0001$; AAV9: $P = 0.035$), and there were no differences between RNA expression in the tongue at 12 weeks ($P > 0.999$). **** $P < 0.0001$, * $P < 0.05$

Table 3-2 | Summary of main and interaction effects of viral DNA copy numbers and RNA expression following a three-way mixed model ANOVA in GraphPad. Variables are tissue (i.e. tongue, diaphragm, gastrocnemius, liver, spleen, heart, brainstem and bladder), time point (i.e. 3- and 12- weeks after viral vector administration), and serotype (i.e. AAV9 or AAVMYO).

	Source of Variation	F (DFn, DFd)	P value
Viral DNA copies	Tissue	F (7, 88) = 19.72	P<0.0001
	Timepoint	F (1, 88) = 18.85	P<0.0001
	Capsid	F (1, 88) = 3.292	P=0.0730
	Tissue x Timepoint	F (7, 88) = 13.86	P<0.0001
	Tissue x Capsid	F (7, 88) = 2.126	P=0.0489
	Timepoint x Capsid	F (1, 88) = 2.533	P=0.1151
	Tissue x Timepoint x Capsid	F (7, 88) = 2.855	P=0.0099
RNA Expression	Tissue	F (7, 88) = 33.09	P<0.0001
	Timepoint	F (1, 88) = 18.32	P<0.0001
	Capsid	F (1, 88) = 2.563	P=0.1130
	Tissue x Timepoint	F (7, 88) = 18.11	P<0.0001
	Tissue x Capsid	F (7, 88) = 2.555	P=0.0192
	Timepoint x Capsid	F (1, 88) = 5.396	P=0.0225
	Tissue x Timepoint x Capsid	F (7, 88) = 5.393	P<0.0001

3.3.2 AAVMYO facilitated more robust light-evoked increases in muscle activity

Three weeks after receiving the AAV9 construct, all animals (n = 6) exhibited robust increases in EMG activity (compared to the previous unstimulated breath) with light application to the tongue surface. At the same time point, after receiving the AAVMYO construct, eight animals exhibited robust increases in EMG activity with light stimulation, and one did not respond to light stimulation (Figure 3-2). Four animals were excluded from the quantitative comparison of light-evoked EMG activity as their data could not be normalised (AAVMYO: n = 2; AAV9: n = 2) due to an absence of endogenous inspiratory genioglossus EMG activity likely caused by a heightened isoflurane sensitivity. However, both these animals had robust light-evoked EMG.

A linear mixed model was used to test genioglossus EMG activity, with animal ID (intercept), serotype (AAV9 or AAVMYO), stimulation (unstimulated or stimulated) and the endogenous group as variables (Table 3-3). 'Endogenous group' was ranked from 1 to 10 based on the percentage of local endogenous EMG activity compared to maximum EMG data (e.g. Figure 3-2, stimulation type: 'none'). This inclusion meant that isoflurane concentration and the subsequent reduction in endogenous muscle activity were considered. Significant main effects were reported for the intercept ($F(1, 9) = 26.930$, $P < 0.001$), endogenous group ($F(9, 225) =$

7.330, P < 0.0001) and stimulation (F(1, 221) = 115.220, P < 0.0001), and significant two-way interactions were reported between serotype and stimulation (F(1, 221) = 38.206, P < 0.0001) and endogenous group and stimulation (F(9, 221) = 4.832, P<0.0001). At three weeks after administration, the AAVMYO serotype facilitated significantly greater increases in EMG activity with light stimulation than the AAV9 serotype (Figure 3-2, Bonferroni, P < 0.0001), with light stimulation increasing EMG activity 193.5% ± 15.1 (mean ± std. error) compared to 66.3% ± 16.6 (mean ± std. error) for AAV9. Univariate tests confirmed that unstimulated EMG activity was equivalent between serotypes (F(1, 10) = 0.056, P = 0.818) and that the differences between serotypes can be attributed to the stimulated EMG data (F(1, 10) = 7.882, P = 0.019).

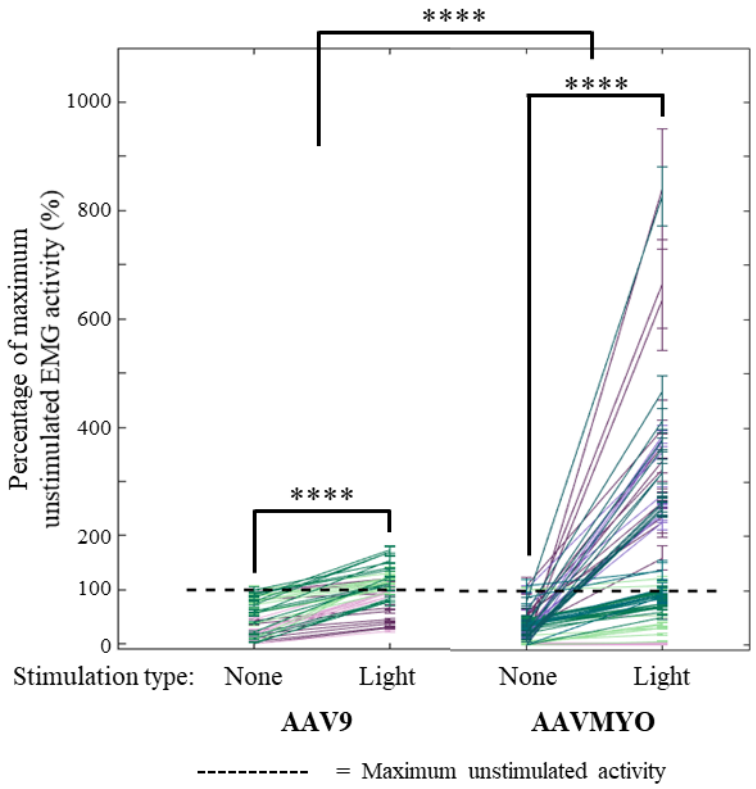

Figure 3-2 | Light-evoked EMG responses in animals receiving AAV9 and AAVMYO packaged optogenetic constructs. Increases in EMG responses with light stimulation were greater in the animals that received the AAVMYO serotype than the AAV9 serotype (linear mixed model, Bonferroni post hoc, P < 0.0001); however, both serotypes facilitated significant EMG increases with light stimulation (Univariant tests, AAVMYO: F(1, 221) = 163.4, P < 0.0001; AAV9: F(1, 221) = 16.0, P < 0.0001). **** P < 0.0001.

Table 3-3 | Summary of main and interaction effects of EMG activity following a linear mixed model in SPSS. Variables are intercept (i.e. animal ID), serotype (i.e. AAV9 or AAVMYO), endogenous group (i.e. method of grouping equivalent levels of endogenous/unstimulated EMG activity – 1 to 10), and stimulation (i.e. unstimulated/endogenous EMG and stimulated EMG).

Source of Variation	F (DFn, DFd)	P value
Intercept	F(1, 9) = 26.930	P<0.001
Serotype	F(1, 9) = 1.760	P=0.218
Endogenous group	F(9, 225) = 7.330	P<0.0001
Stimulation	F(1, 221) = 115.220	P<0.0001
Serotype x Stimulation	F(1, 221) = 38.206	P<0.0001
Endogenous group x Stimulation	F(9, 221) = 4.832	P<0.0001

All animals that displayed an EMG response to light stimulation (6/6 AAV9 animals and 8/9 AAVMYO animals) also displayed visible muscle contractions and tongue movement. Light applied to the surface of the tongue (lateral, dorsal or ventral) via intraoral LED produced asymmetric muscle contraction and movement of the tongue body and tip towards the light. This movement was considerably larger in the AAVMYO cohort and evoked with virtually any LED position. In contrast, the AAV9 cohort required careful LED positioning on the tongue's ventral surface to induce visible tongue contractions.

The light-evoked visible tongue contractions in the AAVMYO cohort were strong enough to allow discrimination between different stimulation protocols. Regardless of pulse width, protocols with frequencies $\leq$ 20 Hz produced unfused tetanic contractions, and protocols with frequencies $\geq$ 40 Hz produced fused tetanic contractions. Contraction strength was also associated with pulse width. 1 ms pulses produced weak contractions, and increases in pulse width produced visible increases in contraction strength until 10 ms pulses were applied. Contractions generated by 20 ms pulses were visually similar to those produced by 10 ms pulses. Continuous ($\geq$ 1 total stimulation duration) 10 ms and 40 Hz stimulation produced sustained tetanic contractions.

3.4 DISCUSSION

In this study, opsin expression and direct optogenetic stimulation of skeletal muscle following intramuscular injections of a novel and highly muscle-specific viral vector AAVMYO were characterised, and the results compared to AAV9, the current, clinically used rAAV serotype for muscle gene therapy. The AAVMYO cohort exhibited stronger light-evoked increases in muscle activity and visible tongue contractions in a rodent model of human sleep-associated

upper airway muscle impairment. The AAVMYO cohort exhibited higher levels of viral DNA copies and transgene RNA expression in the tongue than the AAV9 cohort. AAVMYO viral DNA copies and transgene RNA expression were low or absent in all other tissues, including the spleen, liver, heart, brainstem and blood cells, indicative of a promising safety profile. Finally, reporter fluorescence – a proxy measure of the distribution opsin:reporter protein expression – was robust across both cohorts and not statistically significantly different. These findings confirm that AAVMYO is a highly efficient muscle-preferencing serotype.

For both serotypes, there was strong expression in the tongue and minimal systemic distribution and off-target expression. This indicates that intramuscular injections of an AAVMYO serotype driven by a muscle-specific promoter may produce a similar safety profile to AAV9. However, there was considerable variability in the DNA and RNA expression in the tongue in the AAVMYO cohort, and this requires further research. Despite high viral DNA and RNA expression levels in the tongue three weeks after vector administration, much lower levels were found 12 weeks after administration, regardless of the serotype used. The precise mechanism for this loss in the current study is not yet clear, however transgene loss has been attributed to several non-immunological and immunological processes, including acute and delayed immune responses [507], target cell turnover [508], and promoter silencing [509]. As the timing of expression loss onset can assist in identifying the mechanism of transgene loss [510], future studies using multiple sacrifice time points or repeated recoverable tests of light-evoked muscle responses would provide additional insight. A potential option, ultrasound imaging, will be discussed further below.

While this study confirms that AAVMYO can generate strong opsin expression and functional contraction responses in skeletal muscle, there was a discrepancy between the histology results and the gene quantification and electrophysiology results. While average RNA expression and viral DNA levels in the AAVMYO cohort were over double that of AAV9, there was no difference between the two constructs in terms of the distribution of opsin:reporter expression throughout the tongue. Rat tongues are large (~ 3 cm long [85, 511]) and remarkably complex, composed of eight muscles and profoundly intertwined myofibres [84, 85]. While gene expression was quantified in a large volume of tissue, the distribution of opsin:reporter protein expression was quantified by confocal imaging of only three 80 µm sections, equating to a 0.0024 cm tongue length. Moreover, due to the complexity of the tissue and the absence of exclusively parallel myofibres, quantifying opsin expression by ‘counting’ of fluorescent reporter protein-positive (as per [235, 255]) is not possible. Finally, the comparatively thick (80 µm versus 10 µm [235] or 20 µm [255]) sections may hinder discrimination between

‘background’ and ‘real’ fluorescence due to reporter expression located in ‘deeper’ myofibres running parallel to the transverse tissue plane. While this method successfully discriminated between ‘poor’ and ‘good’ opsin expression in Chapter 2, it may not be sufficiently sensitive to discriminate between opsin expression generated by these two functionally effective constructs. Future studies will aim to combat these issues by quantifying opsin expression in more tongue sections, using alternate thresholding methods (e.g. [512]), and reducing section thickness. Enhancing fluorescent reporters may also aid the ease of discriminating between ‘real’ and ‘background’ fluorescence.

Light-evoked responses were more robust and readily obtained in the AAVMYO cohort. Compared to the AAV9 serotype, AAVMYO facilitated three-fold higher light-evoked EMG responses and greater light-evoked visible muscle contractions and tongue movements. The contractions more closely tracked the input stimulation parameters, with increasing pulse widths applied at frequencies greater than 20 Hz producing increasingly strong tetanic contractions, supporting data described in Chapter 2. This superior functional performance following AAVMYO administration corroborates well with the higher DNA copy numbers and mRNA expression levels, and supports the prior statement regarding the insufficient sensitivity of current histological analysis for quantifying opsin:reporter expression.

Visible light-evoked contractions were asymmetric and typically induced tongue retraction towards the light source. This could be attributed to two factors; (1) to view light-evoked movement the tongue was mechanically drawn out of the mouth (but not fixed, as required for measures of tongue contraction force [60]). Light-stimulation and the associated myofibre contractions then drew the tongue back into a more ‘natural’ position. Alternatively, (2) the poorly penetrating blue light exclusively activated local opsins expressed in myofibres with multiple orientations. As a result, local multi-directional contractions of individual myofibres were generated, and local tongue ‘stiffening’ rather than global protrusion occurred [36, 37]. While these observations demonstrated that robust tongue movement could be generated with light stimulation, it did not clarify whether tongue illumination could translate to airway dilation, which is the end-goal of an optogenetic stimulation therapy for OSA. This could be achieved using magnetic resonance imaging [97, 100, 103, 104] or ultrasound imaging [43, 112]. Moreover, using recoverable imaging experiments could enable repeat assessment of light-evoked airway dilation over an extended period of time. This will allow us to determine when light-evoked muscle responses start declining and subsequently indicate why they decline, and how this can be avoided in future experiments. Imaging will be the basis of experiments undertaken in Chapter 4.

Naturally occurring serotypes and pseudo-types (transgenes flanked by AAV2 ITRs and packaged in a natural rAAV) are used in 87% of clinical trials [338] and all FDA-approved rAAV-based gene therapies. Further, before this thesis, viral vector-mediated direct optogenetic activation of skeletal muscle exclusively used AAV9, a naturally occurring rAAV serotype, to achieve opsin expression [235, 255, 496]. While this body of literature on wild-type rAAVs provides strong efficacy and safety data, significant limitations remain. First, due to the high prevalence of pre-existing anti-AAV antibodies [346] and the subsequent risk of loss of therapeutic levels of transgene expression [313, 348], eligibility for clinical trials and therapeutic administration is commonly restricted to patients with an absence of neutralising anti-AAV antibodies [371] or low anti-AAV antibody titres $\leq$ 1:50 [505], regardless of neutralising ability. Second, naturally occurring rAAVs have been associated with severe adverse events due to liver sequestering, including toxicity, liver failure, and potential death [337, 350]. The risk of these outcomes increases with greater doses administered [334, 349, 350] and highlights the importance of targeted rAAV administration (systemic delivery requires higher viral loads [338]), active liver detargeting, minimal viral loads and thorough biodistribution analysis. This Chapter (and Chapter 2) support the use of intramuscular injections of an engineered serotype (AAVMYO) driven by a muscle-specific promoter (tMCK) for maximising functional responses to light stimulation and subsequently permitting minimal viral loads in future clinical applications. Despite a 27% lower titre, tMCK provided superior expression compared to CAG in Chapter 2. This study demonstrates that AAVMYO further improves functional performance. Moreover, AAVMYO has demonstrated liver detargeting compared to AAV9 in mice [344], and the data reported here show minimal off-target expression and systemic distribution. Finally, unlike wild-type rAAV serotypes, an engineered alternative like AAVMYO may facilitate reduced immune surveillance and responses upon administration and remove exclusion criteria based on anti-AAV antibody seropositivity.

The work presented in this Chapter demonstrates that a novel expression cassette (pAAV-tMCK-ChR2(H134R):mCherry) packaged into an engineered highly myotropic rAAV serotype, AAVMYO, can improve on the already strong performance of the AAV9 serotype. In addition to robust increases in muscle activity in response to light stimulation, visible muscle contractions that are titratable via stimulation protocol changes were observed. The AAVMYO serotype may provide additional benefits for the clinical translation of the proposed therapy for OSA by reducing immune surveillance and responses in anti-AAV antibody seropositive individuals and improving safety profiles by detargeting the liver. A full suite of preclinical safety trials is required, however initial biodistribution studies look promising.

Chapter 4 QUANTIFYING LIGHT-EVOKED AIRWAY DILATION

4.1 INTRODUCTION

Chapters 2 and 3 are submitted as proof-of-concept for a novel optogenetics-based therapy for obstructive sleep apnoea (OSA). First, strong opsin expression was generated in the tongue muscles with minimal off-target expression. Second, in an acute model of sleep-associated upper airway muscle atonia, light-evoked increases in muscle activation, as measured by electromyography (EMG), were achieved. However, EMG alone does not fully characterise the effects of light-evoked muscle activation of airway geometry as it measures electrical activity rather than mechanical output. Moreover, fine wire EMG measures local activity at the electrode location rather than global activity. This is compounded by the anatomical complexity of tongue muscles [26, 84], whereby electrical activity recorded may not correspond to contractions that produce airway dilation. In the current context, EMG recordings are highly dependent on the relative positions of the EMG electrodes, the light source, and the regions of opsin expression. Differences in these positions may have contributed to the discrepancies reported between the amplitude of the light-evoked EMG activity and the observed strength of the light-evoked visible muscle contractions in Chapter 3. Whether light-induced tongue muscle activation is a suitable therapy for OSA depends on the potential for it to stiffen or dilate the pharyngeal airway [71, 86]

Two imaging modalities are feasible options for quantifying airway dilation and/or stiffening during light stimulation in rodents. First, tagged magnetic resonance imaging (MRI) uses a series of radio frequency and magnetic field gradient pulses to superimpose evenly spaced grids or ‘tags’ on targeted tissues. These tag patterns distort with tissue motion and can be used to quantify endogenous and stimulation-induced muscle contractions. Originally developed to image the myocardium [101, 102], tagged MRI has been used to understand better upper airway biomechanics in rats [97, 100, 103, 104] and humans [99, 105, 106]. It has also been used to predict treatment outcomes of mandibular advancement splints in OSA patients [107-109] and, due to its high temporal resolution, to quantify tongue movement during phonation [110, 111]. A second option is ultrasound imaging. In humans, ultrasound imaging has provided a ‘real-time’ method of quantifying airway dilation and tongue movement in OSA patients and healthy controls [43, 112] and is at least as effective as MRI in doing so [43]. Ultrasound has not been used to quantify upper airway function in rodents but has been extensively used to quantify muscle contractions in skeletal [113] and cardiac applications [114]. Compared to MR imaging,

preclinical ultrasounds are low-cost and time-effective. Moreover, protocols are simple to establish and require minimal technical expertise.

This chapter aims to assess ultrasound imaging as a method of quantifying upper airway muscle contractions and airway dilation and to determine whether the EMG data presented in Chapters 2 and 3 translates to light-evoked muscle contractions and airway dilation, thus providing further support for an optogenetics-based therapy for OSA. Moreover, this study aims to provide additional information on the longevity of opsin function following intramuscular injections of an AAVMYO serotype driven by a muscle-specific promoter, using time-evolution of ultrasound-measured light-evoked muscle contractions as a proxy measure of opsin expression. This will assist in identifying the mechanism(s) underpinning the loss of transgene expression, as observed at 12 weeks in Chapter 3.

4.2 METHODS

4.2.1 Animals

All procedures were approved by the University of New South Wales Animal Care and Ethics Committee and follow The Australian Code of Practice for the Care and Use of Animals. Sprague-Dawley (SD) rats were purchased from the Animal Resources Centre (Perth, Australia). All animals were group-housed in a dedicated housing room under a 12-hour light/12-hour dark cycle, and food and water were available ad libitum.

4.2.2 AAV vectors

Based on the strong expression of the opsin with the muscle-specific promoter (tMCK, [330]) in Chapter 2, and AAVMYO [344] in Chapter 3, the construct used in this study was AAVMYO-tMCK-ChR2(H134R):mCherry. The complete expression cassette included the muscle-specific promoter, tMCK, a channelrhodopsin-2 variant with a gain of function substitution (ChR2(H134R)) fused to mCherry, a red fluorescent reporter (pAAV-tMCK-ChR2(H134R):mCherry). This expression cassette sequence (pAAV-tMCK-ChR2(H134R)-mCherry) was developed by GenScript (New Jersey, USA) and packaged into AAVMYO vectors by the Vector and Genome Engineering Facility (Children's Medical Research Institute, Westmead, Australia). The AAVMYO plasmid was provided by Dirk Grimm (University of Heidelberg, Germany) [344].

The AAVMYO-tMCK-ChR2(H134R)-mCherry had a titre of 3.54×10^{13} vg/mL. To maintain consistent vector copies and volume as used in Chapter 3 (20 μL at 4.75×10^{13} vg/mL equating

to 1. 81 × 10^{11} vector copies), 5.1 µL of the AAVMYO construct was diluted in 14.9 µL of injectable saline per animal, equating to 1.81 × 10^{11} vector copies.

4.2.3 Intramuscular AAV injection

Four female SD rats (mean ± SD, age = 7 ± 0 weeks, weight = 175.9 ± 8.0 g) and four male SD rats (mean ± SD, age = 7 ± 0 weeks, weight = 251.8 ± 3.3 g) received intramuscular injections of the AAVMYO construct under general anaesthesia induced with 5% isoflurane in oxygen (1 L/min) in an induction chamber and maintained using 2-3% isoflurane in oxygen (1 L/min) through a nose cone. Adequacy of the anaesthesia was assessed using the negative pedal withdrawal response.

A 25 µL syringe (model 702 LT SYR, Hamilton Company) connected to a sterile 26-gauge needle was used to inject 20 µL of the viral vector construct into four locations (5µL per site) in the animal's tongue (bilateral injections applied to the middle and base of the tongue, see Figure 1A in Chapter 2). The solutions were injected slowly, and the syringe was held in place for 30 seconds after the injection before being slowly retracted from the muscle to minimise vector loss. Animals recovered from the anaesthesia before being returned to their home cage.

4.2.4 High-resolution ultrasound imaging

Three weeks following vector administration to allow for sufficient ChR2(H134R) expression in the tongue, ultrasound imaging was conducted using a fixed MX400 ultra-high frequency linear array transducer (18–38 MHz, centre transmit: 30 MHz, axial resolution: 50 µm) together with a Vevo3100 high-resolution Imaging System (FUJIFILM VisualSonics, Toronto, Ontario, Canada). At this time, the animal cohort was: female (n=4): mean ± SD, age = 9.7 ± 0 weeks, weight = 227.0 ± 13.5 g; male (n=4): mean ± SD, age = 9.9 ± 0 weeks, weight = 388.1 ± 18.1 g.

Anaesthesia was induced using 5% isoflurane in oxygen (1 L/min) in an induction chamber and maintained by using 1.5-3% isoflurane in oxygen (1 L/min) through a nose cone. Adequacy of the anaesthesia was regularly assessed throughout the procedure and based on the negative pedal withdrawal response. The animal's body temperature, heart rate and respiratory rate were monitored using a physiology monitoring platform (Figure 4-1A) (FUJIFILM, VisualSonics, ON, Canada).

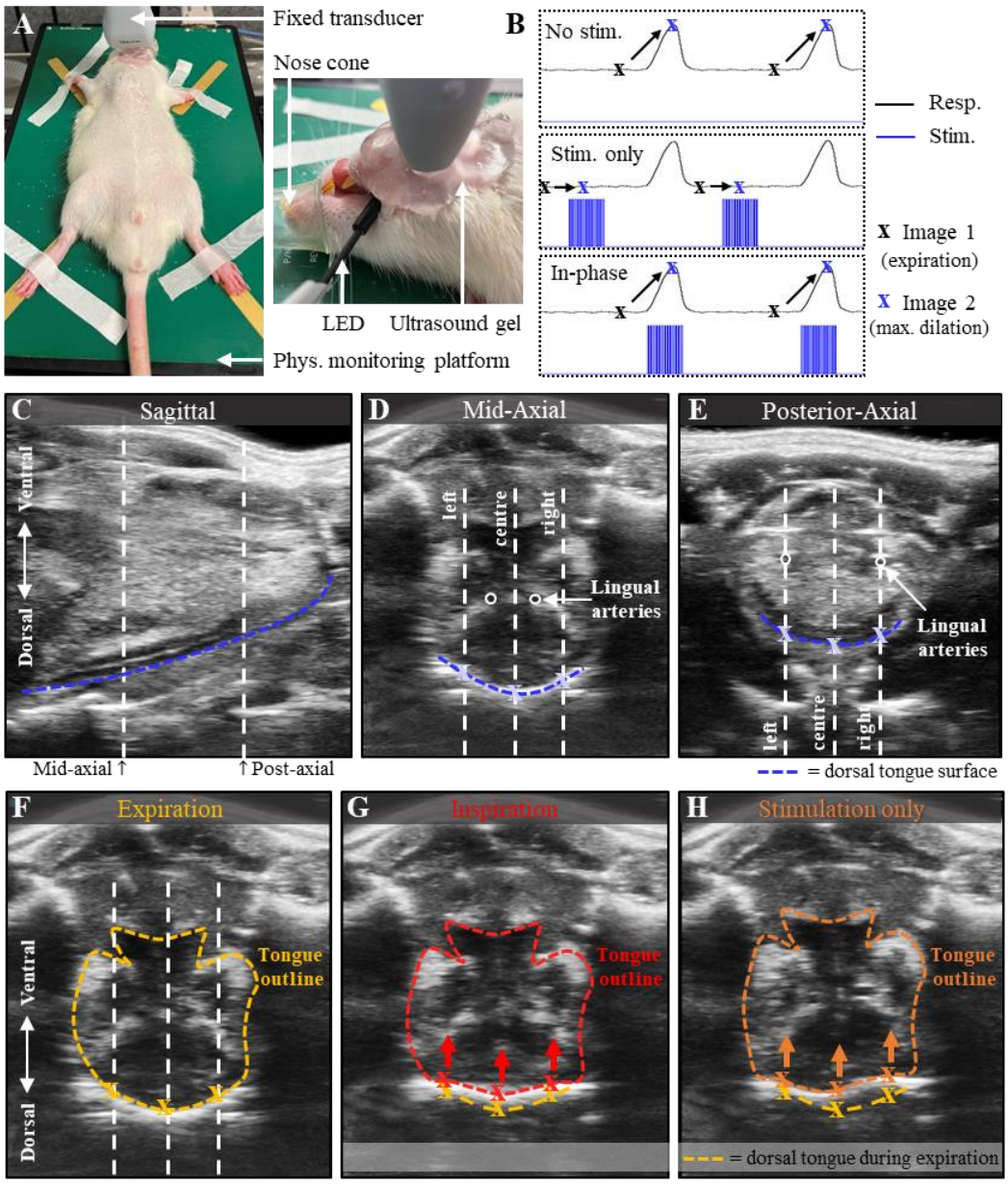

Figure 4-1 | Ultrasound imaging for airway dilation. (A) During ultrasound imaging, animals were placed supine on a physiological monitoring platform, and images were acquired using a fixed transducer. **(B)** The airway was imaged during three conditions; i) no stimulation, ii) stimulation only (i.e. stimulation applied 'out-of-phase' with the respiratory cycle), and iii) light stimulation applied 'in-phase' with the respiratory cycle. **(C)** B-mode images (400 frames, acquired at 45 frames per second) were captured in a sagittal plane, **(D)** a mid-axial plane, and **(E)** a posterior-axial plane. Airway dilation was quantified as the vertical displacement of the dorsal surface of the tongue along three vertical lines, labelled 'left', 'centre' and 'right'. **(F)** The coordinates of the dorsal surface and vertical line intersections were recorded during expiration, **(G)** and inspiration (no stimulation), and when **(H)** stimulation was applied 'out-of-phase' with inspiration (stimulation only), and 'in-phase' with inspiration (not pictured). These coordinates were then used to calculate the ventral displacement of the tongue's dorsal surface.

After depilation, pre-warmed ultrasound gel was applied to the submandibular region while the animal was supine (Figure 4-1A). When using the transducer, care was taken to minimise soft tissue deformation, applying only enough pressure to make complete contact with the gel. B-Mode images (400 frames, 45 fps, transducer fixed at 90°) were acquired using during three conditions; 1) no light stimulation, 2) light stimulation applied 'out-of-phase' with the respiratory cycle i.e. between expiration and inspiration when endogenous tongue movement was minimal, and 3) light stimulation applied 'in-phase' with the respiratory cycle, i.e. light stimulation was applied at inspiration onset (Figure 4-1B). The primary stimulation protocol used in this study was based on the outcomes described in Chapter 2, where 10 ms pulse widths applied at 40 Hz produced strong and consistent EMG activity. This stimulation was applied to the tongue for ~ 300 ms by a 470 nm fibre-coupled LED (Thorlabs, Lastek, SA Australia). Other stimulation protocols tested include low-frequency stimulation (10 ms pulse widths at 10 Hz), high-frequency stimulation (10 ms pulse widths at 60 Hz), and continuous pulsed stimulation (10 ms, 40 Hz applied over 1 second). B-mode images were acquired in three planes. A mid-sagittal plane was positioned between the lingual arteries and extended from the base of the tongue to where the teeth created an image artefact (e.g. Figure 4-1C). The positions of a mid-axial plane (Figure 4-1D) and a posterior-axial plane (Figure 4-1E) are indicated by the orange and red dotted lines in Figure 4-1C, respectively. Sample videos demonstrating 'out-of-phase' light-evoked airway dilation in the sagittal and mid-axial planes are included in the Appendix (Video A4-1 and Video A4-2).

Ultrasound imaging was repeated 6, 8, 10 and 12 weeks after intramuscular injections to assess longevity of the functional response. To minimise impact on the animals, subsequent ultrasound imaging sessions ceased when an animal failed to exhibit any light-evoked muscle movement.

All acquired images were digitally stored in DICOM format for offline analysis.

4.2.5 Ultrasound image analysis

Quantitative analysis was manually performed in ImageJ on mid-axial and posterior-axial images. Three images sequences were analysed per animal to measure maximum dilation; (1) when no stimulation was applied and movement was due to endogenous inspiration-linked muscle contractions (Figure 4-1B, G); (2) when stimulation was applied 'out-of-phase' with inspiration, and movement was due to light stimulation only (Figure 4-1B, F), and (3) when stimulation was applied 'in-phase' with inspiration, and movement was due to the combined effects of endogenous inspiration-related muscle contractions and light-evoked muscle contractions (Figure 4-1B). In each sequence (400 B-mode images), there were 4 or 5 'maximum dilations' where vertical displacement of the tongues dorsal surface was quantified.

In both axial planes, three vertical lines were placed on the first frame of each sequence and were maintained throughout. In the mid-axial plane, the 'centre' line was placed between the two lingual arteries, and the 'left' and 'right' lines were placed between a lingual artery and the lateral border of the tongue (Figure 4-1D). In the posterior-axial plane, the 'centre' line was placed between the two lingual arteries, and the 'left' and 'right' lines were placed on the lingual arteries (Figure 4-1E). A single point was placed at each of the three intersections between the tongues dorsal surface and the three vertical lines (Figure 4-1D-H). Throughout the image sequences, as the muscles contracted, the movement of the points along the vertical lines was manually tracked. When the dorsal surface was maximally displaced (i.e. the three points had reached a turning point between ventral and dorsal movement) due to inspiration (Figure 4-1B, G), stimulation (Figure 4-1B, H), or both (Figure 4-1B), the 'maximum dilation' y-coordinates were recorded. The vertical displacement of the points was calculated by subtracting the y-coordinates of the preceding 'baseline' or 'expiration' point, where there was no visible contraction (Figure 4-1B, F). For example, in Figure 4-1H, the y-coordinates of the yellow markers that represent the tongue's location during 'expiration' (i.e. Figure 4-1F) were subtracted from the y-coordinates of the orange markers that represent the tongue's location during 'stimulation'. This produces the vertical displacement of the three points, indicating the amount of airway dilation achieved when stimulation is applied.

All displacements obtained from the same sequence were averaged, producing three sets (inspiration, stimulation only, in-phase stimulation) of three data points (left, centre, and right).

4.3 RESULTS

4.3.1 Ultrasound-recorded light-evoked airway dilation was variable between animals

Three weeks after injections, light-evoked muscle contractions were observed during ultrasound imaging in 4 of the 8 animals (50%, Table 4-1). Only two animals produced sufficient light-evoked muscle contractions to dilate the airway (25%, Table 4-1).

In animal E5 (Table 4-1,
Figure **4-2**), light-evoked muscle contractions and airway dilation were strong in the mid-axial plane, shifting the dorsal surface of the tongue 0.75 ± 0.03 mm ventrally (maximum) when stimulation was applied 'out-of-phase' with inspiration. The maximum vertical displacement was maintained with 'in-phase' stimulation (0.71 ± 0.03 mm maximum displacement) and exceeded the maximum vertical displacement associated with a standard breath (no stimulation, 0.21 ± 0.02 mm maximum displacement) (
Figure **4-2**B, Figure 4-3). Maximum dilation was recorded in the tongue region closest to the

light source, i.e. it was laterally dominant (the other side of the dorsal tongue surface moved 0.14±0.05 mm ventrally,
Figure **4-2**B). Airway dilation was larger and more even across the dorsal surface in the posterior region of the tongue (as illustrated in the sagittal section in
Figure **4-2**C), however posterior-axial images were not collected three weeks post-injection (with one exception: Animal E6, see Appendix Figure A4-1), so this dilation was not quantified.

Table 4-1 | Qualitative ultrasound observations from three to twelve weeks after vector administration. 'Any' indicates when light-evoked contractions were visible regardless of whether they were associated with airway dilation, and 'Dilate' indicates when light-evoked muscle contractions achieved airway dilation. No further ultrasounds were performed (indicated by '-') on animals in which no light-evoked movement was detected (×)

Animal	Week 3		Week 6		Week 8		Week 10		Week 12	
	Contractions visible in axial planes									
	Any	Dilate	Any	Dilate	Any	Dilate	Any	Dilate	Any	Dilate
E1	×	×	-	-	-	-	-	-	-	-
E2	×	×	-	-	-	-	-	-	-	-
E3	✓	×	✓	×	✓	×	✓	×	✓	×
E4	×	×	-	-	-	-	-	-	-	-
E5	✓	✓	✓	✓	✓	✓	✓	×	✓	×
E6	✓	✓	✓	✓	✓	✓	✓	×	✓	×
E7	×	×	-	-	-	-	-	-	-	-
E8	✓	×	✓	×	✓	×	✓	×	✓	×

In Animal E6 (Figure 4-3A and Appendix Figure A4-1) no light-evoked airway dilation was visible in the mid-axial plane, however light-evoked muscle contractions and airway dilation were recorded in the posterior-axial plane. The tongue's dorsal surface moved 0.57±0.06 mm ventrally (maximum), improving the absence of movement recorded during inspiration (0.00±0.08 mm maximum vertical displacement). Airway dilation was laterally dominant, and the side of the tongue furthest from the light source displayed no muscle contractions or airway dilation with light stimulation (0.06±0.12 mm).

Two animals (Animal ID: E3, E8, Figure 4-3A and Appendix Figure A4-1) had weak light-evoked responses. E3 displayed limited airway dilation with inspiration, only visible in the mid-sagittal plane. E8 displayed small muscle contractions, but airway dilation was not visible in the planes imaged. The small contractions in both animals were difficult to obtain as they required specific positioning of the LED against the tongue.

The remaining four animals (Animal ID: E1, E2, E4, and E7) displayed no visible light-evoked muscle contractions (Figure 4-3A and Appendix Figure A4-1).

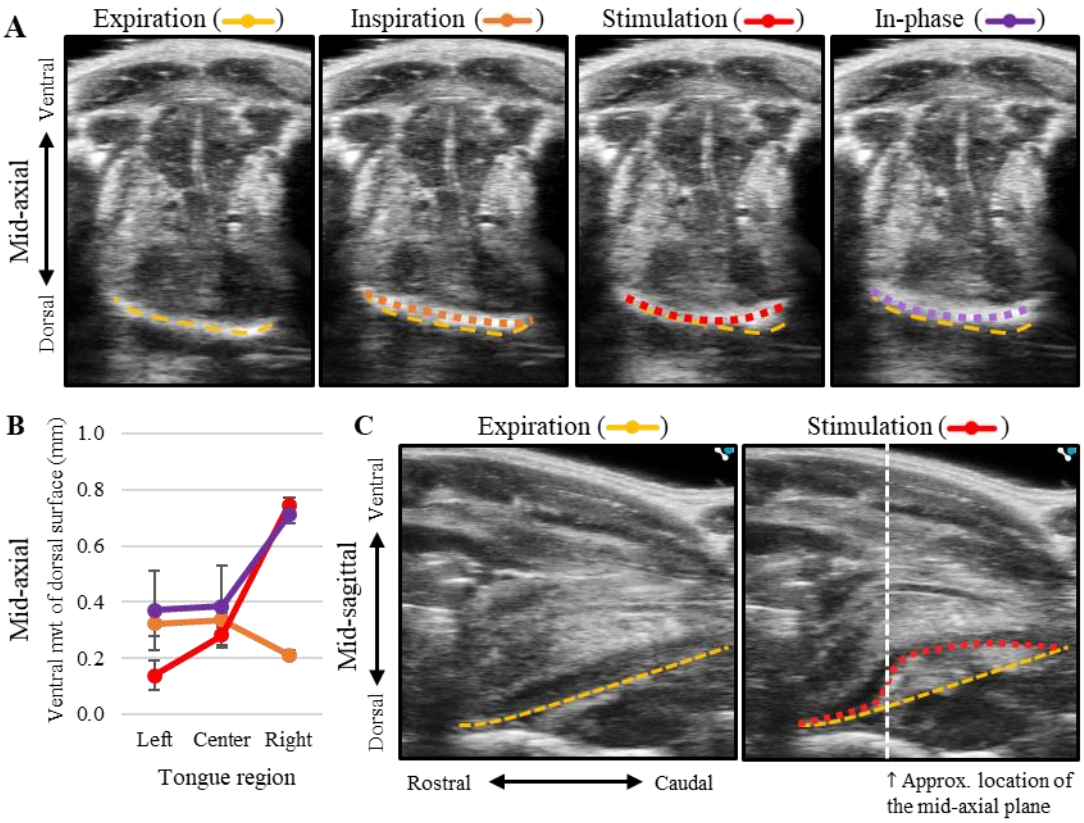

Figure 4-2 | Sample data from three weeks after intramuscular injections in an animal where light-evoked upper airway muscle contraction and airway dilation was observed. (A) Dorsal surfaces of the tongue during expiration (yellow dashed lines), inspiration (i.e. no stimulation, orange dashed lines), stimulation only (red dashed lines), and 'in-phase' stimulation (i.e. stimulation and inspiration, purple dashed lines) are indicated. **(B)** Light stimulation produces laterally dominant airway dilation (red), which persists when light stimulation is applied in phase with inspiration. **(C)** Airway dilation is strongest in the caudal/posterior region of the tongue rather than the rostral/anterior region where the mid-axial plane is located.

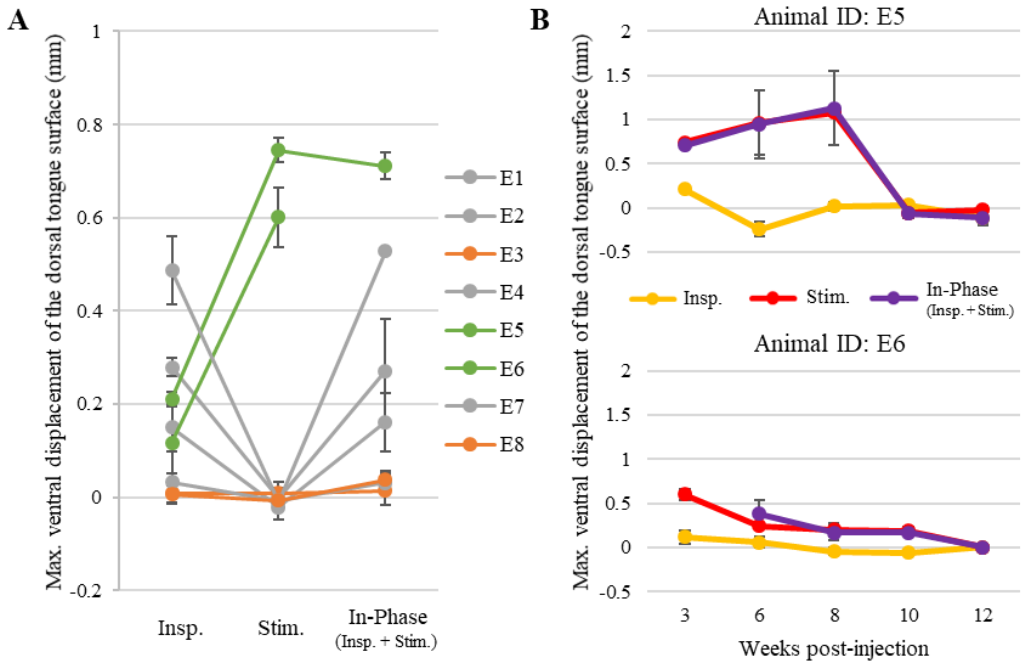

Figure 4-3 | Light-evoked airway dilation following intramuscular injections of an optogenetics construct . (A) At three weeks, two animals (green) displayed light-evoked muscle contractions and airway dilation and two (orange) displayed light-evoked muscle contractions but did not achieve light-evoked airway dilation. The four remaining animals (grey) did not display any light-evoked muscle contractions **(B)** The animals that displayed light-evoked airway dilation at three weeks maintained these responses until ~ 8 to 10 weeks after injections. At this time, light-evoked muscle contractions weakened and airway dilation was not visible in an axial plane.

4.3.2 Persistence of light-evoked muscle contractions 12 weeks after intramuscular injections

In animals where light-evoked muscle contractions were seen three weeks after receiving intramuscular injections of the optogenetics construct (n = 4/8), these light-evoked muscle contractions remained visible at 12 weeks. However, contraction strength, quantified by the amount of airway dilation it generates and/or the volume of tissue that is visibly contracting (where airway dilation does not occur), began to decline between the 8 and 10-week ultrasounds (Figure 4-3B, Figure 4-4 and Appendix Figure A4-2). Additionally, contractions were less likely to achieve airway dilation and were harder to generate, i.e. they required more precise LED positioning and/or firmer pressure of the LED onto the tongue surface.

The animal who was the best responder (E5) at three weeks exhibited strong muscle contractions and airway dilation during the ultrasound conducted eight weeks after injections (Figure 4-3B and Figure 4-4A, B). The posterior-axial images exhibited a maximum ventral displacement of 1.08±0.05 mm when light stimulation was applied out-of-phase with inspiration (Figure 4-3B), exceeding the maximum achieved during the ultrasound conducted 3

weeks post-injections. Dilation occurred along the entire dorsal surface, with a minimum ventral displacement of 0.84±0.08 mm. At 10 weeks, only a slight light-evoked airway dilation was visible at the extreme caudal end of the tongue (see the mid-sagittal images, Figure 4-4C) but was not evident in either axial plane. At 12 weeks, light-evoked muscle contractions were present but did not produce airway dilation (Figure 4-3B and Figure 4-4B).

Similar declines in responses were seen after 8 weeks in all other animals that responded to light stimulation three weeks after viral vector injections, whether the light stimulation generated small airway dilations (E6, Figure 4-3B and Appendix Figure A4-2) or muscle contractions with no dilation (E3 and E8, Appendix Figure A4-2), exhibited similar declines, with light-evoked responses persisting until 8-weeks after vector administration. Animal E6, which had initially dilated the airway by 0.57±0.06 mm with stimulation at 3 weeks, produced only 0.20±0.07 mm with stimulation at 8 weeks, 0.19±0.04 mm at 10 weeks (Figure 4-3B and Appendix Figure A4-2), and while quantitative measures of displacement could not be made at 12 weeks due to poor clarity of the dorsal surface, no displacement was observed. The animals who responded to light stimulation 3 weeks after injections with small and localised muscle contractions (no dilation) similarly maintained some light-evoked responses at 12 weeks, but achieving those contractions became increasingly difficult.

Twelve weeks after injections, clear ultrasound images were challenging to obtain in the male rats, likely due to the greater size of the animals (male rat weight at 3-week ultrasound: 251.8 ± 3.3 g; weight at 12-week ultrasound: 552.0 ± 42.9 g, mean ± sd). While this increase represented a healthy weight gain over this time period (female rats also exhibited healthy weight gain, however their maximum weight was 291.0 ± 17.2 g), the larger animals made airway imaging via ultrasound difficult. In both axial frames, global muscle contractions remained visible (endogenous and light-stimulated), but deeper edges (mainly the dorsal surface in the mid-axial plane) were blurred and often not sufficiently defined for the semi-automated image analysis. Anatomy was better visualised in the mid-sagittal plane, however light-evoked contractions were challenging to capture as they tended to be more lateral (closer to the LED).

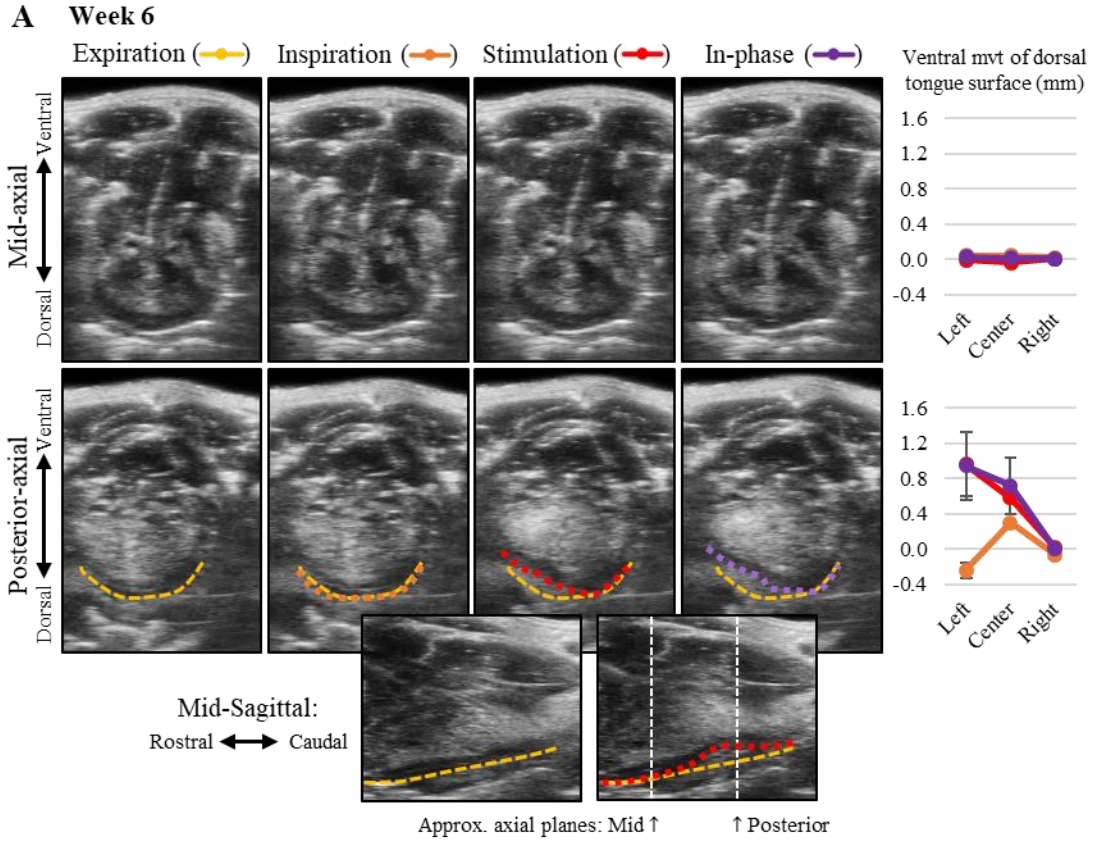
A
Week 6
Expiration
Inspiration
Stimulation
In-phase
Ventral mvt of dorsal tongue surface (mm)
Mid-axial
Ventral
Dorsal
Posterior-axial
1.6
1.2
0.8
0.4
0.0
-0.4
Left
Center
Right
Mid-Sagittal:
Rostral
Caudal
Approx. axial planes: Mid
Posterior

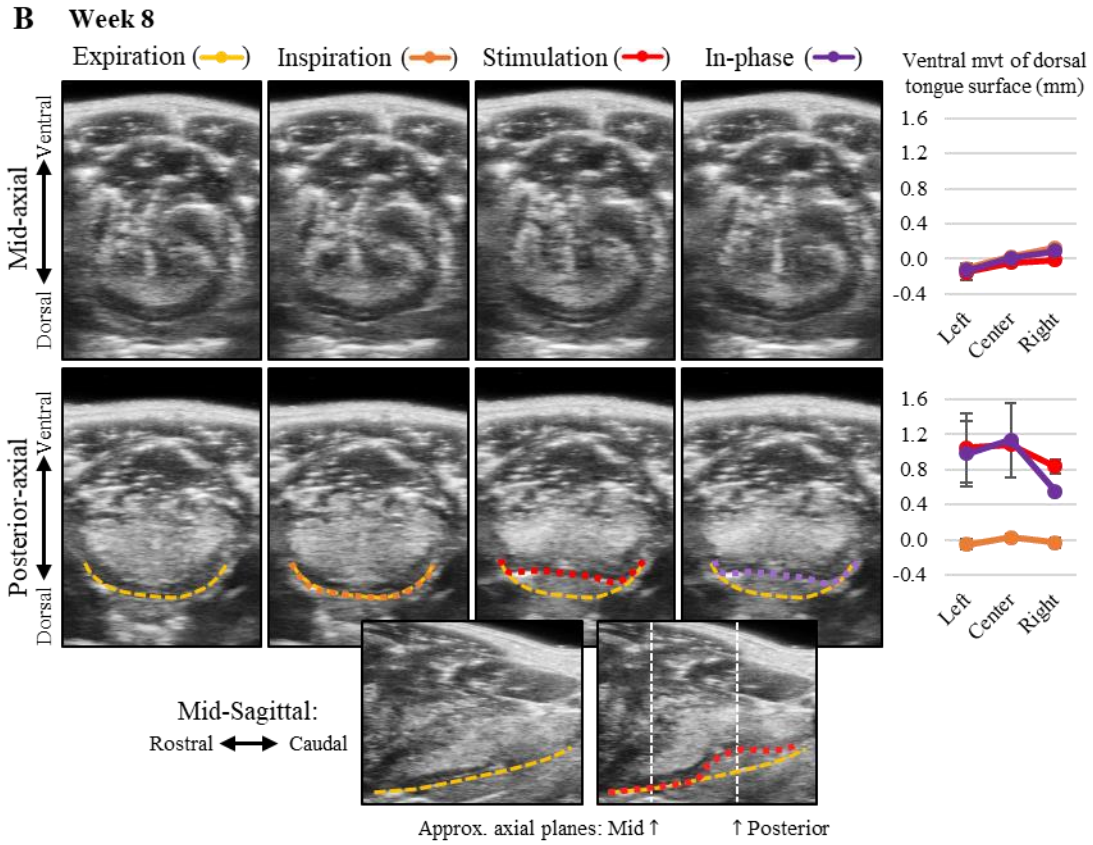
B
Week 8
Expiration
Inspiration
Stimulation
In-phase
Ventral mvt of dorsal tongue surface (mm)
Mid-axial
Ventral
Dorsal
Posterior-axial
1.6
1.2
0.8
0.4
0.0
-0.4
Left
Center
Right
Mid-Sagittal:
Rostral
Caudal
Approx. axial planes: Mid
Posterior

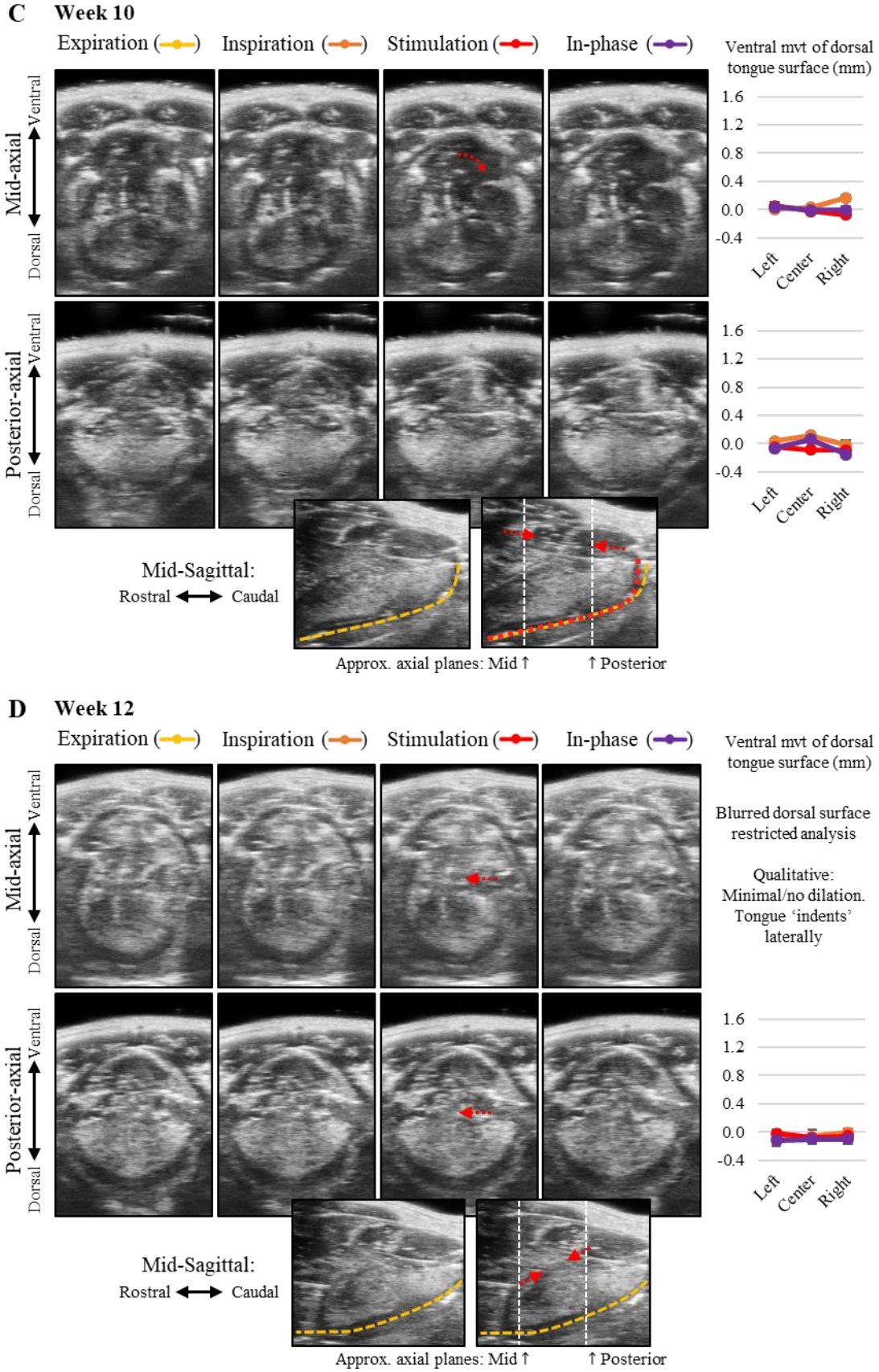
C
Week 10
Expiration
Inspiration
Stimulation
In-phase
Ventral mvt of dorsal tongue surface (mm)
Mid-axial
Ventral
Dorsal
Posterior-axial
1.6
1.2
0.8
0.4
0.0
-0.4
Left
Center
Right
Mid-Sagittal:
Rostral
Caudal
Approx. axial planes: Mid
Posterior
D
Week 12
Blurred dorsal surface restricted analysis
Qualitative: Minimal/no dilation. Tongue 'indents' laterally

Figure 4-4 | Sample data from 6 to 12 weeks after intramuscular injections indicates that when functional responses to light are present three weeks after injections, they persist, albeit at reduced strengths for 9 weeks. (A) At 6 weeks and **(B)** 8 weeks after injection, airway dilation remains strong. Dilation is greater on one side of the tongue, and in the posterior-axial frame. **(C)** 10 weeks after injection, contraction strength declined and airway dilation is minimal. In this animal, it has not been captured in either axial plane, but can be seen in the mid-sagittal plane 'behind' the tongue following light-evoked geniohyoid contraction. **(D)** 12 weeks after injection, contraction strength has declined further, and airway dilation is no longer visible. In all panels, dashed lines indicate the dorsal surface of the tongue during expiration (yellow), inspiration (no stimulation, orange), stimulation only (red), and in-phase stimulation (stimulation and inspiration, purple).

4.3.3 Light-evoked muscle contractions and airway dilation are dependent on the stimulation protocol and are visibly different to endogenous contractions

All tetanic contractions described above were generated by 10 ms pulse widths at 40 Hz stimulation. Low-frequency stimulation (10 ms applied at 10 Hz) produced twitches rather than tetanic contractions, i.e. an isolated contraction per light pulse. High-frequency stimulation (60 Hz) produced strong tetanic contractions over the standard stimulation time (~ 300 ms), however when high-frequency stimulation was maintained for more than 1 second, contraction strength gradually declined and eventually disappeared. In contrast, continuous stimulation using the 10 ms and 40 Hz protocol produced strong contractions that persisted throughout the stimulation period, which exceeded 1 second.

The movements generated with light stimulation did not always match those occurring in a natural (unstimulated) breath. Unstimulated contractions recorded in the sagittal plane tended to appear as a caudal 'shift' of the tongue during inspiration. In contrast, light-evoked muscle contractions were more likely to present as localised airway dilation perpendicular to the posterior pharyngeal wall. In the axial plane, this difference was also evident. Endogenous contractions often presented as a 'flattening' of the tongue's dorsal surface, and light-stimulated contractions were more likely to generate airway dilation by shifting the dorsal surface ventrally away from the posterior pharyngeal wall. Notably, the best-performing animals (E5 and E6) exhibited varying movement patterns with different LED positions, suggesting that some of this variation may be due to LED positioning.

4.4 DISCUSSION

The key finding of this Chapter is that, following intramuscular injections of a novel muscle-specific optogenetic construct to the tongue, light-evoked muscle contractions and airway dilation were observed. While there was considerable variation between animals, these data support previous Chapters' evidence for a novel optogenetics-based muscle-stimulation therapy for OSA. In achieving this, this study has also demonstrated the first use of ultrasound imaging

to examine upper airway anatomy and function in rodents. This first attempt is promising, but will require further development and assessment to determine validity and reliability.

Three weeks after receiving intramuscular injections of the optogenetic construct, varied strengths of light-evoked muscle contractions and airway dilation were achieved. Of eight animals, only two had sufficient light-evoked contractions to achieve airway dilation, two displayed only small light-evoked contractions and no airway dilation, and four did not respond to light stimulation. This poor success rate contrasts with the animals that received the equivalent construct and underwent electrophysiology experiments described in Chapter 3. During these experiments, 8 of 9 animals produced strong visible tongue contractions with very few limitations regarding LED position. Both cohorts followed identical protocols; rats were the same strain and received identical intramuscular injections at approximately seven weeks of age. The same rAAV serotype, expression cassette, viral loads, volumes and distributions were applied (AAVMYO-tMCK-ChR2(H134R):mCherry, 1.81 x 10^{11} genome copies). The delay between injections and functional testing (three weeks until the first ultrasound and three weeks until the electrophysiology experiments) and the mode of light delivery were identical. The sole difference between cohorts was the viral vector 'batch' or 'lot', i.e. two different production runs of the same construct were used. After consultation with the viral vector facility, it was concluded that the discrepancy in light-evoked functional responses was most likely due to a manufacturing fault in the second 'batch' used in the ultrasound cohort resulting in vector genome instability and increasing variability. Sequencing analysis is currently underway to confirm this.

When light-evoked muscle contractions were present three weeks after vector administration, they persisted until the final ultrasound was conducted nine weeks later (12 weeks post-injection), albeit at reduced strengths after 8-10 weeks. This is consistent with the data presented in Chapter 3, where DNA copy numbers and RNA expression in the tongue three weeks after injections were substantial, but much reduced levels were detected at 12 weeks. The current ultrasound study indicates that the reduction in light-evoked muscle strength – here a proxy for opsin expression – seemed to occur between the ultrasounds conducted 8 and 10 weeks after vector administration. This delayed decline suggests that the viral vector and transgene evaded acute initial immune responses associated with pre-existing antibodies to the AAV capsid, pre-existing t-cell immunity and acute innate immunity [507]. Instead, the reduction in muscle contractions may be due to a delayed immune response [507], skeletal muscle cell turnover [508], and/or promoter silencing [509]. As promoter silencing is more commonly reported for viral promoters than non-viral promoters, such as tMCK used here [406,

416-418, 509], this is a less likely mechanism for reduced expression. Future experiments are required to isolate the cause of transgene losses could include an immune suppression protocol to inhibit T cell activation and antibody formation over the 12-week monitoring period. Should light-evoked muscle contractions be maintained at consistent strengths, it will be possible to conclude that immune responses rather than skeletal muscle cell turnover caused the declines in light-evoked muscle contractions and airway dilation reported in this Chapter, and viral DNA copy numbers and RNA expression level reported in Chapter 3.

The initial aim of the intramuscular injections described throughout this thesis was to 'saturate' the tongue muscles with opsin expression. This decision followed electrical stimulation studies where activation of multiple tongue muscles (i.e. intrinsic and extrinsic, protruders and retractors) generated greater airway dilation, pharyngeal stiffening and/or airflow than stimulation of a single muscle group [37, 46, 72]. While earlier chapters reported that light stimulation could generate strong contractions, they were highly localised and typically drew a small region of the tongue's dorsal surface away from the posterior pharyngeal wall. These contractions did not reflect endogenous contractions, which presented in the mid-sagittal plane as an anterior-posterior shift of the tongue. This difference in the spatial patterns of contraction between the endogenous and stimulated contractions is likely due to the single blue light source ineffectively penetrating tissue and thus incompletely activating all transduced myofibres, despite widespread expression (as shown in the histology images in Chapter 3). Preclinical studies of hypoglossal nerve stimulation typically quantify stimulation efficacy by comparing stimulated and unstimulated cross-sectional areas and anteroposterior and lateral dimensions of axial airways [46, 72, 498], which is challenging with ultrasound, especially in the larger male rats. In non-imaging protocols, measures of flow mechanics are typically used (e.g. rate of airflow, pharyngeal critical closing pressure, pharyngeal resistance) [37]. In humans, efficacy is defined via polysomnography outcomes and quality-of-life measures. The results reported here suggest that airway dilation is achievable, and it is therefore highly likely that the use of red-shifted opsins and LED arrays, to improve light penetration and thus more widespread contractions, will provide greater airway dilation and thus patency, regardless of whether the induced muscle contractions exactly mimic endogenous contractions. Indeed, the clinically approved Inspire device unilaterally stimulates the hypoglossal nerve [170, 171], which, while improving airflow, can also induce tongue deviation [71], supporting the contention that airway dilation is more critical than the specific pattern of contractions that generate it.

The results presented in this chapter have demonstrated that, light stimulation of optogenetically transduced upper airway muscles can dilate the upper airway to a similar extent to endogenous

respiratory-related contractions in a rodent model of upper airway muscle hypotonia mimicking sleep-related drop in dilator muscle drive where sufficient opsin expression has been generated. However, additional work to improve consistency between animals is required. Moreover, it was found that light-evoked responses persisted for up to 12 weeks in animals who responded well three weeks after receiving the optogenetic construct, albeit declining in strength after 8-10 weeks, indicating the successful evasion of pre-existing and acute immune responses. The reasons for the late decline in functional response require further study.

Chapter 5 QUANTIFYING THE EFFECTS OF CHRONIC LIGHT STIMULATION

5.1 INTRODUCTION

Optogenetics applied in the periphery is a niche field of research that has inspired some creative solutions for light delivery in freely behaving animals, often in combination with traditional physiological or behavior methods. Recent examples include cuff-based optics for motor neuron or peripheral nerve stimulation [456], flexible and stretchable polymer optical fibres for vagus nerve stimulation [513], wireless LEDs implanted opposing the colon wall and powered by resonant cavity for colonic motility [514], and a fully implanted system that combines a flexible sensor encircling the bladder to continuously monitor organ function and microscale LEDs to activate bladder sensory afferents [252]. These examples represent bespoke solutions to specific experimental and translational challenges.

In the context of an optogenetic therapy for OSA, it is also important to understand the longer-term effects of regular optogenetic-based stimulation on the tongue musculature. This includes establishing that chronic stimulation does not cause reduced dilator muscle performance over time, undesirable tissue changes, or major sleep disturbance.

To date, only four studies have reported direct optogenetic activation of skeletal muscle [235, 254, 255, 464], none have done so without anaesthesia, and only one has reported on the effects of daily light stimulation. In that study, 1 hour per day of transcutaneous light stimulation (500 ms pulsed stimulation, repeated every 6 seconds) was applied to the skin directly above the denervated muscle expressing ChR2(H134R) with the animal under isoflurane anaesthesia. After 10 days, the animals that received daily light stimulation demonstrated significantly less force attenuation and muscle atrophy than those that did not receive daily light stimulation [254]. For the purposes of the novel optogenetics-based muscle stimulation therapy for OSA studied in this thesis, an experimental protocol is required that allows quantification of the effects of *chronic* light stimulation (optimal OSA therapy use is 7 to 8 hours per night, indefinitely) and determine whether light-evoked muscle contractions differ during REM and NREM sleep. This requires hardware and a surgical protocol that is suitable for extended (chronic) stimulation and recording of both muscle activity (EMG), and respiratory and sleep parameters via electroencephalography (EEG).

Several studies have successfully implanted hook electrodes and skull-mounted hardware to monitor rodent genioglossus activity during wakefulness, REM sleep and NREM sleep [87, 188,

455, 515], to investigate upper airway muscle responses to CO_2 administration [87] and GABAA receptor antagonism [515]. Similar hardware has also been used in chemogenetic and optogenetic studies where DREADD (Designer Receptors Exclusively Activated by Designer Drugs) ligands or light stimulation administered to engineered hypoglossal motor nuclei altered downstream muscle activity in the tongue [188, 455]. While these protocols did implant EMG and EEG hardware for monitoring genioglossus activity and identifying sleep stages, recordings were taken at a single time point, one week [87, 515] or 2 weeks [188, 455] post-surgery, rather than repeatedly over several weeks. Additionally, the optogenetic study delivered light centrally, at the motor nucleus, using well-established methodology and off-the-shelf optogenetic consumables (e.g. rigid silica optical fibre:ferrules implanted into the brainstem and fixed to skull). This hardware is unsuitable for light delivery to the tongue.

This thesis chapter describes five pilot studies aiming to develop novel methods that integrate muscle optogenetics, electrophysiology, and whole-body plethysmography, to enable long-term physiological studies in freely behaving animals. Our primary objective was to optically stimulate the tongue and measure the long-term efficacy of tongue optical stimulation via EMG in sleeping animals. To do this, it was necessary to (1) design, fabricate and test novel optical hardware for implantation to deliver blue light to the base of the tongue, (2) integrate this with hardware for chronic electrophysiological recordings of EMG, EEG, heart rate (HR), and temperature, (3) integrate this equipment into a custom-made whole-body plethysmography recording chamber for non-invasive monitoring of breathing, behaviour and natural sleep.

5.2 HARDWARE DEVELOPMENT

Future research investigating the effects of chronic light stimulation of muscle requires the implantation of hardware able to deliver light to the tongue and enable phasic stimulation of muscle with the onset of inspiration. The hardware must also record the subsequent changes in muscle activity and facilitate the identification of wakefulness and sleep stages (REM and NREM). While optimal hardware for behaviour-related experiments is untethered, a skull-secured connection point is acceptable when the targeted behaviour is sleep.

5.2.1 Light delivery requirements

The hardware that delivers light to the tongue must fulfil the following requirements:

1. Light intensity: The device must receive sufficient power to generate the light intensities required to induce muscle contractions.
2. Minimal tethering: As noted, while optimal hardware for behavioural experiments is untethered, a skull-secured connection point is acceptable for sleep-based experiments.

A tethered point also simplifies data recording, reduces costs, increases the ease of fabrication, and reduces power restrictions commonly associated with wholly implantable devices.

3. Robust: The device must withstand surgical implantation and long-term use without incurring damage or functional deficits.
4. Flexible: The device must be sufficiently flexible to minimise tissue damage during implantation and allow free movement and animal comfort post-surgery.
5. Inexpensive: The device should use commercially available components that are low-cost and/or sterilisable and reusable.
6. Adaptable: An adaptable device that can incorporate additional recording components may benefit later experiments (e.g. a thermistor to measure local heating at the stimulation site).

Three methods of light delivery were considered; (1) a flexible printed circuit board, (2) an optical fibre, and (3) a wholly implanted device.

1. A flexible printed circuit board (PCB)

A PCB for light delivery to the upper airway muscles received power via a skull-secured pedestal. The power was then directed along a highly flexible PCB, which extends subcutaneously from the skull and posterior to the animal's ear before projecting anteriorly towards the tongue tissue. LEDs soldered to the end of the PCB were secured within the tongue tissue. Commercial fabrication of a completely customisable PCB (without electrical components) is less than AUD$10 per unit (WellPCB, ShijiaTzhuang Hebei, China), and standard surface mount chip LEDs cost less than $1 per unit (element14, Sydney, Australia). The completely customisable design means spare soldering sites can be included, and future studies can integrate other surface-mounted components and record additional data without additional hardware or altered surgical protocols. For instance, exposed terminals can record surface EMG activity, or thermistors can monitor localised heating.

2. An optical fibre

An optical fibre delivers light generated by an external source via a skull-secured component (fibre optic ferrule). There are no restrictions concerning power and light intensity, and while the fibre is less flexible than the PCB option, it should be sufficient for this application, i.e. to extend subcutaneously from the skull to the mandible. Fibre optic fabrication is cost-effective at approximately AUD$10 per unit (Lastek, South Australia, Australia), assuming the LED driver,

fibre-coupled LED and patch cables are already available. If these must be purchased, there is an additional one-off cost of approximately AUD$1,400 (Lastek, South Australia, Australia).

3. A completely implanted device

Wholly implanted devices that are wirelessly recharged, e.g. by inductive [516] or resonance magnetic coupling [252], are untethered and have demonstrated biomechanical compatibility and efficacy for wireless, 'closed-loop' optogenetic stimulation of peripheral tissue e.g. light stimulation of the bladder in response to data acquired from an encircling stretchable strain gauge that identifies filling and voiding behaviours [252]. Devices using commercially available materials and electronic components that can be processed and assembled using standard fabrication techniques have been developed [516]. However, these devices remain significantly more complex and expensive than the PCB and optical fibre alternatives.

These options and how they fulfil the listed requirements are summarised in Table 5-1. For this project, the flexible PCB with integrated LED chips was selected as our preferable light source, and the optical fibre was selected as our alternative. Methods for the fabrication of both options are outlined below.

Table 5-1 | Summary of devices able to deliver light stimulation to the tongue. Flexible PCBs, optical fibres and fully implanted devices have different characteristics that make them suitable for the presented application.

Device	Light intensity	Untethered	Flexible	Robust	Inexpensive	Adaptable
1. PCB	×	×	✓	✓	✓	✓
2. Optical fibre	✓	×	✓	✓	✓	×
3. Implanted	×	✓	✓	✓	×	×

5.2.1.1 Flexible printed circuit board with embedded LED

The progression of the flexible PCB development is pictured in Figure 5-1. All PCBs were designed via CAD software[2] and manufactured by WellPCB (ShijiaTzhuang Hebei, China). The initial prototype used a 'serpentine' connection between the LEDs and the skull-secured pedestal. This prototype was discarded as it increased the risk of soft tissue catching during implantation and therefore increased surgery difficultly and the risk of tissue damage. It may also increase the risk of tissue damage and animal discomfort during post-surgery movement. The second prototype was manufactured to connect to a 12-channel electrode pedestal (P1 Technologies, Bioscientific, NSW, Australia). This prototype was discarded due to the expense of the 12-channel system components, the predicted difficulty connecting all pins to a single

[2] All CAD files for PCB manufacturing were created by Tom Kulaga, Graduate School of Biomedical Engineering, University of New South Wales

pedestal with dense ports, and the increased risk of between electrode contacts and noise during data collection. The third prototype was manufactured to connect to the cheaper 6-channel pedestal system (P1 Technologies, Bioscientific, NSW, Australia). The final iteration (Figure 5-1B) added four suture points so the PCB could be firmly secured to soft tissue. Two LED chips were soldered to the 'front' of the PCB, and an additional recording component could be soldered to the 'back' should it be required in future research.

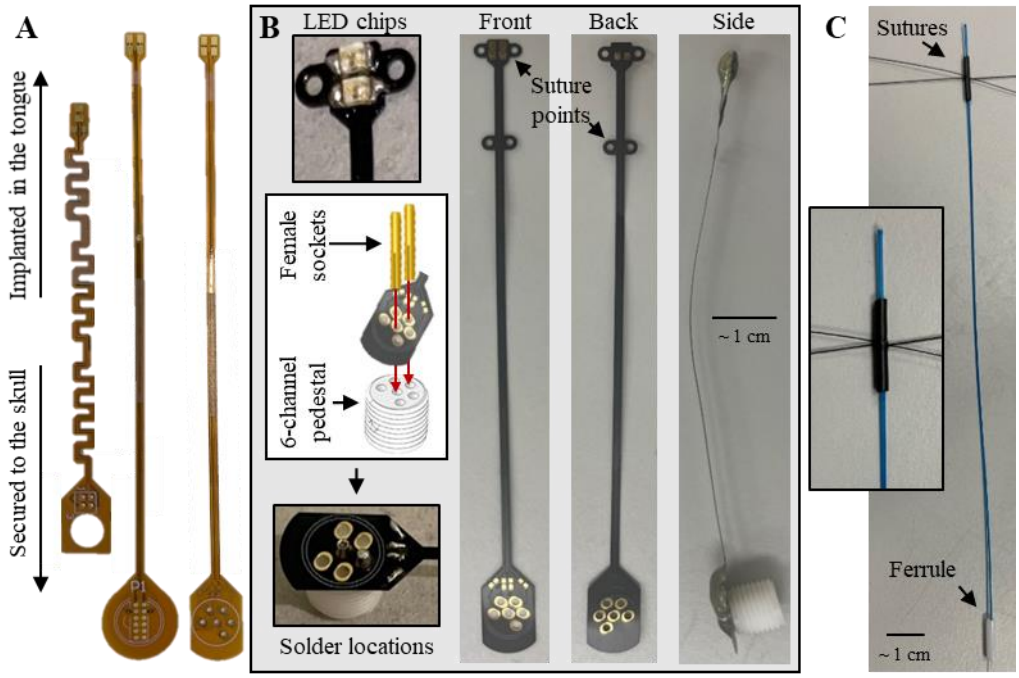

Figure 5-1 | Construction of light-delivery hardware (A) Iterations of the implantable flexible printed circuit boards (PCBs, WellPCB, ShijiaTzhuang Hebei, China) with locations for soldering two light emitting diodes (LEDs). The progression of the development goes from left to right. (**B)** The final flexible PCB design, employs a six-channel electrode system, with two locations for surface-mounted chip LEDs and one for an additional recording component. Four suture points for securing the PCB within the tongue are included. (**C)** Implantable optical fibre for the delivery of visible light from an external source to the tongue. Two suture points are included.

5.2.1.2 Optical fibre

The optical fibre (Figure 5-1C) was constructed based on the protocol described by Sparta et al., 2012 [517]. The primary differences from Sparta et al., 2012 are listed below.

- The optical fibre should be ~ 150 mm long, excluding the ferrule.
- The optical fibre was secured within the tongue via sutures attached to the fibre with heat shrink (1 mm long, ~ 1.5 mm diameter) approximately 5 mm from the exposed optical fibre tip.

5.2.2 Recording hardware

As the proposed light delivery methods used a skull-secured component, so too did the recording components. All components projected from their target (e.g. genioglossus muscle) to a skull secured, 6-channel pedestal (P1 Technologies, Bioscientific, NSW, Aus) via a subcutaneous tunnel. During data acquisition, a patch cable connected to the pedestal and transmit data to amplifiers.

Three recording components are required. First, light stimulation must be synchronised with the respiratory cycle. The respiratory cycle can be monitored using implanted diaphragm EMG electrodes (invasive) or a plethysmograph-like chamber (non-invasive) where chamber pressure indicates the respiratory cycle. Second, muscle activity within the tongue must be recorded to quantify the effect of light stimulation. EMG electrodes originating at the skull-secured pedestal extend behind the animal's ear and then project anteriorly towards the mandibular symphysis to insert into the tongue muscles. Finally, wakefulness and sleep stages are identified by the indicator of the respiratory cycle (and therefore respiration rate) and transcranial electroencephalograph (EEG) electrodes that connect to the skull-secured pedestal. This allows us to determine whether light-evoked muscle responses differ when applied during REM and NREM sleep.

5.3 METHODS

5.3.1 Animals

All procedures were approved by the Animal Ethics Committee, Macquarie University, Australia and accord with The Australian Code of Practice for the Care and Use of Animals. Sprague-Dawley (SD) rats were purchased from the Animal Resources Centre (Perth, Australia). All animals were group-housed in a dedicated housing room under a 12-hour light/12-hour dark cycle, and food and water were available ad libitum.

5.3.2 AAV vectors

Similar to Chapter 3, identical expression cassettes were packaged in either an AAV9 or AAVMYO [344] capsid. The expression cassette contained a muscle-specific promoter (tMCK, [330]) and a channelrhodopsin-2 variant with a gain of function substitute (ChR2(H134R)) fused to mCherry, i.e. pAAV-tMCK-ChR2(H134R):mCherry. The expression cassette was developed by GenScript (New Jersey, USA), and packaged into AAV9 and AAVMYO by the Vector and Genome Engineering Facility (Children's Medical Research Institute, Westmead, Australia). The AAVMYO plasmid was provided by Dirk Grimm (University of Heidelberg, Germany) [344].

The AAV9 construct (AAV9-tMCK-ChR2(H134R)-mCherry) titre was 9.04×10^{12} vg/mL, and the AAVMYO construct (AAVMYO-tMCK-ChR2(H134R)-mCherry) titre was 4.75×10^{13} vg/mL. When the AAV9 construct was injected, 20 µL equated to 1.81×10^{11} vg per animal. When the AAVMYO construct was injected, 3.8 µL of the construct was diluted in 16.2 µL of injectable saline, equating to the same viral load ($1.\ 81 \times 10^{11}$ vg) and total volume (20µm) per animal.

5.3.3 Intramuscular AAV injection

Anaesthesia was established in an induction chamber using 5% isoflurane in oxygen delivered at 1 L/min. The animal was removed from the chamber and placed on a nose cone where 2-3% isoflurane (1 L/min) was delivered and maintained. When adequate anaesthesia was reached (determined via a negative pedal withdrawal response), the animals received intramuscular injections of one of the two viral vectors described (AAV9-tMCK-ChR2(H134R):mCherry or AAVMYO-tMCK-ChR2(H134R):mCherry). A 25 µL syringe (model 702 LT SYR, Hamilton Company) connected to a sterile 26-gauge needle was used to inject 20 µL of the viral vector construct into four locations in the animal's tongue (5µL per site, Figure 5-2). The solutions were slowly injected, and the syringe was held in place within the tongue for an additional 15 seconds post-injection before being slowly retracted to avoid virus loss. Animals were allowed to recover from the anaesthesia before being returned to their cage.

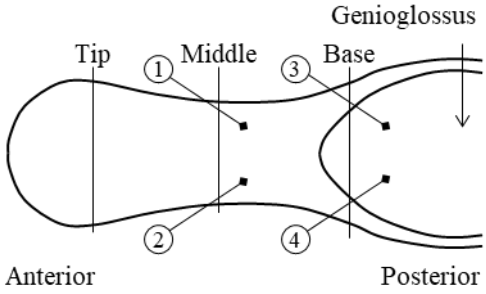

Figure 5-2 | Ventral surface of a rat tongue. Four intramuscular injection locations are labelled 1 to 4.

5.4 PILOT STUDY #1

5.4.1 Surgical method

One week following direct intramuscular injections of AAV9-tMCK-ChR2(H134R):mCherry, two Sprague-Dawley (SD) rats (IDs: H1 and H2) underwent a surgical procedure for the implantation of a flexible PCB, two genioglossus EMG electrodes, two diaphragm EMG electrodes and three EEG electrodes.

Anaesthesia was established in an induction chamber using 5% isoflurane in oxygen delivered at 1 L/min. The animal was removed from the chamber and placed on a nose cone where 2-3% isoflurane (1 L/min) was delivered and maintained. Throughout the surgery, the adequacy of anaesthesia was regularly assessed via negative pedal withdrawal responses, and core temperature was maintained between ~36°C to ~37.5°C via a rectal thermometer and heat mat.

The animal received a subcutaneous injection of an NSAID (carprofen, 5 mg/kg) and an intramuscular injection of an antibiotic (cefazolin, 100 mg/kg). Ophthalmic lubricant was applied ad-lib throughout the surgery to prevent corneal desiccation.

Three sites, the skull, submandibular and diaphragm sites (Figure 5-3), were prepared for surgery by shaving and sterilising with an antiseptic solution (Betadine).

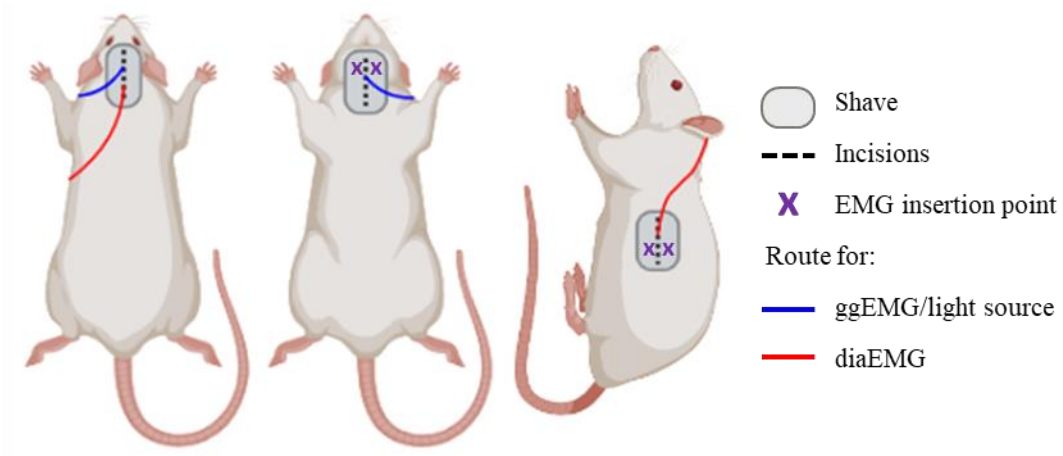

Figure 5-3 | Preparation for hardware implantation. Skull, submandibular and diaphragm (left to right) regions must be shaved and sterilised (grey ovals) and incisions made (black dotted lines). Approximate subcutaneous tunnelling routes and the insertion locations for EMG electrodes are indicated. Created with BioRender.com

Implantation of the light source and genioglossus electrodes

Incisions were made at the skull and submandibular sites (Figure 5-3, black dotted lines), and a subcutaneous tunnel between the incisions was created (Figure 5-3, blue line). A narrow polyethylene tube and the light source were pulled through the tunnel from the skull to the submandibular incision.

The connective tissue at the submandibular site was separated using blunt forceps to expose the tongue muscle under the mandibular symphysis. Two EMG hook electrodes were inserted into the tongue (Figure 5-3, purple 'x'). Electrodes were ~150 mm long (PFA-coated stainless steel 0.005" bare, 0.008" coated; A-M Systems, WA, USA), and a stripped hook end was inserted into the muscle by a 26G hypodermic needle at an angle of ~ 45°. The electrode slack was

threaded through the polyethylene tube until the ends exited at the skull. The tube was removed via the skull incision, and the electrodes remained within the subcutaneous tunnel.

Using the incorporated suture points (Figure 5-1B), the light source was secured between the two EMG electrodes and within the separated muscle tissue.

The submandibular incision was closed with staples, and Vetbond tissue adhesive was applied as required.

Implantation of diaphragm electrodes

An incision was made at the diaphragm site (Figure 5-3, black dotted line), and a subcutaneous tunnel extending to the skull incision was created. A narrow polyethylene tube was pulled through the tunnel from the skull to the diaphragm incision (Figure 5-3, red line).

The base of the ribs were palpated, and two EMG hook electrodes (identical to the genioglossus electrodes) were inserted between the caudal intercostal space and into the costal diaphragm. The electrode slack was threaded through the polyethylene tube until the ends exited at the skull. The tube was removed via the skull incision, and the electrodes remained within the subcutaneous tunnel. The diaphragm incision was closed with sutures, and Vetbond tissue adhesive was applied as required.

Insertion of electroencephalography electrodes

With the animal secured on a stereotaxic frame, a scalpel was used to detach and push aside the periosteum. The remaining tissue covering the skull surface was removed using 3% hydrogen peroxide. Three burr holes were created (Figure 5-4A, green), and screws (0-80 thread, 4.8 mm long; P1 Technologies) were inserted. Approximately 1 mm of the screw thread remained exposed. 15 mm of exposed wire (total electrode length ~ 30 mm) was tightly wrapped around the thread, and the screws were tightened to compact the wire onto the skull surface.

Securing the pedestals

All EMG electrodes (two diaphragm and two genioglossus EMG electrodes) were trimmed, leaving ~30 mm of slack. Female sockets (Figure 5-4D) were crimped onto ~ 2 mm of exposed wire on all 7 electrodes (four EMG and three EEG). The female pins were inserted into the illustrated pedestal locations (Figure 5-4B). All electrode slack was stored in a subcutaneous pocket behind the skull (Figure 5-4A).

The pedestal was secured to the skull with a two-part dental composite (Vertex Self-Curing acrylic) gradually built up to ~ ½ way up the pedestals (Figure 5-4C). When the dental

composite had cured, sutures or stables were used to close the skull incision, and Vetbond adhesive was applied where required.

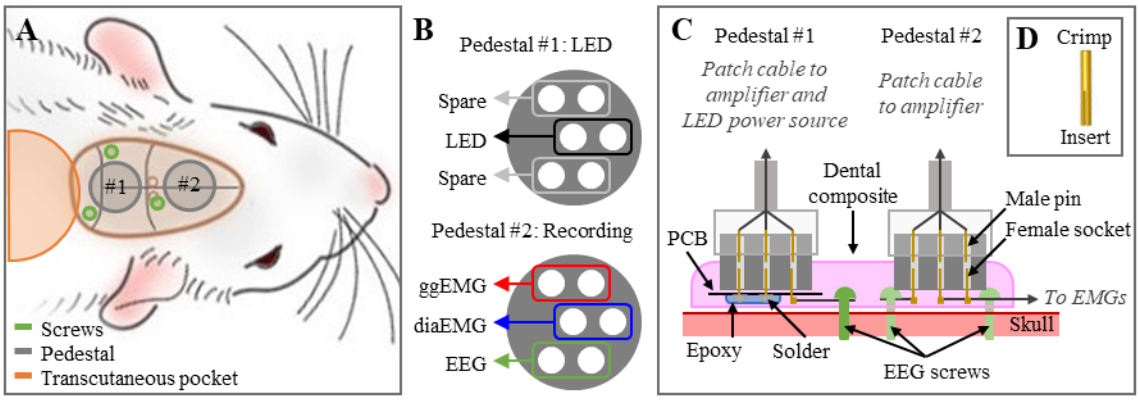

Figure 5-4 | Head stage set up for Pilot 1 and Pilot 2 A) Approximate locations for screws, pedestals, and the transcutaneous pocket for electrode slack storage. **B)** Two diaphragm EMG (diaEMG) electrodes, two genioglossus EMG (ggEMG) electrodes, two EEG electrodes, and two LED connections were connected to specific sites on two six-channel electrode pedestals. The 'spare' connection points were reserved for the third EEG electrode and any additional recording components. The figure indicates pedestal orientation from the insertion side (the larger holes). **C)** The pedestals were secured to the skull via dental composite. Patch cables deliver data from the pedestal to amplifiers and power to the flexible PCB via the pedestals. Epoxy resin was used to isolate the PCB pins. **D)** Female sockets were crimped to the EMG and EEG electrodes and inserted into the 6-channel pedestals, split end first.

Post-operative care

After surgery, the animal was placed into a clean, empty, heated, and padded cage. The animal was provided with water and moistened food, and respiration rate, righting behaviours, grooming, and feeding were monitored. When required, analgesics were administered.

Once ambulatory, the animal was placed in a solo home cage for a minimum of 24 hours before being returned to its group cage. The animal was closely monitored for a minimum of 3 days post-surgery to ensure adequate wound closure, weight gain, and the absence of pain. When required, additional analgesics and antibiotics were administered.

Habituation

A cost-effective plethysmograph was fabricated by combining a pressure sensor and a glass vacuum desiccator (Figure 5-5). A week after surgery, animals started bi-weekly habituation sessions in the chamber for ~ 4 to 6 hours per session. The animal remained untethered during the first week of habituation to allow two full weeks of recovery post-surgery. During week 2 of habituation, patch cables were connected to the pedestals so the animal acclimatised to the additional forces imposed on the implanted hardware. The animal underwent at least four

habituation sessions, and 1L/min active air inflow and passive air outflow were maintained at all times.

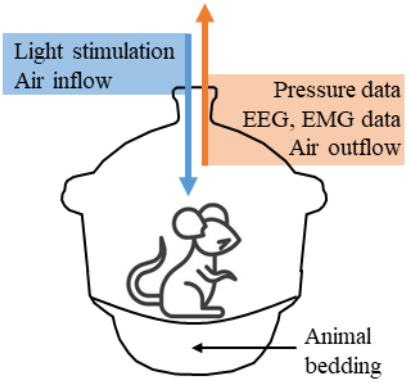

Figure 5-5 | The recording chamber was fabricated by combining a pressure sensor and a glass vacuum desiccator. Light stimulation and air (1 L/min) enter the chamber, and recorded data (chamber pressure, EEG and EMG) and air (passive) exit.

Data Acquisition

At least three weeks after intramuscular injections and two weeks after surgery, the animal underwent the first data acquisition session. Two data acquisition sessions were conducted per animal, separated by at least one day.

Before being placed in the recording chamber, the rats were anaesthetised in an induction chamber using 5% isoflurane in oxygen delivered at 1 L/min. The animal was removed from the chamber and placed on a nose cone where 2-3% isoflurane (1 L/min) was delivered and maintained. Adequacy of anaesthesia was assessed via negative pedal withdrawal responses.

Two custom patch cables were connected to the pedestals, and EEG and EMG activity was recorded for approximately 15 minutes. EMG and EEG signals were amplified and band-pass filtered (EMG: 0.1 – 50 kHz, EEG: 0.03 – 0.1 kHz) via an AC/DC Preamplifier (BMA-400 Four-channel AC/DC Preamplifier, CWE Inc.). A CED Power 1401 (Cambridge Electronic Design Limited) digitised signals at a sampling rate of 5 kHz for EMG and EEG recordings and 1 kHz for chamber pressure (plethysmograph). Data was stored on a computer using Spike2 software.

The animals were then removed from isoflurane and placed in the recording chamber. Chamber pressure, EEG and EMG activity were recorded continuously for ≥ 4 hours. Light stimulation was applied intermittently throughout and was triggered ‘in phase’ with inspiration, i.e. with inspiration onset, and ‘out-of-phase’ with inspiration, i.e. between expiration and inspiration

when no endogenous muscle activity was present. Diaphragm EMG activity or chamber pressure was used to monitor the respiratory cycle and trigger light stimulation.

Necropsy

After data acquisition, a necropsy was conducted to confirm the location of the light source, the EEG electrodes and the EMG electrodes. The general health of organs and tissues was checked, particularly near the implanted hardware.

5.4.2 Results

Both animals (H1 and H2) recovered well from surgery. All incision sites healed, and the pedestals remained firmly in place despite some deterioration of the dental composite around the edges and some skin withdrawal.

5.4.2.1 Data Acquisition (EMG, EEG)

In one animal (H1), only brief periods of low-amplitude endogenous genioglossus activity were recorded (Figure 5-6A). Phasic diaphragm EMG recordings were not obtained, and both EMG channels had significant electrocardiogram (ECG) artefacts (Figure 5-6A, B). Chamber pressure (plethysmography) consistently conveyed the respiratory cycle and was used to trigger 'in-phase' and 'out-of-phase' light stimulation. Light stimulation produced increases in genioglossus EMG activity (Figure 5-6C) and artefacts (Figure 5-6D) at different stages of the data acquisition sessions. Artefacts were identifiable as they were also presented in the EEG recordings as bands of activity at the frequency of the applied light, e.g. 20 Hz, and their associated harmonics, e.g. 40 Hz, 60 Hz and 80 Hz (Figure 5-6D).

EEG activity and respiration rate (derived from the chamber pressure channel) were sufficient to determine sleep stage (Figure 5-7A, B); however, some basic data processing was required as EEG channel gain was insufficient. NREM sleep was characterised by slow wave EEG activity (delta, 1-4 Hz, Figure 5-7B, C) and regular slow breathing. REM sleep was characterised by theta activity bands (~ 7 Hz, Figure 5-7B, D) and occasionally erratic breathing rates. Wakefulness was characterised by high-frequency EEG activity (~ 10 to 20 Hz) and irregular breathing (Figure 5-7A, ~ 5400 s). Augmented breaths, e.g. sighs and arousal from sleep, were detected and aided in identifying transitions between sleep stages, i.e. from REM to NREM, or NREM to wakefulness.

Light-stimulated genioglossus EMG activity was recorded during NREM (Figure 5-7C) and REM (Figure 5-7D) sleep. While the amplitude of the stimulated EMG appears smaller in REM sleep (Figure 5-7D), this was likely due to the stimulation protocol (1 ms pulse widths) rather than sleep stage.

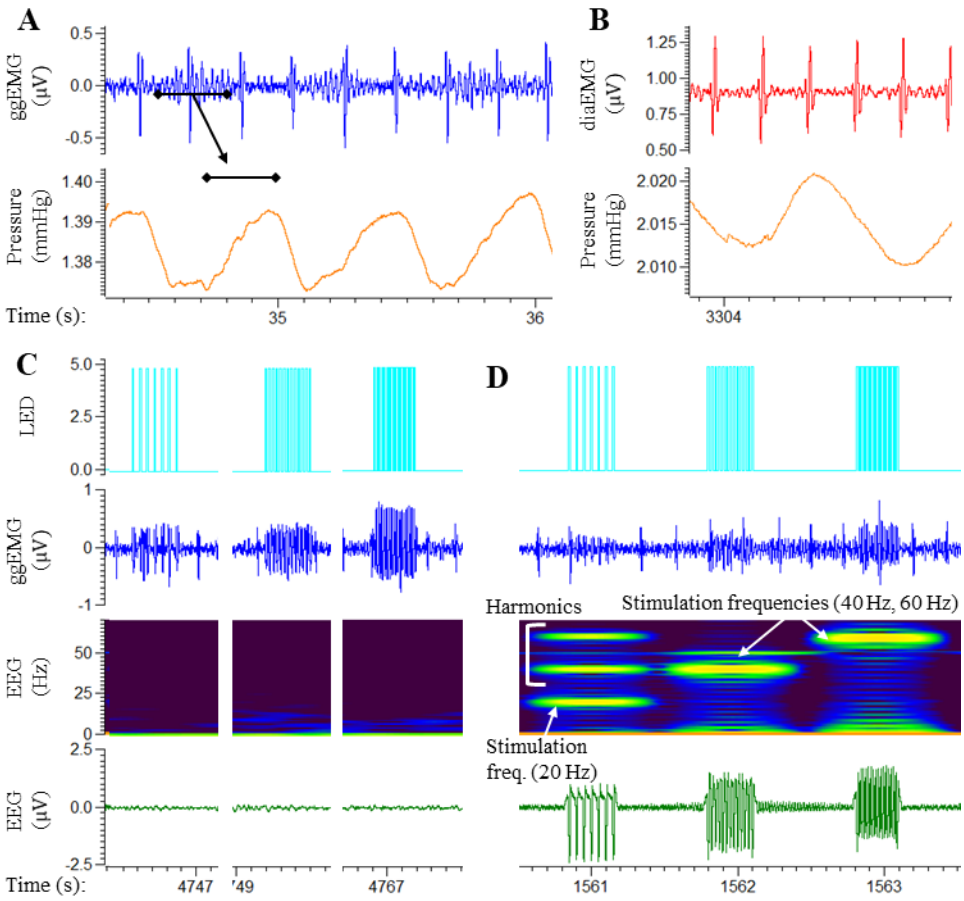

Figure 5-6 | Endogenous EMG recording was difficult to obtain, and light stimulation produced increases in muscle activity and artefacts (A) Brief and low amplitude periods of endogenous respiratory-linked genioglossus EMG (ggEMG) were present. However, no endogenous respiration-linked diaphragm EMG (diaEMG) was recorded. ECG artefacts were present in the **(A)** ggEMG and **(B)** diaEMG channels. Light stimulation induced **(C)** increases in ggEMG activity and **(D)** artefacts in both the EMG and EEG channels. **D) A**rtefacts generated by 10 ms pulses repeated at 20 Hs, 40 Hz and 60 Hz. Artefacts in the EEG channel are evident at the stimulating frequency and the associated harmonics.

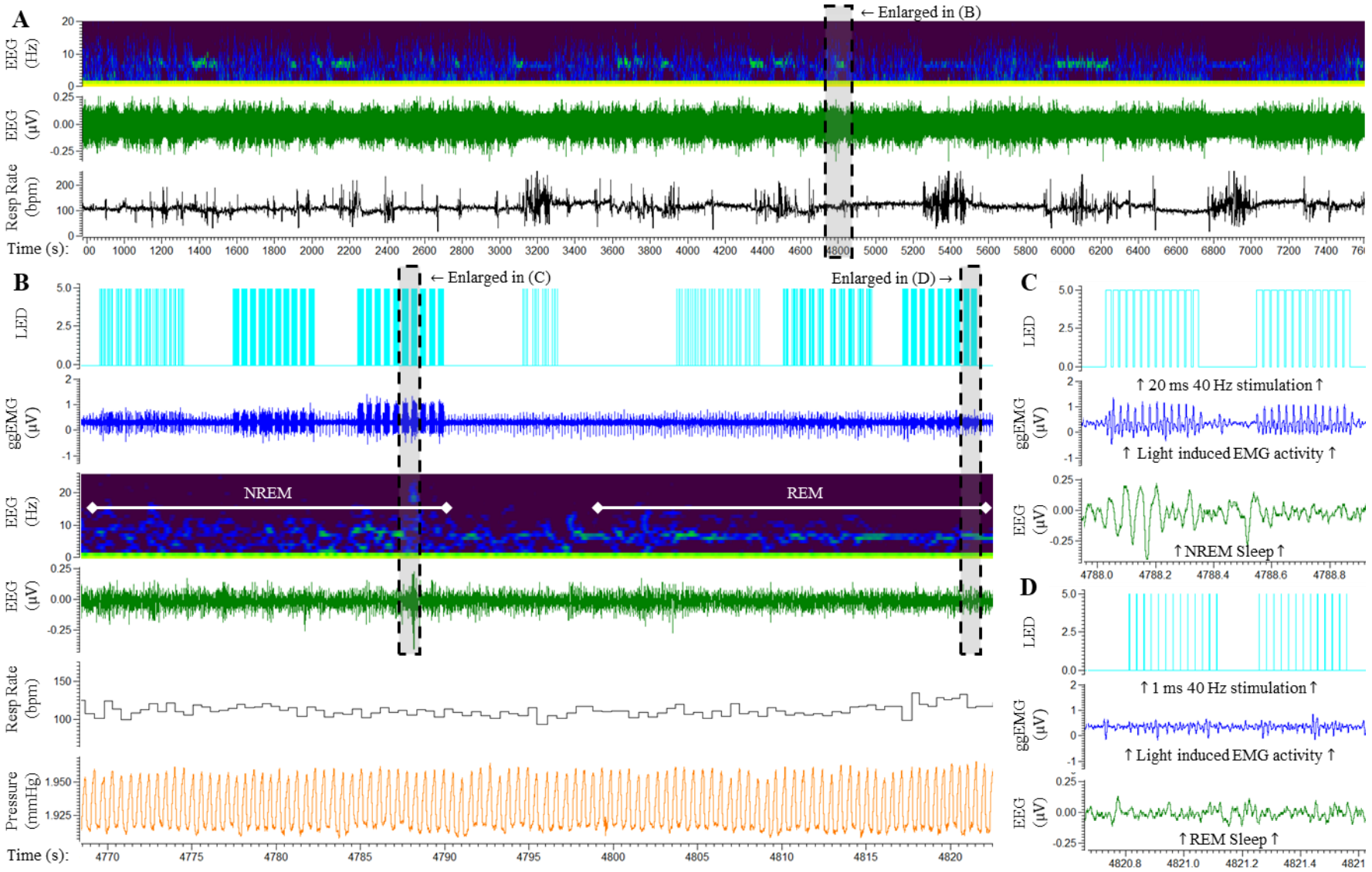
A
← Enlarged in (B)
EEG (Hz)
EEG (μV)
Resp Rate (bpm)
Time (s):
B
← Enlarged in (C)
Enlarged in (D) →
LED
ggEMG (μV)
NREM
REM
EEG (Hz)
EEG (μV)
Resp Rate (bpm)
Pressure (mmHg)
Time (s):
C
LED
↑ 20 ms 40 Hz stimulation ↑
ggEMG (μV)
↑ Light induced EMG activity ↑
EEG (μV)
↑ NREM Sleep ↑
D
LED
↑ 1 ms 40 Hz stimulation ↑
ggEMG (μV)
↑ Light induced EMG activity ↑
EEG (μV)
↑ REM Sleep ↑

Figure 5-7 | Pilot study #1 recorded periods of EEG, genioglossus EMG (ggEMG) and respiratory data (pressure). (A) ~ 2 hours of data show distinct periods of theta activity (~ 7 Hz). When high-frequency respiratory rates are also recorded (RespRate), the animal is likely awake (e.g. ~ 5400 s). When the RespRate is stable with only occasional bursts of activity the animal is likely in REM sleep. The grey box identifies a transition period between REM and NREM. This is enlarged in **(B),** where the periods of NREM and REM are identified. Light-induced ggEMG activity was recorded during **(C)** NREM and **(D)** REM sleep

All channels (EMG and EEG) had significant periods of noise that temporarily obscured all useful data. The genioglossus EMG recordings were particularly susceptible to noise due to animal movement.

During data acquisition for the second animal (H2), commercially available patch cables were used (6-channel cable with open-ended connections, P1 Technologies, Bioscientific, NSW, Aus). These cables are very fine wires wrapped with non-conducting fibres. Unfortunately, they were susceptible to failure due to ineffective soldering to the plugs that connect to the amplifiers (i.e. the fibre rather than the wire was soldered to the plug). Cable failure occurred during this animal's data acquisition, so no EMG or EEG data was recorded. As this was the first cohort to undergo data acquisition, backup cables were unavailable. New customise patch cables were fabricated for later recording sessions.

5.4.2.2 Necropsy

At necropsy, the genioglossus electrodes and the LED appeared well secured within the muscle. The diaphragm electrodes had dislodged and migrated approximately 40 mm rostrally along the subcutaneous tunnelling route. All EMG electrode slack was caught in the dental composite caudal to the pedestals, hampering their ability to extend with animal movement to minimise the risk of electrode displacement at their insertion point. The three EEG screws remained secured in the skull and dental composite. However, when the crown of the skull was removed, substantial indentations in the brain tissue were evident. These findings were present in both animals.

Infection was present in one animal (H2), caudal to the skull. This may have been caused by irritation from the electrode slack that was caught in the dental cement.

The PCB was cut during the necropsy of H1, so functionality could not be tested upon removal. The PCB implanted in H2 remained intact but was no longer functional. As no EMG data was collected, and the necropsy was conducted four days after the data acquisition session, it is not possible to conclusively state when the PCB stopped functioning.

5.4.2.3 Conclusions

Pilot study #1 produced promising initial data for the novel surgical protocol, obtaining periods of EEG and endogenous and light-evoked genioglossus EMG activity. The primary concerns were associated with the confinement of the electrode slack within the dental cement, the displacement of the diaphragm EMG electrodes, the soft tissue damage imparted to the brain tissue by the EEG screws and the occasional light stimulation induced artefacts.

5.5 PILOT STUDY #2

5.5.1 Surgical method - Changes

One week following direct intramuscular injections of AAV9-tMCK-ChR2(H134R):mCherry, two SD rats (IDs: H3 and H4) underwent a surgical procedure for the implantation of a flexible PCB, two genioglossus EMG electrodes, two diaphragm EMG electrodes and three EEG electrodes.

Two main changes were made to the protocol described in Section 5.4.1. First, as the dental composite restricted the EMG electrode slack in Pilot 1, the electrode storage site was changed. In this pilot, electrode slack was stored within the subcutaneous tunnels that approached the submandibular and diaphragm incision sites (Figure 5-8). A loose suture secured a single loop of slack at both locations. Minimal slack was maintained caudal to the skull. This change aims to reduce the likelihood of generating an infection caudal to the skull and reduce the risk of EMG electrode migration. Second, due to the indentations found in the brain tissue following Pilot 1, the 4.8 mm long screws were replaced with 2.4 mm screws (P1 Technologies).

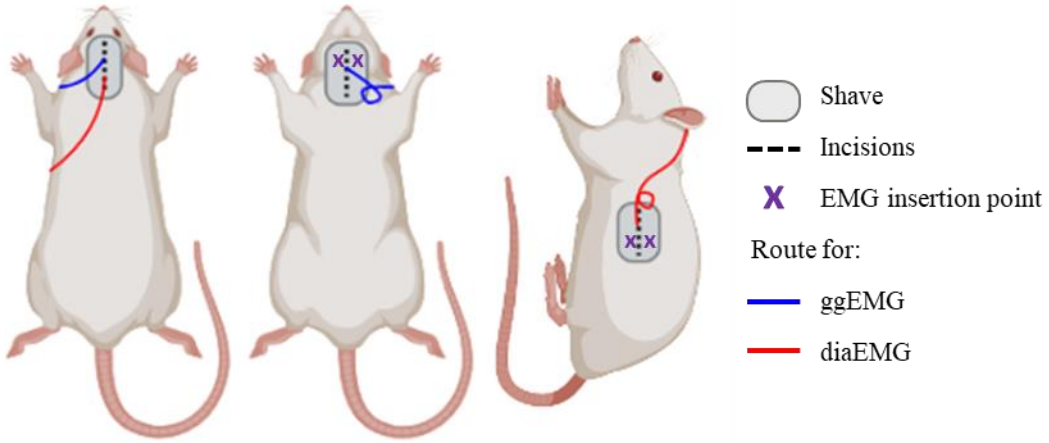

Figure 5-8 | Adapted version of Figure 5-3 indicates the new locations for electrode 'slack', i.e. the loops included in the genioglossus EMG (ggEMG) and diaphragm EMG (diaEMG) electrode routes. Created with BioRender.com

5.5.2 Results

One animal (H4) did not survive the surgery. At necropsy, evidence of a pre-existing respiratory condition was found. It was concluded that extended isoflurane exposure negatively interacted with the condition, resulting in the animal's death.

The other animal (H3) completed the surgery. While the diaphragm and submandibular incisions healed well, there was a bulbous region near the diaphragm at the approximate location of the electrode slack. As the animal did not display indicators of stress or discomfort, data acquisition continued, and the site was monitored.

Mild dental composite deterioration and skin withdrawal from the dental composite were present.

5.5.2.1 Data Acquisition (EMG, EEG)

In the animal that completed the surgery, no respiratory cycle recording was obtained as the chamber pressure sensor was not functioning, and the diaphragm electrodes had broken and protruded through the skin ($\leq$ 1 mm). Fortunately, the animal did not display indicators of stress or discomfort due to the electrode, so the data acquisition continued. Due to the above failures, it was not possible to automatically trigger light stimulation 'in-phase' or 'out-of-phase' with inspiration.

Pedestal-to-patch cable connections for the genioglossus and EEG electrodes were difficult to establish as the dental composite clogged the pedestal ports. While the animal was anaesthetised, the ports were cleared, and brief periods of stereotypical anaesthetised EEG activity were acquired (Figure 5-9A). No endogenous inspiration-linked EMG data were recorded while the animal was anaesthetised.

When the animal recovered from isoflurane in the recording chamber, there were significant periods where noise obscured all useful data. When noise was minimised, brief periods of low amplitude inspiration-related activity (Figure 5-9B) and high amplitude behaviour-related activity (grooming, teeth grinding and whiskering, Figure 5-9C) were found in the genioglossus EMG channel. Periods of EEG were recorded where wakefulness, REM sleep and NREM sleep could be identified. The activity in the genioglossus EMG channel that correlated with animal behaviour allowed us to discriminate between wakefulness and REM sleep, as theta bands characterise EEG activity in both. This was essential as the faulty plethysmograph and diaphragm electrodes did not provide respiratory rate data.

Finally, light stimulation exclusively produced artefacts that obscured all data.

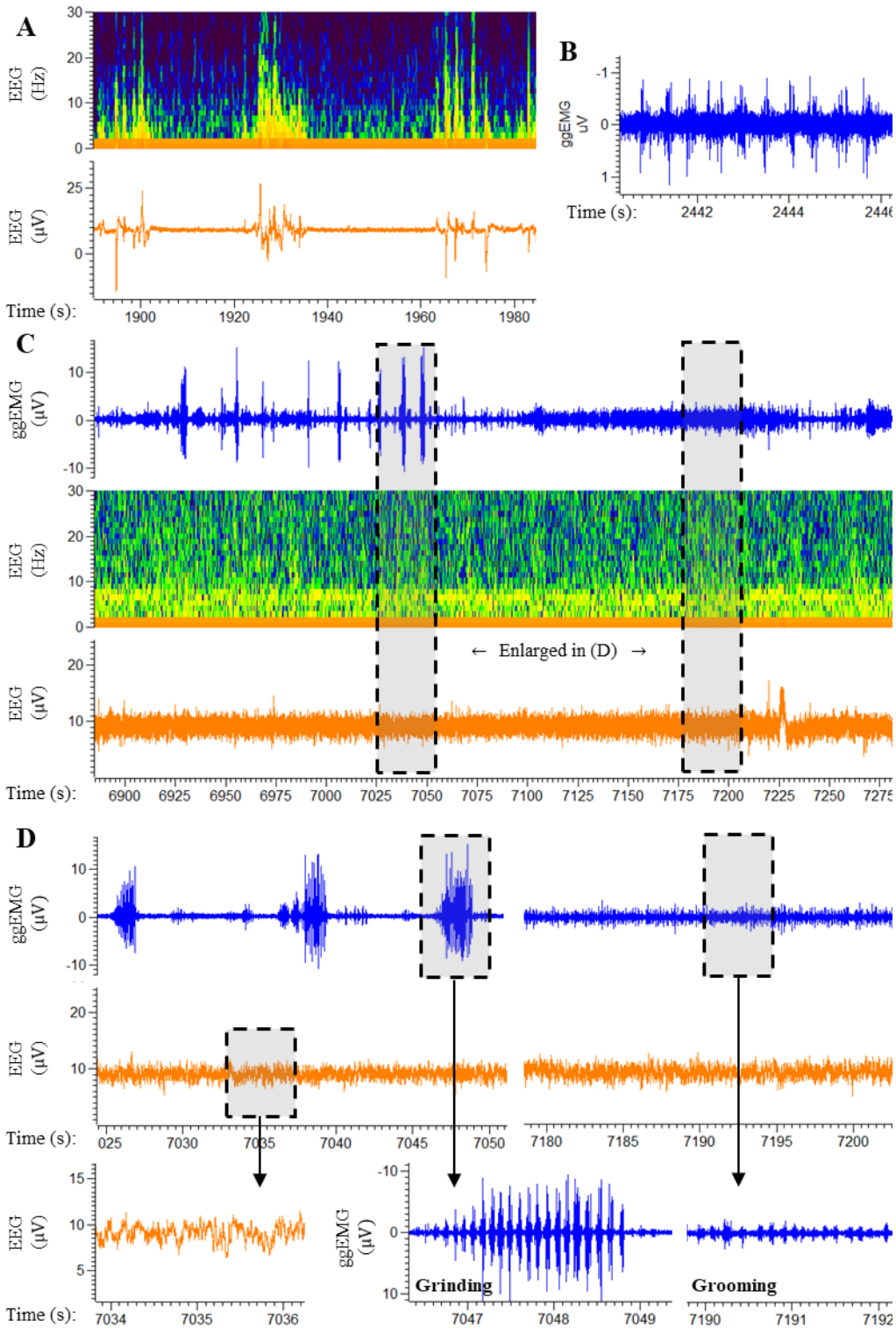

Figure 5-9 | Pilot #2 produced periods of clear EEG and genioglossus EMG (ggEMG) data. (A) Under isoflurane anaesthesia, clean EEG data was recorded. **(B)** In the recording chamber (not anaesthetised), brief periods of endogenous ggEMG activity were recorded. **(C)** Wakefulness could be identified by a weak theta band (~ 7 Hz) in the EEG channel and behaviour-related activity in the ggEMG channel, i.e. **(D)** teeth grinding and grooming.

5.5.2.2 Necropsy

At necropsy, genioglossus EMG electrodes remained secured within the muscle. Despite intact sutures, the PCB had migrated superficially at the submandibular site, and the LED no longer functioned upon removal. This may have been due to minor damage the PCB sustained during removal.

The diaphragm electrodes remained securely anchored within the muscle despite the protrusion of the electrode tips through the skin. However, minor localised infections were present at the diaphragm incision site, and the location at which the electrodes had broken and protruded from the skin (posterior to the forelimb).

No indentations were seen in the brain when the skull cap was removed.

5.5.2.3 Conclusions

Pilot study #2 produced periods of clear EMG data that allowed the identification of sleep stages and behaviour-associated genioglossus EMG activity. Using the shorter transcranial screws prevented brain tissue damage, and changing the electrode slack location seemed to reduce the risk of infection caudal to the skull cap.

However, only brief periods of low-amplitude endogenous genioglossus EMG activity and no endogenous diaphragm EMG activity were recorded during this pilot study, and light stimulation exclusively produced artefacts. These findings contrast with successful intraoperative recordings.

Finally, there were extended periods where noise obscured all data, potentially due to poor connections between the female sockets within the pedestals and the male pins of the patch cables.

5.6 PILOT STUDY #3

5.6.1 Surgical method - Changes

One week following direct intramuscular injections of AAVMYO-tMCK-ChR2(H134R):mCherry, two SD rats (IDs: H5 and H6) underwent a surgical procedure for the implantation of a flexible PCB, two genioglossus EMG electrodes, and three EEG electrodes.

Several changes were made to the protocol described in Section 5.4.1. In pilot studies 1 and 2, the diaphragm electrodes failed to provide EMG data and potentially caused the animal discomfort due to electrode breakage or migration. While implanted diaphragm EMG electrodes have been successful in other studies, they necessitated direct sutures to the costal diaphragm

through an abdominal incision [455]. As diaphragm EMG electrodes in the current application were included solely to provide respiratory cycle data and trigger light stimulation, a role chamber pressure data can similarly and non-invasively provide with less impact on the animals, they would no longer be implanted.

To reduce the risk of light stimulation-induced artefacts, additional isolation of the electrical components of the PCB by the two-part epoxy was applied. Additionally, when securing the pedestals to the skull with dental composite, the six connection points were temporarily covered to avoid blockages. This allowed more effective connections between the pedestal and patch cable during data acquisition and reduced the risk of noise in the data channels.

Greater separation of the submandibular connective tissue and muscle fibres allowed the LED to be secured deeper in the tissue to ensure adequate illumination.

5.6.2 Results

One animal (H5) healed well from the surgery. The second animal (H6) developed some inflammation around the dental composite that appeared painful when touched. As this was likely due to sharp dental composite edges, the animal was briefly anaesthetised (5% isoflurane induction in the chamber, then 2-3% isoflurane via nose cone), and the dental composite was trimmed. After the correction, visible irritation had reduced, and the animal healed well at all incision sites. However, two electrode wires were cut or exposed during the dental composite trimming.

Dental composite deterioration was evident in both animals. H6 showed considerable skin withdrawal from the dental composite but displayed no indicators of pain or discomfort.

5.6.2.1 Data Acquisition (EMG, EEG)

Respiratory signals were consistently obtained via the chamber pressure channel and allowed ‘closed loop’ stimulation. ‘In-phase’ light stimulation was triggered by the respiratory signal rising over a threshold that indicated inspiration onset (Figure 5-10A), and ‘out-of-phase’ light stimulation was triggered by the trace falling below a specified threshold that indicated the end of expiration. The respiratory signals consistently indicated augmented breaths, pauses in breathing, and changes in respiration rate (Figure 5-10D) that contributed to sleep stage identification.

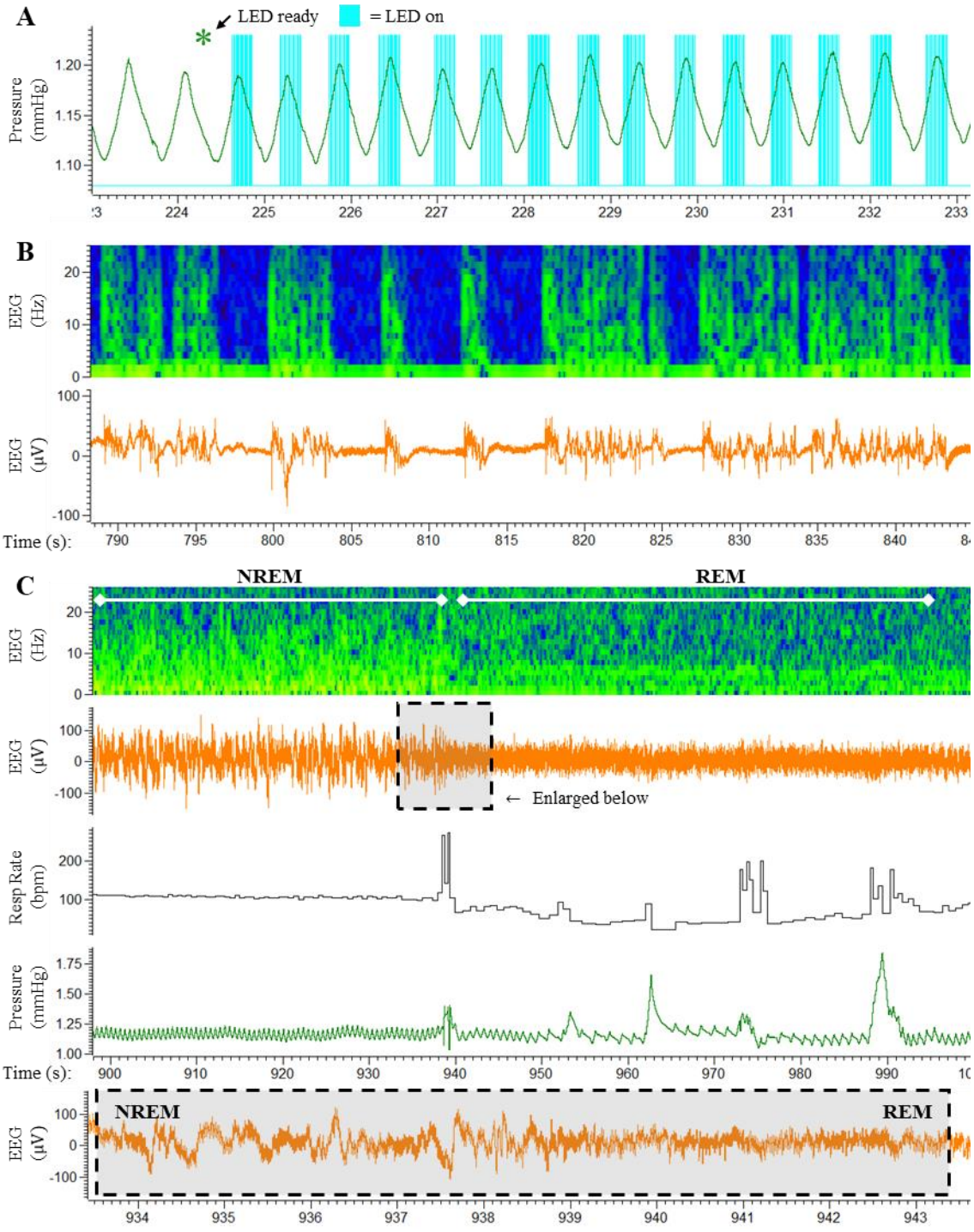

Figure 5-10 | Data acquired during Pilot #4. (**A)** The chamber pressure signal afforded closed-loop light stimulation. **B)** EEG data was recorded while the animal was under isoflurane, and **C)** during NREM and REM sleep. Augmented breaths indicated transitions between sleep stages or REM sleep when accompanied by slowed breathing.

EEG signals improved in clarity and consistency. This cohort provided clear EEG signals when anaesthetised (Figure 5-10B) and during wakefulness and natural sleep in the recording chamber (Figure 5-10C). The improved EEG and respiratory signals allowed efficient sleep stage identification. Figure 5-10C shows a transition period between NREM and REM sleep, identifiable by the change in EEG activity from delta (0.5 to 4.5 Hz) to theta (~ 7 Hz) wave dominance. The respiratory signal also indicates a NREM to REM transition. During NREM, breathing is consistent at ~ 110 breaths per minute. The change to REM sleep is first indicated by an augmented breath (possibly a micro-arousal) and a shift to more variable and intermittently erratic breathing.

No phasic inspiration-related genioglossus EMG activity was obtained, and the activity in the EMG channel correlated to animal behaviour (grooming, teeth grinding and whisking). Light stimulation exclusively generated artefacts that obscured all EMG activity despite increased efforts to isolate the electrical components of the PCB.

The dental composite again caused difficulty establishing patch cable connections as it clogged pedestal ports; subsequently, the risk of noise due to potentially impeded contacts was elevated. During the second data acquisition session for H6, the skull cap (i.e. the two pedestals, the dental composite and the underlying skull) spontaneously detached, and the animal was immediately terminated under isoflurane.

5.6.2.2 Necropsy results

At necropsy of H6 (post-emergency termination via isoflurane), the animal seemed to be in otherwise good health. The EEG screws had not produced any soft tissue damage to the skull, and the skull cap did not exhibit any obvious damage that may have contributed to spontaneous detachment. Other factors that may have contributed to the detachment include insufficient preparation of the skull's surface prior to dental composite application, poor dental composite curing, and/or disruption of the dental composite/skull interface during the additional corrective surgery that smoothed the composite edges. LED function was not tested as it was cut when the animal was removed from the recording chamber for termination.

5.6.2.3 Conclusions

Pilot study #3 greatly improved respiratory and EEG data acquisition, allowing easy identification of sleep stages. However, an alternate method for securing the hardware to the skull is required due to repeated issues related to the dental composite, i.e. general deterioration, skull cap detachment, and clogged pedestal ports. This is essential for future preclinical studies where data acquisition sessions may be repeated over several weeks. Additionally, despite

increased efforts to isolate the electrical components of the PCB, light stimulation continued to generate artefacts in the EMG channel, and a new light delivery method is required.

5.7 PILOT STUDY #4

5.7.1 Surgical method - Changes

The primary purpose of pilot study #4 was to test the feasibility of implanting an optical fibre rather than a flexible PCB and to confirm the absence of artefacts when light stimulation was triggered. The single animal (H7) did not receive any intramuscular injections and underwent surgery to implant an optical fibre for light delivery to the tongue (optical fibre construction is outlined in Section 5.2.1.2), two genioglossus EMG electrodes, and three EEG electrodes.

Following the persistence of light stimulation artefacts in the prior pilot studies, an optical fibre rather than a flexible PCB was implanted. An optical fibre delivers light generated by an external source (laser or LED), and unlike the PCB, no power transfers across any implanted components. The optical fibre was connected to the skull via an optic ferrule, and all EMG and EEG electrodes projected to one 6-channel pedestal (Figure 5-11A-C). The optical fibre followed the same route as the flexible PCB, i.e. alongside the ggEMG electrodes that extend from the skull, behind the ear, and to the submandibular incision (Figure 5-8).

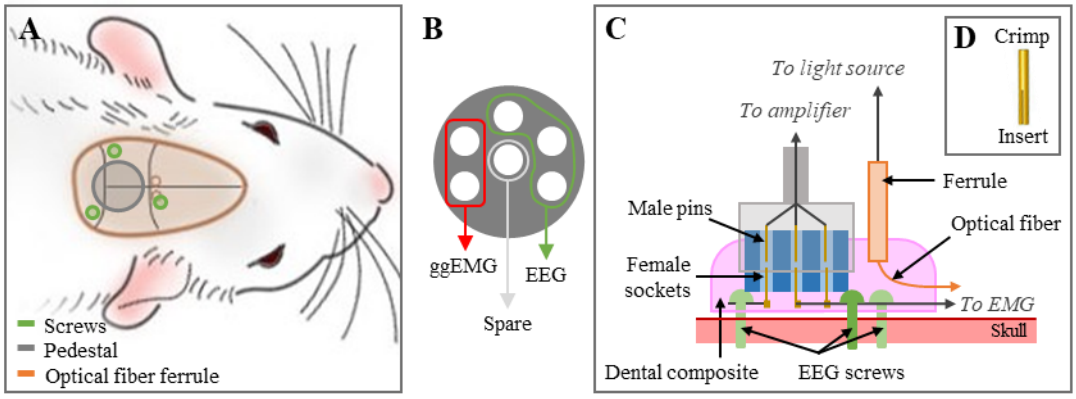

Figure 5-11 | Altered version of Figure 5-4, describing head stage set up for Pilots 4 and 5. (**A**) Approximate locations for screws, pedestal, and optical fibre ferrule. (**B**) Two genioglossus EMG (ggEMG) electrodes and three EEG electrodes connect to specific sites on a six-channel electrode pedestal. The figure indicates the orientation from the insertion side of the pedestals (the larger holes). (**C**) The pedestal and ferrule are secured to the skull by a dental composite and, during recording, connect to patch cables for data and light transfer, respectively. (**D**) The female pins are crimped to the wires at the solid end and inserted into the pedestal split end first.

Due to the previous dental composite deterioration, clogged pedestal connection ports, and the detachment of the skull cap during data collection in Pilot 3, an alternate method of securing the pedestals was used. In this pilot study, the skull was prepared using OptiBond Primer and

OptiBond Adhesive (as per product instructions), and the pedestal and ferrule were secured in place by Tetric EvoFlow dental composite (as per product instructions). The new dental composite was gradually built up and intermittently cured until ~ ½ of the pedestal and ~ ¼ of the ferrule was covered (Figure 5-11A).

This pilot study also used a pen-style cordless drill for craniotomies. The new drill allows better control that minimises soft tissue damage and improves EEG connections when combined with the shorter screws added in Pilot 2.

5.7.2 Results

The new skull preparation and dental composite were more straightforward and quicker to apply than the previous method, reducing anaesthesia time. Patch cable connections were easy to establish, and no composite deterioration was evident.

During the three days of close monitoring after the surgery, the animal lost over 10% of its pre-surgery weight. While there were no behavioural indicators of pain or discomfort, and all wounds healed well, data acquisition was brought forward and performed under anaesthesia.

5.7.2.1 Data Acquisition (EMG, EEG)

No stimulation-induced artefacts were recorded in the genioglossus EMG channel, and EEG activity was consistent throughout.

5.7.2.2 Necropsy

At necropsy, the sub-mandibular incision was reopened, and the external LED was triggered, confirming that the optical fibre was intact and able to deliver light stimulation to the base of the tongue. While the sutures securing the optical fibre remained in place, the optical fibre tip shifted slightly laterally from the original location. This shift was likely due to the comparatively stiffer material and the single set of sutures used to secure the fibre.

One of the genioglossus electrodes protruded into the oral cavity, and the hooked tip was lodged in the ventral surface of the tongue. This was likely the cause of the animal's weight loss.

5.7.2.3 Conclusions

The optical fibre and new dental composite were successful in this pilot study. No light stimulation-induced artefacts were recorded, and no dental composite deterioration occurred. Additional sutures are required to hold the optical fibre in place and avoid lateral displacement.

5.8 PILOT STUDY #5

5.8.1 Surgical method – Changes

One week following direct intramuscular injections of AAVMYO-tMCK-ChR2(H134R):mCherry, one SD rat (ID: H8) underwent a surgical procedure for the implantation of an optical fibre, two genioglossus EMG electrodes, and three EEG electrodes.

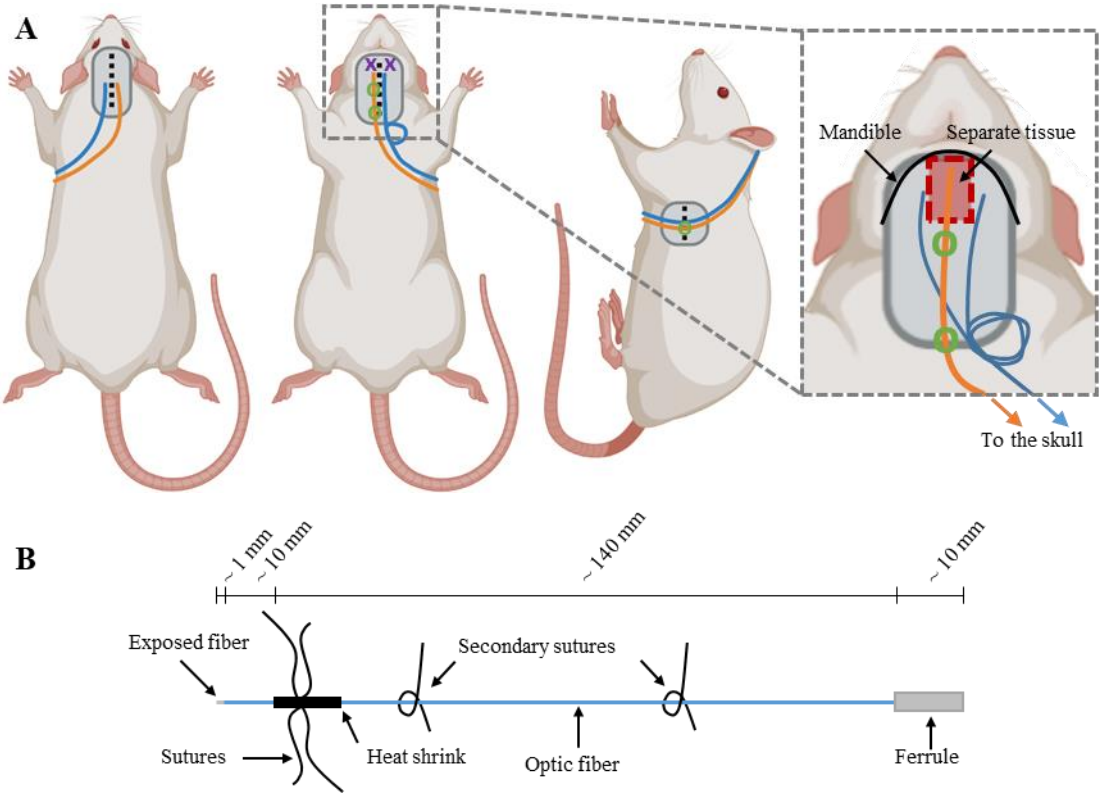

Figure 5-12 | Chronic implantation of an optical fibre for Pilot 5. A) Skull, sub-mandibular and shoulder (left to right) regions must be shaved and sterilised (grey ovals) prior to incisions (black dotted lines). Approximate routes for subcutaneous tunnelling for the genioglossus EMG (ggEMG) electrodes (blue) and optical fibre (orange) are indicated. The optical fibre was secured at three points (green), and the EMG electrodes were inserted at two points (purple). The inset image displays the region where the tissue was separated (red) immediately posterior to the mandibular symphysis for effective light source placement. Created with BioRender.com **B)** One set of sutures was secured to the optical fibre via shrink wrap, and two additional single sutures were unattached and loosely applied.

Due to the displacement of the optical fibre tip in Pilot 4, a different subcutaneous tunnelling route between the submandibular and skull incisions was used (Figure 5-12A). This change reduced the amount of flexion in the fibre before insertion into the tongue muscles. Two additional sutures were included (Figure 5-12A, B). One suture secured the fibre immediately upon entering the submandibular incision, and the second secured the fibre at a new incision site located posterior to the forelimb. The genioglossus electrodes also followed this altered route to minimise the tunnelling (Figure 5-12A).

5.8.2 Results

After surgery, all wounds healed well, but the animal lost weight during the first recovery week (≤ 5% of body weight). A minor infection at the sub-mandible incision site was found during the removal of the external stitches (under isoflurane anaesthesia) and was attributed to internal sutures protruding from the incision site. The wound was reopened and cleared of infection. The internal sutures were trimmed, and the wound was closed. Additional antibiotics (cefazolin, 100 mg/kg) and painkillers (carprofen, 5 mg/kg) were administered. The infection resolved quickly, and regular weight gain was reinstated.

5.8.2.1 Data Acquisition (EMG, EEG)

Excellent EEG signals were obtained throughout the recording sessions. Under anaesthesia, EEG recordings displayed dose-dependent changes. Greater concentrations of isoflurane produced sparse and high amplitude spikes of EEG activity, which increased in density and decreased amplitude when isoflurane concentration was reduced (Figure 5-13A).

While the animal was in the recording chamber, EEG was recorded for approximately 4 hours without significant interference. Figure 5-13B shows approximately 1.5 hours of uninterrupted data. When combined with the pressure channel that indicates respiration rate, wakefulness and sleep stages were easily identifiable. Figure 5-13B (~ 600 and 1400 seconds) shows repetitive periods of NREM sleep separated by micro-arousals, i.e. single peaks in the respiration rate channel, and a clear transition to REM sleep at ~ 1550 seconds, indicated by the dominance of the theta band in the EEG channel and the increased variability in the respiration rate.

Two distinct EEG channels were created when the patch cable from one of the three EEG electrodes was ‘daisy chained’ (Figure 5-14). ‘EEG #1’ has greater activity in the theta wave band (~ 7 Hz) during NREM sleep than ‘EEG #2’ (Figure 5-14B). Conversely, during REM sleep, both channels show increased delta wave activity (~ 0.5 to 4 Hz, Figure 5-14C).

Figure 5-13 | Pilot #5 generated excellent EEG recordings (A) while the animal was anaesthetised, with sparser activity when greater isoflurane concentrations were applied. **(B)** EEG was also consistently recorded when the animal was in the recording chamber, and wakefulness (e.g. 100 to 400 seconds) and sleep stage identification were possible. A NREM and a REM stage are identified.

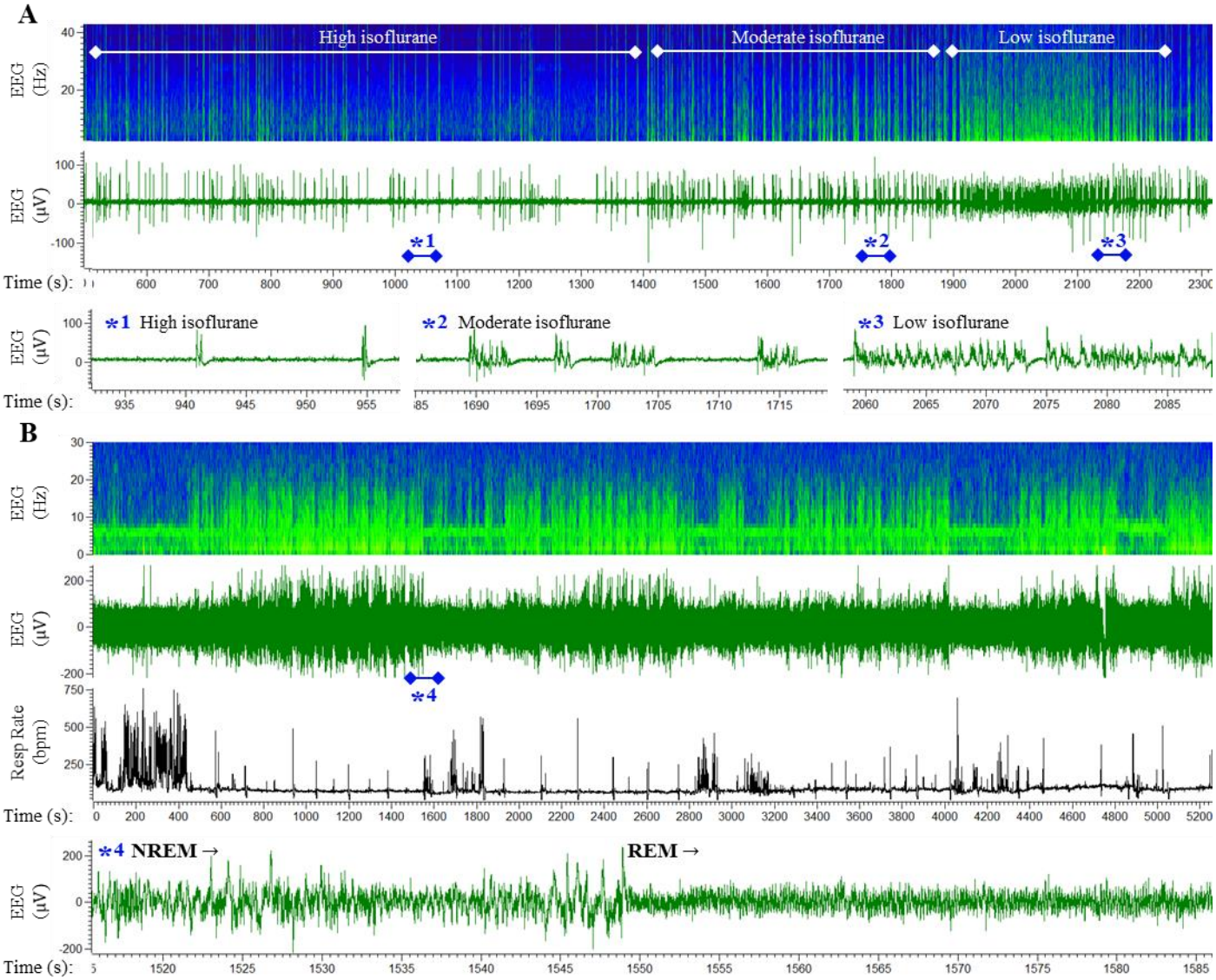
A
High isoflurane
Moderate isoflurane
Low isoflurane
EEG (Hz)
EEG (μV)
*1
*2
*3
Time (s):
*1 High isoflurane
*2 Moderate isoflurane
*3 Low isoflurane
B
Resp Rate (bpm)
*4
*4 NREM →
REM →

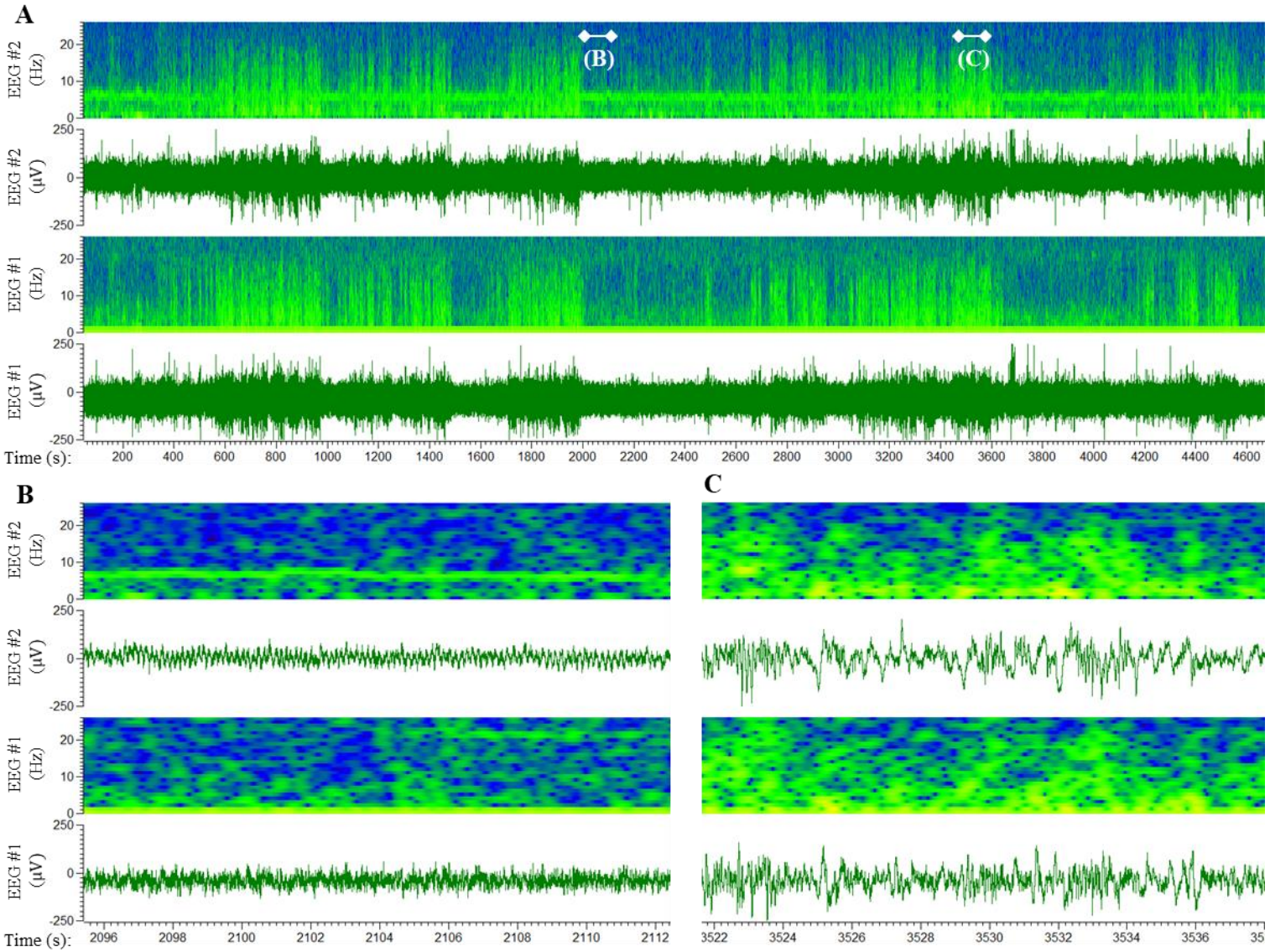
A
(B)
(C)
EEG #2 (Hz)
EEG #2 (µV)
EEG #1 (Hz)
EEG #1 (µV)
Time (s):
200 400 600 800 1000 1200 1400 1600 1800 2000 2200 2400 2600 2800 3000 3200 3400 3600 3800 4000 4200 4400 4600
B
C
2096 2098 2100 2102 2104 2106 2108 2110 2112
3522 3524 3526 3528 3530 3532 3534 3536 35

Figure 5-14 | Daisy-chained EEG patch cables produce two different EEG channels. (A) Each channel displays different intensities of activity bands characteristic of wakefulness, REM and NREM. **(B)** During REM sleep, the 'EEG #2' channel displayed theta wave activity (~ 7 Hz). This was absent in the 'EEG #1' channel. **(C)** Both channels display increases in delta wave activity (0 to 4 Hz) during NREM sleep

Despite visible tongue contractions generated when an external light source was applied intraorally, no visible movement or EMG activity was observed or recorded when the implanted optical fibre delivered light stimulation. It is unclear whether this was due to poor optical fibre positioning or poor EMG electrode position in relation to the regions of opsin expression.

5.8.2.2 Necropsy

At necropsy, the optical fibre was functional and in its original location.

One genioglossus EMG electrode was slightly dislodged. This likely occurred when the submandibular incision was reopened to reduce infection rather than during natural animal movement.

5.8.2.3 Conclusions

Pilot study #5 produced clear and consistent EEG and respiration cycle signals, and wakefulness and sleep stages were easily identifiable. The excellent EEG signals were attributed to the new cordless drill, the smaller screws, and the new dental composite that optimally secured the hardware and improved the pedestal-to-patch cable connections.

Clear and consistent EMG signals from the genioglossus were not achieved. As a result, it was not possible to confirm that the optical fibre was in the correct position to stimulate the tongue muscles. However, this study did demonstrate that an optical fibre is the preferred method for light delivery, as stimulation-induced artefacts were not produced in any recording channels, and the optical fibre remained functional at necropsy.

5.9 DISCUSSION

This chapter presents a series of pilot studies aimed at developing a surgical protocol for the chronic implantation of hardware to deliver light stimulation to upper airway muscles during natural sleep and records subsequent changes in muscle activity (the complete protocol is available in the Appendix). While methods for achieving high-quality EEG recordings, from which it is possible to consistently discriminate between wakefulness and sleep stages, and respiratory data from a custom plethysmography setup were achieved, further developments are

required to achieve reliable genioglossus EMG signals and to confirm that positioning of the optical fibre is suitable for evoking light-stimulated muscle activity.

The EEG channel successfully recorded high-amplitude low-frequency waves (delta activity, 0.5 – 4.5 Hz) indicative of NREM sleep and low-amplitude mixed-frequency activity (theta activity, 4 – 8 Hz) indicative of REM sleep. Wakefulness presented a similar EEG profile to REM sleep but could be identified by rapid and irregular breathing (e.g. Figure 5-13B, 200 to 400 seconds) in the plethysmography channel. In contrast, REM sleep was identifiable with slower breathing with sporadic augmented breaths (e.g. Figure 5-13B, 4000 to 4400 seconds). The plethysmograph also detected micro-arousals, pauses in breathing, deep breaths and gasps (e.g. Figure 5-10 and Figure 5-14). These events also aid in sleep stage identification as they are common at transitions between sleep stages. Finally, the respiratory data derived from the plethysmography channel allows inspiration-linked light stimulation to be triggered automatically (e.g. Figure 5-10A). As this pressure signal is likely delayed compared to inspiratory muscle activity, a small study to calibrate the signal to a more temporally precise indicator of inspiration onset, e.g. pre-inspiratory genioglossus muscle activity measured via standard intraoral EMG electrodes (i.e. not implanted, described in Chapter 2), may be beneficial. Finally, where EEG and respiratory data were sufficient for sleep stage identification, all animals experienced REM and NREM sleep in the recording chamber.

It was concluded that implanted optical fibres were the best method for delivering light stimulation to the tongue as they did not produce artefacts, likely because they transmitted light rather than power. Moreover, optical fibres are cost-effective, robust, and relatively flexible. However, despite the difficulties faced when using flexible PCBs, they may still have utility as a chronically implanted device but will require significant improvements in encapsulation to avoid generating artefacts. Their ability to incorporate a broad range of recording options in addition to LEDs for a relatively low cost, and with no additional surgical steps or hardware, is particularly advantageous.

Despite recording genioglossus activity via the pedestals and patch cables during the implantation procedure, consistent recordings of endogenous or light-induced genioglossus activity were not achieved during sleep, wakefulness or under anaesthesia approximately two weeks later. Future work should focus on determining a better method of securing the implanted hook electrodes or an alternative method for monitoring the effects of chronic light stimulation on upper airway muscles that express opsins. As noted previously, monitoring upper airway muscle activity via implanted genioglossus EMG electrodes during natural sleep in rodents has been done previously, however, it is typically limited acute responses to acute intervention

administration [87, 188, 455, 515], and no literature described instrumentation procedures with recording sessions more than two weeks after surgery. One method used to secure genioglossus electrodes was introducing a knot in the electrode lead (~1 mm diameter) and burying the knot within a pocket in the tongue muscle. The pocket was then closed using non-absorbable coated-silk sutures, and the electrode lead was knotted to the suture to maintain its position [455]. This is a potential option for future studies.

It is important to note that, as in these pilot studies, previous research in non-anaesthetised mice has reported no discernible respiratory-related tongue muscle activity in awake and sleeping mice despite anaesthetised mice exhibiting clear respiratory modulation [188, 455]. Instead, tongue muscle activity was minimal during REM and NREM sleep except for transient activation during REM sleep, and activity during wakefulness was primarily associated with behaviours such as grooming [455]. This contrast between phasic muscle activity recorded in anaesthetised and non-anaesthetised animals was explained by reports that some anaesthetics can induce strong phasic inspiratory activity in the hypoglossal nerve via altering activity in pre-motor neurons [518]. While this is unlikely to have caused the absence of phasic activity in these pilot studies (phasic genioglossus activity was also challenging to acquire when the animals were anaesthetised prior to being placed in the recording chamber), it is an important factor to consider in future research.

While stimulation-induced tongue muscle activity has been achieved during wakefulness and sleep [515], it was not achieved in these pilot studies. Fortunately, EMG recordings are not the sole method for quantifying the efficacy of muscle-stimulation therapies for OSA during natural sleep. Instead of chronically implanting EMG electrodes, daily recordings (~ 7 hours per day, 7 days per week) of EEG and chamber pressure (i.e. respiratory cycle) to monitor sleep stages and trigger light stimulation could be conducted. Across the 8 weeks, regular experiments under anaesthesia using intra-oral genioglossus EMG electrodes (insertion described in Chapter 2) could determine whether the chronic light stimulation applied in the chamber during natural sleep altered acute light-evoked muscle responses. Provided the plethysmography setup is sufficiently sensitive to detect changes in inspiratory flow following light stimulation during REM and NREM sleep (which remains to be determined), this approach may provide the same information without the added complications of the chronically implanted EMG electrodes. A similar approach has been used in investigations into DREADDs (Designer Receptors Exclusively Activated by Designer Drugs) for OSA [15, 16]. In these studies, genioglossus EMG responses to DREADD ligand administration were quantified under anaesthesia, and efficacy during natural sleep was quantified using polysomnography parameters (total sleep

time, sleep efficacy, the percentage time in REM and NREM, and number and duration of sleep bouts) and maximal inspiratory flow [16].

This pilot work outlines the early development of a novel surgical protocol that will allow determination of whether chronic light stimulation alters acute light-evoked muscle responses. As it stands, animals typically tolerated the surgery well, and by the final study, EEG and respiratory data were consistently recorded and allowed the identification of wakefulness, REM and NREM sleep. These studies also established optical fibres as the best method for delivering light stimulation to the tongue throughout a multi-week protocol and demonstrated that said light stimulation could be synchronised with the respiratory cycle. While additional pilot studies are still required to determine how best to record EMG activity in the tongue, considerable progress has been made.

Chapter 6 SUMMARY, DISCUSSION, AND CONCLUSIONS

6.1 SUMMARY OF RESULTS

This thesis presents a series of studies with the overarching objective of providing preclinical proof-of-concept for a minimally invasive, optogenetics-based muscle stimulation therapy for obstructive sleep apnoea (OSA). This encompassed the development of a suitable optogenetic construct for targeted opsin expression in, and light-evoked stimulation of, the tongue muscles of rats (Chapters 2,3), leading to upper airway dilation (Chapter 4), and development of both an acute model of OSA that recapitulates the sleep-related decrements in dilatory muscle activity (Chapter 2), and a protocol for long-term studies of regular light stimulation (Chapter 5).

The first two studies generated and refined a novel optogenetics construct with improved expression levels and biodistribution profile compared to previous muscle-directed gene therapies, through the use of a muscle-specific promoter (tMCK, Chapter 2) and a highly myotropic capsid (AAVMYO, Chapter 3). Specifically, the muscle-specific promoter, tMCK, produced 470% greater opsin expression in the tongue than the non-specific CAG promoter ($p=0.013$, RM-ANOVA) that has been used in all previous studies [235, 255]. Also, there was minimal systemic expression and no CNS expression following retrograde transmission despite AAV9s proven ability to do so [499, 500]. In a newly established rodent model of OSA that recapitulates human sleep-associated upper airway muscle hypotonia, this tMCK driven optogenetic construct facilitated a ~66% increase in muscle activity over that recorded during unstimulated breaths ($p<0.001$, linear mixed model) under light stimulation. The light-evoked responses were independent of the level of endogenous activity, confirming that this approach can boost impaired dilator muscle function (Chapter 2). An engineered and highly myotropic rAAV serotype, AAVMYO, driven by tMCK further increased muscle activity with light stimulation to ~194% of that recorded during unstimulated breaths ($p<0.001$, linear mixed model) with a similar biodistribution profile to the tMCK-AAV9 construct (Chapter 3). Ultrasound imaging demonstrated that light-evoked muscle contractions translated into airway dilation, and that contraction strength could be altered with changes in stimulation protocol. Where light-evoked muscle contractions were present, these persisted 12 weeks post-injection, albeit at reduced strengths at the final timepoint (Chapter 4). Finally, a surgical protocol was developed for the chronic implantation of light delivery hardware and recording electrodes in rodents and a pilot study conducted (Chapter 5), although further work is required for reliable EMG recordings of genioglossus activity. This will allow us to determine the effects of acute and chronic light stimulation on opsin-expressing upper airway muscles during natural sleep.

6.2 DEVELOPING AN OPTOGENETIC STIMULATION THERAPY FOR OSA

While there is no 'one size fits all' approach to the design of preclinical gene therapy studies, there are general objectives that aim to support and guide the design of preclinical data needed to support Phase 1 Clinical Trials. First, 'proof-of-concept' for the proposed gene therapy product should be established. Second, a pharmacologically effective dose range needs to be identified (i.e. minimally effective and optimal biological doses). These are used as the basis for dose-escalation studies for human clinical trials. Third, preclinical studies should describe the biodistribution of the gene therapy product, provide data on all organs (target or non-target), identify potential toxicities, and confirm gene therapy persistence, mobilisation and shedding. These studies should use the clinically proposed gene therapy product and route of administration and should be longitudinal, monitoring potential acute and chronic effects in terms of efficacy, biodistribution and potential toxicities. Concerning viral vectors specifically, replication incompetence, absence of integration, and latency must also be confirmed. Potential immunogenicity should be investigated, and methods of evading immune responses, should they be required, should be established [519, 520]. Upon completion, the gene therapy can then progress to first in human trials and Clinical Trials, Phases 1 to 3.

This thesis presents preclinical proof-of-concept for a novel optogenetics-based muscle stimulation therapy for OSA – the first step in this preclinical research process. It establishes a candidate viral vector platform for delivering a standard channelrhodopsin to the upper airway muscles, reporting that an engineered rAAV serotype (AAMYO) driven by a muscle-specific promoter (tMCK) generates strong and specific opsin expression in the upper airway muscles following direct intramuscular injection. The opsin expression produced in the tongue was sufficient for light stimulation to restore or boost muscle contractions and airway dilation in a rodent model of human sleep-associated upper airway hypotonia. This thesis also provided early biodistribution data indicative of a strong safety profile. The novel construct and local intramuscular route of administration generated minimal systemic expression and no CNS expression, and the strong light-evoked responses may allow further reductions of an already low viral load (3.4- and 4.6-fold lower viral loads than reported in similar rodent applications of optogenetics-based muscle stimulation [255, 496]). Finally, this thesis has commenced the development of surgical protocols that will allow long-term efficacy and safety data to be acquired.

Prior to translation to clinical trials, significant work is still required. We must (1) optimise light-evoked responses by determining which opsin can be most effectively activated in larger human muscles; (2) We must confirm that we can consistently induce strong opsin expression

with low viral loads that (3) persist over time. Next, (4) we must establish a strong safety profile by optimising tissue specificity and minimising systemic distribution or expression; and finally we must (5) develop appropriate light delivery hardware for human OSA patients.

6.2.1 Light stimulation

Effective optogenetics-based muscle stimulation requires sufficient opsin expression in the targeted muscle and sufficient illumination of the targeted muscles. Experiments achieved strong light-evoked muscle contractions and airway dilation, more predominantly localised to the region of tissue closest to the light source. This can be attributed to the poor penetration ability of blue light and the single (focal) light source, resulting in the illumination of only a small portion of the opsin-expressing tongue muscle tissue. This reflects a key issue associated with the translation of optogenetics from preclinical studies to clinical studies, i.e. the increase in the tissue volume combined with the poor penetration abilities of visible light. Fortunately, considered opsin selection and light-delivery technology can circumvent these issues.

6.2.1.1 Opsins

Experimental work (Chapters 2 and 3) clearly showed that the channelrhodopsin-2 (ChR2) variant, ChR2(H134R), achieved strong, albeit localised, light-evoked muscle contractions and airway dilation (Chapter 4). ChR2(H134R) and ChR2 are both activated by blue light and are currently the only opsins used for optogenetics-based muscle stimulation in rodents [235, 255, 496]. There are some limitations of developing ChR2-based stimulation, including poor tissue penetration of blue light, which restricts the depth at which opsins can be activated [276], and the slow kinetics of ChR2(H134R), which restricts the frequencies at which pulsed stimulation can be effective [235, 455, 460]. These limitations hinder the generation of longer duration light-evoked muscle contractions which is important for translation to humans, due to significantly larger tissue volumes and a slower respiratory cycle.

An obvious next step for this research is to assess other opsins that may generate stronger light-evoked responses and facilitate the activation of large volumes of tissue. Red-shifted opsins, e.g. ChrimsonR [268], are of particular interest due to the greater penetration of red light through tissue [276] which will allow myofibers further from the light source to be activated and therefore more complete muscle contractions and airway dilation to be generated. Similarly, CatCh, a higher sensitivity opsin with fast kinetics [281], can be activated at lower light levels, which may similarly aid in increasing the volumes of activated tissues. Furthermore, due to CatCh's greater Ca^{2+} permeability than ChR2 [283], it is particularly suitable for Ca^{2+} influx induced muscle contraction. In contrast, ChRmine [267], while red-light sensitive, has very low Ca^{2+} conductance so may be less effective for muscle activation [283]. In silico research in

cardiac muscle suggests that red-shifted and/or highly photosensitive opsins are likely to be required for rodent-to-human translation [250, 521]. Another advantage of ChrimsonR is that has been used in humans (partial restoration of vision has been achieved following rAAV-mediated ChrimsonR expression in retinal ganglion cells of retinitis pigmentosa patients [256-259]), so it has existing safety and efficacy data that may be leveraged for future clinical research.

Ultra-fast opsins such as ChETA [268, 272, 461] may also be useful, as their faster kinetics allow rapid opsin reactivation and reduce EMG 'decay' after rapid sequential pulses [235, 455, 456], as was reported with ChR2(H134R) in Chapter 2. Tetanic contractions were generated using 10 ms pulses applied at 40 Hz in Chapter 4, however the amplitude and tunability of these contractions could be further improved. Tunability could be improved with higher frequency stimulation [254], as evident when short pulse widths (≤ 5 ms) were applied during the stimulation protocol testing in Chapter 2. However, the small amplitude responses generated per pulse need improvement. Ultrafast opsins would balance these characteristics, by allowing longer pulses that individually generate greater amplitude responses to be applied at greater frequencies, with the fast kinetics allowing repolarization in shorter 'latency periods' between pulses. Unlike ChR2(H134R), which exhibits declines when 10 ms pulses are applied for more than 40 Hz (Chapter 2), this will allow greater amplitude responses to be generated and sustained over the prolonged human respiratory cycle, with frequencies exceeding 60 Hz.

Should red light not provide sufficient muscle penetration in the human upper airway for activation of deeper transduced cells, alternatives, including step-function opsins, could be explored to increase tonic muscle activity and/or reduce depolarisation thresholds that the activation of spectrally distinct red-shifted opsins must overcome [271]. Alternatively, opsins expressed in the tongue could be activated by nanoparticle technology that emits light when activated by ultrasound [482]. This technology uses rechargeable nanoparticles injected into the bloodstream that are activated by ultrasound when passing through lingual blood vessels, and emit visible light [482]. Upconversion nanoparticle devices (2 mm length, ~ 500 μm diameter) could also be implanted in the tongue to trigger optogenetic activation of the dilator muscles. These devices convert highly penetrating near infrared light into the visible spectrum, thereby stimulating expressed opsins sensitive to a matching frequency [481].

6.2.1.2 Light delivery

In addition to blue light incompletely penetrating rodent upper airway muscles, use of a single focal light source (LED) likely also contributed to the localised light-evoked muscle contractions and airway dilation. For future preclinical studies, it would be useful to trial LED

arrays to distribute light evenly across the tongue and increase the number of opsins activated and the size and uniformity of contractions generated. Preclinical technology for optogenetics research is rapidly evolving, and fully implantable flexible LED arrays have also been reported [472, 474-476], which may be useful for chronic stimulation studies, although their use in the tongue would be challenging due to the large movements involved in other tasks such as swallowing and mastication.

For future translation to humans, the technology required for minimally invasive illumination is often cited as a potential barrier to many applications for peripherally targeted direct optogenetics due to the target tissue's volume and distance from transdermal light delivery hardware. As the upper airway muscles are relatively small and accessible via the oral cavity, this could be overcome for this application through the use of an oral appliance to deliver light. In parallel with the work presented in this thesis, a 'smart' oral device for non-invasive light delivery is being developed in collaboration with biomedical engineering researchers at the University of New South Wales, Australia. An embedded sensor suite (using signal quality weighted inputs from a microphone, accelerometer, gyroscopic and photoplethysmography sensors) will monitor the respiratory cycle and deliver light to the targeted optogenetically transduced upper airway dilator muscles prior to the onset of inspiration. The light-evoked muscle contractions will subsequently mimic endogenous pre-inspiratory muscle contractions that 'set' the airway and defend against large negative inspiration-related pressure swings. As a removable device, device powering can be achieved through a 'charging station' that can also provide data transfer. Importantly, oral appliances are already well tolerated by OSA patients in the form of mandibular advancement splints, suggesting this is a practical approach from both an engineering and clinical perspective.

6.2.2 Targeted opsin expression and optimised safety profiles

Gene therapies for optogenetics-based muscle stimulation must balance efficacy and safety. First, viral vector constructs should achieve opsin expression sufficient to generate functionally effective responses to light stimulation. Second, opsin expression should be specific to the targeted skeletal muscle and delivered at the lowest effective doses to reduce risks associated with off-target expression and high viral particle titres, including immune responses and toxicities [330, 334-337], motor neuron death and muscle atrophy [335]. Optimising elements of the viral vector platform for gene delivery, including the promoter, the capsid and the route of administration, play significant roles in achieving strong targeted opsin expression, restricted biodistribution profiles and low viral loads.

6.2.2.1 Promoter

By restricting transgene expression to targeted cell types, tissue-specific promoters can maximise opsin expression while minimising the potentially harmful effects of off-target expression and high viral loads [319, 330]. Chapter 2 showed that a muscle-specific promoter (tMCK) generated stronger and muscle-restricted expression than a non-specific promoter (CAG) when packaged in a wild-type serotype (AAV9) and administered via intralingual injections. Three weeks after administration, the tMCK driven construct generated 4.7-fold greater opsin:reporter protein expression in the tongue than an otherwise equivalent CAG driven construct. This translated into strong light-evoked increases in muscle activity and visible muscle contractions in a rodent model of human sleep-associated hypotonia of the upper airway dilator muscles. Notably, this was achieved despite a 3.6-fold lower viral load than our original construct (AAV9-CAG), and a 3.4- and 4.6-fold lower viral load than equivalent non-specific promoter driven constructs used in other studies investigating optogenetics-based stimulation of skeletal muscle [255, 496].

tMCK also showed some potential safety benefits over a non-specific promoter. In contrast with the CAG driven construct, tMCK did not generate any opsin:reporter protein expression in the CNS, despite AAV9s demonstrated ability to do so following intralingual injections [499, 500]. This was an important finding considering that PNS and CNS targets for optogenetics have been associated with motor neuron death and muscle atrophy, thought to be chiefly elicited by ChR-mediated immunogenicity [335]. Moreover, there was minimal systemic distribution and uptake by internal organs (liver, spleen, heart) and other skeletal muscles (diaphragm, gastrocnemius). Like many wild-type rAAVs, AAV9 is prone to liver sequestering following systemic delivery [344], and intralingual injections [500] when driven by a non-specific promoter. Reducing off-target expression, particularly managing expression in the liver, is often cited as a priority as sequestering has been associated with limited transduction efficacy and increased risks of toxicities and liver failure with high viral loads [342, 349]. Conversely, liver-directed rAAV gene therapies have induced systemic tolerance to transgene products [522] and may promote long-term expression [523]. These conflicting reports will be taken into account in future work. This safety profile was maintained when AAVMYO replaced AAV9 in Chapter 3.

These findings indicate that, in addition to inducing strong and localised expression and robust functional responses to light stimulation, tMCK combined with intramuscular injections, may allow reduced viral loads, and minimise the risk of toxicities, immune responses, and other adverse events associated with off-target delivery. While numerous muscle-specific promoters are available, and some have been used in clinical trials [364, 524], at this time, tMCK appears

to meet the requirements for this application, however there may be further improvements in muscle-specific promoters in future that could also be suitable for the proposed therapy.

6.2.2.2 Capsid

When work on this PhD project commenced, AAV9 was the benchmark rAAV serotype for muscle transduction, was clinically approved for delivery of spinal muscular atrophy therapy, and was the only serotype used in preclinical optogenetics-based muscle stimulation [235, 255, 496]. Chapter 2 confirmed AAV9 could generate strong opsin:reporter expression in the tongue following intramuscular injections. However, engineered rAAVs were investigated as an alternative in an attempt to mitigate some of the disadvantages associated with wild-type rAAVs, including the high prevalence of anti-AAV seropositive patients [346], which restricts patient eligibility for rAAV-mediated gene therapies due to immune responses [313, 348, 371, 505]. However, improvements to capsids for muscle-targeted gene therapy have occurred since, including the development of the highly-myotropic capsid AAVMYO. Key advantages of relevance here include that when delivered systemically in mice, AAVMYO driven by a non-specific promoter produced significantly greater RNA expression in skeletal muscles (~ 61-fold and 17-fold greater in the diaphragm and quadriceps femoris, respectively) and 9-fold greater liver detargeting compared to AAV9 [344]. Chapter 3 showed that these advantages persist in rats, and when combined with intramuscular injections and muscle-specific promoters, AAVMYO further enhanced the tissue and location specificity reported in Chapter 2 with AAV9. Moreover, light stimulation in AAVMYO-injected animals elicited measurable upper airway dilations in some animals. Compared to AAV9, AAVMYO may lower effective viral loads, minimise the risk of therapy-limiting toxicities [349, 350], reduce immune surveillance and responses [344, 345, 351], and be clinically accessible to more individuals.

More recently, research into the development and enhancement of highly myotropic rAAVs using similar methods to those used to develop AAVMYO, i.e. directed evolution followed by high-throughput testing of large ‘barcoded’ rAAV libraries, has accelerated. AAVMYO has received rational additions to further reduce off-target expression [55]. Another highly myotropic capsid, MyoAAV was also described, with similar properties. Like AAVMYO, systemic delivery of MyoAAV generated greater RNA and transgene expression in skeletal muscle and greater liver detargeting than AAV9 [345]. Significantly, MyoAAV performed well after intramuscular delivery, similar to methods used in this thesis. In particular, while the experiments outlined in Chapter 3 report twice as much RNA expression following intramuscular injections into our targeted muscles than AAV9, MyoAAV produced 14 times greater RNA expression following intramuscular injections. Notably, it was also tested in

human myocytes, and transduction was 35 to 52 times greater [345] – a promising result for human translation. There is considerable commercial interest in this area as well. Following successful clinical trials using a wild-type rAAV for a Duchenne Muscular Dystrophy gene therapy, Sarepta Therapeutics was granted a license for MyoAAV use for various neuromuscular and cardiac indications. Regarding the proposed therapy for OSA, future studies will need to confirm whether MyoAAV would further improve on AAVMYO's functional responses to light stimulation, but it may present an opportunity to leverage safety and efficacy data produced from ongoing preclinical and clinical research targeting other muscles.

6.2.2.3 Route of administration

In the context of the proposed optogenetics-based muscle stimulation therapy for OSA, the benefits of intramuscular injections over systemic distribution are; (1) Intramuscular injections are associated with strong safety profiles and efficient transgene expression. As a result, they will facilitate (2) effective light-evoked airway dilation and (3) may enable targeted therapy aimed at patient-specific sites of collapse.

6.2.2.3.1 Biodistribution and safety

Compared to systemic delivery, intramuscular injections result in relatively modest vector uptake in non-targeted tissue [366], are less susceptible to pre-existing anti-AAV humoral immunity [367, 368], and are associated with fewer serious adverse events [323]. Targeted delivery allows reduced viral loads, with clinical trials administering a maximum of 7.5×10^{15} vector copies versus 1.5×10^{17} for systemic administration [338]. In this thesis, intralingual injections of either AAV9 or AAVMYO driven by tMCK generated robust opsin:reporter fusion protein and RNA expression, and high viral DNA copy numbers in the tongue, but no expression in the CNS and minimal or no systemic distribution or uptake by all other tissues, including the liver. This early biodistribution data contrasts with existing data using systemic administration of a tMCK-driven by a wild-type rAAV, which generated efficient skeletal muscle targeting, but found that the greatest vector copy numbers remained in the liver and required 16.6- and 33.1-fold higher viral loads (3×10^{12} and 6×10^{12} vector copies) to generate functionally effective transgene expression [525]. The results from this thesis add to the existing literature on the relative safety benefits of intramuscular injections compared to systemic administration for muscle-targeted gene therapy.

It should be noted that intramuscular injections have been associated with a greater risk of anti-transgene immune responses than systemic administration [526, 527], however minimal research has been conducted regarding optogenetics. ChR2-mediated immunogenicity has been reported following injections into the lower limb's anterior compartment, producing severe

adverse events, including motor neuron death and muscle atrophy. This immune response and associated adverse events were moderated using slow-release immunosuppressants, and opsin expression was maintained for up to 12 weeks post-administration [335]. Regardless, future preclinical studies for the proposed OSA therapy will need to conduct thorough biodistribution and toxicity studies to monitor the presence or absence of immune responses, including anti-AAV and anti-opsin antibodies over an extended period of time and to determine whether adjunct immune suppression is required.

6.2.2.3.2 Tongue contraction versus dilation

All experiments described in this thesis aimed to saturate the tongue with opsin expression via four 5 µL intramuscular injections distributed throughout the tongue. This decision was based on reports that electrical stimulation of multiple tongue muscles (i.e. intrinsic and extrinsic, protruders and retractors) generated greater airway dilation, pharyngeal stiffening and/or increased airflow than electrical stimulation of a single muscle group [36, 37, 46, 72]. In Chapter 4, it was demonstrated that the opsin expression achieved strong but highly localised light-evoked muscle contractions and airway dilation. While promising, it was noted that the light-evoked contractions did not mimic endogenous contractions associated with a standard breath. The reasons for this were likely two-fold; (1) simultaneous activation of indiscriminately expressed opsins in myofibres of the intermingled muscles of the tongue does not reflect natural physiological muscle activation in the tongue [31, 73, 77]; and (2) the single light source delivering blue light ineffectively penetrates tissue and thus activates only the local area where light penetration is sufficient. As a result, light stimulation produced intense local contractions rather than an anterior-posterior ‘shift’ of the tongue. While interesting, a non-physiological pattern of may not be a barrier to effective maintenance of airway patency clinically. In clinical research studies investigating hypoglossal nerve stimulation for OSA, treatment success is defined by polysomnography data and quality of life outcomes [170, 171], and in preclinical research, stimulation success is defined by airway dilation and measures of flow mechanics [46, 72, 498]. To generate preclinical evidence of efficacy for an optogenetics-based therapy, achieving strong and titratable airway dilation should therefore be the priority. In this context, the main concern is the focal nature of airway dilation induced here. This limitation may be able to be overcome using red-shifted opsins and LED arrays that will increase the volume of illuminated tissue and extend the strong light-evoked contractions along the length of the tongue. It remains to be proven that such stimulation would maintain airway patency and airflow during natural sleep, and in the presence of anatomical compromise.

6.2.2.4 Targeting site of collapse

While saturating the tongue with opsins did achieve strong dilation in animals that responded, and is expected to improve using red-shifted opsins and LED arrays, this 'broad brush' approach may not be suitable for all OSA patients. Airway collapse typically occurs at multiple levels – predominantly at the palatal and tongue base levels, and less commonly at the oropharyngeal and epiglottis levels [528]. Similar to the initial approach followed here, hypoglossal nerve stimulation focuses on the muscles of the tongue. By stimulating the medial branch of the nerve the 'protruder' muscles, including the genioglossus, vertical and transverse muscles, contract and airway patency should be maintained. While this may be effective in some patients, it is ineffective in patients with complete concentric collapse at the velopharynx [528], and these patients are excluded from this therapy. These patients in particular may benefit from targeted stimulation of palatal muscles, including the tensor palatini which has been shown to stiffen the soft palate to promote nasal breathing [49, 50] or the palatoglossus which couples the soft palate to the tongue [21, 49, 51].

In principle, an optogenetics-based muscle stimulation therapy could use targeted intramuscular injections to deliver opsins to specific regions to tailor light-evoked airway dilation to patient-specific sites of collapse, building on experiments reported here that saturate the tongue with opsin expression using several intramuscular injections. This achieved robust opsin:reporter protein expression throughout the tongue (Chapters 2 and 3), and strong light-evoked muscle contractions and airway dilation, with little dependence on LED position (Chapters 3 and 4), but localised to the area near the LED. As discussed above, the region of dilation could be expanded by red-shifted opsins and LED arrays, but this also indicates that targeted muscle activation is possible. In addition, the successful use of ultrasound to image rodent upper airway muscles indicates that ultrasound guidance could be an effective method for administering injections to specific muscles. Clinically, ultrasound guiding is commonly used for injections and biopsies, e.g. delivering corticosteroids to joints, tendons and bursas, or extracting tissue samples to check potentially cancerous cells. Based on the imaging data obtained to date, practical preclinical targets could include the genioglossus and the geniohyoid to generate longitudinal contractions and dilation at the tongue's posterior. Injections in the oblique genioglossus and vertical muscles are expected to generate vertical contractions and airway dilation in the mid-axial plane. Successful targeting, confirmed by quantifying opsin:reporter protein expression in the tongue, and functional light-evoked responses under ultrasound, would provide support for patient specific, targeted muscle stimulation approaches. Finally, in the context of safety, targeted intramuscular injections may also improve safety profile by reducing the required viral loads compared to whole-tongue saturation.

6.2.2.5 Variability

This thesis reported significant inter- and intra-cohort variations, particularly in the AAVMYO cohorts. In Chapter 3, variation was seen in the light-evoked increases in EMG and in the tongue's viral DNA and RNA expression. In Chapter 4, variation was seen in the light-evoked muscle contractions and airway dilation; where, of the 8 animals that received the construct, only two produced sufficient contractions to generate airway dilation, and four animals did not respond to light stimulation at all. Inter-cohort variation was also evident between these chapters. In Chapter 3, strong light-evoked muscle contractions were visible in 8 of 9 animals, whereas Chapter 4, equivalent strength contractions were visible in only 1 of 8 animals. While all animals in these cohorts underwent identical vector administration protocols and experimental timetables, they did receive different 'batches' or 'lots' of the theoretically identical constructs. The two lots had different titres (4.75×20^{13} vg/mL and 2.43×10^{13} vg/mL), but were diluted to deliver 1.81×10^{11} vector copies. At this time, we have confirmed the originally stated titers and have concluded that the variation is due to the manufacturing process – plasmid sequencing in underway.

Both intra- and inter-lot variation can occur at various stages of the viral vector manufacturing process, and lot-to-lot variation has been reported between theoretically identical constructs manufactured by different vector cores and those manufactured within a single core [529, 530]. Lot-to-lot variation has been reported with various serotypes, including AAV9, however the cause of variation is not always evident [530]. Potential sources of variation include differences in the proportion of empty versus full capsids [529, 531, 532], viral particle aggregation [533], the presence of various impurities [534, 535] and action by residual cesium chloride (CsCl) following CsCl-based purification [530, 536, 537]. The latter is of particular note as all constructs reported in the thesis were generated via this method. The cell platform used for production can also alter outcomes (insect cells (SF9) vs mammalian cells (HEK293)) [529], and incomplete plasmid transfection can result in low titer and incomplete viral packaging. Finally, the integrity of the vector genome can also have an effect on production quality and can lead to poor stability and transduction efficiency of the product [538]. ITR instability in particular has been flagged as a potential source of variation in our constructs following investigations by the manufacturer. Further testing is required to isolate the source(s) of this variability.

Recommendations for preclinical trials [519, 520], require evidence of product consistency by thoroughly characterising at least three successive batches of the bulk product for identity,

purity, potency, and safety. Once this is achieved, a more limited battery of tests can be used on later viral vector lots.

6.2.3 Long term considerations

6.2.3.1 Persistent opsin expression

The success of rAAV-mediated gene therapies depends on the magnitude and persistence of the transgene expression. Chapter 4 of this thesis reported that when animals exhibited light-evoked muscle contractions and airway dilation three weeks after intramuscular injections of an optogenetic construct, light-evoked muscle contractions persisted for three months, albeit at reduced strengths after 8-10 weeks. This is consistent with data presented in Chapter 2 where viral DNA and RNA expression was robust in the tongue three weeks after vector administration, but at low levels 12 weeks after administration. Importantly, the ultrasound studies showing that functional declines started 8-10 weeks after vector administration, indicate that the construct successfully evaded pre-existing and acute immune responses, and thus late functional loss is more likely to be caused by delayed adaptive immune responses [507], skeletal muscle cell turnover [508], and/or promoter silencing [509]. As silencing is less prevalent with non-viral promoters, such as tMCK used here, than viral promoters, e.g. CMV [416, 417], and transgene expression in skeletal muscle has been reported up to 10 years after rAAV administration in humans [332] due to slow myocyte turnover rates [539], these mechanisms are less likely cause expression losses. Future studies could determine whether inhibiting delayed adaptive immune responses will allow persistent opsin expression. Based on previous literature where long term expression was achieved [335, 385], these studies could use sustained immunosuppressant administration to prevent B-cell and T-cell formation throughout the three months of repeated functional testing could be performed. Persistent light-evoked responses by the upper airway muscles – a proxy for opsin expression – would indicate that immune responses rather than skeletal muscle turnover produced the declines reported in Chapters 3 and 4, therefore informing potential immunosuppression requirements for clinical trials. Other avenues to address this challenge are possible. For example, rAAV vector re-administration has been achieved when the initial dose is administered concurrently with synthetic vaccine particles encapsulating immunosuppressants [386], and in seropositive animals and in in-vitro human plasma samples when endopeptidase infusions that degrade circulating antibodies are applied prior to rAAV administration [387]. Muscle cell turn over in opsin expressing muscle could also be analysed using BrdU or EdU assays that ‘tag’ cells generated after the animals receive rAAV treatments. Immunohistochemistry based experiments at the end point (i.e. 12-weeks after vector administration) would calculate the percentage of

BrdU or EdU positive cells verses opsin:reporter positive cells to determine whether transgene losses are due to new cell proliferation [540].

6.2.3.2 Chronic light stimulation

Upon achieving long-term opsin expression, studies investigating the effects of chronic light stimulation on the upper airway muscles and their responses to acute light stimulation are required. The sole study that has investigated 'chronic' light stimulation in rodent skeletal muscle found that 1 hour of pulsed light stimulation per day for 10 days mitigated muscle atrophy and force losses following muscle denervation [254]. As optimal OSA therapy use is 7 to 8 hours per night, repeated indefinitely, this duration of light stimulation is insufficient. Clinically, the most comparable data is from long-term use of hypoglossal nerve stimulation. After 5 years of device use, therapeutic efficacy and adherence remain high, and stimulation-induced side effects that were highly prevalent after 12 months of use (40% of participants reported discomfort during stimulation, and 21% reported tongue soreness) had significantly declined [171, 172]. While this is promising data regarding the tolerability of stimulated contractions of the upper airway muscles, application-specific data is required.

Chapter 5 outlines the development of a surgical protocol that will enable generation of this data, using a plethysmograph-like chamber to monitor the respiratory cycle non-invasively and trigger light stimulation 'in phase' with inspiration and during natural sleep (as identified via chronically implanted EEG electrodes) while recording evoked muscle activity and. In addition to providing information regarding the effects of chronic light stimulation on muscle properties, these experiments could also determine whether light stimulation disturbs sleep, based on the presence of arousals following stimulation, and whether light-evoked muscle contractions are effective during both REM and NREM sleep. The latter is of interest because recent studies investigating a chemogenetic approach to inducing airway dilation use 'designer receptors exclusively activated by designer drugs' (DREADDs). By targeting hypoglossal motor neurons, this approach successfully increased dilator muscle tone [16, 232] but was found to be more efficacious in NREM than REM sleep [16]. As Chapters 2 and 3 of this thesis found that light stimulation was able to restore or boost near-eliminated muscle activity in a rodent model of human sleep-associated upper airway muscle hypotonia, it seems likely that stimulation efficacy can be maintained during REM sleep; however, this does require confirmation.

6.3 CONTRIBUTIONS TO KNOWLEDGE

This thesis has made several contributions to current preclinical research and future clinical applications of optogenetics-based muscle stimulation; (1) This thesis presents two novel

techniques for rodent research, i.e. a rodent model of upper airway muscle hypotonia that mimics muscle activity reductions seen during sleep onset in humans, and the first data using ultrasound to quantify upper airway muscle function. (2) This thesis has improved targeting of opsin expression for direct optogenetic control of skeletal muscle. As a result, (3) it has further developed biotechnology that has potential utility in multiple disorders associated with loss of muscle function.

6.3.1 Rodent research methods

6.3.1.1 A novel rodent model of human sleep-associated upper airway muscle impairment

Rodents make up approximately 95% of laboratory animals due to their small size, which facilitates easy housing and maintenance, their short reproductive cycle and lifespan, the ease of genetic manipulation and their genetic similarities to humans [81]. Prior to this thesis, rodent models of OSA were restricted to obese or leptin-deficit animals with significant comorbidities [92, 97, 220], mechanical occlusion that collapse or block the upper airway [224-227, 494] and models of intermittent hypoxia [222]. None were suitable for quantifying pharyngeal muscle activity restoration.

Here a novel model of sleep-associated upper airway hypotonia in humans was developed, inspired by the clinical problem where general anesthesia using isoflurane caused upper airway hypotonia and increased upper airway collapsibility [495]. In Chapter 2, a simple model where increased isoflurane concentration produced reversible reductions in phasic inspiratory dilator activity of the genioglossus in otherwise healthy Sprague-Dawley rats while having minimal effects on diaphragm inspiratory activity was described. The development of this model has application to preclinical testing of other novel therapies targeting the common poor muscle responsiveness endotype that contributes to OSA [11].

6.3.1.2 Ultrasound imaging as a cost-effective method of quantifying rodent upper airway function

Until this thesis, dynamic and static imaging of the rodent upper airway had exclusively used magnetic resonance imaging (MRI) [15, 16, 72, 97, 100, 103]. While MRI is highly effective and provides excellent spatial resolution and tissue contrast, it is time-consuming, expensive, has relatively poor temporal resolution, and requires significant technological expertise. In comparison, ultrasound is a ‘real-time’ imaging modality and is much cheaper to run. Unlike MRIs which require dedicated magnet and control rooms with restricted access, pre-clinical ultrasound can be housed with other equipment in standard PC2 laboratories. Finally, while ultrasound has a more limited penetration depth than MR imaging, this did not present an issue

in rodent upper airways until the rats reached ~ 550 g. This limitation in larger animals could be overcome by changing to an alternate transducer with greater scan depths (e.g. MX400 to MX250S, FUJIFILM, VisualSonics, ON, Canada).

6.3.2 Improved targeting of direct optogenetic control of skeletal muscle

This thesis presents the first use of muscle-specific promoters and engineered rAAV serotypes for direct optogenetic control of skeletal muscle. Previously, research had exclusively used a standard rAAV serotype, AAV9, driven by a non-specific promoter, CAG [235, 255, 496]. Two of the three existing reports, both published in 2022, demonstrated light-evoked EMG responses in the diaphragm and tongue following intrapleural and intralingual injections respectively. The study investigating optogenetic control of the diaphragm, also provided evidence that light stimulation could generate respiratory airflow.

As outlined in this thesis, the shift from CAG to tMCK, and AAV9 to AAVMYO significantly improved the specificity of opsin expression and the light-evoked muscle responses. AAV9 driven by tMCK rather than CAG generated 4.7-fold greater opsin:reporter expression in the tongue. Next, using AAVMYO rather than AAV9, generated over double the RNA expression and viral DNA copy numbers in the tongue, and significantly greater functional responses to light stimulation. Notably, this was achieved despite the new construct being administered at a 3.6-fold lower viral load, which equated to a 3.4- and 4.6-fold reduction than that administered in the earlier studies [255, 496].

This thesis also presented the first investigation of viral DNA, and protein and RNA expression distribution outside of the targeted muscle. In Chapter 2 it was reported that the tMCK promoter eliminated opsin:reporter expression in the CNS. This is particularly important for pre-clinical research considering PNS and CNS targets have been associated with motor neuron death and muscle atrophy, thought to be elicited by ChR-mediated immunogenicity [335]. Moreover, RNA expression and viral DNA copies numbers in all tissues excluding the tongue were low or absent. This promising safety profile persisted when the AAV9 capsid was replaced with AAVMYO in Chapter 3.

Finally, this data presents the first application of AAVMYO outside of systemic administration in mice [345], indicating that the stronger muscle-specific expression achieved by AAVMYO compared to AAV9 persists with different promoters, administration routes, and animal species. Moreover, this data supports AAVMYO and other similarly engineered myotropic rAAV serotypes (e.g. MyoAAV) as an essential tool for future clinical, skeletal muscle-directed gene therapies.

6.3.3 Clinical applications outside of OSA

While this thesis has specifically targeted the upper airway muscles to provide proof-of-concept for a novel OSA therapy, as a pain-free, spatially and temporally precise method of muscle function restoration, the technology developed has potential application in other neuromuscular disorders.

Direct optogenetic activation of skeletal muscle could be applied in disorders or injuries where patients have sustained damage to the neural pathways connecting the skeletal muscle and the CNS. Early proof-of-concept for an optogenetics-based therapy for diaphragm dysfunction used intrapleural injections of a non-specific promoter-driven optogenetics construct (similar to that described in Chapter 2) to generate opsin expression in the diaphragm [255]. While phrenic nerve stimulation for diaphragm control is an option for some patients, those with damage to the nerve or the phrenic motor pool are commonly ineligible as the descending stimulation will not reach the skeletal muscle target. By directly activating diaphragm myofibers with optogenetics, the damage is bypassed. Impaired diaphragm activation is common in many neuromuscular diseases and spinal cord injuries, and diaphragm-targeted optogenetics may prove life-changing for ventilated individuals with damaged or vulnerable phrenic nerves or motor pools. This example is representative of a larger clinical population, i.e. patients with impaired descending motor neuronal tracts (upper or lower motor neurons, peripheral nerves, motor neuronal pools, and/or neuromuscular synapses), that may benefit from direct optogenetic stimulation of skeletal muscle due to exclusion from, or an absence of, functional electrical stimulation options. Clinical populations include those with muscle function losses following peripheral nerve or spinal cord injury and disorders such as motor neurone diseases, e.g. amyotrophic lateral sclerosis, and muscular dystrophies. Within these populations, potential muscle targets that may benefit from spatially and temporally precise, closed-loop, optogenetics-based stimulation are virtually limitless, e.g. fine control of the muscles required for grasping objects, or ankle and foot dorsiflexors to prevent foot drop. Moreover, direct optogenetic stimulation may also reduce muscle atrophy following denervation [254].

Direct optogenetic stimulation also has utility in selectively activating muscles innervated by mixed peripheral nerves, where electrical stimulation could not provide selectivity. Moreover, spectrally distinct opsins could be used to allow alternating activation, or simultaneous activation and inhibition, of an agonists and antagonists. Optogenetics also has the major advantage that it can also allow endogenous motor neuron activity to function in parallel, a characteristic particularly beneficial in muscles with multiple roles. The mammalian larynx is a good example, as the laryngeal nerve innervates all skeletal muscles that control the position of

the vocal cords. As contraction of the posterior cricoarytenoid muscle opens the vocal cords and contractions of other intralaryngeal muscles close the vocal cords, electrical stimulation of the laryngeal nerve may not effectively modulate vocal cord opening. One of the first studies of direct optogenetic control of skeletal muscle provided ex vivo proof that this method could be used to manipulate the vocal cords [235]. Notably, like the upper airway muscles, laryngeal muscles are comparatively small and shallow and, therefore, more likely to be accessible by transdermal illumination.

6.4 CONCLUSIONS

This thesis has provided proof-of-concept for a direct optogenetics approach for boosting or restoring upper airway muscle activity and generating airway dilation in a rodent model of human sleep-associated upper airway muscle hypotonia. Local intramuscular injections, a muscle-specific promoter and an engineered and highly myotropic rAAV serotype maximised the efficiency and specificity of opsin expression, and light stimulation protocols facilitated highly customisable and temporally precise stimulation. Moreover, the strong expression and strong light-evoked responses were achieved with a low viral load, no CNS expression, and minimal systemic distribution, providing a promising safety profile. Future studies exploring novel opsins to optimise airway dilation, immunosuppression studies to facilitate long-term opsin expression, and thorough biodistribution and toxicology studies are required to establish the required preclinical evidence base for human clinical trials.

This thesis has also made significant contributions to preclinical research by developing a novel rodent model of upper airway muscle hypotonia and describing the first use of ultrasound to quantify rodent upper airway function. Finally, by introducing muscle-specific promoters and engineered rAAVs, this thesis has advanced the viral technology used to generate opsin expression in skeletal muscle, which has potential application beyond OSA in other diseases/disorders associated with muscle function loss, particularly those where the integrity of the descending motor tract is compromised.

REFERENCES

1. Benjafield, A.V., et al., *Estimation of the global prevalence and burden of obstructive sleep apnoea: a literature-based analysis.* The Lancet Respiratory Medicine, 2019. **7**(8): p. 687-698.
2. *Modern Management of Obstructive Sleep Apnea*. 2019white, Cham: Cham : Springer International Publishing : Imprint: Springer.
3. Heinzer, R., et al., *Prevalence of sleep-disordered breathing in the general population: the HypnoLaus study.* Lancet Respir Med, 2015. **3**(4): p. 310-8.
4. Peppard, P.E., et al., *Increased prevalence of sleep-disordered breathing in adults.* Am J Epidemiol, 2013. **177**(9): p. 1006-14.
5. Weaver, T.E. and R.R. Grunstein, *Adherence to continuous positive airway pressure therapy: the challenge to effective treatment.* Proceedings of the American Thoracic Society, 2008. **5**(2): p. 173-178.
6. Kompelli, A.R., et al., *The outcomes of hypoglossal nerve stimulation in the management of OSA: A systematic review and meta-analysis.* World J Otorhinolaryngol Head Neck Surg, 2019. **5**(1): p. 41-48.
7. Phillips, C., et al., *Health Outcomes of Continuous Positive Airway Pressure versus Oral Appliance Treatment for Obstructive Sleep Apnea.* Am. J. Respir. Crit. Care Med., 2013. **187**(8): p. 879-887.
8. Kribbs, N.B., et al., *Objective Measurement of Patterns of Nasal CPAP Use by Patients with Obstructive Sleep Apnea.* American Review of Respiratory Disease, 1993. **147**(4): p. 887-895.
9. Jullian-Desayes, I., et al., *Impact of concomitant medications on obstructive sleep apnoea*. British Journal of Clinical Pharmacology, 2017. **83**(4): p. 688-708.
10. Eckert, D.J., et al., *Defining phenotypic causes of obstructive sleep apnea. Identification of novel therapeutic targets.* American journal of respiratory and critical care medicine, 2013. **188**(8): p. 996.
11. Eckert, D., *Phenotypic approaches to obstructive sleep apnoea - New pathways for targeted therapy.* Sleep Med. Rev., 2018. **37**: p. 45-59.
12. Costantino, A., et al., *Hypoglossal nerve stimulation long-term clinical outcomes: a systematic review and meta-analysis.* Sleep and Breathing, 2019.
13. Eastwood, P.R., et al., *Bilateral hypoglossal nerve stimulation for treatment of adult obstructive sleep apnoea.* European Respiratory Journal, 2020. **55**(1): p. 1901320.
14. Kezirian, E.J., et al., *Hypoglossal nerve stimulation improves obstructive sleep apnea: 12-month outcomes.* J Sleep Res, 2014. **23**(1): p. 77-83.
15. Fleury Curado, T., et al., *Chemogenetic stimulation of the hypoglossal neurons improves upper airway patency.* Sci Rep, 2017. **7**: p. 44392.
16. Fleury Curado, T., et al., *Designer Receptors Exclusively Activated by Designer Drugs Approach to Treatment of Sleep-disordered Breathing.* Am J Respir Crit Care Med, 2021. **203**(1): p. 102-110.
17. Butler, J.E., A.L. Hudson, and S.C. Gandevia, *The neural control of human inspiratory muscles.* Progress in brain research, 2014. **209**: p. 295-308.
18. Emura, F., T.H. Baron, and I.M. Gralnek, *The pharynx: examination of an area too often ignored during upper endoscopy.* Gastrointest Endosc, 2013. **78**(1): p. 143-9.
19. Anatomy, S.S.G.s., *The anatomical basis of clinical practice. Churchill Livingstone*. 2008, Elsevier.
20. Ayappa, I. and D.M. Rapoport, *The upper airway in sleep: physiology of the pharynx.* Sleep Med Rev, 2003. **7**(1): p. 9-33.
21. Edwards, B.A. and D.P. White, *Control of the pharyngeal musculature during wakefulness and sleep: implications in normal controls and sleep apnea.* Head & neck, 2011. **33 Suppl 1**(Suppl 1): p. S37-S45.

22. Ciscar, M.A., et al., *Magnetic resonance imaging of the pharynx in OSA patients and healthy subjects.* 2001. **17**(1): p. 79-86.

23. Isono, S., et al., *Static Properties of the Passive Pharynx in Sleep Apnea.* Sleep, 1996. **19**(suppl_10): p. S175-S177.

24. Isono, S., et al., *Anatomy of pharynx in patients with obstructive sleep apnea and in normal subjects.* J Appl Physiol (1985), 1997. **82**(4): p. 1319-26.

25. Mu, L., et al., *Innervation of human soft palate muscles.* Anat Rec (Hoboken), 2021. **304**(5): p. 1054-1070.

26. Sanders, I. and L. Mu, *A three-dimensional atlas of human tongue muscles.* Anat Rec (Hoboken), 2013. **296**(7): p. 1102-14.

27. Tamura, T., et al., *Relationships between maximum tongue pressure and second formant transition in speakers with different types of dysarthria.* PLoS One, 2022. **17**(3): p. e0264995.

28. Sasegbon, A. and S. Hamdy, *The anatomy and physiology of normal and abnormal swallowing in oropharyngeal dysphagia.* Neurogastroenterology and motility : the official journal of the European Gastrointestinal Motility Society, 2017. **29**(11).

29. Cheng, S., et al., *Movement of the tongue during normal breathing in awake healthy humans.* The Journal of physiology, 2008. **586**(17): p. 4283-4294.

30. Mu, L. and I. Sanders, *Human tongue neuroanatomy: Nerve supply and motor endplates.* Clinical anatomy (New York, N.Y.), 2010. **23**(7): p. 777-791.

31. Saboisky, J.P., et al., *Tonic and phasic respiratory drives to human genioglossus motoneurons during breathing.* Journal of Neurophysiology, 2006. **95**(4): p. 2213-2221.

32. Bailey, E.F. and R.F. Fregosi, *Coordination of intrinsic and extrinsic tongue muscles during spontaneous breathing in the rat.* J Appl Physiol (1985), 2004. **96**(2): p. 440-9.

33. Fregosi, R.F. and C.L. Ludlow, *Activation of upper airway muscles during breathing and swallowing.* Journal of applied physiology (Bethesda, Md. : 1985), 2014. **116**(3): p. 291.

34. Kier, W.M. and K.K. Smith, *Tongues, tentacles and trunks: the biomechanics of movement in muscular-hydrostats.* Zoological Journal of the Linnean Society, 1985. **83**(4): p. 307-324.

35. Kubin, L., *Neural Control of the Upper Airway: Respiratory and State-Dependent Mechanisms.* Compr Physiol, 2016. **6**(4): p. 1801-1850.

36. Fuller, D., J.H. Mateika, and R.F. Fregosi, *Co-activation of tongue protrudor and retractor muscles during chemoreceptor stimulation in the rat.* J Physiol, 1998. **507 (Pt 1)**: p. 265-76.

37. Fuller, D.D., et al., *Effect of co-activation of tongue protrudor and retractor muscles on tongue movements and pharyngeal airflow mechanics in the rat.* J Physiol, 1999. **519 Pt 2**(Pt 2): p. 601-13.

38. Netter, F.H., *Atlas of human anatomy*. 6th ed. ed. 2014, London: London : Elsevier Health Sciences.

39. Wilkinson, V., et al., *Discharge patterns of human genioglossus motor units during sleep onset.* Sleep, 2008. **31**(4): p. 525-33.

40. Wilkinson, V., et al., *Discharge patterns of human genioglossus motor units during arousal from sleep.* Sleep, 2010. **33**(3): p. 379-87.

41. Yeung, J., et al., *Task-dependent neural control of regions within human genioglossus.* J Appl Physiol (1985), 2022. **132**(2): p. 527-540.

42. Jugé, L., et al., *Regional respiratory movement of the tongue is coordinated during wakefulness and is larger in severe obstructive sleep apnoea.* J Physiol, 2020. **598**(3): p. 581-597.

43. Kwan, B.C.H., et al., *Sagittal Measurement of Tongue Movement During Respiration: Comparison Between Ultrasonography and Magnetic Resonance Imaging.* Ultrasound in Medicine & Biology, 2019. **45**(4): p. 921-934.

44. Kwan, B.C.H., et al., *Influence of respiratory mechanics and drive on genioglossus movement under ultrasound imaging.* PLOS ONE, 2018. **13**(4): p. e0195884.

45. Sakamoto, Y., *Configuration of the extrinsic muscles of the tongue and their spatial interrelationships.* Surg Radiol Anat, 2017. **39**(5): p. 497-506.

46. Bailey, E.F., Y.H. Huang, and R.F. Fregosi, *Anatomic consequences of intrinsic tongue muscle activation.* J Appl Physiol (1985), 2006. **101**(5): p. 1377-85.

47. Sakamoto, Y., *Structural arrangement of the intrinsic muscles of the tongue and their relationships with the extrinsic muscles.* Surg Radiol Anat, 2018. **40**(6): p. 681-688.

48. Rodenstein, D.O. and D.C. Stănescu, *Soft palate and oronasal breathing in humans.* J Appl Physiol Respir Environ Exerc Physiol, 1984. **57**(3): p. 651-7.

49. Tangel, D.J., W.S. Mezzanotte, and D.P. White, *Respiratory-related control of palatoglossus and levator palatini muscle activity.* 1995. **78**(2): p. 680-688.

50. Tangel, D.J., W.S. Mezzanotte, and D.P. White, *Influence of sleep on tensor palatini EMG and upper airway resistance in normal men.* J Appl Physiol (1985), 1991. **70**(6): p. 2574-81.

51. Mortimore, I. and N. Douglas, *Palatopharyngeus has respiratory activity and responds to negative pressure in sleep apnoeics.* 1996. **9**(4): p. 773-778.

52. Shimada, K. and R.F.J.C.A. Gasser, *Variations of the pharyngeal raphe.* 1988. **1**.

53. Mu, L. and I. Sanders, *Neuromuscular Specializations within Human Pharyngeal Constrictor Muscles.* Ann Otol Rhinol Laryngol, 2007. **116**(8): p. 604-617.

54. Sakamoto, Y., *Classification of pharyngeal muscles based on innervations from glossopharyngeal and vagus nerves in human.* Surg Radiol Anat, 2009. **31**(10): p. 755-761.

55. Kuna, S.T., *Respiratory-related activation and mechanical effects of the pharyngeal constrictor muscles.* Respir Physiol, 2000. **119**(2-3): p. 155-61.

56. McClung, J. and S. Goldberg, *Organization of the hypoglossal motoneurons that innervate the horizontal and oblique components of the genioglossus muscle in the rat.* Brain research, 2002. **950**: p. 321-4.

57. McClung, J.R. and S.J. Goldberg, *Organization of motoneurons in the dorsal hypoglossal nucleus that innervate the retrusor muscles of the tongue in the rat.* Anat Rec, 1999. **254**(2): p. 222-30.

58. Aldes, L.D., *Subcompartmental organization of the ventral (protrusor) compartment in the hypoglossal nucleus of the rat.* Journal of Comparative Neurology, 1995. **353**(1): p. 89-108.

59. Sokoloff, A.J. and T.W. Deacon, *Musculotopic organization of the hypoglossal nucleus in the cynomolgus monkey, Macaca fascicularis.* Journal of Comparative Neurology, 1992. **324**(1): p. 81-93.

60. Fregosi, R.F. and D.D. Fuller, *Respiratory-related control of extrinsic tongue muscle activity1Paper presented at the conference on Neural Control of Breathing: Molecular to Organismal Perspectives, Madison, WI, 21–25 July 19961.* Respiration Physiology, 1997. **110**(2): p. 295-306.

61. Jordan, A.S., et al., *Genioglossus muscle activity at rest and in response to brief hypoxia in healthy men and women.* J Appl Physiol (1985), 2002. **92**(1): p. 410-7.

62. Eastwood, P.R., et al., *Heterogeneous activity of the human genioglossus muscle assessed by multiple bipolar fine-wire electrodes.* J Appl Physiol (1985), 2003. **94**(5): p. 1849-58.

63. Fogel, R.B., et al., *Genioglossal activation in patients with obstructive sleep apnea versus control subjects. Mechanisms of muscle control.* Am J Respir Crit Care Med, 2001. **164**(11): p. 2025-30.

64. Bailey, E.F., A.D. Rice, and A.J. Fuglevand, *Firing Patterns of Human Genioglossus Motor Units During Voluntary Tongue Movement.* Journal of Neurophysiology, 2007. **97**(1): p. 933-936.

65. Richardson, P.A. and E.F. Bailey, *Tonically discharging genioglossus motor units show no evidence of rate coding with hypercapnia.* J Neurophysiol, 2010. **103**(3): p. 1315-21.

66. Carberry, J.C., et al., *Upper Airway Collapsibility (Pcrit) and Pharyngeal Dilator Muscle Activity are Sleep Stage Dependent.* Sleep, 2016. **39**(3): p. 511-21.

67. Mateika, J.H., et al., *Response of human tongue protrudor and retractors to hypoxia and hypercapnia.* Am J Respir Crit Care Med, 1999. **160**(6): p. 1976-82.

68. Powell, G.L., et al., *Respiration-related discharge of hyoglossus muscle motor units in the rat.* 2014. **111**(2): p. 361-368.

69. Fregosi, R.F. and D.D. Fuller, *Respiratory-related control of extrinsic tongue muscle activity.* Respir Physiol, 1997. **110**(2-3): p. 295-306.

70. Pittman, L.J. and E.F. Bailey, *Genioglossus and intrinsic electromyographic activities in impeded and unimpeded protrusion tasks.* J Neurophysiol, 2009. **101**(1): p. 276-82.

71. Eisele, D.W., et al., *Direct hypoglossal nerve stimulation in obstructive sleep apnea.* Arch Otolaryngol Head Neck Surg, 1997. **123**(1): p. 57-61.

72. Brennick, M.J., et al., *MRI study of pharyngeal airway changes during stimulation of the hypoglossal nerve branches in rats.* J Appl Physiol (1985), 2001. **90**(4): p. 1373-84.

73. Nicholas, C.L., et al., *Discharge Patterns of Human Tensor Palatini Motor Units During Sleep Onset.* Sleep, 2012. **35**(5): p. 699-707.

74. Launois, S.H., J. Tsui, and J.W. Weiss, *Respiratory function of velopharyngeal constrictor muscles during wakefulness in normal adults.* J Appl Physiol (1985), 1997. **82**(2): p. 584-591.

75. Wiegand, D.A., et al., *Geniohyoid muscle activity in normal men during wakefulness and sleep.* J Appl Physiol (1985), 1990. **69**(4): p. 1262-9.

76. Wiegand, D.A., et al., *Upper airway resistance and geniohyoid muscle activity in normal men during wakefulness and sleep.* J Appl Physiol (1985), 1990. **69**(4): p. 1252-61.

77. Brown, E.C., et al., *Single motor unit recordings in human geniohyoid reveal minimal respiratory activity during quiet breathing.* J Appl Physiol (1985), 2011. **110**(4): p. 1054-9.

78. Kuna, S.T., J.S. Smickley, and C.R. Vanoye, *Respiratory-related pharyngeal constrictor muscle activity in normal human adults.* Am J Respir Crit Care Med, 1997. **155**(6): p. 1991-1999.

79. Palmer, J.B., et al., *Coordination of mastication and swallowing.* Dysphagia, 1992. **7**(4): p. 187-200.

80. Kuna, S.T., *Respiratory-related activation and mechanical effects of the pharyngeal constrictor muscles.* Respir Physiol, 2000. **119**(2): p. 155-161.

81. Hickman, D.L., et al., *Chapter 7 - Commonly Used Animal Models*, in *Principles of Animal Research for Graduate and Undergraduate Students*, M.A. Suckow and K.L. Stewart, Editors. 2017, Academic Press: Boston. p. 117-175.

82. Harkema, J.R., et al., *6 - Nose, Sinus, Pharynx, and Larynx*, in *Comparative Anatomy and Histology*, P.M. Treuting and S.M. Dintzis, Editors. 2012, Academic Press: San Diego. p. 71-94.

83. Laitman, J.T. and J.S. Reidenberg, *Specializations of the human upper respiratory and upper digestive systems as seen through comparative and developmental anatomy.* Dysphagia, 1993. **8**(4): p. 318-325.

84. Aoyagi, H., S.i. Iwasaki, and T.J.S.S. Asami, *Three-Dimensional Architecture of the Mouse Tongue Muscles Using Micro-CT with a Focus on the Transverse, Vertical, and Genioglossus Muscles.* 2015. **6**: p. 358-368.

85. McClung, J.R. and S.J. Goldberg, *Functional anatomy of the hypoglossal innervated muscles of the rat tongue: a model for elongation and protrusion of the mammalian tongue.* Anat Rec, 2000. **260**(4): p. 378-86.

86. Oliven, A., et al., *Effect of coactivation of tongue protrusor and retractor muscles on pharyngeal lumen and airflow in sleep apnea patients.* J Appl Physiol (1985), 2007. **103**(5): p. 1662-8.

87. Horner, R.L., et al., *Effects of sleep-wake state on the genioglossus vs.diaphragm muscle response to CO(2) in rats.* J Appl Physiol (1985), 2002. **92**(2): p. 878-87.

88. LaCross, A., P.J. Watson, and E.F. Bailey, *Association between Laryngeal Airway Aperture and the Discharge Rates of Genioglossus Motor Units.* Front Physiol, 2017. **8**: p. 27.

89. Bamagoos, A.A., et al., *Dose-dependent effects of mandibular advancement on upper airway collapsibility and muscle function in obstructive sleep apnea.* Sleep, 2019. **42**(6).

90. Wellman, A., et al., *A simplified method for determining phenotypic traits in patients with obstructive sleep apnea.* J Appl Physiol (1985), 2013. **114**(7): p. 911-22.

91. Osman, A.M., et al., *Upper airway collapsibility measured using a simple wakefulness test closely relates to the pharyngeal critical closing pressure during sleep in obstructive sleep apnea.* Sleep, 2019. **42**(7).

92. Polotsky, M., et al., *Effects of leptin and obesity on the upper airway function.* Journal of applied physiology (Bethesda, Md. : 1985), 2012. **112**(10): p. 1637-1643.

93. Polotsky, M., et al., *Effect of age and weight on upper airway function in a mouse model.* 2011. **111**(3): p. 696-703.

94. Matsuo, K. and J.B. Palmer, *Coordination of Mastication, Swallowing and Breathing.* Jpn Dent Sci Rev, 2009. **45**(1): p. 31-40.

95. Ma, J., *Dixon techniques for water and fat imaging.* J Magn Reson Imaging, 2008. **28**(3): p. 543-58.

96. McRobbie, D.W., et al., *MRI from Picture to Proton*. 2 ed. 2006, Cambridge: Cambridge University Press.

97. Brennick, M.J., et al., *Tongue fat infiltration in obese versus lean Zucker rats.* Sleep, 2014. **37**(6): p. 1095.

98. Kim, A.M., et al., *Tongue fat and its relationship to obstructive sleep apnea.* Sleep, 2014. **37**(10): p. 1639.

99. Jugé, L., et al., *Effect of upper airway fat on tongue dilation during inspiration in awake people with obstructive sleep apnea.* Sleep, 2021.

100. Brennick, M.J., et al., *Pharyngeal airway wall mechanics using tagged magnetic resonance imaging during medial hypoglossal nerve stimulation in rats.* The Journal of physiology, 2004. **561**(Pt 2): p. 597-610.

101. Zerhouni, E.A., et al., *Human heart: tagging with MR imaging--a method for noninvasive assessment of myocardial motion.* Radiology, 1988. **169**(1): p. 59-63.

102. Axel, L. and L. Dougherty, *MR imaging of motion with spatial modulation of magnetization.* Radiology, 1989. **171**(3): p. 841-5.

103. Brennick, M., et al., *Phasic Respiratory Pharyngeal Mechanics by Magnetic Resonance Imaging in Lean and Obese Zucker Rats.* American Journal of Respiratory and Critical Care Medicine, 2006. **173**(9): p. 1031-7.

104. Brennick, M.J., et al., *Altered Upper Airway and Soft Tissue Structures in the New Zealand Obese Mouse.* Am J Respir Crit Care Med, 2009. **179**(2): p. 158-169.

105. Tong, J., et al., *Respiratory-related displacement of the trachea in obstructive sleep apnea.* J Appl Physiol (1985), 2019. **127**(5): p. 1307-1316.

106. Juge, L., et al., *Regional respiratory movement of the tongue is coordinated during wakefulness and is larger in severe obstructive sleep apnoea.* J Physiol, 2019.

107. Brown, E.C., et al., *Mandibular advancement splint response is associated with the pterygomandibular raphe.* Sleep, 2020. **44**(4).

108. Jugé, L., et al., *The Relationship Between Mandibular Advancement, Tongue Movement, and Treatment Outcome in Obstructive Sleep Apnea.* Sleep, 2022.

109. Jugé, L., et al., *Influence of mandibular advancement on tongue dilatory movement during wakefulness and how this is related to oral appliance therapy outcome for obstructive sleep apnea.* Sleep, 2021. **44**(3).

110. Niitsu, M., et al., *Tongue displacement: visualization with rapid tagged magnetization-prepared MR imaging.* Radiology, 1994. **191**(2): p. 578-80.

111. Stone, M., et al., *Modeling the motion of the internal tongue from tagged cine-MRI images.* J Acoust Soc Am, 2001. **109**(6): p. 2974-82.

112. Kwan, B.C., et al., *A novel ultrasound technique to measure genioglossus movement in vivo.* J Appl Physiol (1985), 2014. **117**(5): p. 556-62.

113. Lee, S.A., et al., *Displacement Imaging for Focused Ultrasound Peripheral Nerve Neuromodulation.* IEEE Trans Med Imaging, 2020. **39**(11): p. 3391-3402.

114. Moran, C.M., et al., *High-resolution echocardiography in the assessment of cardiac physiology and disease in preclinical models.* 2013. **98**(3): p. 629-644.

115. Streatfeild, J., et al., *The social and economic cost of sleep disorders.* Sleep, 2021. **44**(11).

116. Lechat, B., et al., *Multinight Prevalence, Variability, and Diagnostic Misclassification of Obstructive Sleep Apnea.* Am J Respir Crit Care Med, 2022. **205**(5): p. 563-569.

117. Kapur Vishesh, K., et al., *Clinical Practice Guideline for Diagnostic Testing for Adult Obstructive Sleep Apnea: An American Academy of Sleep Medicine Clinical Practice Guideline.* Journal of Clinical Sleep Medicine. **13**(03): p. 479-504.

118. Garbarino, S., et al., *Risk of Occupational Accidents in Workers with Obstructive Sleep Apnea: Systematic Review and Meta-analysis.* Sleep, 2016. **39**(6): p. 1211-8.

119. Peppard, P.E., et al., *Prospective study of the association between sleep-disordered breathing and hypertension.* The New England Journal of Medicine, 2000. **342**(19): p. 1378-1384.

120. Shamsuzzaman, A.S.M., B. Gersh, and V. Somers, *Obstructive sleep apnea - Implications for cardiac and vascular disease.* JAMA-J. Am. Med. Assoc., 2003. **290**(14): p. 1906-1914.

121. Somers, V.K., et al., *Sleep apnea and cardiovascular disease: an American Heart Association/American College of Cardiology Foundation Scientific Statement from the American Heart Association Council for High Blood Pressure Research Professional Education Committee, Council on Clinical Cardiology, Stroke Council, and Council on Cardiovascular Nursing.* J Am Coll Cardiol, 2008. **52**(8): p. 686-717.

122. Peppard, P.E., et al., *Longitudinal association of sleep-related breathing disorder and depression.* Archives of Internal Medicine, 2006. **166**(16): p. 1709-1715.

123. Baldwin, C.M., et al., *The association of sleep-disordered breathing and sleep symptoms with quality of life in the Sleep Heart Health Study.* Sleep, 2001. **24**(1): p. 96.

124. Yaffe, K., et al., *Sleep-disordered breathing, hypoxia, and risk of mild cognitive impairment and dementia in older women.* JAMA, 2011. **306**(6): p. 613.

125. Shi, L., et al., *Sleep disturbances increase the risk of dementia: A systematic review and meta-analysis.* Sleep Med Rev, 2018. **40**: p. 4-16.

126. Young, T., et al., *Sleep disordered breathing and mortality: eighteen-year follow-up of the Wisconsin sleep cohort.* Sleep, 2008. **31**(8): p. 1071-8.

127. Punjabi, N.M., et al., *Sleep-disordered breathing and mortality: a prospective cohort study.* PLoS Med, 2009. **6**(8): p. e1000132.

128. Carberry, J.C., J. Amatoury, and D.J. Eckert, *Personalized Management Approach for OSA.* Chest, 2018. **153**(3): p. 744-755.

129. Segal, Y., A. Malhotra, and G. Pillar, *Upper airway length may be associated with the severity of obstructive sleep apnea syndrome.* International Journal of the Science and Practice of Sleep Medicine, 2008. **12**(4): p. 311-316.

130. Carlisle, T., et al., *Upper airway factors that protect against obstructive sleep apnoea in healthy older males.* The European respiratory journal, 2014. **44**(3): p. 685.

131. Schwab, R., et al., *Identification of upper airway anatomic risk factors for obstructive sleep apnea with volumetric magnetic resonance imaging.* American Journal of Respiratory and Critical Care Medicine, 2003. **168**(5): p. 522-30.

132. Ito, E., et al., *Oropharyngeal Crowding Closely Relates to Aggravation of OSA.* Chest, 2016. **150**(2): p. 346-352.

133. Neelapu, B., et al., *Craniofacial and upper airway morphology in adult obstructive sleep apnea patients: A systematic review and meta-analysis of cephalometric studies.* Sleep Med. Rev., 2017. **31**: p. 79-90.

134. Ho, A.W., D.E. Moul, and J. Krishna, *Neck Circumference-Height Ratio as a Predictor of Sleep Related Breathing Disorder in Children and Adults.* J Clin Sleep Med, 2016. **12**(3): p. 311-7.

135. Caron, C.J.J.M., et al., *Obstructive sleep apnoea in craniofacial microsomia: analysis of 755 patients.* International journal of oral and maxillofacial surgery, 2017. **46**(10): p. 1330.

136. Chi, L., et al., *Identification of craniofacial risk factors for obstructive sleep apnoea using three-dimensional MRI.* 2011. **38**(2): p. 348-358.

137. Sands, S.A., et al., *Enhanced upper-airway muscle responsiveness is a distinct feature of overweight/obese individuals without sleep apnea.* Am J Respir Crit Care Med, 2014. **190**(8): p. 930-7.

138. Cheng, S., et al., *Healthy humans with a narrow upper airway maintain patency during quiet breathing by dilating the airway during inspiration.* J Physiol, 2014. **592**(21): p. 4763-74.

139. Eckert, D. and M. Younes, *Arousal from sleep: implications for obstructive sleep apnea pathogenesis and treatment.* J. Appl. Physiol., 2014. **116**(3): p. 302-313.

140. Eckert, D.J., et al., *Eszopiclone increases the respiratory arousal threshold and lowers the apnoea/hypopnoea index in obstructive sleep apnoea patients with a low arousal threshold.* Clin Sci (Lond), 2011. **120**(12): p. 505-14.

141. Ratnavadivel, R., et al., *Upper airway function and arousability to ventilatory challenge in slow wave versus stage 2 sleep in obstructive sleep apnoea.* Thorax, 2010. **65**(2): p. 107-12.

142. Younes, M., *Role of arousals in the pathogenesis of obstructive sleep apnea.* Am. J. Respir. Crit. Care Med., 2004. **169**(5): p. 623-633.

143. Gray Emma, L., K. McKenzie David, and J. Eckert Danny, *Obstructive Sleep Apnea without Obesity Is Common and Difficult to Treat: Evidence for a Distinct Pathophysiological Phenotype.* Journal of Clinical Sleep Medicine. **13**(01): p. 81-88.

144. Younes, M., et al., *Chemical control stability in patients with obstructive sleep apnea.* American Journal of Respiratory and Critical Care Medicine, 2001. **163**(5): p. 1181-1190.

145. Bratton, D.J., et al., *Comparison of the effects of continuous positive airway pressure and mandibular advancement devices on sleepiness in patients with obstructive sleep apnoea: a network meta-analysis.* The Lancet Respiratory Medicine, 2015. **3**(11): p. 869-878.

146. Weaver, T.E., et al., *Relationship between hours of CPAP use and achieving normal levels of sleepiness and daily functioning.* Sleep, 2007. **30**(6): p. 711-719.

147. Barbé, F., et al., *Long-term effect of continuous positive airway pressure in hypertensive patients with sleep apnea.* Am J Respir Crit Care Med, 2010. **181**(7): p. 718-26.

148. Antic, N.A., et al., *The Effect of CPAP in Normalizing Daytime Sleepiness, Quality of Life, and Neurocognitive Function in Patients with Moderate to Severe OSA.* Sleep, 2011. **34**(1): p. 111-119.

149. Tregear, S., et al., *Obstructive Sleep Apnea and Risk of Motor Vehicle Crash: Systematic Review and Meta-Analysis.* J. Clin. Sleep Med., 2009. **5**(6): p. 573-581.

150. Zimmerman, M.E., et al., *Normalization of Memory Performance and Positive Airway Pressure Adherence in Memory-Impaired Patients With Obstructive Sleep Apnea.* Chest, 2006. **130**(6): p. 1772-1778.

151. Kuhn, E., et al., *Effects of CPAP and Mandibular Advancement Devices on Health-Related Quality of Life in OSA: A Systematic Review and Meta-analysis.* Chest, 2017. **151**(4): p. 786-794.

152. Sutherland, K., et al., *Oral appliance treatment for obstructive sleep apnea: an update.* Journal of clinical sleep medicine : JCSM : official publication of the American Academy of Sleep Medicine, 2014. **10**(2): p. 215-227.

153. Tan, Y.K., et al., *Mandibular advancement splints and continuous positive airway pressure in patients with obstructive sleep apnoea: a randomized crossover trial.* The European Journal of Orthodontics, 2002. **24**(3): p. 239-249.

154. Engleman, H.M., et al., *Randomized crossover trial of two treatments for sleep apnea/hypopnea syndrome: continuous positive airway pressure and mandibular repositioning splint.* Am J Respir Crit Care Med, 2002. **166**(6): p. 855-9.

155. Edwards, B.A., et al., *Upper-Airway Collapsibility and Loop Gain Predict the Response to Oral Appliance Therapy in Patients with Obstructive Sleep Apnea.* Am J Respir Crit Care Med, 2016. **194**(11): p. 1413-1422.

156. Vena, D., et al., *Predicting sleep apnea responses to oral appliance therapy using polysomnographic airflow.* Sleep, 2020. **43**(7).

157. Caples, S.M., et al., *Surgical modifications of the upper airway for obstructive sleep apnea in adults: a systematic review and meta-analysis.* Sleep, 2010. **33**(10): p. 1396-407.

158. Martínez Ruiz de Apodaca, P., et al., *Development of positional obstructive sleep apnea (POSA) after upper airway surgery in OSA patients.* Sleep Breath, 2020. **24**(3): p. 849-856.

159. MacKay, S., et al., *Effect of Multilevel Upper Airway Surgery vs Medical Management on the Apnea-Hypopnea Index and Patient-Reported Daytime Sleepiness Among Patients With Moderate or Severe Obstructive Sleep Apnea: The SAMS Randomized Clinical Trial.* Jama, 2020. **324**(12): p. 1168-1179.

160. Rojo-Sanchis, C., et al., *Impact of Bimaxillary Advancement Surgery on the Upper Airway and on Obstructive Sleep Apnea Syndrome: a Meta-Analysis.* Scientific Reports, 2018. **8**(1): p. 5756.

161. Camacho, M., et al., *The effect of nasal surgery on continuous positive airway pressure device use and therapeutic treatment pressures: a systematic review and meta-analysis.* Sleep, 2015. **38**(2): p. 279-86.

162. Pang, K.P., et al., *Upper airway surgery for obstructive sleep apnea reduces blood pressure.* Laryngoscope, 2018. **128**(2): p. 523-527.

163. Huntley, C., et al., *Comparison of Traditional Upper Airway Surgery and Upper Airway Stimulation for Obstructive Sleep Apnea.* Ann Otol Rhinol Laryngol, 2021. **130**(4): p. 370-376.

164. Joosten, S.A., et al., *Loop Gain Predicts the Response to Upper Airway Surgery in Patients With Obstructive Sleep Apnea.* Sleep, 2017. **40**(7).

165. Wong, A.M., et al., *The impact of upper airway surgery on the pathophysiological traits causing obstructive sleep apnea (OSA).* Sleep Medicine, 2019. **64**: p. S421.

166. Wong, A.M., et al., *Examining the impact of multilevel upper airway surgery on the obstructive sleep apnoea endotypes and their utility in predicting surgical outcomes.* Respirology, 2022.

167. Du, A.L., et al., *Obesity and outcomes in patients undergoing upper airway surgery for obstructive sleep apnea.* PLoS One, 2022. **17**(8): p. e0272331.

168. MacKay, S.G., et al., *Surgical management of obstructive sleep apnoea: A position statement of the Australasian Sleep Association().* Respirology, 2020. **25**(12): p. 1292-1308.

169. FDA, *Inspire® Upper Airway Stimulation – System Implant Manual.* 2020.

170. Strollo, P.J., et al., *Upper-Airway Stimulation for Obstructive Sleep Apnea.* New England Journal of Medicine, 2014. **370**(2): p. 139-149.

171. Woodson, B.T., et al., *Three-Year Outcomes of Cranial Nerve Stimulation for Obstructive Sleep Apnea: The STAR Trial.* Otolaryngol Head Neck Surg, 2016. **154**(1): p. 181-8.

172. Woodson, B.T., et al., *Upper Airway Stimulation for Obstructive Sleep Apnea: 5-Year Outcomes.* Otolaryngol Head Neck Surg, 2018. **159**(1): p. 194-202.

173. Heiser, C., et al., *Bilateral vs Unilateral Hypoglossal Nerve Stimulation in Patients With Obstructive Sleep Apnea.* OTO Open, 2022. **6**(3): p. 2473974x221109794.

174. Lewis, R., et al., *Control of OSA in a patient with CCC of soft palate using bilateral hypoglossal nerve stimulation.* Clin Case Rep, 2021. **9**(4): p. 2222-2224.

175. Bisogni, V., et al., *Electrical stimulation for the treatment of obstructive sleep apnoea: a review of the evidence.* Expert Rev Respir Med, 2017. **11**(9): p. 711-720.

176. Friedman, M., et al., *Targeted hypoglossal nerve stimulation for the treatment of obstructive sleep apnea: Six-month results.* Laryngoscope, 2016. **126**(11): p. 2618-2623.

177. van Bremen, T., et al., *Spot light on skeletal muscles: optogenetic stimulation to understand and restore skeletal muscle function.* J Muscle Res Cell Motil, 2017. **38**(3-4): p. 331-337.

178. Op de Beeck, S., et al., *Endotypic Mechanisms of Successful Hypoglossal Nerve Stimulation for Obstructive Sleep Apnea.* Am J Respir Crit Care Med, 2021. **203**(6): p. 746-755.

179. Taranto-Montemurro, L., et al., *Desipramine increases genioglossus activity and reduces upper airway collapsibility during non-REM sleep in healthy subjects.* Am J Respir Crit Care Med, 2016. **194**(7): p. 878-885.

180. Taranto-Montemurro, L., et al., *Desipramine improves upper airway collapsibility and reduces OSA severity in patients with minimal muscle compensation.* Eur Respir J, 2016. **48**(5): p. 1340-1350.

181. Lim, R., et al., *The noradrenergic agent reboxetine plus the antimuscarinic hyoscine butylbromide reduces sleep apnoea severity: a double-blind, placebo-controlled, randomised crossover trial.* The Journal of physiology, 2021. **599**(17): p. 4183-4195.

182. Perger, E., et al., *Reboxetine Plus Oxybutynin for OSA Treatment: A 1-Week, Randomized, Placebo-Controlled, Double-Blind Crossover Trial.* Chest, 2022. **161**(1): p. 237-247.

183. Altree, T.J., et al., *The norepinephrine reuptake inhibitor reboxetine alone reduces obstructive sleep apnea severity: a double blind, placebo controlled, randomized, cross-over trial.* J Clin Sleep Med, 2022.

184. Taranto-Montemurro, L., et al., *The Combination of Atomoxetine and Oxybutynin Greatly Reduces Obstructive Sleep Apnea Severity. A Randomized, Placebo-controlled, Double-Blind Crossover Trial.* Am J Respir Crit Care Med, 2019. **199**(10): p. 1267-1276.

185. Taranto-Montemurro, L., et al., *Effects of the Combination of Atomoxetine and Oxybutynin on OSA Endotypic Traits.* Chest, 2020. **157**(6): p. 1626-1636.

186. Aishah, A., et al., *Different antimuscarinics when combined with atomoxetine have differential effects on obstructive sleep apnea severity.* J Appl Physiol (1985), 2021. **130**(5): p. 1373-1382.

187. Roth, B.L., *DREADDs for Neuroscientists.* Neuron, 2016. **89**(4): p. 683-694.

188. Horton, G.A., et al., *Activation of the Hypoglossal to Tongue Musculature Motor Pathway by Remote Control.* Sci Rep, 2017. **7**: p. 45860.

189. Horner, R.L., K.P. Grace, and A. Wellman, *A resource of potential drug targets and strategic decision-making for obstructive sleep apnoea pharmacotherapy*. 2017: Chichester, UK. p. 861-873.

190. Daniel, F.M., et al., *The DREADD agonist clozapine N-oxide (CNO) is reverse-metabolized to clozapine and produces clozapine-like interoceptive stimulus effects in rats and mice.* Scientific Reports, 2018. **8**(1): p. 1-10.

191. Gunja, N., *The clinical and forensic toxicology of Z-drugs.* J Med Toxicol, 2013. **9**(2): p. 155-62.

192. Berry, R.B., et al., *Triazolam in patients with obstructive sleep apnea.* Am J Respir Crit Care Med, 1995. **151**(2 Pt 1): p. 450-4.

193. Cirignotta, F., et al., *Zolpidem-polysomnographic study of the effect of a new hypnotic drug in sleep apnea syndrome.* Pharmacology Biochemistry and Behavior, 1988. **29**(4): p. 807-809.

194. Carter, S.G., et al., *Zopiclone Increases the Arousal Threshold without Impairing Genioglossus Activity in Obstructive Sleep Apnea.* Sleep, 2016. **39**(4): p. 757-766.

195. Messineo, L., et al., *Zolpidem increases sleep efficiency and the respiratory arousal threshold without changing sleep apnoea severity and pharyngeal muscle activity.* J Physiol, 2020. **598**(20): p. 4681-4692.

196. Carter, S.G., et al., *Effect of 1 month of zopiclone on obstructive sleep apnoea severity and symptoms: a randomised controlled trial.* 2018. **52**(1): p. 1800149.

197. Carter, S.G., et al., *Randomized Trial on the Effects of High-Dose Zopiclone on OSA Severity, Upper Airway Physiology, and Alertness.* Chest, 2020. **158**(1): p. 374-385.

198. Edwards, B.A., et al., *The Combination of Supplemental Oxygen and a Hypnotic Markedly Improves Obstructive Sleep Apnea in Patients with a Mild to Moderate Upper Airway Collapsibility.* Sleep, 2016. **39**(11): p. 1973-1983.

199. Edwards, B.A., et al., *Acetazolamide improves loop gain but not the other physiological traits causing obstructive sleep apnoea.* J Physiol, 2012. **590**(5): p. 1199-211.

200. Eskandari, D., et al., *Acetazolamide Reduces Blood Pressure and Sleep-Disordered Breathing in Patients With Hypertension and Obstructive Sleep Apnea: A Randomized Controlled Trial.* J Clin Sleep Med, 2018. **14**(3): p. 309-317.

201. Eskandari, D., et al., *Zonisamide reduces obstructive sleep apnoea: a randomised placebo-controlled study.* 2014. **44**(1): p. 140-149.

202. Espinoza, H., et al., *The effects of aminophylline on sleep and sleep-disordered breathing in patients with obstructive sleep apnea syndrome.* Am Rev Respir Dis, 1987. **136**(1): p. 80-4.

203. Messineo, L., et al., *The Combination of Betahistine and Oxybutynin Increases Respiratory Control Sensitivity (Loop Gain) in People with Obstructive Sleep Apnea: A Randomized, Placebo-Controlled Trial.* Nat Sci Sleep, 2022. **14**: p. 1063-1074.

204. Heinzer, R., et al., *Prevalence and characteristics of positional sleep apnea in the HypnoLaus population-based cohort.* Sleep Med, 2018. **48**: p. 157-162.

205. van Maanen, J.P. and N. de Vries, *Long-term effectiveness and compliance of positional therapy with the sleep position trainer in the treatment of positional obstructive sleep apnea syndrome.* Sleep, 2014. **37**(7): p. 1209-15.

206. Zuberi, N.A., K. Rekab, and H.V. Nguyen, *Sleep Apnea Avoidance Pillow Effects on Obstructive Sleep Apnea Syndrome and Snoring.* Sleep and Breathing, 2004. **8**(4): p. 201-207.

207. Permut, I., et al., *Comparison of positional therapy to CPAP in patients with positional obstructive sleep apnea.* J Clin Sleep Med, 2010. **6**(3): p. 238-43.

208. Hudgel, D.W., et al., *The Role of Weight Management in the Treatment of Adult Obstructive Sleep Apnea. An Official American Thoracic Society Clinical Practice Guideline.* Am J Respir Crit Care Med, 2018. **198**(6): p. e70-e87.

209. Mitchell, L.J., et al., *Weight loss from lifestyle interventions and severity of sleep apnoea: a systematic review and meta-analysis.* Sleep Med, 2014. **15**(10): p. 1173-83.

210. Dixon, J.B., et al., *Surgical vs Conventional Therapy for Weight Loss Treatment of Obstructive Sleep Apnea: A Randomized Controlled Trial.* JAMA, 2012. **308**(11): p. 1142-1149.

211. Young, T., P.E. Peppard, and D.J. Gottlieb, *Epidemiology of obstructive sleep apnea: a population health perspective.* Am J Respir Crit Care Med, 2002. **165**(9): p. 1217-39.

212. Wellman, A., et al., *Effect of oxygen in obstructive sleep apnea: role of loop gain.* Respir Physiol Neurobiol, 2008. **162**(2): p. 144-51.

213. Smith, P.L., E.F. Haponik, and E.R. Bleecker, *The effects of oxygen in patients with sleep apnea.* Am Rev Respir Dis, 1984. **130**(6): p. 958-63.

214. Sun, X., J. Luo, and Y. Wang, *Comparing the effects of supplemental oxygen therapy and continuous positive airway pressure on patients with obstructive sleep apnea: a meta-analysis of randomized controlled trials.* Sleep & breathing, 2021. **25**(4): p. 2231-2240.

215. Eckert, D.J. and A. Malhotra, *Pathophysiology of adult obstructive sleep apnea.* Proc Am Thorac Soc, 2008. **5**(2): p. 144-53.

216. Dieltjens, M., et al., *A promising concept of combination therapy for positional obstructive sleep apnea.* Sleep Breath, 2015. **19**(2): p. 637-44.

217. Tong, B.K., et al., *CPAP combined with oral appliance therapy reduces CPAP requirements and pharyngeal pressure swings in obstructive sleep apnea.* J Appl Physiol (1985), 2020. **129**(5): p. 1085-1091.

218. Hendricks, J.C., et al., *The English bulldog: a natural model of sleep-disordered breathing.* J Appl Physiol (1985), 1987. **63**(4): p. 1344-50.

219. Christon, J., et al., *Effects of inspired gas on sleep-related apnea in the rat.* 1996. **80**(6): p. 2102-2107.

220. Hernandez, A.B., et al., *Novel whole body plethysmography system for the continuous characterization of sleep and breathing in a mouse.* J Appl Physiol (1985), 2012. **112**(4): p. 671-80.

221. Sood, S., et al., *Genioglossus muscle activity and serotonergic modulation of hypoglossal motor output in obese Zucker rats.* 2007. **102**(6): p. 2240-2250.

222. Fletcher, E.C., et al., *Repetitive, episodic hypoxia causes diurnal elevation of blood pressure in rats.* Hypertension, 1992. **19**(6): p. 555-561.

223. Polotsky, V.Y., et al., *Intermittent hypoxia causes REM sleep deficits and decreases EEG delta power in NREM sleep in the C57BL/6J mouse.* Sleep Medicine, 2006. **7**(1): p. 7-16.

224. Farré, R., et al., *Collapsible upper airway segment to study the obstructive sleep apnea/hypopnea syndrome in rats.* Respiratory Physiology and Neurobiology, 2003. **136**(2-3): p. 199-209.

225. Iwasaki, Y., et al., *Atrial Fibrillation Promotion With Long-Term Repetitive Obstructive Sleep Apnea in a Rat Model.* J. Am. Coll. Cardiol., 2014. **64**(19): p. 2013-2023.

226. Farré, R., et al., *Rat model of chronic recurrent airway obstructions to study the sleep apnea syndrome.* Sleep, 2007. **30**(7): p. 930.

227. Carreras, A., et al., *Non-invasive system for applying airway obstructions to model obstructive sleep apnea in mice.* Respiratory physiology & neurobiology, 2011. **175**(1): p. 164.

228. Crossland, R.F., et al., *A new rodent model for obstructive sleep apnea: effects on ATP-mediated dilations in cerebral arteries.* American journal of physiology. Regulatory, integrative and comparative physiology, 2013. **305**(4): p. R334.

229. Yoshioka, M., et al., *Pharmacological characterization of 5-hydroxytryptamine-induced apnea in the rat.* Journal of Pharmacology and Experimental Therapeutics, 1992. **260**(2): p. 917.

230. Calik, M.W., M. Radulovacki, and D.W. Carley, *Intranodose ganglion injections of dronabinol attenuate serotonin-induced apnea in Sprague-Dawley rat.* Respiratory physiology & neurobiology, 2014. **190**(1): p. 20.

231. Michael, W.C. and W.C. David, *Cannabinoid type 1 and type 2 receptor antagonists prevent attenuation of serotonin-induced reflex apneas by dronabinol in Sprague-Dawley rats.* PLoS ONE, 2014. **9**(10): p. e111412.

232. Fleury Curado, T.A., et al., *Silencing of Hypoglossal Motoneurons Leads to Sleep Disordered Breathing in Lean Mice.* Front Neurol, 2018. **9**: p. 962.

233. Crick, F., *The Impact of Molecular Biology on Neuroscience.* Philosophical Transactions: Biological Sciences, 1999. **354**(1392): p. 2021-2025.

234. *Method of the Year 2010.* Nature Methods, 2010. **8**: p. 1.

235. Bruegmann, T., et al., *Optogenetic control of contractile function in skeletal muscle.* Nat Commun, 2015. **6**: p. 7153.

236. Guru, A., et al., *Making Sense of Optogenetics.* The international journal of neuropsychopharmacology, 2015. **18**(11): p. pyv079-pyv079.

237. Chang, R.B., *Optogenetic Control of the Peripheral Nervous System.* 2019.

238. Mattis, J., et al., *Principles for applying optogenetic tools derived from direct comparative analysis of microbial opsins.* Nat Methods, 2011. **9**(2): p. 159-72.

239. Delbeke, J., et al., *And Then There Was Light: Perspectives of Optogenetics for Deep Brain Stimulation and Neuromodulation.* 2017. **11**(663).

240. Barnett, S.C., et al., *Optogenetic stimulation: Understanding memory and treating deficits.* Hippocampus, 2018. **28**(7): p. 457-470.

241. Mirzayi, P., et al., *Optogenetics: implications for Alzheimer's disease research and therapy.* Molecular Brain, 2022. **15**(1): p. 20.

242. Magno, L.A.V., et al., *Optogenetic Stimulation of the M2 Cortex Reverts Motor Dysfunction in a Mouse Model of Parkinson's Disease.* J Neurosci, 2019. **39**(17): p. 3234-3248.

243. Kravitz, A.V., et al., *Regulation of parkinsonian motor behaviours by optogenetic control of basal ganglia circuitry.* Nature, 2010. **466**(7306): p. 622-6.

244. Peled, A., *Optogenetic neuronal control in schizophrenia.* Med Hypotheses, 2011. **76**(6): p. 914-21.

245. Liu, S., et al., *Potential Application of Optogenetic Stimulation in the Treatment of Pain and Migraine Headache: A Perspective from Animal Studies.* Brain Sci, 2019. **9**(2).

246. Zhang, H., et al., *Optogenetic activation of 5-HT neurons in the dorsal raphe suppresses seizure-induced respiratory arrest and produces anticonvulsant effect in the DBA/1 mouse SUDEP model.* Neurobiol Dis, 2018. **110**: p. 47-58.

247. Entcheva, E. and M.W. Kay, *Cardiac optogenetics: a decade of enlightenment.* Nat Rev Cardiol, 2021. **18**(5): p. 349-367.

248. Zgierski-Johnston, C.M., et al., *Cardiac pacing using transmural multi-LED probes in channelrhodopsin-expressing mouse hearts.* Prog Biophys Mol Biol, 2020. **154**: p. 51-61.

249. Bruegmann, T., et al., *Optogenetic termination of atrial fibrillation in mice.* Cardiovasc Res, 2018. **114**(5): p. 713-723.

250. Bruegmann, T., et al., *Optogenetic defibrillation terminates ventricular arrhythmia in mouse hearts and human simulations.* J Clin Invest, 2016. **126**(10): p. 3894-3904.

251. Bruegmann, T., et al., *Optogenetic control of heart muscle in vitro and in vivo.* Nature Methods, 2010. **7**: p. 897.

252. Mickle, A.D., et al., *A wireless closed-loop system for optogenetic peripheral neuromodulation.* Nature, 2019. **565**(7739): p. 361-365.

253. Park, J.H., et al., *Optogenetic Modulation of Urinary Bladder Contraction for Lower Urinary Tract Dysfunction.* Sci Rep, 2017. **7**: p. 40872.

254. Magown, P., et al., *Direct optical activation of skeletal muscle fibres efficiently controls muscle contraction and attenuates denervation atrophy.* Nature Communications, 2015. **6**: p. 8506.

255. Benevides, E.S., et al., *Optogenetic activation of the diaphragm.* Scientific Reports, 2022. **12**(1): p. 6503.

256. *Efficacy and Safety of of vMCO-010 Optogenetic Therapy in Adults With Retinitis Pigmentosa RESTORE*. https://ClinicalTrials.gov/show/NCT04945772.

257. *RST-001 Phase I/II Trial for Advanced Retinitis Pigmentosa*. https://ClinicalTrials.gov/show/NCT02556736.

258. *Dose-Escalation Study to Evaluate the Safety and Tolerability of Intravitreal vMCO-I in Patients With Advanced Retinitis Pigmentosa*. https://ClinicalTrials.gov/show/NCT04919473.

259. *Dose-escalation Study to Evaluate the Safety and Tolerability of GS030 in Subjects With Retinitis Pigmentosa*. https://ClinicalTrials.gov/show/NCT03326336.

260. Sahel, J.-A., et al., *Partial recovery of visual function in a blind patient after optogenetic therapy.* Nature Medicine, 2021. **27**(7): p. 1223-1229.

261. Haupts, U., et al., *General concept for ion translocation by halobacterial retinal proteins: the isomerization/switch/transfer (IST) model.* Biochemistry, 1997. **36**(1): p. 2-7.

262. Zhang, F., et al., *The microbial opsin family of optogenetic tools.* Cell, 2011. **147**(7): p. 1446-1457.

263. Nagel, G., et al., *Channelrhodopsin-2, a directly light-gated cation-selective membrane channel.* 2003. **100**(24): p. 13940-13945.

264. Boyden, E.S., et al., *Millisecond-timescale, genetically targeted optical control of neural activity.* Nat Neurosci, 2005. **8**(9): p. 1263-8.

265. Nagel, G., et al., *Light activation of channelrhodopsin-2 in excitable cells of Caenorhabditis elegans triggers rapid behavioral responses.* Curr Biol, 2005. **15**(24): p. 2279-84.

266. Zhao, S., et al., *Improved expression of halorhodopsin for light-induced silencing of neuronal activity.* Brain Cell Biol, 2008. **36**(1-4): p. 141-54.

267. Chen, R., et al., *Deep brain optogenetics without intracranial surgery.* Nature Biotechnology, 2021. **39**(2): p. 161-164.

268. Klapoetke, N.C., et al., *Independent optical excitation of distinct neural populations.* Nature Methods, 2014. **11**: p. 338.

269. Mager, T., et al., *High frequency neural spiking and auditory signaling by ultrafast red-shifted optogenetics.* Nature Communications, 2018. **9**(1): p. 1750.

270. Kishi, K.E., et al., *Structural basis for channel conduction in the pump-like channelrhodopsin ChRmine.* Cell, 2022. **185**(4): p. 672-689.e23.

271. Gong, X., et al., *An Ultra-Sensitive Step-Function Opsin for Minimally Invasive Optogenetic Stimulation in Mice and Macaques.* Neuron, 2020. **107**(1): p. 38-51.e8.

272. Gunaydin, L.A., et al., *Ultrafast optogenetic control.* Nat Neurosci, 2010. **13**(3): p. 387-92.

273. Lin, S., et al., *Locomotor-related V3 interneurons initiate and coordinate muscles spasms after spinal cord injury.* J Neurophysiol, 2019. **121**(4): p. 1352-1367.

274. Maimon, B.E., et al., *Spectrally distinct channelrhodopsins for two-colour optogenetic peripheral nerve stimulation.* Nat Biomed Eng, 2018. **2**(7): p. 485-496.

275. Yizhar, O., et al., *Optogenetics in Neural Systems.* Neuron, 2011. **71**(1): p. 9-34.

276. Acker, L., et al., *FEF inactivation with improved optogenetic methods.* 2016. **113**(46): p. E7297-E7306.

277. Klapoetke, N.C., et al., *Independent optical excitation of distinct neural populations.* Nature methods, 2014. **11**(3): p. 338-346.

278. Lin, J.Y., et al., *ReaChR: a red-shifted variant of channelrhodopsin enables deep transcranial optogenetic excitation.* Nature Neuroscience, 2013. **16**: p. 1499.

279. Maimon, B.E., et al., *Transdermal optogenetic peripheral nerve stimulation.* Journal of Neural Engineering, 2017. **14**(3): p. 034002.

280. Stujenske, J.M., T. Spellman, and J.A. Gordon, *Modeling the Spatiotemporal Dynamics of Light and Heat Propagation for In Vivo Optogenetics.* Cell Rep, 2015. **12**(3): p. 525-34.

281. Kleinlogel, S., et al., *Ultra light-sensitive and fast neuronal activation with the Ca^{2+}-permeable channelrhodopsin CatCh.* Nat Neurosci, 2011. **14**(4): p. 513-8.

282. Bedbrook, C.N., et al., *Machine learning-guided channelrhodopsin engineering enables minimally invasive optogenetics.* Nature Methods, 2019. **16**(11): p. 1176-1184.

283. Fernandez Lahore, R.G., et al., *Calcium-permeable channelrhodopsins for the photocontrol of calcium signalling.* Nat Commun, 2022. **13**(1): p. 7844.

284. Wang, H., et al., *High-speed mapping of synaptic connectivity using photostimulation in Channelrhodopsin-2 transgenic mice.* Proceedings of the National Academy of Sciences, 2007. **104**(19): p. 8143.

285. Marshel, J.H., et al., *Cortical layer-specific critical dynamics triggering perception.* 2019. **365**(6453): p. eaaw5202.

286. Berndt, A., et al., *Bi-stable neural state switches.* Nature Neuroscience, 2009. **12**(2): p. 229-234.

287. Arenkiel, B.R., et al., *In vivo light-induced activation of neural circuitry in transgenic mice expressing channelrhodopsin-2.* Neuron, 2007. **54**(2): p. 205-18.

288. Ting, J.T. and G. Feng, *Development of transgenic animals for optogenetic manipulation of mammalian nervous system function: Progress and prospects for behavioral neuroscience.* Behavioural Brain Research, 2013. **255**: p. 3-18.

289. G, N., et al., *Channelrhodopsins: visual regeneration and neural activation by a light switch.* N Biotechnol, 2013. **30**(5): p. 461-74.

290. Bitzenhofer, S.H., J. Ahlbeck, and I.L. Hanganu-Opatz, *Methodological Approach for Optogenetic Manipulation of Neonatal Neuronal Networks.* Front Cell Neurosci, 2017. **11**: p. 239.

291. Cervia, L.D. and F. Yuan, *Current Progress in Electrotransfection as a Nonviral Method for Gene Delivery.* Molecular Pharmaceutics, 2018. **15**(9): p. 3617-3624.

292. Engelke, L., et al., *Recent insights into cutaneous immunization: How to vaccinate via the skin.* Vaccine, 2015. **33**(37): p. 4663-74.

293. Ita, K., *Perspectives on Transdermal Electroporation.* Pharmaceutics, 2016. **8**(1): p. 9.

294. Mori, K., et al., *Effect of electric field on the enhanced skin permeation of drugs by electroporation.* Journal of Controlled Release, 2003. **90**(2): p. 171-179.

295. Gibot, L. and M.-P. Rols, *Gene transfer by pulsed electric field is highly promising in cutaneous wound healing.* Expert Opinion on Biological Therapy, 2016. **16**(1): p. 67-77.

296. Young, J.L. and D.A. Dean, *Electroporation-mediated gene delivery.* Adv Genet, 2015. **89**: p. 49-88.

297. Wu, M. and F. Yuan, *Membrane binding of plasmid DNA and endocytic pathways are involved in electrotransfection of mammalian cells.* PloS one, 2011. **6**(6): p. e20923-e20923.

298. Chun-Chi, C., W. Mina, and Y. Fan, *Role of specific endocytic pathways in electrotransfection of cells.* Molecular Therapy: Methods & Clinical Development, 2014. **1**(C).

299. Markelc, B., et al., *Inhibitor of endocytosis impairs gene electrotransfer to mouse muscle in vivo.* Bioelectrochemistry, 2015. **103**: p. 111-119.

300. Mir, L.M., *Electroporation-based gene therapy: recent evolution in the mechanism description and technology developments.* Methods Mol Biol, 2014. **1121**: p. 3-23.

301. Esmaeili, N. and M. Friebe, *Electrochemotherapy: A Review of Current Status, Alternative IGP Approaches, and Future Perspectives %J Journal of Healthcare Engineering.* 2019. **2019**: p. 11.

302. Mir, L.M., et al., *Effective treatment of cutaneous and subcutaneous malignant tumours by electrochemotherapy.* British journal of cancer, 1998. **77**(12): p. 2336-2342.

303. Escoffre, J.M. and M.P. Rols, *Electrochemotherapy: progress and prospects.* Curr Pharm Des, 2012. **18**(23): p. 3406-15.

304. Donà, M., et al., *Functional in vivo gene transfer into the myofibers of adult skeletal muscle.* Biochemical and biophysical research communications, 2003. **312**(4): p. 1132.

305. Sokołowska, E. and A.U. Błachnio-Zabielska, *A Critical Review of Electroporation as A Plasmid Delivery System in Mouse Skeletal Muscle.* 2019. **20**(11): p. 2776.

306. Jt, V., et al., *Electrotransfer of naked DNA in the skeletal muscles of animal models of muscular dystrophies.* Gene Therapy, 2001. **8**(14): p. 1097.

307. Hiroyuki, A. and M. Jun-Ichi, *Gene transfer into muscle by electroporation in vivo.* Nature Biotechnology, 1998. **16**(9): p. 867.

308. Murakami, T., et al., *Full-length dystrophin cDNA transfer into skeletal muscle of adult mdx mice by electroporation.* Muscle & Nerve, 2003. **27**(2): p. 237-241.

309. Vilquin, J.T., et al., *Electrotransfer of naked DNA in the skeletal muscles of animal models of muscular dystrophies.* Gene Ther, 2001. **8**(14): p. 1097-107.

310. Durko, M., et al., *CT-GalNAc transferase overexpression in adult mice is associated with extrasynaptic utrophin in skeletal muscle fibres.* J Muscle Res Cell Motil, 2010. **31**(3): p. 181-93.

311. Cervia, L.D., et al., *Distinct effects of endosomal escape and inhibition of endosomal trafficking on gene delivery via electrotransfection.* PLoS One, 2017. **12**(2): p. e0171699.

312. Chang, C.C., et al., *Improvement in Electrotransfection of Cells Using Carbon-Based Electrodes.* Cell Mol Bioeng, 2016. **9**(4): p. 538-545.

313. Lotfinia, M., et al., *Adeno-associated virus as a gene therapy vector: strategies to neutralize the neutralizing antibodies.* Clinical and Experimental Medicine, 2019. **19**(3): p. 289-298.

314. Donate, A., et al., *Thermal Assisted In Vivo Gene Electrotransfer.* Current gene therapy, 2016. **16**(2): p. 83-89.

315. Donate, A., et al., *Application of increased temperature from an exogenous source to enhance gene electrotransfer.* Bioelectrochemistry, 2015. **103**: p. 120-123.

316. Olaiz, N., et al., *Tissue damage modeling in gene electrotransfer: The role of pH.* Bioelectrochemistry, 2014. **100**: p. 105-111.

317. Lyu, C., J. Wang, and B. Rubinsky, *Non-electrolytic microelectroporation.* Biomed Microdevices, 2017. **19**(3): p. 65.

318. Sugibayashi, K., et al., *Electric field analysis on the improved skin concentration of benzoate by electroporation.* International Journal of Pharmaceutics, 2001. **219**(1): p. 107-112.

319. Naso, M.F., et al., *Adeno-Associated Virus (AAV) as a Vector for Gene Therapy.* BioDrugs : clinical immunotherapeutics, biopharmaceuticals and gene therapy, 2017. **31**(4): p. 317-334.

320. Alsaggar, M. and D. Liu, *Physical Methods for Gene Transfer.* Advances in Genetics, 2015. **89**: p. 1-24.

321. Atchison Robert, W., C. Casto Bruce, and D. Hammon William Mc, *Adenovirus-Associated Defective Virus Particles.* Science, 1965. **149**(3685): p. 754-756.

322. Hoggan, M.D., N.R. Blacklow, and W.P. Rowe, *Studies of small DNA viruses found in various adenovirus preparations: physical, biological, and immunological characteristics.* Proc Natl Acad Sci U S A, 1966. **55**(6): p. 1467-74.

323. Kuzmin, D.A., et al., *The clinical landscape for AAV gene therapies.* Nat Rev Drug Discov, 2021. **20**(3): p. 173-174.

324. Dunbar, C.E., et al., *Gene therapy comes of age.* Science, 2018. **359**(6372): p. eaan4672.

325. Brady, J.M., D. Baltimore, and A.B. Balazs, *Antibody gene transfer with adeno-associated viral vectors as a method for HIV prevention.* Immunological Reviews, 2017. **275**(1): p. 324-333.

326. Dismuke, D.J., L. Tenenbaum, and R.J. Samulski, *Biosafety of recombinant adeno-associated virus vectors.* Curr Gene Ther, 2013. **13**(6): p. 434-52.

327. Aguti, S., A. Malerba, and H. Zhou, *The progress of AAV-mediated gene therapy in neuromuscular disorders.* Expert Opin Biol Ther, 2018. **18**(6): p. 681-693.

328. Ramos, J.N., et al., *Development of Novel Micro-dystrophins with Enhanced Functionality.* Molecular Therapy, 2019. **27**(3): p. 623-635.

329. Geisler, A. and H. Fechner, *MicroRNA-regulated viral vectors for gene therapy.* World J Exp Med, 2016. **6**(2): p. 37-54.

330. Wang, B., et al., *Construction and analysis of compact muscle-specific promoters for AAV vectors.* Gene Therapy, 2008. **15**: p. 1489.

331. Chamberlain, J.S., *Gene therapy of muscular dystrophy.* Human Molecular Genetics, 2002. **11**(20): p. 2355-2362.

332. Buchlis, G., et al., *Factor IX expression in skeletal muscle of a severe hemophilia B patient 10 years after AAV-mediated gene transfer.* Blood, 2012. **119**(13): p. 3038-41.

333. Leroy, B.P., et al., *Gene Therapy for Inherited Retinal Disease: Long-Term Durability of Effect.* Ophthalmic Research, 2023: p. 179-196.

334. Hösel, M., et al., *Toll-like receptor 2–mediated innate immune response in human nonparenchymal liver cells toward adeno-associated viral vectors.* Hepatology, 2012. **55**(1): p. 287-297.

335. Maimon, B.E., et al., *Optogenetic Peripheral Nerve Immunogenicity.* Scientific reports, 2018. **8**(1): p. 14076-14076.

336. Hartigan-O'Connor, D., et al., *Immune evasion by muscle-specific gene expression in dystrophic muscle.* Mol Ther, 2001. **4**(6): p. 525-33.

337. Feldman, A.G., et al., *Subacute Liver Failure Following Gene Replacement Therapy for Spinal Muscular Atrophy Type 1.* The Journal of Pediatrics, 2020. **225**: p. 252-258.e1.

338. Au, H.K.E., M. Isalan, and M. Mielcarek, *Gene Therapy Advances: A Meta-Analysis of AAV Usage in Clinical Settings.* Front Med (Lausanne), 2022. **8**: p. 809118.

339. Miraldi Utz, V., et al., *Gene therapy for RPE65-related retinal disease.* Ophthalmic Genet, 2018. **39**(6): p. 671-677.

340. Srivastava, A., *In vivo tissue-tropism of adeno-associated viral vectors.* Current opinion in virology, 2016. **21**: p. 75-80.

341. Wu, Z., A. Asokan, and R.J. Samulski, *Adeno-associated virus serotypes: vector toolkit for human gene therapy.* Mol Ther, 2006. **14**(3): p. 316-27.

342. Zincarelli, C., et al., *Analysis of AAV serotypes 1-9 mediated gene expression and tropism in mice after systemic injection.* Mol Ther, 2008. **16**(6): p. 1073-80.

343. Davidsson, M., et al., *A novel process of viral vector barcoding and library preparation enables high-diversity library generation and recombination-free paired-end sequencing.* Sci Rep, 2016. **6**: p. 37563.

344. Weinmann, J., et al., *Identification of a myotropic AAV by massively parallel in vivo evaluation of barcoded capsid variants.* Nature Communications, 2020. **11**(1): p. 5432.

345. Tabebordbar, M., et al., *Directed evolution of a family of AAV capsid variants enabling potent muscle-directed gene delivery across species.* Cell, 2021. **184**(19): p. 4919-4938.e22.

346. Boutin, S., et al., *Prevalence of serum IgG and neutralizing factors against adeno-associated virus (AAV) types 1, 2, 5, 6, 8, and 9 in the healthy population: implications for gene therapy using AAV vectors.* Human gene therapy, 2010. **21**(6): p. 704.

347. Rapti, K., et al., *Neutralizing antibodies against AAV serotypes 1, 2, 6, and 9 in sera of commonly used animal models.* Mol Ther, 2012. **20**(1): p. 73-83.

348. Leborgne, C., et al., *Prevalence and long-term monitoring of humoral immunity against adeno-associated virus in Duchenne Muscular Dystrophy patients.* Cell Immunol, 2019. **342**: p. 103780.

349. Hinderer, C., et al., *Severe Toxicity in Nonhuman Primates and Piglets Following High-Dose Intravenous Administration of an Adeno-Associated Virus Vector Expressing Human SMN.* Hum Gene Ther, 2018. **29**(3): p. 285-298.

350. Morales, L., et al., *Broader Implications of Progressive Liver Dysfunction and Lethal Sepsis in Two Boys following Systemic High-Dose AAV.* Molecular Therapy, 2020. **28**(8): p. 1753-1755.

351. Narendra, M., et al., *Directed evolution of adeno-associated virus yields enhanced gene delivery vectors.* Nature Biotechnology, 2006. **24**(2): p. 198.

352. Lee, E.J., C.M. Guenther, and J. Suh, *Adeno-Associated Virus (AAV) Vectors: Rational Design Strategies for Capsid Engineering.* Curr Opin Biomed Eng, 2018. **7**: p. 58-63.

353. Wang, D., P.W.L. Tai, and G. Gao, *Adeno-associated virus vector as a platform for gene therapy delivery.* Nature Reviews Drug Discovery, 2019. **18**(5): p. 358-378.

354. El Andari, J., et al., *Semirational bioengineering of AAV vectors with increased potency and specificity for systemic gene therapy of muscle disorders.* 2022. **8**(38): p. eabn4704.

355. Rost, B.R., et al., *Optogenetic Tools for Subcellular Applications in Neuroscience.* Neuron, 2017. **96**(3): p. 572-603.

356. Chamberlain, K., J.M. Riyad, and T. Weber, *Expressing Transgenes That Exceed the Packaging Capacity of Adeno-Associated Virus Capsids.* Human Gene Therapy Methods, 2016. **27**(1): p. 1-12.

357. Baldo, A., et al., *General considerations on the biosafety of virus-derived vectors used in gene therapy and vaccination.* Current gene therapy, 2013. **13**(6): p. 385-394.

358. Duan, D., *Systemic AAV Micro-dystrophin Gene Therapy for Duchenne Muscular Dystrophy.* Molecular Therapy, 2018. **26**(10): p. 2337-2356.

359. Hu, C. and G.S. Lipshutz, *AAV-based neonatal gene therapy for hemophilia A: long-term correction and avoidance of immune responses in mice.* Gene therapy, 2012. **19**(12): p. 1166.

360. Burton, M., et al., *Coexpression of factor VIII heavy and light chain adeno-associated viral vectors produces biologically active protein.* Proceedings of the National Academy of Sciences of the United States of America, 1999. **96**(22): p. 12725-12730.

361. Strings, V., et al., *"Silence and Replace" : Development of a single AAV vector system for the treatment of oculopharyngeal muscular dystrophy (OPMD).* Hum. Gene Ther., 2017. **28**(12): p. A8-A8.

362. Ali, H.G., et al., *Gene therapy for spinal muscular atrophy: the Qatari experience.* Gene Ther, 2021. **28**(10-11): p. 676-680.

363. Salva, M.Z., et al., *Design of tissue-specific regulatory cassettes for high-level rAAV-mediated expression in skeletal and cardiac muscle.* Mol Ther, 2007. **15**(2): p. 320-9.

364. Mendell, J.R., et al., *Assessment of Systemic Delivery of rAAVrh74.MHCK7.micro-dystrophin in Children With Duchenne Muscular Dystrophy: A Nonrandomized Controlled Trial.* JAMA Neurol, 2020. **77**(9): p. 1122-1131.

365. Philippidis, A., *Novartis Confirms Deaths of Two Patients Treated with Gene Therapy Zolgensma.* Hum Gene Ther, 2022. **33**(17-18): p. 842-844.

366. Arruda, V.R., et al., *Lack of germline transmission of vector sequences following systemic administration of recombinant AAV-2 vector in males.* Mol Ther, 2001. **4**(6): p. 586-92.

367. Catherine, S.M., et al., *Successful transduction of liver in hemophilia by AAV-Factor IX and limitations imposed by the host immune response.* Nature Medicine, 2006. **12**(3): p. 342.

368. Greig, J.A., et al., *Intramuscular administration of AAV overcomes pre-existing neutralizing antibodies in rhesus macaques.* Vaccine, 2016. **34**(50): p. 6323.

369. Verdera, H.C., K. Kuranda, and F. Mingozzi, *AAV Vector Immunogenicity in Humans: A Long Journey to Successful Gene Transfer.* Molecular Therapy, 2020. **28**(3): p. 723-746.

370. Kuranda, K., et al., *Exposure to wild-type AAV drives distinct capsid immunity profiles in humans.* The Journal of Clinical Investigation, 2018. **128**(12): p. 5267-5279.

371. Li, N. and Y. Song, *Strategies for Bottlenecks of rAAV-Mediated Expression in Skeletal and Cardiac Muscle of Duchenne Muscular Dystrophy.* Genes (Basel), 2022. **13**(11).

372. Scallan, C.D., et al., *Human immunoglobulin inhibits liver transduction by AAV vectors at low AAV2 neutralizing titers in SCID mice.* Blood, 2006. **107**(5): p. 1810-1817.

373. Jiang, H., et al., *Effects of transient immunosuppression on adenoassociated, virus-mediated, liver-directed gene transfer in rhesus macaques and implications for human gene therapy.* Blood, 2006. **108**(10): p. 3321-3328.

374. Fitzpatrick, Z., et al., *Influence of Pre-existing Anti-capsid Neutralizing and Binding Antibodies on AAV Vector Transduction.* Molecular Therapy - Methods & Clinical Development, 2018. **9**: p. 119-129.

375. Wang, L., et al., *The Pleiotropic Effects of Natural AAV Infections on Liver-directed Gene Transfer in Macaques.* Molecular Therapy, 2010. **18**(1): p. 126-134.

376. Mingozzi, F., et al., *CD8+ T-cell responses to adeno-associated virus capsid in humans.* Nature Medicine, 2007. **13**(4): p. 419-422.

377. Mingozzi, F., et al., *Overcoming preexisting humoral immunity to AAV using capsid decoys.* Sci Transl Med, 2013. **5**(194): p. 194ra92.

378. Lee, G.K., et al., *PEG conjugation moderately protects adeno-associated viral vectors against antibody neutralization.* Biotechnol Bioeng, 2005. **92**(1): p. 24-34.

379. Mok, H., J.W. Park, and T.G. Park, *Microencapsulation of PEGylated adenovirus within PLGA microspheres for enhanced stability and gene transfection efficiency.* Pharm Res, 2007. **24**(12): p. 2263-9.

380. Gyorgy, B., et al., *Naturally enveloped AAV vectors for shielding neutralizing antibodies and robust gene delivery in vivo.* Biomaterials, 2014. **35**(26): p. 7598-609.

381. Gyorgy, B. and C.A. Maguire, *Extracellular vesicles: nature's nanoparticles for improving gene transfer with adeno-associated virus vectors.* Wiley Interdiscip Rev Nanomed Nanobiotechnol, 2018. **10**(3): p. e1488.

382. Monteilhet, V., et al., *A 10 patient case report on the impact of plasmapheresis upon neutralizing factors against adeno-associated virus (AAV) types 1, 2, 6, and 8.* Mol Ther, 2011. **19**(11): p. 2084-91.

383. Mendell, J.R., et al., *Single-Dose Gene-Replacement Therapy for Spinal Muscular Atrophy.* New England Journal of Medicine, 2017. **377**(18): p. 1713-1722.

384. Chirmule, N., et al., *Humoral Immunity to Adeno-Associated Virus Type 2 Vectors following Administration to Murine and Nonhuman Primate Muscle.* J Virol, 2000. **74**(5): p. 2420-2425.

385. Meliani, A., et al., *Antigen-selective modulation of AAV immunogenicity with tolerogenic rapamycin nanoparticles enables successful vector re-administration.* Nat Commun, 2018. **9**(1): p. 4098.

386. Meliani, A., et al., *Antigen-selective modulation of AAV immunogenicity with tolerogenic rapamycin nanoparticles enables successful vector re-administration.* Nature Communications, 2018. **9**(1): p. 4098.

387. Leborgne, C., et al., *IgG-cleaving endopeptidase enables in vivo gene therapy in the presence of anti-AAV neutralizing antibodies.* Nat Med, 2020. **26**(7): p. 1096-1101.

388. Chai, Z., et al., *Optimization of Dexamethasone Administration for Maintaining Global Transduction Efficacy of Adeno-Associated Virus Serotype 9.* Hum Gene Ther, 2019. **30**(7): p. 829-840.

389. Cramer, M.L., et al., *Induction of T-Cell Infiltration and Programmed Death Ligand 2 Expression by Adeno-Associated Virus in Rhesus Macaque Skeletal Muscle and Modulation by Prednisone.* Hum Gene Ther, 2017. **28**(6): p. 493-509.

390. Bowles, D.E., et al., *Phase 1 gene therapy for Duchenne muscular dystrophy using a translational optimized AAV vector.* Mol Ther, 2012. **20**(2): p. 443-55.

391. Tenenbaum, L., E. Lehtonen, and P.E. Monahan, *Evaluation of risks related to the use of adeno-associated virus-based vectors.* Curr Gene Ther, 2003. **3**(6): p. 545-65.

392. Mingozzi, F. and K.A. High, *Therapeutic in vivo gene transfer for genetic disease using AAV: progress and challenges.* Nat Rev Genet, 2011. **12**(5): p. 341-55.

393. Roberto, E. and M.W. James, *Humoral immune response to AAV.* Frontiers in Immunology, 2013. **4**.

394. Doroudchi, M.M., et al., *Virally delivered Channelrhodopsin-2 Safely and Effectively Restores Visual Function in Multiple Mouse Models of Blindness.* Molecular Therapy, 2011. **19**(7): p. 1220-1229.

395. Sugano, E., et al., *Local and systemic responses following intravitreous injection of AAV2-encoded modified Volvox channelrhodopsin-1 in a genetically blind rat model.* Gene Ther, 2016. **23**(2): p. 158-66.

396. Sugano, E., et al., *Immune responses to adeno-associated virus type 2 encoding channelrhodopsin-2 in a genetically blind rat model for gene therapy.* Gene Therapy, 2011. **18**(3): p. 266-274.

397. Simpson, E., *A historical perspective on immunological privilege.* Immunological Reviews, 2006. **213**(1): p. 12-22.

398. Ertl, H.C.J., *T Cell-Mediated Immune Responses to AAV and AAV Vectors.* Front Immunol, 2021. **12**: p. 666666.

399. Lin, J., et al., *Vaccines based on novel adeno-associated virus vectors elicit aberrant CD8+ T-cell responses in mice.* J Virol, 2007. **81**(21): p. 11840-9.

400. Li, H., et al., *Capsid-specific T-cell responses to natural infections with adeno-associated viruses in humans differ from those of nonhuman primates.* Mol Ther, 2011. **19**(11): p. 2021-30.

401. Gaudet, D., et al., *Efficacy and long-term safety of alipogene tiparvovec (AAV1-LPLS447X) gene therapy for lipoprotein lipase deficiency: an open-label trial.* Gene Ther, 2013. **20**(4): p. 361-9.

402. Al-Zaidy, S., et al., *Health outcomes in spinal muscular atrophy type 1 following AVXS-101 gene replacement therapy.* Pediatr Pulmonol, 2019. **54**(2): p. 179-185.

403. Mendell, J.R., et al., *Single-Dose Gene-Replacement Therapy for Spinal Muscular Atrophy.* N Engl J Med, 2017. **377**(18): p. 1713-1722.

404. Powell, S.K., R. Rivera-Soto, and S.J. Gray, *Viral expression cassette elements to enhance transgene target specificity and expression in gene therapy.* Discov Med, 2015. **19**(102): p. 49-57.

405. Husain, T., et al., *Long-term AAV vector gene and protein expression in mouse brain from a small pan-cellular promoter is similar to neural cell promoters.* Gene Therapy, 2009. **16**(7): p. 927-932.

406. Qin, J.Y., et al., *Systematic Comparison of Constitutive Promoters and the Doxycycline-Inducible Promoter.* PLOS ONE, 2010. **5**(5): p. e10611.

407. Xu, L., et al., *CMV-beta-actin promoter directs higher expression from an adeno-associated viral vector in the liver than the cytomegalovirus or elongation factor 1 alpha promoter and results in therapeutic levels of human factor X in mice.* Hum Gene Ther, 2001. **12**(5): p. 563-73.

408. Gray, S.J., et al., *Optimizing promoters for recombinant adeno-associated virus-mediated gene expression in the peripheral and central nervous system using self-complementary vectors.* Hum Gene Ther, 2011. **22**(9): p. 1143-53.

409. Kornegay, J.N., et al., *Widespread muscle expression of an AAV9 human mini-dystrophin vector after intravenous injection in neonatal dystrophin-deficient dogs.* Mol Ther, 2010. **18**(8): p. 1501-8.

410. Lange, A.M., et al., *Overexpression of factor VIII after AAV delivery is transiently associated with cellular stress in hemophilia A mice.* Mol Ther Methods Clin Dev, 2016. **3**: p. 16064.

411. Chandler, R.J., et al., *Vector design influences hepatic genotoxicity after adeno-associated virus gene therapy.* J Clin Invest, 2015. **125**(2): p. 870-80.

412. Xiong, W., et al., *AAV cis-regulatory sequences are correlated with ocular toxicity.* Proc Natl Acad Sci U S A, 2019. **116**(12): p. 5785-5794.

413. Klein, R.L., et al., *Efficient neuronal gene transfer with AAV8 leads to neurotoxic levels of tau or green fluorescent proteins.* Mol Ther, 2006. **13**(3): p. 517-27.

414. Watakabe, A., et al., *Comparative analyses of adeno-associated viral vector serotypes 1, 2, 5, 8 and 9 in marmoset, mouse and macaque cerebral cortex.* Neurosci Res, 2015. **93**: p. 144-57.

415. Gernoux, G., et al., *Early Interaction of Adeno-Associated Virus Serotype 8 Vector with the Host Immune System Following Intramuscular Delivery Results in Weak but Detectable Lymphocyte and Dendritic Cell Transduction.* Human Gene Therapy, 2014. **26**(1): p. 1-13.

416. Takeshita, F., et al., *Muscle creatine kinase/SV40 hybrid promoter for muscle-targeted long-term transgene expression*. Vol. 19. 2007. 309-15.

417. Harms, J.S. and G.A. Splitter, *Interferon-gamma inhibits transgene expression driven by SV40 or CMV promoters but augments expression driven by the mammalian MHC I promoter.* Hum Gene Ther, 1995. **6**(10): p. 1291-7.

418. McCown, T.J., et al., *Differential and persistent expression patterns of CNS gene transfer by an adeno-associated virus (AAV) vector.* Brain Res, 1996. **713**(1-2): p. 99-107.

419. Lee, Y., et al., *GFAP promoter elements required for region-specific and astrocyte-specific expression.* Glia, 2008. **56**(5): p. 481-93.

420. Zheng, C. and B.J. Baum, *Evaluation of promoters for use in tissue-specific gene delivery.* Methods Mol Biol, 2008. **434**: p. 205-19.

421. Hauser, M.A., et al., *Analysis of Muscle Creatine Kinase Regulatory Elements in Recombinant Adenoviral Vectors.* Molecular Therapy, 2000. **2**(1): p. 16-25.

422. Wang, B., et al., *Construction and analysis of compact muscle-specific promoters for AAV vectors.* Gene Ther, 2008. **15**(22): p. 1489-99.

423. Mendell, J.R., et al., *Limb-girdle muscular dystrophy type 2D gene therapy restores alpha-sarcoglycan and associated proteins.* Ann Neurol, 2009. **66**(3): p. 290-7.

424. Müller, O.J., et al., *Improved cardiac gene transfer by transcriptional and transductional targeting of adeno-associated viral vectors.* Cardiovasc Res, 2006. **70**(1): p. 70-8.

425. Burke, R.E., et al., *Physiological types and histochemical profiles in motor units of the cat gastrocnemius.* J Physiol, 1973. **234**(3): p. 723-48.

426. Kandel, E.R., *Principles of neural science*. 5th ed. ed. 2013, New York: New York : McGraw-Hill Medical.

427. Henneman, E., *Relation between size of neurons and their susceptibility to discharge.* Science, 1957. **126**(3287): p. 1345-7.

428. Calderon, J.C., P. Bolanos, and C. Caputo, *The excitation-contraction coupling mechanism in skeletal muscle.* Biophys Rev, 2014. **6**(1): p. 133-160.

429. Mendell, L.M., *The size principle: a rule describing the recruitment of motoneurons.* J Neurophysiol, 2005. **93**(6): p. 3024-6.

430. Llewellyn, M.E., et al., *Orderly recruitment of motor units under optical control in vivo.* Nat Med, 2010. **16**(10): p. 1161-5.

431. Hultman, E., et al., *Evaluation of methods for electrical stimulation of human skeletal muscle in situ.* 2004. **398**: p. 139-141.

432. Hasse, B.A., et al., *Restoration of complex movement in the paralyzed upper limb.* J Neural Eng, 2022. **19**(4).

433. Rowald, A., et al., *Activity-dependent spinal cord neuromodulation rapidly restores trunk and leg motor functions after complete paralysis.* Nat Med, 2022. **28**(2): p. 260-271.

434. Biasiucci, A., et al., *Brain-actuated functional electrical stimulation elicits lasting arm motor recovery after stroke.* Nature Communications, 2018. **9**(1): p. 2421.

435. Ajiboye, A.B., et al., *Restoration of reaching and grasping movements through brain-controlled muscle stimulation in a person with tetraplegia: a proof-of-concept demonstration.* Lancet, 2017. **389**(10081): p. 1821-1830.

436. Currier, D. and R. Mann, *Pain complaint: comparison of electrical stimulation with conventional isometric exercise.* J Orthop Sports Phys Ther, 1984. **5**(6): p. 318-23.

437. Tyler, D.J. and D.M. Durand, *Functionally selective peripheral nerve stimulation with a flat interface nerve electrode.* IEEE Transactions on Neural Systems and Rehabilitation Engineering, 2002. **10**(4): p. 294-303.

438. Gregory, C.M. and C.S. Bickel, *Recruitment patterns in human skeletal muscle during electrical stimulation.* Phys Ther, 2005. **85**(4): p. 358-64.

439. Srinivasan, S.S., et al., *Closed-loop functional optogenetic stimulation.* Nature Communications, 2018. **9**(1): p. 5303.

440. Llewellyn, M.E., et al., *Orderly recruitment of motor units under optical control in vivo.* Nature Medicine, 2010. **16**(10): p. 1161-1165.

441. Mendell, L.M., *The size principle: a rule describing the recruitment of motoneurons.* Journal of Neurophysiology, 2005. **93**(6): p. 3024-3026.

442. Maffiuletti, N.A., *Physiological and methodological considerations for the use of neuromuscular electrical stimulation.* Eur J Appl Physiol, 2010. **110**(2): p. 223-34.

443. Ibáñez, J., et al., *Recruitment order of motor neurons promoted by epidural stimulation in individuals with spinal cord injury.* Journal of Applied Physiology, 2021. **131**(3): p. 1100-1110.

444. Dreibati, B., et al., *Influence of electrical stimulation frequency on skeletal muscle force and fatigue.* Annals of Physical and Rehabilitation Medicine, 2010. **53**(4): p. 266-277.

445. Vromans, M. and P.D. Faghri, *Functional electrical stimulation-induced muscular fatigue: Effect of fiber composition and stimulation frequency on rate of fatigue development.* Journal of Electromyography and Kinesiology, 2018. **38**: p. 67-72.

446. Buckmire, A.J., et al., *Mitigation of excessive fatigue associated with functional electrical stimulation.* Journal of Neural Engineering, 2018. **15**(6): p. 066004.

447. Perez-Medina, A.L. and J.J. Galligan, *Optogenetic analysis of neuromuscular transmission in the colon of ChAT-ChR2-YFP BAC transgenic mice.* Am J Physiol Gastrointest Liver Physiol, 2019. **317**(5): p. G569-G579.

448. Vogt, M., et al., *Direct optogenetic stimulation of smooth muscle cells to control gastric contractility.* Theranostics, 2021. **11**(11): p. 5569-5584.

449. Bruegmann, T., et al., *Optogenetic control of heart muscle in vitro and in vivo.* Nat Methods, 2010. **7**(11): p. 897-900.

450. Rorsman, N.J.G., et al., *Defining the ionic mechanisms of optogenetic control of vascular tone by channelrhodopsin-2.* Br J Pharmacol, 2018. **175**(11): p. 2028-2045.

451. Senova, S., et al., *Experimental assessment of the safety and potential efficacy of high irradiance photostimulation of brain tissues.* Sci Rep, 2017. **7**: p. 43997.

452. Lin, J.Y., et al., *ReaChR: a red-shifted variant of channelrhodopsin enables deep transcranial optogenetic excitation.* Nat Neurosci, 2013. **16**(10): p. 1499-508.

453. Il Park, S., et al., *Stretchable multichannel antennas in soft wireless optoelectronic implants for optogenetics.* Proceedings of the National Academy of Sciences of the United States of America, 2016. **113**(50): p. E8169.

454. Kampasi, K., et al., *Dual color optogenetic control of neural populations using low-noise, multishank optoelectrodes.* Microsystems & Nanoengineering, 2018. **4**(1): p. 10.

455. Aggarwal, J.A., et al., *Measurement and State-Dependent Modulation of Hypoglossal Motor Excitability and Responsivity In-Vivo.* Sci Rep, 2020. **10**(1): p. 550.

456. Towne, C., et al., *Optogenetic Control of Targeted Peripheral Axons in Freely Moving Animals.* PLOS ONE, 2013. **8**(8): p. e72691.

457. Al-Juboori, S.I., et al., *Light scattering properties vary across different regions of the adult mouse brain.* PloS one, 2013. **8**(7): p. e67626-e67626.

458. Gorini, C.J., et al., *Reversible temporally-specific inhibition of muscle using a light-activated chloride channel.* bioRxiv, 2018: p. 398156.

459. Alilain, W.J., et al., *Light-induced rescue of breathing after spinal cord injury.* J Neurosci, 2008. **28**(46): p. 11862-70.

460. Williams, J.J., et al., *Viral-Mediated Optogenetic Stimulation of Peripheral Motor Nerves in Non-human Primates.* 2019. **13**.

461. Lin, J.Y., et al., *Characterization of engineered channelrhodopsin variants with improved properties and kinetics.* Biophysical journal, 2009. **96**(5): p. 1803-1814.

462. Weick, J.P., et al., *Functional Control of Transplantable Human ESC-Derived Neurons Via Optogenetic Targeting.* 2010. **28**(11): p. 2008-2016.

463. Bryson, J.B., et al., *Optical control of muscle function by transplantation of stem cell-derived motor neurons in mice.* Science, 2014. **344**(6179): p. 94-7.

464. Singer, M.L., et al., *Optogenetic activation of the tongue in spontaneously breathing mice.* Respir Physiol Neurobiol, 2023. **309**: p. 103998.

465. Lu, L., et al., *Wireless optoelectronic photometers for monitoring neuronal dynamics in the deep brain.* 2018. **115**(7): p. E1374-E1383.

466. Sridharan, A., S.D. Rajan, and J. Muthuswamy, *Long-term changes in the material properties of brain tissue at the implant-tissue interface.* J Neural Eng, 2013. **10**(6): p. 066001.

467. Gilletti, A. and J. Muthuswamy, *Brain micromotion around implants in the rodent somatosensory cortex.* J Neural Eng, 2006. **3**(3): p. 189-95.

468. McCall, J.G., et al., *Fabrication and application of flexible, multimodal light-emitting devices for wireless optogenetics.* Nat Protoc, 2013. **8**(12): p. 2413-2428.

469. Zhang, Y., et al., *Battery-free, fully implantable optofluidic cuff system for wireless optogenetic and pharmacological neuromodulation of peripheral nerves.* 2019. **5**(7): p. eaaw5296.

470. Khan, W., et al., *Inductively coupled, mm-sized, single channel optical neuro-stimulator with intensity enhancer.* Microsystems & Nanoengineering, 2019. **5**(1): p. 23.

471. Zhang, Y., et al., *Battery-free, lightweight, injectable microsystem for in vivo wireless pharmacology and optogenetics.* 2019. **116**(43): p. 21427-21437.

472. Morikawa, Y., et al. *Highly Stretchable Kirigami Structure with Integrated Led Chips and Electrodes for Optogenetic Experiments on Perfused Hearts*. in *2019 20th International Conference on Solid-State Sensors, Actuators and Microsystems & Eurosensors XXXIII (TRANSDUCERS & EUROSENSORS XXXIII)*. 2019.

473. Kim, D., et al., *Ultraflexible organic light-emitting diodes for optogenetic nerve stimulation.* Proc Natl Acad Sci U S A, 2020. **117**(35): p. 21138-21146.

474. Ji, B., et al., *Flexible and stretchable opto-electric neural interface for low-noise electrocorticogram recordings and neuromodulation in vivo.* Biosensors and Bioelectronics, 2020. **153**: p. 112009.

475. Morikawa, Y., et al., *Donut-Shaped Stretchable Kirigami: Enabling Electronics to Integrate with the Deformable Muscle.* 2019. **8**(23): p. 1900939.

476. Ko, H.C., et al., *Curvilinear Electronics Formed Using Silicon Membrane Circuits and Elastomeric Transfer Elements.* 2009. **5**(23): p. 2703-2709.

477. Song, K.-I., et al., *Compact Optical Nerve Cuff Electrode for Simultaneous Neural Activity Monitoring and Optogenetic Stimulation of Peripheral Nerves.* Scientific Reports, 2018. **8**(1): p. 15630.

478. Berglund, K., et al., *Light-emitting channelrhodopsins for combined optogenetic and chemical-genetic control of neurons.* PLoS One, 2013. **8**(3): p. e59759.

479. Berglund, K., et al., *Step-function luminopsins for bimodal prolonged neuromodulation.* J Neurosci Res, 2020. **98**(3): p. 422-436.

480. Park, S.Y., et al., *Novel luciferase-opsin combinations for improved luminopsins.* J Neurosci Res, 2020. **98**(3): p. 410-421.

481. Wang, Y., et al., *Flexible and fully implantable upconversion device for wireless optogenetic stimulation of the spinal cord in behaving animals.* Nanoscale, 2020. **12**(4): p. 2406-2414.

482. Wu, X., et al., *Sono-optogenetics facilitated by a circulation-delivered rechargeable light source for minimally invasive optogenetics.* Proc Natl Acad Sci U S A, 2019. **116**(52): p. 26332-26342.

483. Chen, Z., et al., *Wireless Optogenetic Modulation of Cortical Neurons Enabled by Radioluminescent Nanoparticles.* ACS Nano, 2021. **15**(3): p. 5201-5208.

484. Sahel, J.A., et al., *Partial recovery of visual function in a blind patient after optogenetic therapy.* Nat Med, 2021. **27**(7): p. 1223-1229.

485. Pisanello, M., et al., *Tailoring light delivery for optogenetics by modal demultiplexing in tapered optical fibers.* Scientific Reports, 2018. **8**(1): p. 4467.

486. Yarmolenko, P.S., et al., *Thresholds for thermal damage to normal tissues: An update.* International Journal of Hyperthermia, 2011. **27**(4): p. 320-343.

487. Goncalves, S.B., et al., *LED Optrode with Integrated Temperature Sensing for Optogenetics.* 2018. **9**(9): p. 473.

488. Xu, L., et al., *3D multifunctional integumentary membranes for spatiotemporal cardiac measurements and stimulation across the entire epicardium.* Nat Commun, 2014. **5**: p. 3329.

489. Srinivasan, S.S., et al., *Closed-loop functional optogenetic stimulation.* Nat Commun, 2018. **9**(1): p. 5303.

490. Won, C.H.J., K.K. Li, and C. Guilleminault, *Surgical Treatment of Obstructive Sleep Apnea.* Proceedings of the American Thoracic Society, 2008. **5**(2): p. 193-199.

491. Wheeler, M.A., et al., *Genetically targeted magnetic control of the nervous system.* Nature Neuroscience, 2016. **19**(5): p. 756-761.

492. Hoy, S.M., *Onasemnogene Abeparvovec: First Global Approval.* Drugs, 2019. **79**(11): p. 1255-1262.

493. Hitoshi, N., Y. Ken-ichi, and M. Jun-ichi, *Efficient selection for high-expression transfectants with a novel eukaryotic vector.* Gene, 1991. **108**(2): p. 193-199.

494. Schoorlemmer, G.H., et al., *A new method to produce obstructive sleep apnoea in conscious unrestrained rats.* Exp Physiol, 2011. **96**(10): p. 1010-8.

495. Eastwood, Peter R., et al., *Collapsibility of the Upper Airway during Anesthesia with Isoflurane.* Anesthesiology, 2002. **97**(4): p. 786-793.

496. Singer, M.L., et al., *Optogenetic activation of the tongue in spontaneously breathing mice.* Respir Physiol Neurobiol, 2022. **309**: p. 103998.

497. Choudhury, S.R., et al., *In Vivo Selection Yields AAV-B1 Capsid for Central Nervous System and Muscle Gene Therapy.* Mol Ther, 2016. **24**(7): p. 1247-57.

498. Brennick, M.J., et al., *Pharyngeal airway wall mechanics using tagged magnetic resonance imaging during medial hypoglossal nerve stimulation in rats.* Journal of Physiology, 2004. **561**(2): p. 597-610.

499. ElMallah, M.K., et al., *Retrograde gene delivery to hypoglossal motoneurons using adeno-associated virus serotype 9.* Hum Gene Ther Methods, 2012. **23**(2): p. 148-56.

500. Elmallah, M.K., et al., *Sustained correction of motoneuron histopathology following intramuscular delivery of AAV in pompe mice.* Mol Ther, 2014. **22**(4): p. 702-12.

501. Vandamme, C., O. Adjali, and F. Mingozzi, *Unraveling the Complex Story of Immune Responses to AAV Vectors Trial After Trial.* 2017. **28**(11): p. 1061-1074.

502. Weeratna, R.D., et al., *Designing gene therapy vectors: avoiding immune responses by using tissue-specific promoters.* Gene Therapy, 2001. **8**(24): p. 1872-1878.

503. Fenno, L., O. Yizhar, and K. Deisseroth, *The Development and Application of Optogenetics.* Annual Review of Neuroscience, 2011. **34**(1): p. 389-412.

504. Jugé, L., et al., *Influence of mandibular advancement on tongue dilatory movement during wakefulness and how this is related to oral appliance therapy outcome for obstructive sleep apnoea.* Sleep, 2020.

505. Chirmule, N., et al., *Immune responses to adenovirus and adeno-associated virus in humans.* Gene Ther, 1999. **6**(9): p. 1574-83.

506. Chan, Y.K., et al., *Engineering adeno-associated viral vectors to evade innate immune and inflammatory responses.* Sci Transl Med, 2021. **13**(580).

507. Verdera, H.C., K. Kuranda, and F. Mingozzi, *AAV Vector Immunogenicity in Humans: A Long Journey to Successful Gene Transfer.* Mol Ther, 2020. **28**(3): p. 723-746.

508. Schmalbruch, H. and D.M. Lewis, *Dynamics of nuclei of muscle fibers and connective tissue cells in normal and denervated rat muscles.* Muscle Nerve, 2000. **23**(4): p. 617-26.

509. Brooks, A.R., et al., *Transcriptional silencing is associated with extensive methylation of the CMV promoter following adenoviral gene delivery to muscle.* J Gene Med, 2004. **6**(4): p. 395-404.

510. Muhuri, M., et al., *Durability of transgene expression after rAAV gene therapy.* Molecular Therapy, 2022. **30**(4): p. 1364-1380.

511. Goździewska-Harłajczuk, K., et al., *Biological aspects of the tongue morphology of wild-captive WWCPS rats: a histological, histochemical and ultrastructural study.* Anatomical Science International, 2018. **93**(4): p. 514-532.

512. Xue, J.-H. and D.M. Titterington, *Median-based image thresholding.* Image and Vision Computing, 2011. **29**(9): p. 631-637.

513. Cao, Y., et al., *Flexible and stretchable polymer optical fibers for chronic brain and vagus nerve optogenetic stimulations in free-behaving animals.* BMC Biol, 2021. **19**(1): p. 252.

514. Spencer, N.J., et al., *Optogenetic control of the enteric nervous system and gastrointestinal transit.* Expert Rev Gastroenterol Hepatol, 2019. **13**(4): p. 281-284.

515. Morrison, J.L., et al., *GABAA receptor antagonism at the hypoglossal motor nucleus increases genioglossus muscle activity in NREM but not REM sleep.* J Physiol, 2003. **548**(Pt 2): p. 569-83.

516. Kim, C.Y., et al., *Soft subdermal implant capable of wireless battery charging and programmable controls for applications in optogenetics.* Nature Communications, 2021. **12**(1): p. 535.

517. Sparta, D.R., et al., *Construction of implantable optical fibers for long-term optogenetic manipulation of neural circuits.* Nature Protocols, 2012. **7**(1): p. 12-23.

518. Roda, F., et al., *Effects of anesthetics on hypoglossal nerve discharge and c-fos expression in brainstem hypoglossal premotor neurons.* 2004. **468**(4): p. 571-586.

519. European Medicines Agency, *Guideline on the non-clinical studies required before first clinical use of gene therapy medicinal products*. 2008.

520. FDA, *Guidance for industry - Preclinical assessment of investigational cellular and gene therapy products.* 2019.

521. Karathanos, T.V., et al., *Opsin spectral sensitivity determines the effectiveness of optogenetic termination of ventricular fibrillation in the human heart: a simulation study.* 2016. **594**(23): p. 6879-6891.

522. Mingozzi, F., et al., *Induction of immune tolerance to coagulation factor IX antigen by in vivo hepatic gene transfer.* The Journal of Clinical Investigation, 2003. **111**(9): p. 1347-1356.

523. Keeler, G.D., D.M. Markusic, and B.E. Hoffman, *Liver induced transgene tolerance with AAV vectors.* Cell Immunol, 2019. **342**: p. 103728.

524. Mendell, J.R., et al., *Gene Delivery for Limb-Girdle Muscular Dystrophy Type 2D by Isolated Limb Infusion.* Hum Gene Ther, 2019. **30**(7): p. 794-801.

525. Sahenk, Z., et al., *Systemic delivery of AAVrh74.tMCK.hCAPN3 rescues the phenotype in a mouse model for LGMD2A/R1.* Mol Ther Methods Clin Dev, 2021. **22**: p. 401-414.

526. Mendell, J.R., et al., *Dystrophin immunity in Duchenne's muscular dystrophy.* N Engl J Med, 2010. **363**(15): p. 1429-37.

527. Poupiot, J., et al., *Role of Regulatory T Cell and Effector T Cell Exhaustion in Liver-Mediated Transgene Tolerance in Muscle.* Molecular Therapy - Methods & Clinical Development, 2019. **15**: p. 83-100.

528. Vanderveken, O.M., et al., *Evaluation of Drug-Induced Sleep Endoscopy as a Patient Selection Tool for Implanted Upper Airway Stimulation for Obstructive Sleep Apnea.* 2013. **09**(05): p. 433-438.

529. Ebberink, E.H.T.M., et al., *Assessing production variability in empty and filled adeno-associated viruses by single molecule mass analyses.* Molecular Therapy - Methods & Clinical Development, 2022. **27**: p. 491-501.

530. O'Connor, D.M., et al., *Lot-to-Lot Variation in Adeno-Associated Virus Serotype 9 (AAV9) Preparations.* Hum Gene Ther Methods, 2019. **30**(6): p. 214-225.

531. Gao, K., et al., *Empty Virions In AAV8 Vector Preparations Reduce Transduction Efficiency And May Cause Total Viral Particle Dose-Limiting Side-Effects.* Mol Ther Methods Clin Dev, 2014. **1**(9): p. 20139.

532. Schnödt, M. and H. Büning, *Improving the Quality of Adeno-Associated Viral Vector Preparations: The Challenge of Product-Related Impurities.* Human Gene Therapy Methods, 2017. **28**(3): p. 101-108.

533. Wright, J.F., et al., *Identification of factors that contribute to recombinant AAV2 particle aggregation and methods to prevent its occurrence during vector purification and formulation.* Molecular Therapy, 2005. **12**(1): p. 171-178.

534. Wright, J.F., *Product-Related Impurities in Clinical-Grade Recombinant AAV Vectors: Characterization and Risk Assessment.* Biomedicines, 2014. **2**(1): p. 80-97.

535. Tenenbaum, L., et al., *Cellular contaminants of adeno-associated virus vector stocks can enhance transduction.* Gene Therapy, 1999. **6**(6): p. 1045-1053.

536. Klein, R.L., et al., *AAV8, 9, Rh10, Rh43 vector gene transfer in the rat brain: effects of serotype, promoter and purification method.* Mol Ther, 2008. **16**(1): p. 89-96.

537. Strobel, B., et al., *Comparative Analysis of Cesium Chloride- and Iodixanol-Based Purification of Recombinant Adeno-Associated Viral Vectors for Preclinical Applications.* Hum Gene Ther Methods, 2015. **26**(4): p. 147-57.

538. Srivastava, A., et al., *Manufacturing Challenges and Rational Formulation Development for AAV Viral Vectors.* Journal of Pharmaceutical Sciences, 2021. **110**(7): p. 2609-2624.

539. Sender, R. and R. Milo, *The distribution of cellular turnover in the human body.* Nature Medicine, 2021. **27**(1): p. 45-48.

540. Mead, T.J. and V. Lefebvre, *Proliferation assays (BrdU and EdU) on skeletal tissue sections.* Methods Mol Biol, 2014. **1130**: p. 233-243.

APPENDICES

CHAPTER 2 OPTIMISING THE VIRAL CONSTRUCT: PROMOTERS

METHODS

Pilot studies

Three vectors were obtained from the AddGene Plasmid Repository; AAV9-CAG-ChR2(H134R)-mCherry (3.3×10^{13} GC/mL, donated to the repository by Karl Deisseroth's lab, Addgene viral prep #100054-AAV9; http://n2t.net/179ncorpo:100054; RRID: Addgene_100054), AAV2-CAG-ChR2(H134R)-eGFP (1.1×10^{13} GC/mL, donated to the repository by Karl Deisseroth's lab, Addgene viral prep #100054-AAV2; http://n2t.net/179ncorpo:100054; RRID: Addgene_100054) and a 'non-functional' vector AAV9-tMCK-eGFP (3.1×10^{13} GC/mL, donated to the repository by James M. Wilson (Addgene viral prep # 105556-AAV9; http://n2t.net/addgene:105556; RRID:Addgene_105556) that induces reporter protein expression only. The first cohort of SD rats, received one of the two 'functional' CAG vectors (AAV2-CAG-ChR2(H134R)-eGFP or AAV9-CAG-ChR2(H134R)-mCherry) via bilateral intramuscular injections to the tongue. The second cohort received four intramuscular injections as outlined in the primary methods. These animals received AAV9-CAG-ChR2(H134R)-mCherry or AAV9-tMCK-eGFP.

DNA/RNA extraction

Primer sequences

Gene target	Forward sequence 5' to 3'	Reverse sequence 5' to 3'
ChR2	AGA GTG GCT GCT CAC TTG TC	GCG CCA TAG CAC AAT CCA AG
RPL13	CAT CGT GAG GTG CCC TAC AG	GCC GAG AAA GCT CGT AGT CA
YWHAZ	CCC ACT CCG GAC ACA GAA TA	TGT CAT CGT ATC GCT CTG CC

Thermal cycling protocols

- ChR2: 50°C 2 minutes, 95°C 10 minutes, [95°C 15 seconds, 60°C 1 minute) × 40 cycles, 95°C 15 seconds, 60°C 1 minute, 95°C 15 seconds
- RPL13 and YWHAZ: 50°C 2 minutes, 95°C 10 minutes, [95°C 15 seconds, 59°C 15 seconds, 72°C 1 minute] × 40 cycles, 95°C 15 seconds, 60°C 1 minute, 95°C 15 seconds

FIGURES

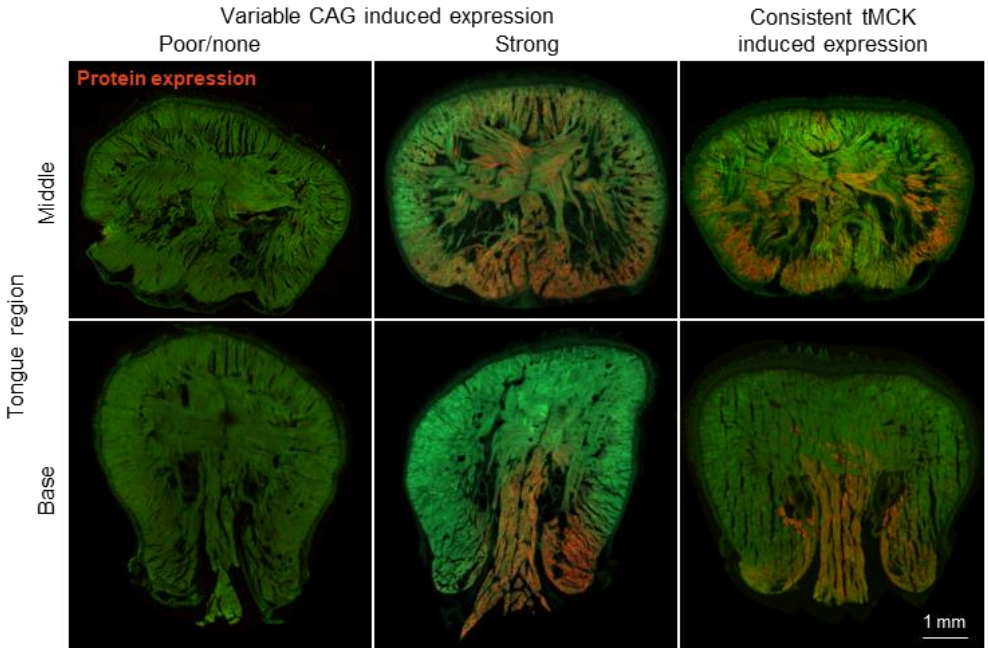

Fig. A2-1. Histology results during pilot studies. The CAG driven vector (AAV9-CAG-ChR2(H134R)-mCherry) drove highly variable levels of expression ranging from absolutely no expression to strong opsin-reporter fusion protein expression and subsequently strong light induced EMG responses. Conversely, a non-functional tMCK driven vector (AAV9-tMCK-eGFP) consistently drove strong expression in all animals, equivalent to the best CAG induced response.

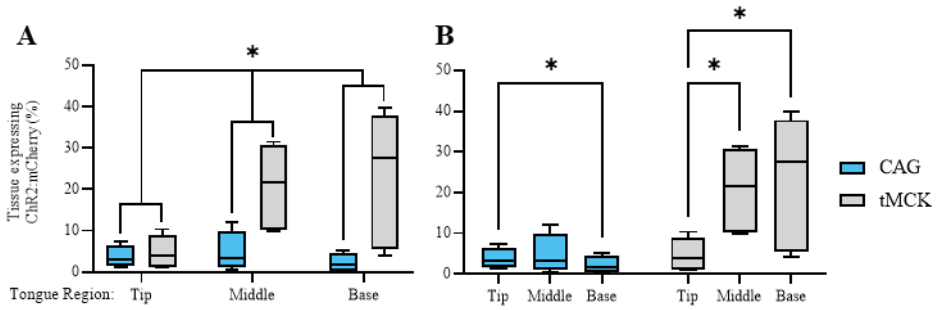

Fig. A2-2. Regional differences of opsin expression within the tongue. (A) Opsin expression varies across the three regions of the tongue ($F(1.563, 12.51) = 4.81$, $p = 0.048$) and this variation is dependent on the promoter employed ($F(2,16) = 4.719$, $p = 0.025$). **(B)** The tMCK construct (grey, $n = 6$) induced the most expression in the middle and base regions of the tongue, i.e. the regions where the vector was injected, indicating that intramuscular injections of the tMCK construct induced very localised skeletal muscle expression (Bonferroni post hoc, tip vs middle, $p = 0.038$; tip vs base, $p = 0.041$). Conversely, the CAG construct (blue, $n = 4$) did not seem to induce sufficient expression to discriminate between tongue regions. The only significant difference was a 0.58-fold difference between the tip and the base region (Bonferroni post hoc, $p = 0.021$).

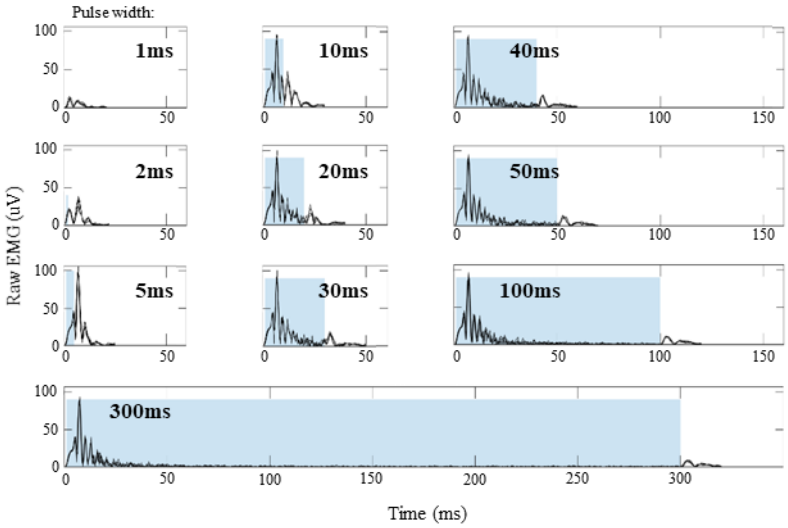

Fig. A2-3. Raw genioglossus EMG activity induced by single light pulses. Pulse durations increase from 1 ms to 300 ms (n = 1), indicated with blue shading.

VIDEOS

Video A2-1: Light-induced visible tongue contractions in rodent model of pharyngeal dilator muscle atonia. Higher levels of isoflurane suppress endogenous phasic inspiratory drive and tongue movements. Pulsed blue light restores tongue contractions and movement. Breathing is indicated by the flashing red asterisks.

FIGURES

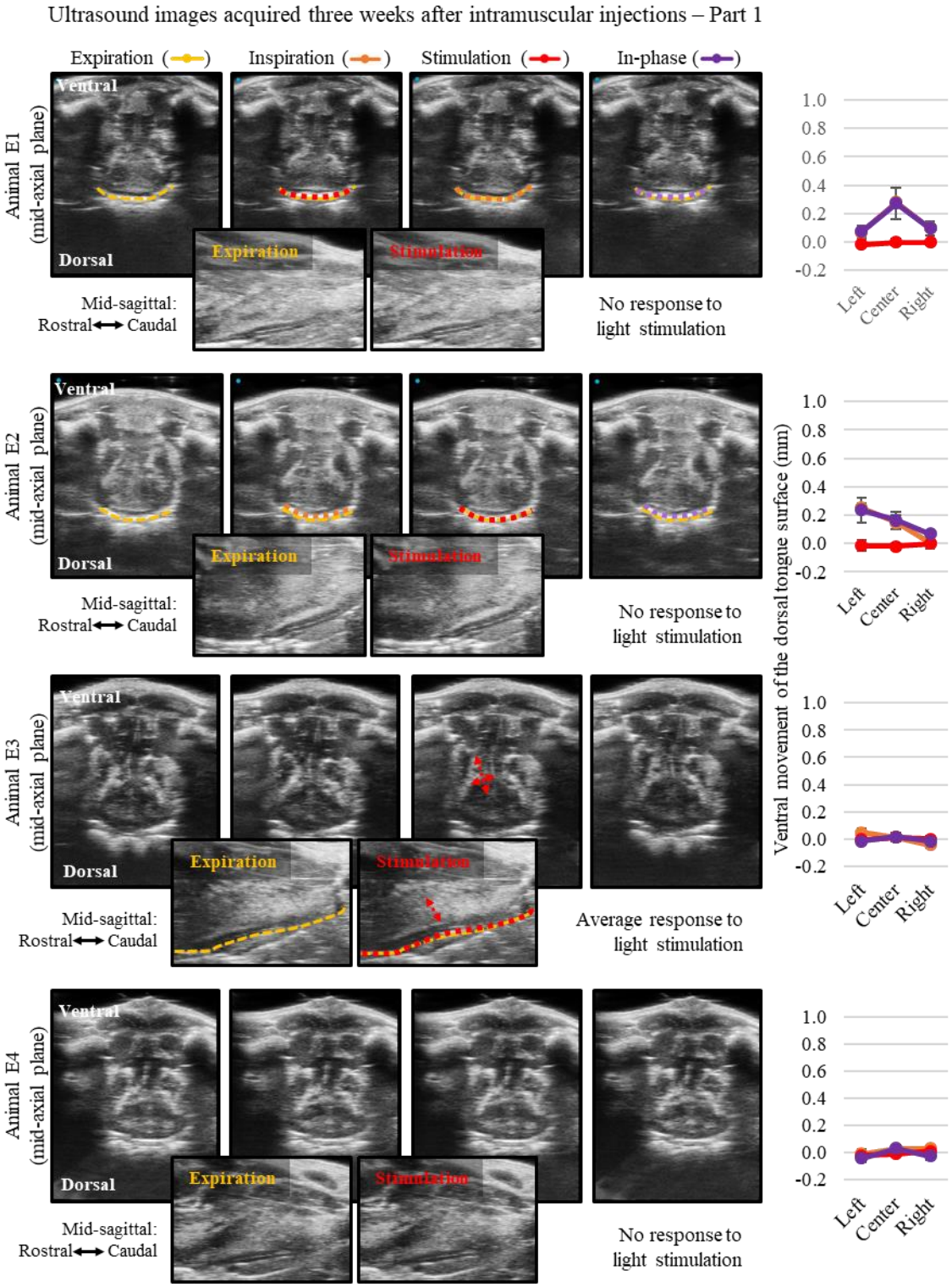
Ultrasound images acquired three weeks after intramuscular injections – Part 1
Expiration
Inspiration
Stimulation
In-phase
Animal E1 (mid-axial plane)
Animal E2 (mid-axial plane)
Animal E3 (mid-axial plane)
Animal E4 (mid-axial plane)
Ventral
Dorsal
Mid-sagittal: Rostral Caudal
No response to light stimulation
Average response to light stimulation
Ventral movement of the dorsal tongue surface (mm)
1.0
0.8
0.6
0.4
0.2
0.0
-0.2
Left
Center
Right

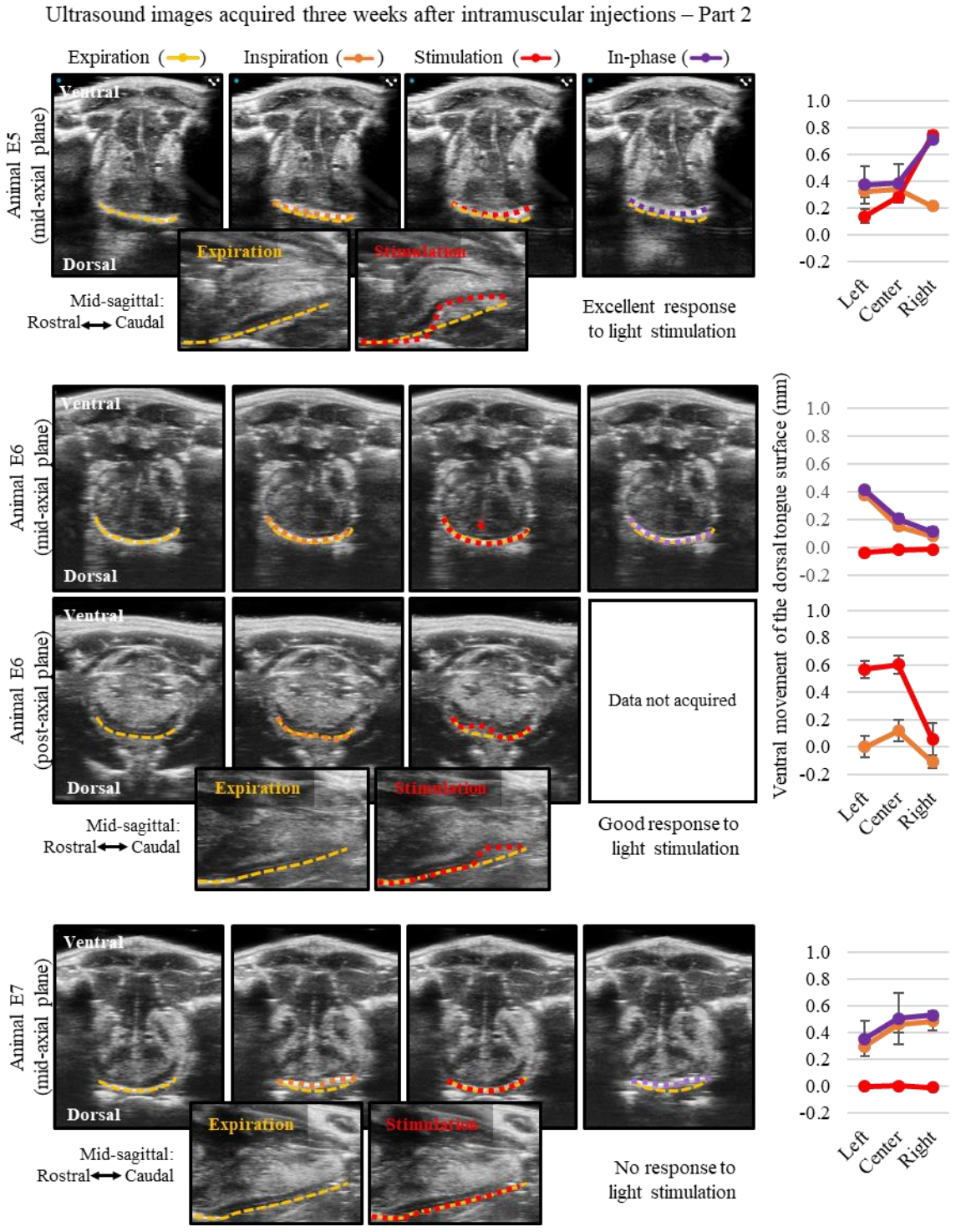
Ultrasound images acquired three weeks after intramuscular injections – Part 2
Expiration
Inspiration
Stimulation
In-phase
Animal E5 (mid-axial plane)
Ventral
Dorsal
Expiration
Stimulation
Mid-sagittal: Rostral Caudal
Excellent response to light stimulation
Animal E6 (mid-axial plane)
Animal E6 (post-axial plane)
Data not acquired
Good response to light stimulation
Animal E7 (mid-axial plane)
No response to light stimulation
Ventral movement of the dorsal tongue surface (mm)
1.0
0.8
0.6
0.4
0.2
0.0
-0.2
Left
Center
Right

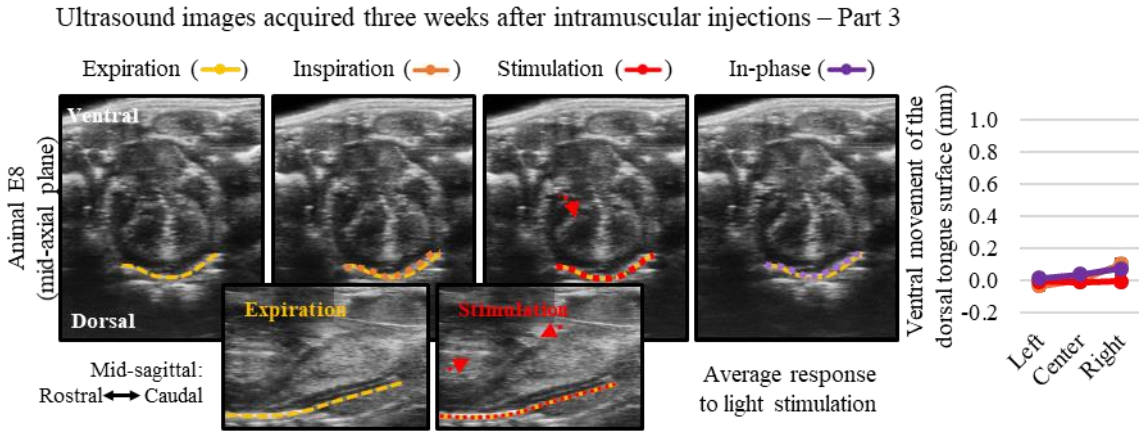

Figure A4-1 | Three weeks after viral vector administration, ultrasound imaging was conducted on 8 animals. Two animals (E5 and E6) displayed light-evoked airway dilation, two animals (E3 and E7) displayed light-evoked muscle contractions (but not airway dilation), and four animals displayed no response to light stimulation. The position of the tongue's dorsal surface during expiration (yellow dashed lines), inspiration (i.e. no stimulation, orange dashed lines), stimulation only (red dashed lines), and 'in-phase' stimulation (i.e. stimulation and inspiration, purple dashed lines) are indicated. In the graphs on the right, each data set represents the ventral movement of the dorsal surface during inspiration (orange), stimulation (red), and 'in-phase' stimulation (purple).

Longitudinal data: Animal ID – E3, Part 1

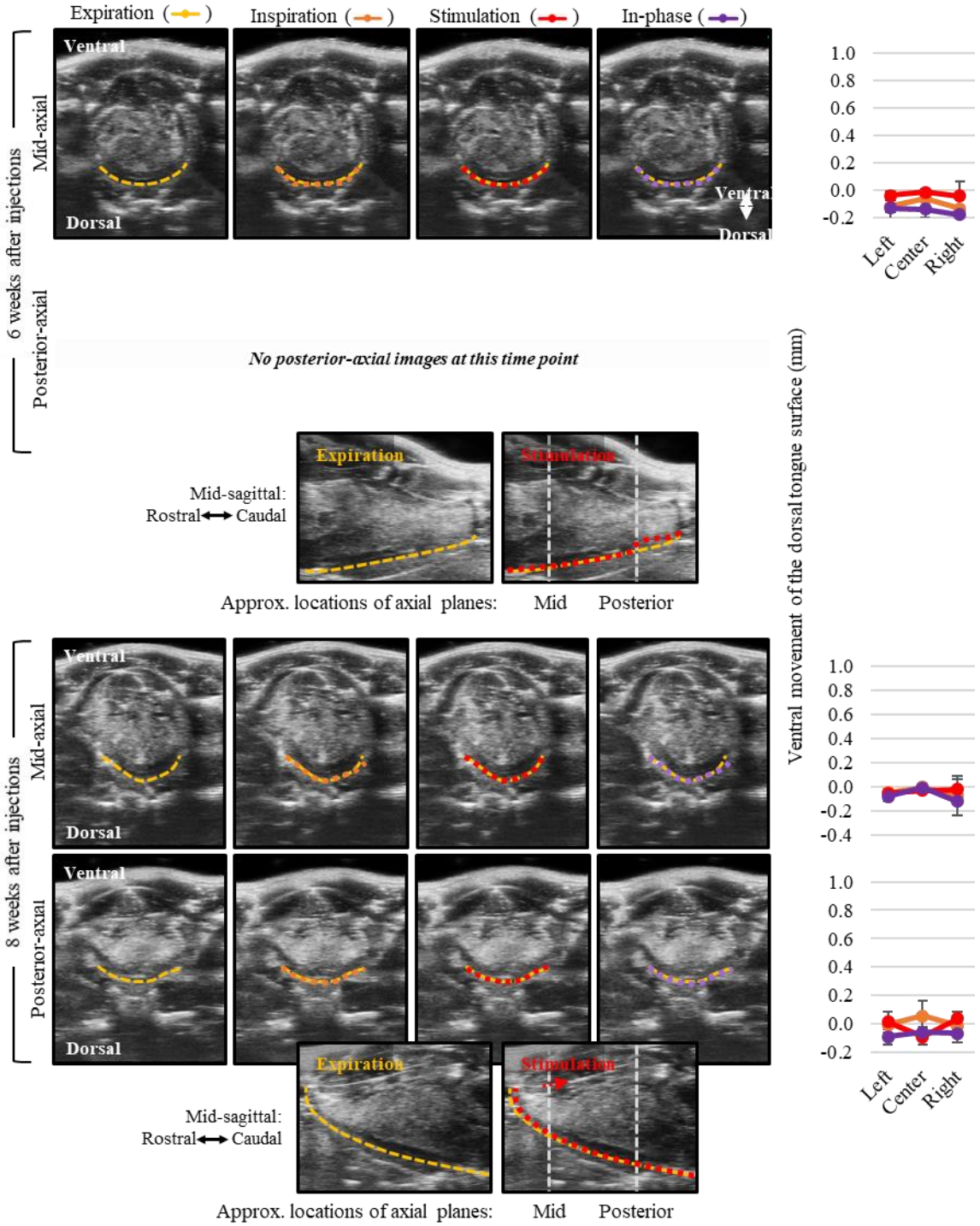

Longitudinal data: Animal ID – E3, Part 2

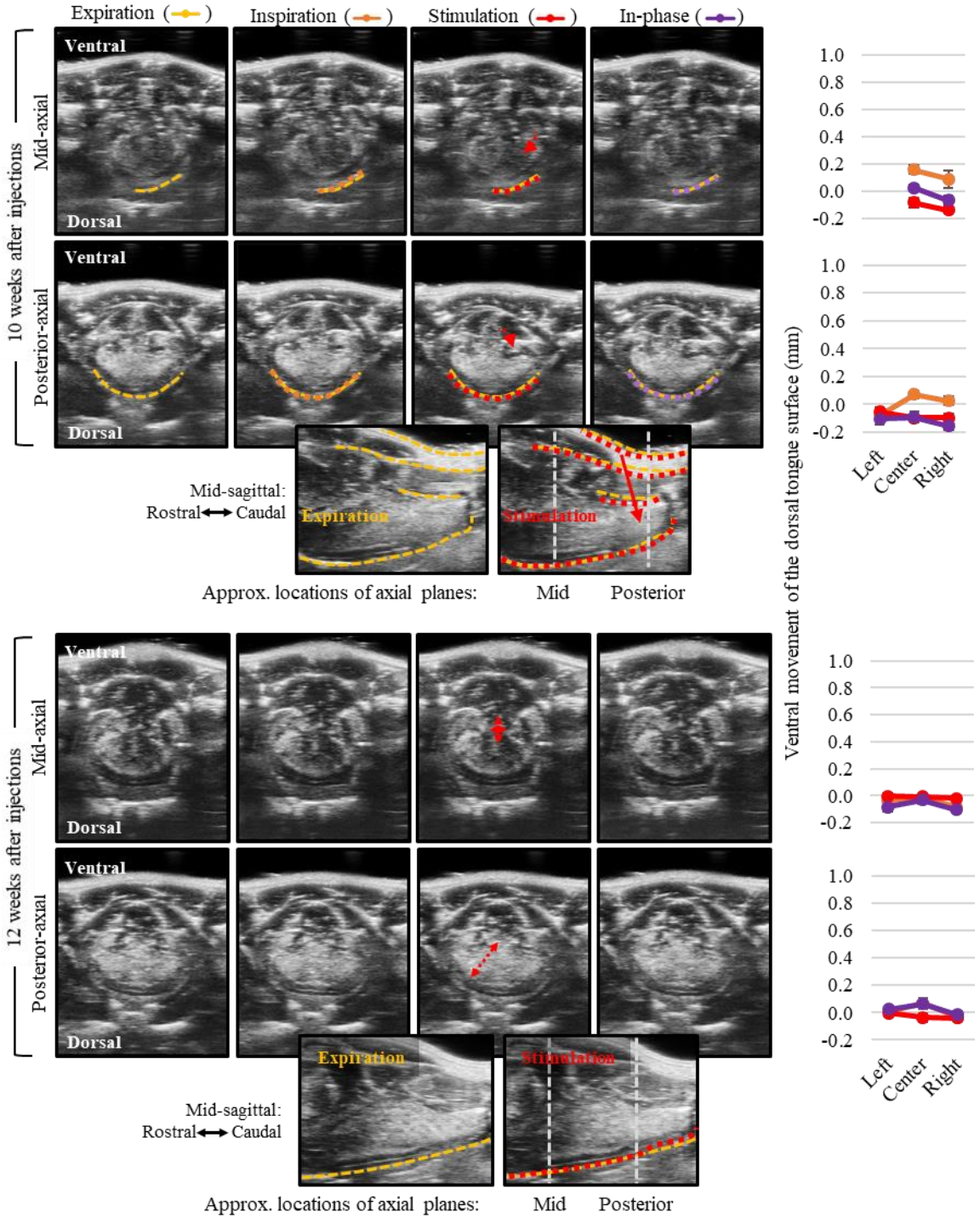

Longitudinal data: Animal ID – E5, Part 1

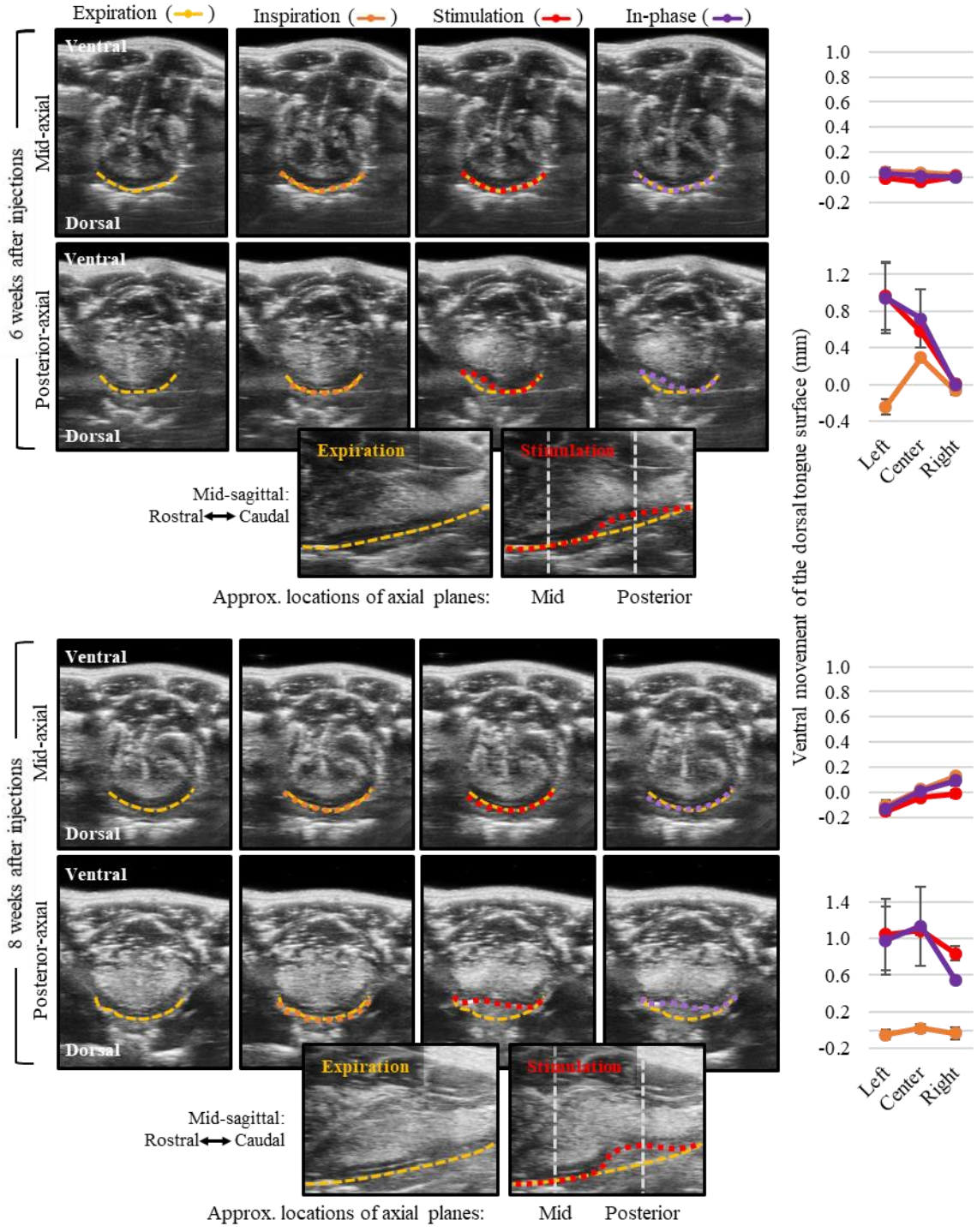

Longitudinal data: Animal ID – E5, Part 2

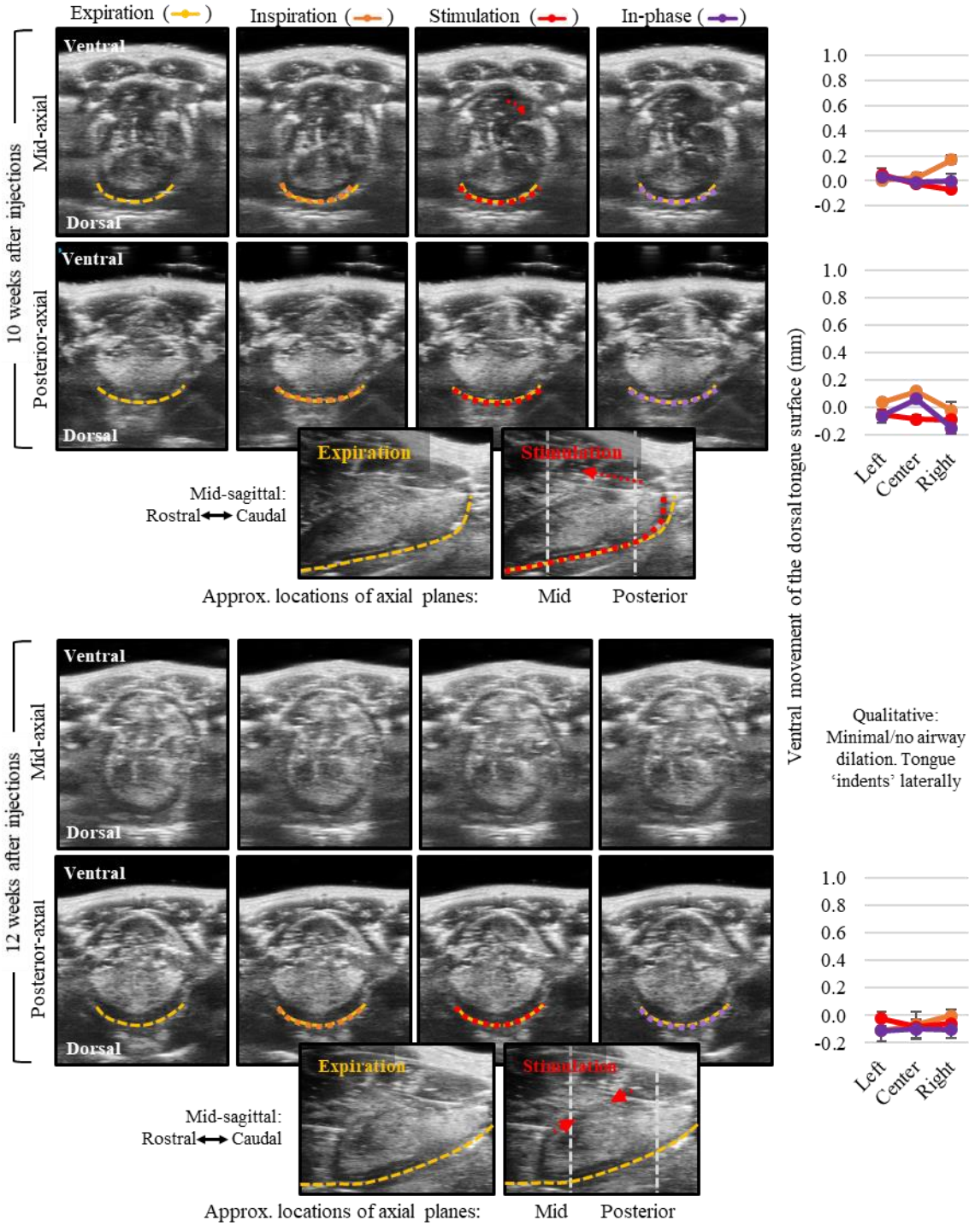

Longitudinal data: Animal ID – E6, Part 1

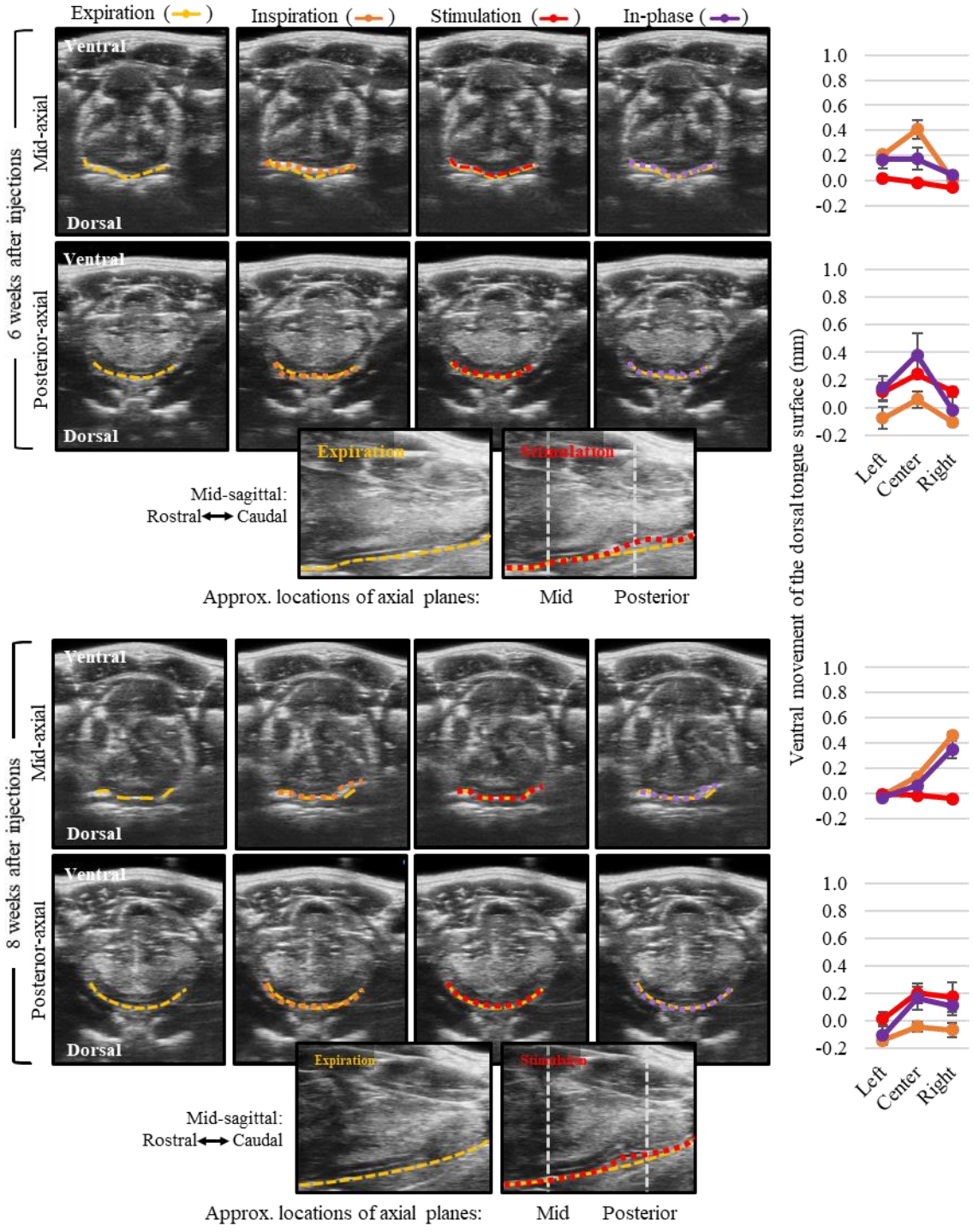

Longitudinal data: Animal ID – E6, Part 2

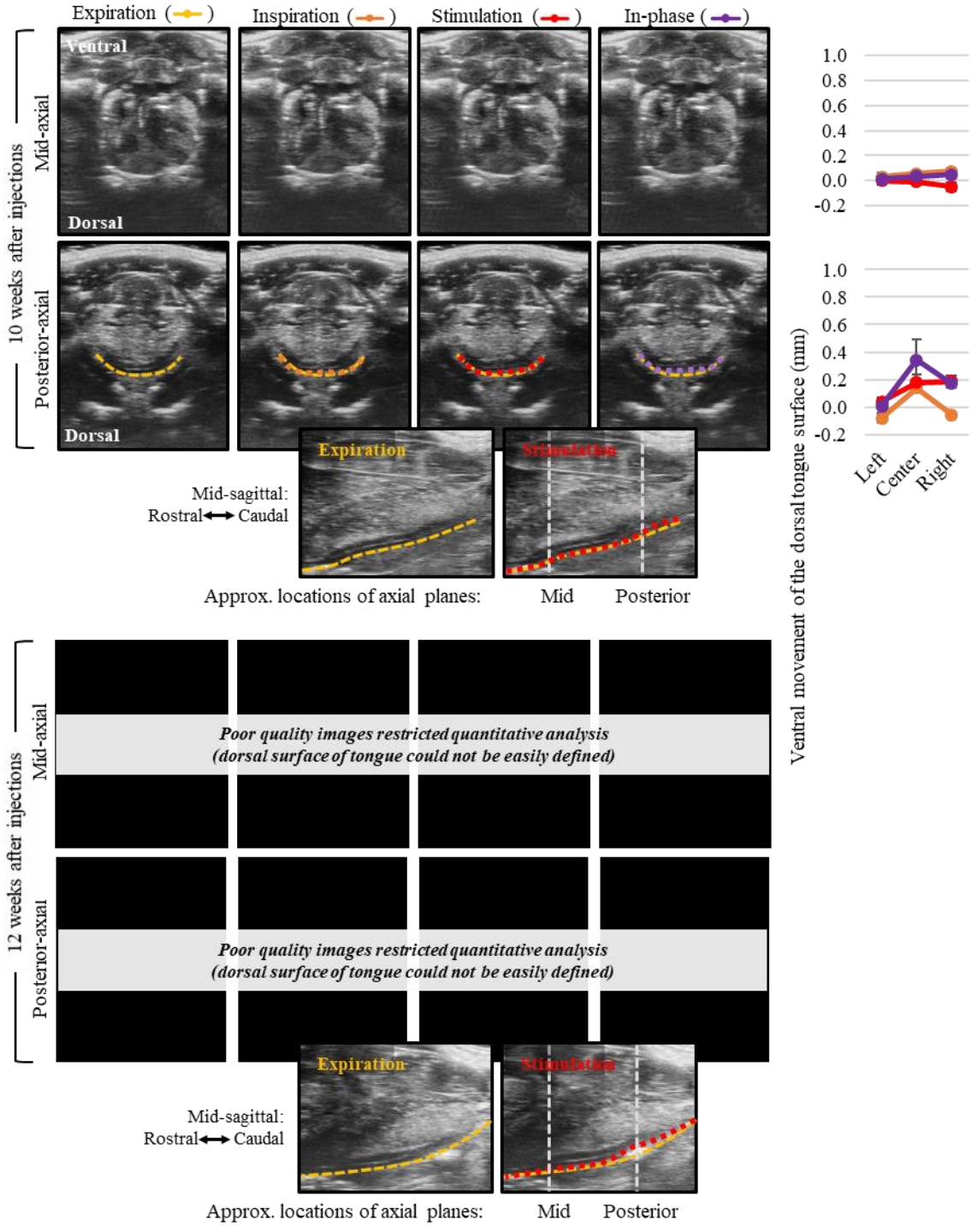

Longitudinal data: Animal ID – E8, Part 1

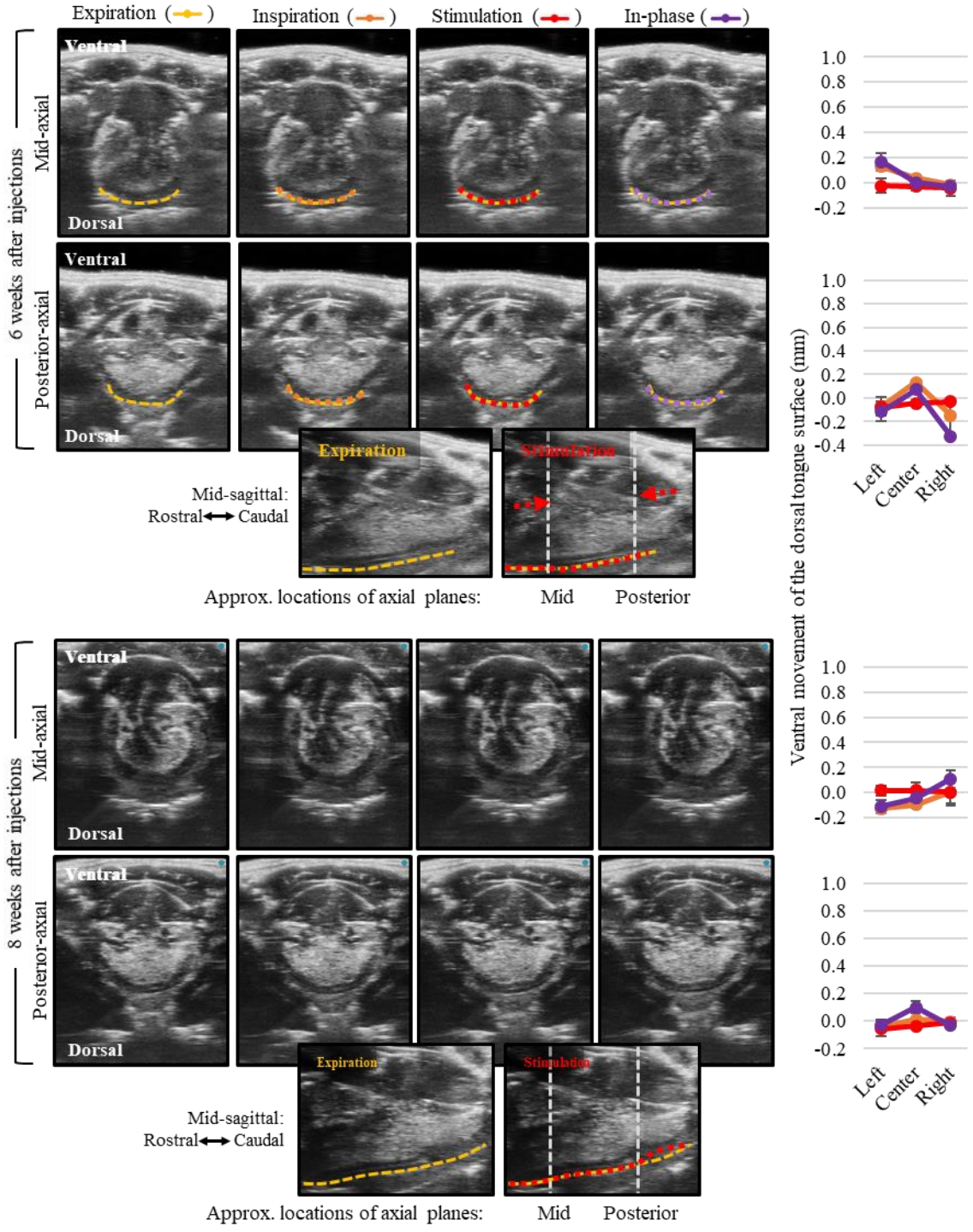

Longitudinal data: Animal ID – E8, Part 2

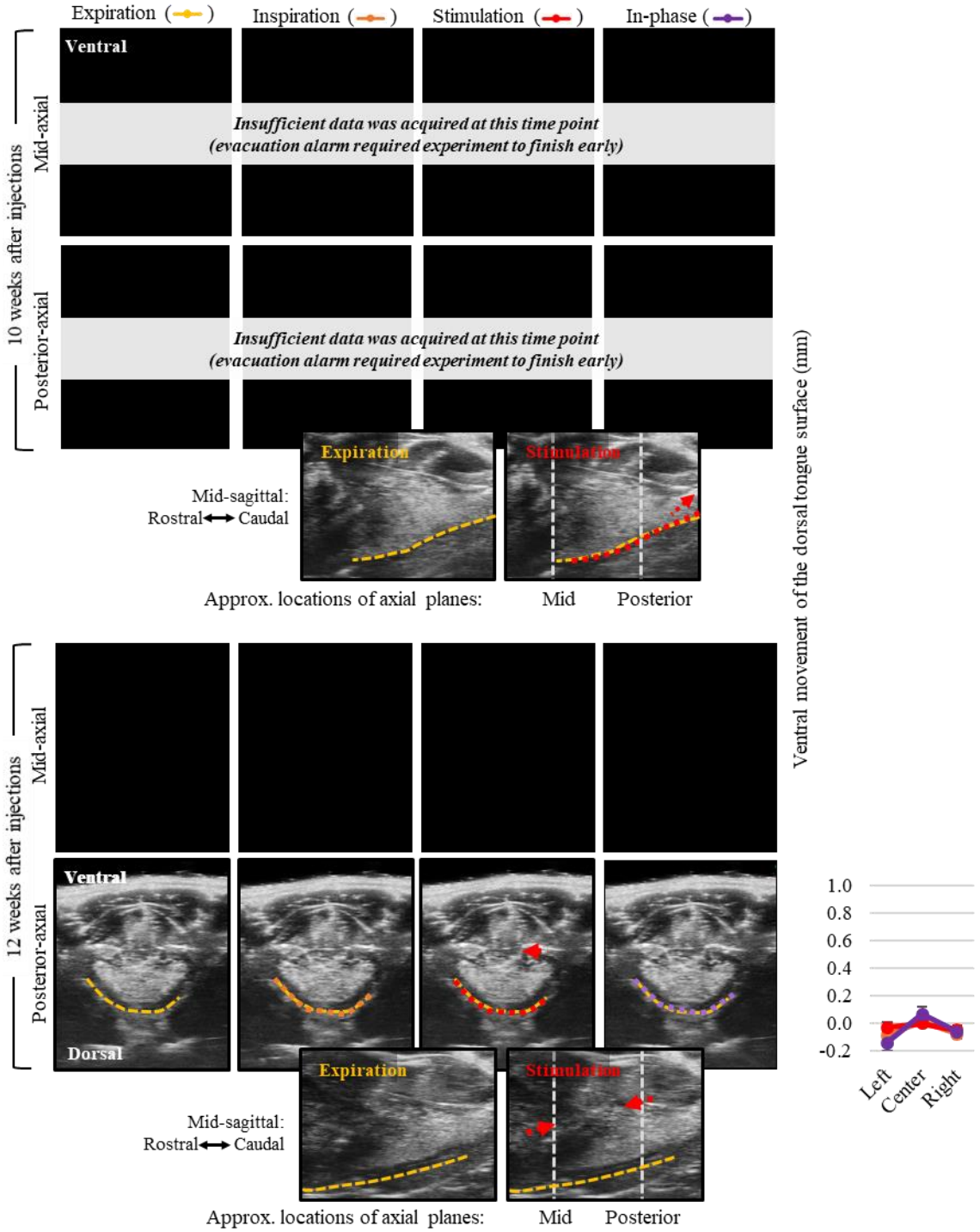

Figure A4-2 | Longitudinal ultrasound imaging data acquired from four animals (E3, E5, E6, E8) at 6, 8, 10 and 12 weeks after vector administration. Where light-evoked responses occurred at 3 weeks, they persisted until 12 weeks after vector administration, but started declining at approximately 9 weeks. The position of the tongue's dorsal surface during expiration (yellow dashed lines), inspiration (i.e. no stimulation, orange dashed lines), stimulation only (red dashed lines), and 'in-phase' stimulation (i.e. stimulation and inspiration, purple dashed lines) are indicated. In the graphs on the right, each data set represents the ventral movement of the dorsal surface during inspiration (orange), stimulation (red), and 'in-phase' stimulation (purple).

VIDEOS

Video A4-1: Sample muscle contractions and airway dilation in the mid-axial plane in response to 'out-of-phase' light stimulation applied to the upper airway muscles. In video text indicates endogenous, inspiratory related contractions and dilation (no stimulation) via 'Inspiration', and light-stimulation induced contractions and dilation via 'Stimulation'.

Video A4-2: Sample muscle contractions and airway dilation in the mid-sagittal plane in response to 'out-of-phase' light stimulation applied to the upper airway muscles. In video text indicates endogenous, inspiratory related contractions and dilation (no stimulation) via 'Inspiration', and light-stimulation induced contractions and dilation via 'Stimulation'.

CHAPTER 5 QUANTIFYING THE EFFECTS OF CHRONIC LIGHT STIMULATION

FINAL SURGICAL PROTOCOL

Preparation of electrodes and implantable light sources

1 | Construct optical fibre

i. Strip ~20 mm off a 200-µm core fibre (Lastek, Aus) using a micro-stripper (Micro Electronics, MA, USA). For easier stripping, keep the fibre attached to the fibre spool (Figure 5-1A).

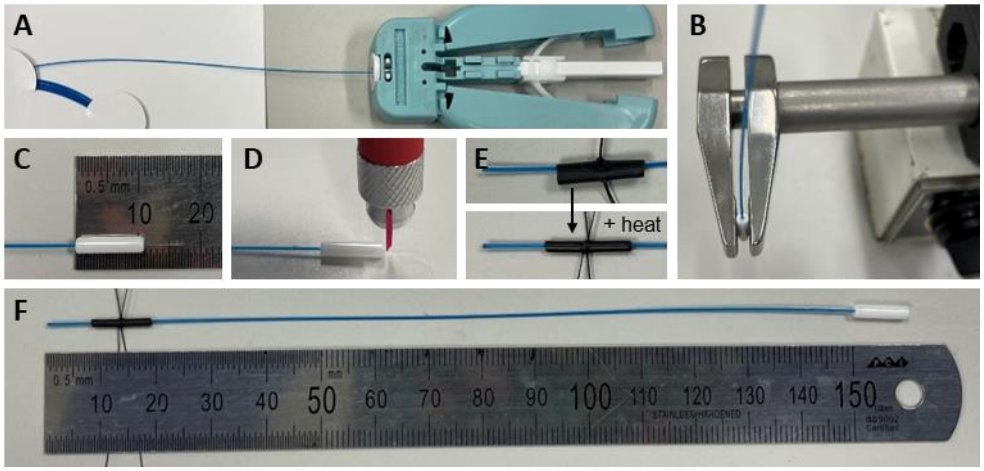

Figure 5-1 | Optical fiber development. **A)** Strip using micro-stripper, **B)** secure the ferrule in a vice, **C)** and let the remaining stripped fiber protrude through the ferrule. **D)** Trim the excess with a ruby-tipped scribe, and **E)** secure the sutures via heat shrink. **F)** The final device should be ~ 150 mm long, but can be altered for different sized animals.

ii. Leaving ~150 mm of unstripped fibre, score the fibre from the spool using a ruby-tipped scribe (ThorLabs, NJ, USA). Gently tap the fibre off with your finger or a glass rod. This will leave ~170 mm of fibre (20 mm stripped, 150 mm unstripped).

When scoring the fiber, hold the scribe perpendicular to the fiber and score in one direction in a single motion. Do not cut the fiber completely with the scribe.

iii. Prepare two-part epoxy, and fill a 1-ml syringe with the mixture. Add a blunted 25-gauge needle.

iv. Secure the ferrule (250 µm diameter; Lastek, Australia) into a vice with the convex side down (Figure 5-1B).

v. Add one drop (enough to fill the ferrule bore) of epoxy to the flat end of the ferrule. Wipe any excess epoxy off the sides of the ferrule.

vi. Insert the stripped end of the fibre into the ferrule (still in the vice) and thread it through until the ferrule contacts the fiber insulation, leaving the excess stripped fibre protruding through the ferrule (e.g. Figure 5-1C)

vii. Allow epoxy to cure as per product instructions

viii. Remove the excess stripped fibre precisely at the convex end of the ferrule using the ruby-tipped scribe (Figure 5-1D).

ix. Polish the convex end of the ferrule by making ~10 figure-eight rotations on five grades of polishing paper (polish using course to fine: 9, 6, 3, 1, 0.3 μm). Polishing must be gentle, and even pressure must be applied perpendicular to the paper to ensure an even ferrule surface and good light output.

x. Strip ~1 mm off the opposite, non-ferrule end of the optical fibre using a micro-stripper. This end will be inserted into tongue

xi. Thread two sutures through the middle of ~ 10 mm of heat shrink (diameter ~ 1.5 mm). Insert the optical fibre into the heat shrink so the heat shrink sits ~ 5 mm from the non-ferrule tip (Figure 5-1E).

xii. Use a heat gun to contract heat shrink around the optical fibre (Figure 5-1E, F).

xiii. Test optical fibre to confirm ≥ 70% of maximum output.

2 | Construct EMG electrodes for genioglossus recording

Note: Unless otherwise stated, all wire used in this protocol is PFA coated stainless steel wire (0.005” bare, 0.008” coated; A-M Systems, WA, USA)

i. Thread two ~150 mm lengths of insulated stainless steel wire through four sterile 26G needles

ii. For all wires strip ~ 4 mm of insulation off the end protruding from the needle tip, and ~ 6 mm of insulation off the other end

iii. Bend the ~4 mm stripped tip in half, forming a hook. The hook will be embedded into the muscle

3 | Construct three EEG electrodes for recording brain activity

i. Strip ~ 2 mm and ~ 15 mm of insulation off each end of three ~ 30 mm lengths of insulated stainless steel wire

Animal preparation

4 | Place the animal in an induction chamber and apply 5% isoflurane in oxygen delivered at a rate of 1 L/min.

5 | When no automatic withdrawal follows a paw pinch, remove animal from the chamber and maintain anaesthesia via nose cone. Isoflurane concentration should be maintained at approximately 2-3% isoflurane in oxygen (1 L/min).
Regularly assess the adequacy of anaesthesia via testing the negative pedal withdrawal response.

6 | Place a heat map under the animal and insert a rectal thermometer.
Regularly assess the animals core temperature, maintaining it at ~36°C to ~37.5°C.

7 | Subcutaneously inject carprofen (NSAID, 5 mg/kg), and intramuscularly inject cefazolin (antibiotic, 100 mg/kg).

8 | Apply an opthalamic lubricant (Viscotears) to prevent corneal desiccation.
Reapply ad lib throughout the surgery.

9 | Shave and sterilise (Betadine antiseptic solution) the regions indicated in Figure 5-2.
Approximate regions:

i. Skull: From immediately posterior to the eyes, to the base of the skull, ear to ear width.
ii. Sub-mandible: From the apex of the mandible to the clavicle, ~ 20 mm wide.
iii. Shoulder: Posterior to the fore limb, ~ 20 mm long, ~ 20 mm wide.

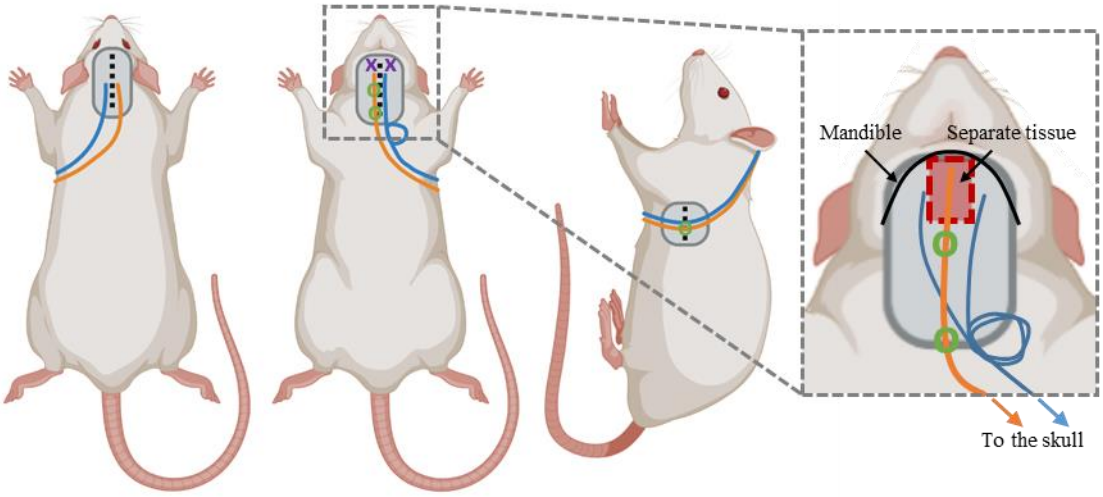

Figure 5-2 | Chronic implantation of an optical fibre and genioglossus EMG electrodes. Skull, sub-mandibular and shoulder (left to right) regions must be shaved and sterilised (grey ovals) prior to incisions (black dotted lines). Approximate routes for subcutaneous tunnelling for the genioglossus EMG (ggEMG) electrodes (blue) and optical fibre (orange) are indicated. The optical fibre was secured at three points (green), and the EMG electrodes were inserted at two points (purple). The inset image displays the region where the tissue was separated (red) immediately posterior to the mandibular symphysis for effective light source placement. Created with BioRender.com

Insertion of genioglossus EMG electrodes and securing the light source

10 | With a scalpel make ~ 25 mm long incisions at the sub-mandible and skull locations and an ~ 15 mm incision posterior to the shoulder (Figure 5-2, black dotted lines)

11 | Using blunt haemostats separate the connective tissue and muscle fibres underneath the chin, and immediately posterior to the rostral end of the sub-mandible incision (Figure 5-2, inset image)

▲CRITICAL STEP▲ Sufficient separation of muscle fibres, and subsequent securing of the light source deep within the muscle is essential for effective illumination of the genioglossus

12 | Using blunt hemostats, tunnel subcutaneously from the sub-mandible incision to the skull incision via the shoulder incision following the approximate route in Figure 5-2 (blue). Do not remove the haemostats when completed.

13 | Use the haemostats to clamp two narrow polyethylene tubes (diameter ~ 2 mm) at the skull incision, and pull the tubing through the subcutaneous tunnel to the sub-mandible incision via the shoulder incision.

14 | Insert the optical fibre into one of the tubes at the skull incision, and push the fiber through the tube until the end is visible at the sub-mandible incision. The ferrule should remain exposed at the skull incision.

15 | Gently remove the tube by pulling it through the tunnel from the sub-mandible incision, thus leaving the optical fibre in place.

16 | Insert two electrodes by inserting the needles at ~ 15° to the rat, ~ 5 mm caudal from the mandible apex, and ~ 3 mm each side of the midline (Figure 5-2, inset image).
Gently withdraw the needle from the muscle, removing it from the electrode wire, and leaving the hook electrode in place within the genioglossus.

17 | Test genioglossus EMG recordings for endogenous respiratory linked muscle activity

18 | Place the light source within the separated tissue and between the EMG electrodes. Secure the light source in place with sutures at the points illustrated in Figure 5-2.

19 | Create a single loop in the electrode (diameter ~ 10 mm) approximately 20 mm after the wires are inserted within the muscle. Secure the loop with a loose suture at the entrance to the subcutaneous tunnel to allow the wire to extend with animal movement.

20 | Thread the remaining EMG electrodes (after the loop) through the polyethylene tube until they exit at the skull incision. Carefully remove the tube by pulling it through the skull incision. This will thus leave the electrodes in place, extending from within the genioglossus to the skull incision site.

21 | Suture closed the chin incision, and apply Vetbond tissue adhesive as required.

Insertion of EEG electrodes

22 | Place rat in the stereotaxic frame, maintaining constant isoflurane (~ 2-3% in oxygen, 1 L/min)

23 | Use a scalpel blade to detach and push aside the periosteum and use haemostats to hold the skin back and ensure maximum exposure of the skull.

24 | Use sterile gauze to clear the skulls surface of blood

25 | Use a cotton tip to cover the exposed skull with 3% hydrogen peroxide to remove remaining tissue

26 | Deactivate the hydrogen peroxide with saline when the skulls surface is clear and the bregma and lambda are identifiable

27 | Using a hand held drill (Woodpecker iLED Curing Light, Ark Health, NSW, Aus), make burr-holes at the three locations identified in Figure 5-3A. Insert screws (0-80 thread, 2.4 mm long; P1 Technologies), leaving ~ 1 mm of the thread exposed

28 | Using fine forceps, tightly wrap the longer uninsulated region of the ~ 30 mm electrodes around the exposed thread of the three screws until there is ~10 mm of wire remaining uncoiled

29 | Tighten the screws on top of the coiled wires

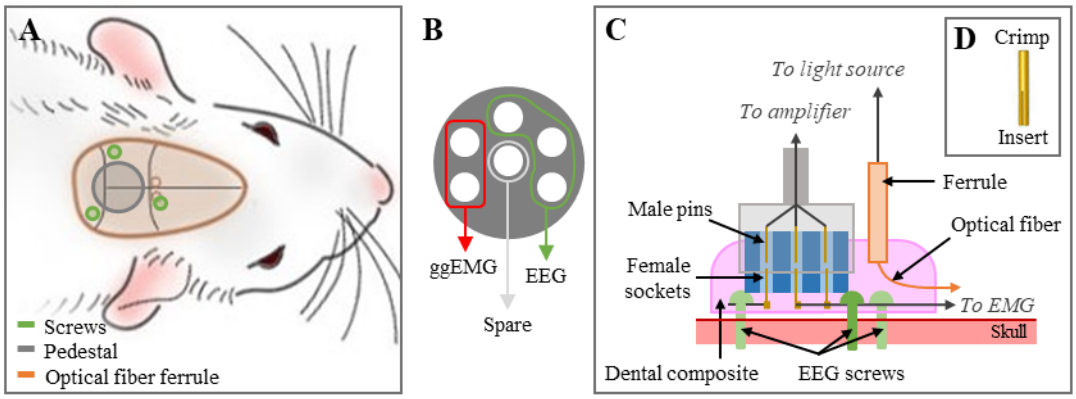

Figure 5-3 | Head stage set up with one pedestal and an optical fiber. (**A)** Approximate locations for screws, pedestal, and optical fibre ferrule. (**B)** Two genioglossus EMG (ggEMG) electrodes and three EEG electrodes connect to specific sites on a six-channel electrode pedestal. The figure indicates the orientation from the insertion side of the pedestals (the larger holes). (**C)** The pedestal and ferrule are secured to the skull by a dental composite and, during recording, connect to patch cables for data and light transfer, respectively. (**D)** The female pins are crimped to the wires at the solid end and inserted into the pedestal split end first.

30 | Trim the excess electrode wire so each will be 'relaxed' upon entering the pedestal. Whilst slack should be minimised, the electrode should not be taut when secured. Strip the insulation from the last ~ 2 mm off all wires.

31 | Crimp the solid end of the female sockets (Figure 5-3D) onto the ~ 2 mm of exposed wire of all 5 electrodes (i.e. 3x EEG, and 2x genioglossus electrodes)

32 | Identify the side of the pedestal with the larger holes and insert the female sockets into locations identified in Figure 5-3B

Securing the pedestals

33 | The skull surface is prepared using OptiBond Primer and OptiBond Adhesive as per product instructions. The pedestal and ferrule are then secured in place (Figure 5-3A) by Tetric EvoFlow dental composite and cured as per product instructions.

34 | Gradually build up the Tetric EvoFlow, intermittently curing the material until ~ ½ of the pedestal and ~ ¼ of the ferrule are covered.

Minimise the development of any sharp edges and take care to avoid blocking the pedestal connection points with Tetric EvoFlow to allow easy patch cable attachments for data acquisition.

35 | If required, use sutures or staples to close the posterior or anterior ends of the skull incision

36 | If required, use Vetbond to secure the skin to the dental composite

Post-operative care

37 | Post-surgery, remove the nose cone and place the rat into a clean, empty, heated and padded cage.

i. Do not leave animal unattended
ii. Provide water and moistened food at bottom of cage
iii. Observe animal respiration rates, righting behaviours, grooming and feeding
iv. Administer post-surgery analgesics if necessary

38 | When ambulatory, place the animal in a solo home cage within the general animal housing room.

The animal will remain in a solo home cage for a minimum of 24 hours following surgery.

39 | Monitor the animal closely for a minimum of 3 days post-surgery.

v. Ensure adequate wound closure at the incision sites, and around the dental composite
vi. Monitor weight, and ensure it does not fall below ~ 80% of pre-surgery weight
vii. If the animals display any characteristics indicative of pain and/or infection, administer additional analgesics and/or antibiotics.

viii. Continue daily monitoring and contact veterinary care if recovery exceeds 3 days

40 | Remove sutures after 7 to 10 days

Recording Chamber Set Up

A cost-effective plethysmograph is fabricated by combining a pressure sensor and a glass vacuum desiccator.

1 | Pour rodent bedding material into the chamber

2 | Feed the below tubes and patch cables through the desiccator lid

i. Air inflow tube: Connected to a compressed air cylinder, for active delivery of air to the recording chamber at ~ 1L/min

ii. Air outflow tube: Allows passive escape of air to the external environment

iii. Pressure sensor tube: Connected to custom device to signify the respiratory cycle

iv. Patch cable: Connects to pedestal, and is comprised of five cables all of which project from pedestal specific male pins (P1 Technologies) to banana plugs.

v. Optical fibre patch: Connects the optical fibre ferrule to the external light source (laser or LED).

Habituation

A week following surgery, animals start bi-weekly chamber habituation sessions, for ~ 4 to 6 hours per session. To allow for 2 complete weeks of recovery post-surgery, the animal remains untethered during the first week of habituation. During week 2 of habituation, patch cables are connected to the animal so they additionally habituate to the forces imposed on the implanted hardware. The animal will undergo at least four habituation sessions before data acquisition commences. 1L/min active air inflow and passive air outflow is maintained at all times when the animal is in the chamber.

Data Acquisition

A minimum of three weeks post i.m. injections, two weeks post-surgery, and at least 4 habituation sessions, the animal will undergo the first data acquisition session. Two data acquisition sessions should be conducted per animal.

1 | Place the animal in an induction chamber and anaesthetise via inhaled 5% isoflurane in oxygen (1 L/min).

2 | When no withdrawal response follows a paw pinch, remove the animal from the chamber and use a nose cone to maintain anaesthesia at 2-3% isoflurane in oxygen (1 L/min).
Regularly assess the adequacy of anaesthesia via negative pedal withdrawal response.

3 | Whilst anaesthetised, patch cables are attached (see above under 'Recording Chamber set up')

4 | Remove animal from isoflurane and place in the recording chamber

5 | Chamber pressure, EEG and EMG activity are recorded continuously for a minimum of 4 hours.
EMG signals are amplified and band-pass filtered (0.3–10 kHz), and EEG signals are amplified and band-pass filtered (0.1-0.3 kHz) via a AC/DC Preamplifier (BMA-400 Four-channel AC/DC Preamplifier, CWE Incorperated). A CED Power 1401 (Cambridge Electronic Design Limited) digitises signals at a sampling rate of 5 kHz for EMG and EEG recordings, and 1 kHz for chamber pressure (plethysmograph). Data is stored on a computer using Spike2 software.

1 | Light stimulation is applied intermittently throughout.
Stimulation is triggered 'in phase' with inspiration, or 'out-of-phase' i.e. during expiration and/or pauses in the respiratory cycle. Inspiration and expiration onset points are determined by chamber pressure.

Necropsy

After the data acquisition sessions were completed, a necropsy was conducted to confirm the locations of the light source, the EEG electrodes and the EMG electrodes. General health of organs and tissues, particularly near the implanted hardware was checked.